THESIS FOR THE DEGREE OF DOCTOR OF PHILOSOPHY IN ARCHITECTURE

Differential geometry and structural action of vaults and shells

EMIL ADIELS

Department of Architecture and Civil Engineering
Division of Architectural Theory and Methods
Architecture and Engineering Research Group
CHALMERS UNIVERSITY OF TECHNOLOGY

Göteborg, Sweden 2024

Differential geometry and structural action of vaults and shells
EMIL ADIELS
ISBN 978-91-7905-985-9

© EMIL ADIELS, 2024

Thesis for the degree of Doctor of Philosophy in Architecture
Doktorsavhandlingar vid Chalmers tekniska högskola
Ny serie nr. 5451
ISSN 0346-718X
Department of Architecture and Civil Engineering
Division of Architectural Theory and Methods
Architecture and Engineering Research Group
Chalmers University of Technology
SE-412 96 Göteborg
Sweden
Telephone: +46 (0)31-772 1000

Cover:
Asymptotic grid shell as an exhibition space, built with students in the course Parametric Design - Digital Tools with bachelor students at the Architecture and Engineering program in 2019. The author was the part of the design team together with I. Naslund, J. Isaksson, H. Moubarak and C. J. K. Williams

Chalmers Reproservice
Göteborg, Sweden 2024

Differential geometry and structural action of vaults and shells
Thesis for the degree of Doctor of Philosophy in Architecture
EMIL ADIELS
Department of Architecture and Civil Engineering
Chalmers University of Technology

Abstract

Masonry vaults and bridges, concrete shells, and steel and timber grid shells are all examples of shell structures. Their beauty, spatial qualities, structural efficiency and manufacturing are closely tied to their geometry. Geometry is central since it does not only describe the shape of the shell but also the building blocks, which together form a pattern or grid dictating its construction and structural behaviour.

History has shown how architects and builders successfully utilized curved shapes to combine architectural qualities with structural efficiency through the use of simple building blocks of local materials. Differential geometry offers a mathematical framework for the investigation of such architectural qualities in both historic and new structures. The focus of this thesis is to investigate *how differential geometry can contribute to the design and production of shell structures in the digital age.*

During the thesis work, different directions for the investigation of differential geometry in architecture and engineering have been explored. Out of these explorations, two main directions have evolved, each of them with a more limited and specific research question:

> *How can differential geometry be used to design structurally efficient shells and shells with surface patterns for simple production?*
>
> *How can differential geometry be applied in a design process supporting the quick production of a grid shell?*

These questions have been treated and investigated in studies reported in the appended Paper A-F. Paper A, D and E cover different aspects of how to design shells where simple building blocks can be used. Paper A and D show different possibilities for designing new brick shells and masonry bridges, while Paper E investigates the architectural application of shells whose boundaries subtend a constant solid angle. Paper B and C describe and discuss the design and construction process of two different timber grid shell structures built of straight planar laths. Paper F takes its point of departure from the fact that shells are generally statically indeterminate structures, allowing several force and moment distributions that can fulfil equilibrium. Our study offers a framework for designing shells using the force method, where the redundant forces and moments in the shell are represented as two surfaces.

Keywords: Differential geometry, Shell, Grid shell, Conceptual design, Structural design, Form finding, Architecture, Engineering, Geometry, Masonry, Bridges

Sammanfattning

Murade valv och broar, betongskal och gitterskal av stål och trä är alla exempel på skalkonstruktioner. Deras skönhet, rumsliga egenskaper, strukturella effektivitet och tillverkning är nära knutna till deras geometri. Geometrin är central då den inte bara beskriver skalets form men också de individuella byggstenarnas utformning och hur de tillsammans formar ett strukturellt och konstruktivt mönster.

Historien har visat hur arkitekter, konstruktörer och hantverkare framgångsrikt använt krökta former för att kombinera arkitektoniska kvaliteter med strukturell effektivitet genom att använda enkla byggstenar av lokala material. Differentialgeometri är den gren av matematik som behandlar ytor och ytmönster och erbjuder ett matematiskt ramverk för undersökning av sådana arkitektoniska kvaliteter i både historiska och nya strukturer. Avhandlingens fokus är *hur differentialgeometri kan bidra till design och produktion av skalstrukturer i en digital tid.*

Avhandlingen undersöker differentialgeometrins möjliga kopplingar till arkitektur och ingenjörskonst. Två huvudriktningar har utvecklats, var och en av dem med en mer begränsad och specifik forskningsfråga:

Hur kan differentialgeometri användas för att designa strukturellt effektiva skal, samt skal med ytmönster för enkel produktion?

Hur kan differentialgeometri tillämpas i en designprocess som stödjer en snabb produktion av gitterskal?

Dessa frågor har behandlats och undersökts i de studier som beskrivs i bifogade Artikel A-F. Artikel A, D och E tar upp olika aspekter av hur man designar skal där enkla byggstenar kan användas. Artikel A och D visar olika möjligheter att designa nya tegelskal och murade broar, medan Artikel E undersöker de arkitektoniska möjligheter som skal vars yta beksrivs genom att varje punkt har en konstant rymdvinkel kopplat till ytans rand kan tillgå. I Artikel B och C beskrivs design- och konstruktionsprocessen för två olika skalstrukturer byggda och konstruerade av raka plana ribbor av plywood. Artikel F tar sin utgångspunkt i att skalkonstuktioner till en hög grad är statiskt obestämda. Det medför att de finns olika alternativ för skalet att bära last. Artikel F ger ett ramverk för hur man kan man kan utforma alternativa kraftmönster vid design och analys av skalkonstruktioner genom att representera strukturens statiskt övertaliga krafter och moment i kraftmetoden som två ytor.

Preface

'Do you live here...?', said the surprised technician from the Swedish energy agency. According to her instructions, this was the facility's boiler room with all technical installations, which was true. Still, to her astonishment, she stepped into a workshop of gears, motorcycle chains where two children were sleeping on the floor. She found herself in almost a medieval workshop where the border between family life and the workshop space was nonexistent.

At that time, my brother and I aimed to become world champions like our hero Tony Rickardsson in a motorsport called *Speedway* where we toured together with our father around Sweden, caring little about much else. It is a motorsport of extreme simplicity. French aviator Antoine de Saint Exupéry describes perfection in his book *Wind Sand And Stars* as 'In anything at all, perfection is finally attained not when there is no longer anything to add, but when there is no longer anything to take away, when a body has been stripped down to its nakedness' (Saint-Exupéry, 1939, p.66). Nothing can be more true for a speedway bike. It is basically an engine on wheels: one cylinder, fixed gear, no brakes and no back-wheel suspension. Since the bike is stripped of all leisure, the skills come to handle the bike and become one with the machine. That also includes service and repair between the races.

During those years my brother and I learned what it takes to be a craftsman, both on and off the track. However, my father was clear that he was not content with me becoming a craftsman like himself, 'Son, if you intend to become a bricklayer like your father, I will strangle you in your sleep. It might sound harsh, but it is, in fact, an act of kindness'. It was not a threat but rather an expression of years of struggles and poor treatment as a bricklayer throughout the '90s recession in Sweden. During several years many of them, if they had any work at all, were forced to work on short contracts, sometimes spanning a week.

It was not that my father did not like his work. We often walked around in the city where he told stories of the former master builder's skills and, with awe, pointed out specific details only a craftsman notice. With simple tools such as a trowel and a plummet, they built masterpieces with their hands using bricks. That level of craftsmanship no living bricklayer could accomplish, he said. He would also often revisit the buildings he had worked on several years later to evaluate the long-term effects. I think the reluctance was due to an industry that did not value his and his colleague's skills and knowledge, which is probably a shared feeling among other professions. I have always found it sad when skilled, committed and passionate people feel badly treated or their knowledge is valued less because they do not have an academic degree. That is why, no matter how much my father loved the work, he did not wish his son to experience the industry's dark side and instructed me to study at the university.

The studies started at the dual program in architecture and engineering—an entirely new world of new references and a different culture. Most important were the study tours in Italy, the United Kingdom and Switzerland. In London, I saw the curved glass roof over the British Museum Court Roof for the first time, and I was amazed by the geometry and the public space it created. It reminded me of the masonry vaults my dad and I had seen and discussed. Several years later, I met Professor Chris Williams, who generated the geometry. Yet, before that, I did an internship between my bachelor's and

my master's on Buro Happold, the structural engineering consultancy behind the British Museum Court Roof. I was fortunate to work with both geometry and code development, developing schemes for similar grid shells. However, sometimes, we were consulted late in the process. During those occasions, it was difficult or impossible to please architects, contractors, manufacturers, and engineers regarding aesthetics, buildability, and structural performance with too many parameters fixed. I understood that there was a relationship between spatial qualities, buildability and structural performance and that geometry was the key. Being part early in the process was equally essential. Hence, I would need to know more theory and work with those parameters simultaneously earlier in the design process. Back at the university, I tried to find courses in geometry, but it was easier said than done. I managed to enroll in a course in differential geometry; I somehow understood that this was what I would need, but it wasn't easy to find direct applications. It was not until I got in touch with Professor Chris Williams that I understood how it could be related to architecture and physics.

During my studies, I was also lucky to be one of the organisers of the big conference *Smartgeometry* in 2016. A symposium where architects, engineers, software developers and researchers meet to investigate the connection between architecture and technology during a four-day hackathon. It was an exciting and open atmosphere with an iterative loop between ideas and experiments. Except for the love of that experimental environment, I became aware of the craft of organising workshops.

Looking back, all these experiences have been important to me going into the thesis work. Seeing the beauty and skills of building brick vaults using simple tools and building elements. Realising geometry was the 'elephant in the room' in my strive to combine spatial qualities, buildability and structural performance during work and studies.

Acknowledgements

First of all, I would also like to thank my supervisors, Prof. Chris Williams, Dr Mats Ander and Prof. Klas Modin. I cannot thank Chris enough for his wisdom, which he generously shares, and for opening up an entirely new world of insights and references, especially in geometry and the connection to architecture physics. Also for advice and generous support during the experiments and workshops. I want to thank Mats for valuable discussions, ideas, endless enthusiasm and encouragement. I am grateful for the conversations about mathematics with Klas and his open-minded attitude towards our way of interpreting mathematics.

I want to thank my examiner, Prof. Karl-Gunnar Olsson, for his support and mentorship both before and during my PhD studies. I am very grateful for all the conversations, discussions, feedback, and exciting events at Chalmers that you have enabled and for which I have had the opportunity to be a part.

I want to thank several people for interesting discussions, comments, encouragement, feedback help or advice during different times including Peter Christensson, Morten Lund, Kia Bengtsson Ekström, Maja Kovacs, Jonas Carlsson, Stefano Delia, Prof. Angela Sasic Kalagasidis, Joosef Leppänen, Prof. Sigrid Adriaenssens, Prof. Philippe Block, Dr Matthias Rippmann, Assoc. Prof. Jan Stevens, Dr Michele Godio, Ulla Antonsson and Stefan Lundin. I want to especially thank my PhD colleagues, Dr Erica Hörteborn, Dr Alexander Sehlström and Dr Jens Olsson, for all the valuable conversations, discussions and support, both at work and off work.

I want to thank those who have been part of, helped or supported the many workshops at Chalmers including Isak Näslund, Emil Poulsen, Nicolo Bencini, Puria Safari, Cecilie Brandt-Olsen, Johanna Isaksson, Habiba Moubarak, Dr Robin Oval, Carl Hoff, Erik Wigh, Fredrik Boman, Alison Martin, Tim Finlay, Dr Al Fisher, Robert Otani, Dr Diederik Veenendaal, Peter Lindblom, Tabita Nilsson, Sebastian Almfeldt, Anders Karlsson, Peter Bäckgren and Tord Hansson. It has been some of the best days in my life, thank you!

Many thanks to Tomas Gustavsson for the support and many exciting conversations regarding brick and masonry structures.

I would like to express much gratitude to Cramo Göteborg and especially Christian Dimitrossopoulus and Mikael Torstensson for supporting and sponsoring the workshops at Chalmers.

I want to thank ARQ research fund for supporting my studies in masonry which has been valuable in my research.

I would also like my former colleagues at Buro Happold, from which I learned a lot, and it was an exciting time. That experience has been influential for my research.

Most of all, I want to thank my wife Linnea and my family for their endless support, especially when there has been a bump in the road in my work, they have helped me get back on track.

Contents

Paper C

Adiels, E., Brandt-Olsen, C., Isaksson, J., Näslund, I., Olsson, K.-G., Poulsen, E., & Williams, C. J. K. (2019). The design , fabrication and assembly of an asymptotic timber gridshell. *Proceedings of the IASS Annual Symposium 2019 - Structural Membranes 2019* (October) (2019), 1–8

Paper D

Adiels, E., & Williams, C. J. K. (2021). The construction of new masonry bridges inspired by Paul Séjourné. *IASS Annual Symposium and Spatial Structures Conference: Inspiring the Next Generation* (August) (2021)

Paper E

Adiels, E., Ander, M., & Williams, C. J. K. (2023). *The architectural application of shells whose boundaries subtend a constant solid angle* [Under review (first revision, October 2023)]

Paper F

Adiels, E., & Williams, C. J. K. (2024). Internal force and moment surfaces for shells. In S. Gabriele, A. Manuello Bertetto, F. Marmo, & A. Micheletti (Eds.), *Shell and spatial structures* (pp. 118–128). Springer Nature Switzerland

Part I
Introduction and overview

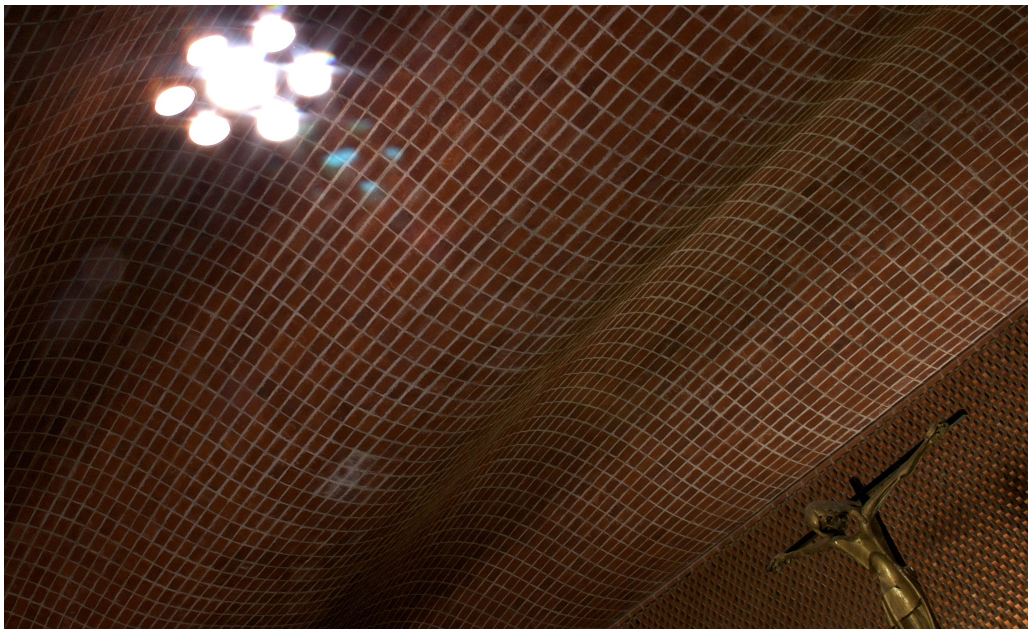

Figure 1: *Church of Christ the Worker (1958–60) in Atlántida, Montevideo, Uruguay, by Eladio Dieste (1917–2000).*

1 Introduction

Shells are characterised by their slender and curved shapes and are perhaps mostly known for their vital function in living organisms. Yet, shells also constitute an essential feature in architecture and our built environment. We see them in masonry vaults and bridges, in concrete shells, and in steel and timber grid shells. Their beauty, spatial qualities, structural efficiency and manufacturing are closely tied to their geometry. Geometry is central since it does not only describe the shape of the shell but also the building blocks, which together form a pattern or grid dictating its construction and structural behaviour.

It is, therefore, no surprise that geometry has had a tremendous importance and impact in the history of architecture, structural engineering and construction. Shelby (1972) wrote 'For medieval masons Euclid had virtually become an eponymous hero of the craft, and the word geometry had become synonymous with masonry'. With Euclidean geometry, master builders and architects designed and built vaults and cathedrals that have survived storms and world wars. Similarly, they designed masonry arch bridges that today carry much heavier and faster trains than they were initially intended for.

While geometry has developed tremendously over the last two hundred years, it is no longer fundamental knowledge among architects, builders or engineers. Instead, they rely on 3D modelling software to describe complicated curved shapes. The overall aim of this thesis is to recapture geometry as a fundamental knowledge and its use in architecture

and structural design, and thus its role in sustainable building.

The modern mathematics of curved surfaces is differential geometry, so called because it relies on differential calculus. In this thesis, the strengths and opportunities of differential geometry are explored through both theoretical and practical explorations. Hopefully, the findings and the described workflows could encourage architects and engineers to include more geometry in their curricula and, in doing so, also enhance their use of computer tools and even write their own software.

History has shown how architects and builders successfully utilised curved shapes to combine architectural qualities with structural efficiency through the use of simple building blocks of local materials. Differential geometry offers a mathematical framework for the investigation of such architectural qualities in both historic structures and the design of new structures. The focus of this thesis is to investigate *how differential geometry can contribute to the design and production of shell structures in the digital age.*

1.1 Differential geometry and physics

Classical differential geometry is the study of curved lines and curved surfaces in the 3-dimensional Euclidean space. Differential geometry was founded by Gauss in the 19th century and relies on a powerful concept. Imagine a coordinate system that follows a curved surface like the brick vault in Atlántida by Eladio Dieste (Figure 1). Even though the vault is curved, each brick represents a small region close to a flat plane tangential to the surface. On each brick, we could use small measuring sticks with the Euclidean geometry learned in elementary school to measure the geometric properties and their relation to the surrounding bricks. From the measured distances and angles of our bricks, we can tell the curvature of the surface. This is one of the most beautiful and powerful mathematical theorems called *Theorema Egregium* (Latin for 'Remarkable Theorem'). One of Gauss's students would later show that the same concept would hold in higher dimensions which is the foundation of Einstein's general theory of relativity.

> In the same way, one can have a curved four-dimensional space immersed in a flat space of a larger number of dimensions. Such a curved space is called a Riemann space. A small region of it is approximately flat. Einstein assumed that physical space is of this nature and thereby laid the foundation for his gravitation theory. (Dirac, 1975, p. 9)

Concepts such as stress, energy and momentum are central to relativity theory and similarly the connection between geometry and the mechanics of shell structures is most naturally described using differential geometry.

1.2 Structural action of shells

The characteristic feature of shells is that they are curved and thin compared to their surface extension. Through their curvature, shells can redirect external loads perpendicular to the surface and create internal forces in the tangent plane of the surface. The dominating and shaping load is usually related to gravity. The structural action of shells means that

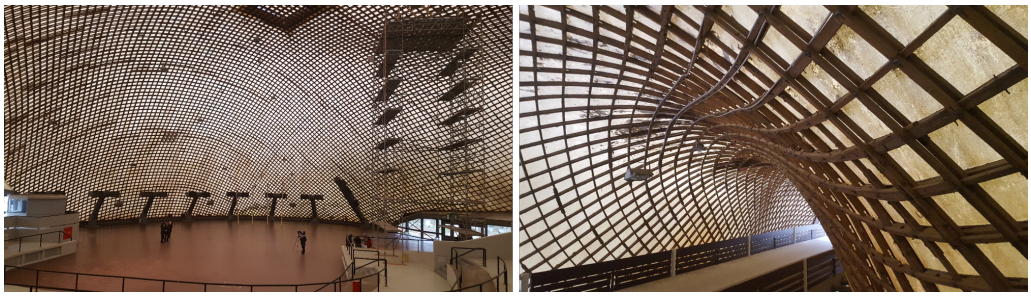

Figure 1.1: *Timber grid shell in Mannheim (1975) by Frei Otto (1925-2015) together with structural engineers Ted Happold (1930 – 1996), Ian Liddell and Chris Williams from Structures Group 3 at Arup.*

they work mainly in pure compression or tension rather than bending, which is why they are superior for large spans.

A quick envelope calculation for a dome spanning a hundred meters in diameter shows its material efficiency. For a shell built in a material like stone or concrete with unit weight $\rho = 2000$ kN per cubic metre and with the radius r, the simple expression $\sigma = \rho r$ computes the stresses at the springing of the dome to 1 MPa (Heyman, 1995). This can be compared to the compressive strength of perhaps 15-30 MPa of concrete. This very efficient way of carrying loads explains why we see such shapes not only in historical structures but also in nature and cells (Thompson, 1917).

Thus, if designed correctly with proper supports, shells can be built using a small amount of material. Pioneers in this aspect include the German architect and engineer Frei Otto, in the works of the Olympic stadium and the timber grid shell in Mannheim (Figure 1.1), and the Swiss engineer Heinz Isler who designed slender concrete shells. Shell structures are also suited for using weak materials with low embodied carbon. An example of such a project is the *Mapungubwe Interpretation Center* in South Africa by Peter Rich Architects, Michael Ramage and John Ochsendorf, where they used compressed earth tiles from local soil (Figure 1.2). Both aspects tie into the biggest challenges for the building industry in reducing *greenhouse gas* emissions to mitigate climate change (IEA, 2019).

1.3 Design and production of shells

What makes shells structurally efficient also makes them complex in terms of manufacturing. Especially if they are to be assembled of simple building blocks by a person or a machine and where the geometrical constraints include both the shape and the surface pattern. This connects to the overall challenge of sustainable building. Besides fulfilling the architectural and structural requirements, an adaption of the manufacturing to locally available materials and labour skills, as well as to the economic conditions and cultural context of the local community is needed. This is highlighted in the 2018 Davos declaration (Swiss federal Office of Culture, 2018) where the European Ministers of Culture call for a high-quality *Baukultur*. Baukultur includes the architectural quality

Figure 1.2: *Mapungubwe Interpretation Center. Team: Peter Rich Architects, Michael Ramage at Cambridge University and John Ochsendorf at MIT*

of the final building or architectural design but also stresses the need for a sustainable building culture. A sustainable building culture that includes the design process and the construction process, and how these processes and the final design are anchored in the local context. Christopher Alexander (1977) addresses some of the aspects related to this issue:

> The central problem of materials, then, is to find a collection of materials which are small in scale, easy to cut on site, easy to work on site without the aid of huge and expensive machinery, easy to vary and adapt, heavy enough to be solid, longlasting or easy to maintain, and yet easy to build, not needing specialized labor, not expensive in labor, and universally obtainable and cheap. (p. 956)

The question is whether differential geometry could be an aid or tool in the design process to address the construction constraints connected to the local context while also achieving structural and material efficiency.

The Russian mathematician Chebyshev showed an early example of how differential geometry could be applied to understand the complex cutting patterns of textiles, which, according to Chebyshev (1887/1946), can be applied to any body:

> I touched on another question about fabrics, the solution of which with the help of mathematics may be of certain interest, namely, the cutting of fabrics in the manufacture of clothing or, in general, the shells of any kinds of bodies.[1] (p. 38)

The Chebyshev nets means that each side of the quadrilaterals in the net is equal in length, but its internal angles change with the curvature. Such net was applied in the form finding of the timber grid shell of the Mannheim Multihalle (Figure 1.1). The hanging chain-net (Figure 1.3) form finding method is meant to reflect the inverted shape in pure compression with respect to gravity. The result was a Chebyshev net in compression

[1]Translated from Russian to English with the help of Konstantin Mina

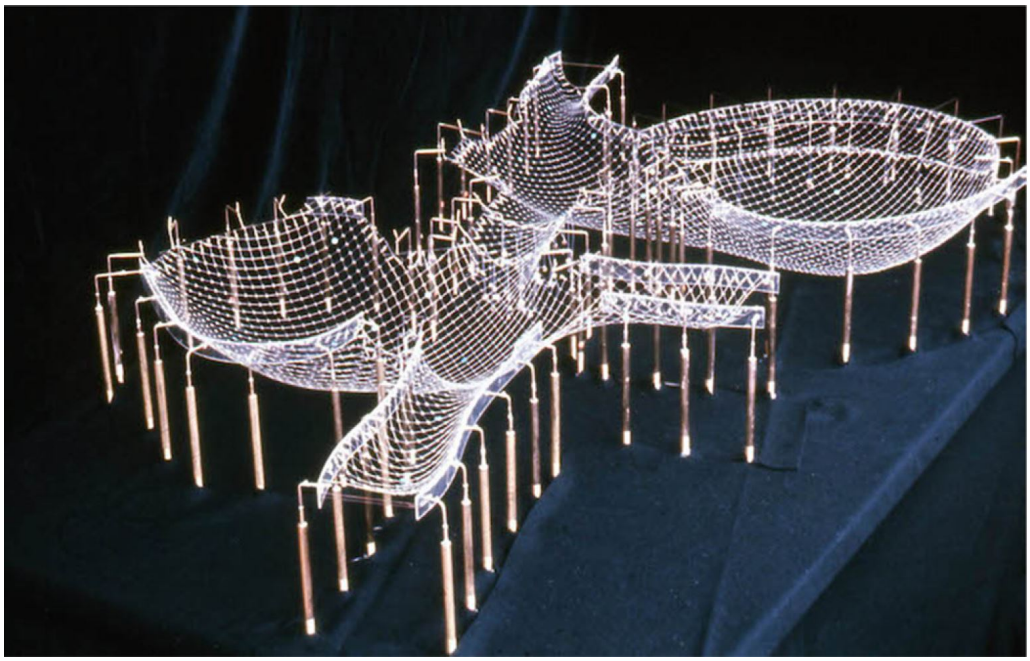

Figure 1.3: *Final hanging chain model for the timber grid shell of Mannheim Multihalle (1975), which is also Chebyshev net where the length in each quadrilateral is equal in length but with varying angles.*

which could be built from straight continuous timber laths, where the widest span is 60 metres with a structural depth of roughly 20 cm. The relative thickness is three times the thickness of an eggshell[2]. The Mannheim Multihalle showcases one of the possibilities of combining differential geometry and shell theory to span large distances using simple building elements.

1.4 Research questions and methodology

Differential geometry offers a natural link between structural action, production and architectural qualities of shells and grid shells. The current lack of knowledge in geometry in architecture and civil engineering calls for studies using differential geometry to achieve the structural benefits of shells while still adapting manufacturing requirements for sustainable design. Different directions for investigating these aspects have been explored during the thesis work. Out of these explorations, two main directions have evolved, each of them with a more limited and specific research question:

[2]The span to thickness ratio of an eggshell is 100 for an eggshell (Heyman, 1995) compared to 300 for the Mannheim grid shell with a grid size of 50x50 cm.

1. How can differential geometry be used to design structurally efficient shells and shells with surface patterns for simple production?

2. How can differential geometry be applied in a design process supporting the quick production of a grid shell?

The research methods used are taken from both engineering science and from the field of art and design, and can be divided into five main categories:

(1) A literature review was conducted on both historical and contemporary architecture and mathematics, as well as the theory of geometry and its connection to physical phenomena related to architectural design.

(2) Theory development was used as a qualitative approach described in (Hammond & Wellington, 2021) to explore, explain and uncover phenomena and generate new theoretical insights in geometry connected to architecture.

(3) Simulations and digital experiments have been performed to evaluate the geometric and structural concepts developed. It has been done through programming computer programs or scripts linked to architects' and engineers' digital toolbox and digital environments, such as *Rhinoceros3D* and *Grasshopper3d*.

(4) Design inquiries, or design challenges, were used to organize experiments around research questions and generate new research questions — the type of action research described in the category of Research through art and design by Frayling (1993) and Borgdorff (2007). The design and applications were intended for the conceptual and early-stage design process and physical prototypes in controlled environments.

(5) Documentation of the experiments and the design processes has been made using film and moving pictures. The purpose has been twofold. Firstly, it has been vital for communication and a tool for discussions during and after experiments on geometric, structural, manufacturing, and architectural aspects. Secondly, it was used as a forum or tool to discuss new insights or aspects of these buildings and experiments with others. It could be the architectural qualities, theories from craftsmen on how things were made, mechanical phenomena in the models, or possible methods to analyze the behaviour.

These methods have been combined into specific methodologies for each research question, described in more detail in Sections 5.3.2 and 5.3.3, along with a broader description of the research methods used in architectural research in Section 5.2.

1.5 An architecture and engineering research culture

The research has been conducted in the *Architecture and Engineering Research Group*, an interdisciplinary research group of architects, engineers and artists part of the *Research School of Architecture* at Chalmers University of Technology. The research group is closely related to the dual degree program *Architecture and Engineering* (Caldenby et al., 2017; Olsson et al., 2019) at Chalmers. Prof. Karl-Gunnar Olsson, the founder of the program, described the inspiration and the concept of the program as follows:

> Inspired by the work and attitudes of architects and engineers like Jörg Schlaich, Renzo Piano, Piero Luigi Nervi, Sverre Fehn, Ted Happold, and environments like ILEK in Stuttgart and ETH in Zürich, a vision of a new kind

> of architects and engineers ... where the fundamentals from the engineering science: mathematics, mechanics, physics and materials, is combined with history of architecture and engineering, artistic explorative courses, and the fundamentals of the architectural design process. (Olsson et. al, 2019, p.1)

The research group has four similar basic elements (Figure 1.4) that characterize the working method of the group: *(1) Contextual anchoring in contemporary and historically based references, (2) Mathematical modelling, simulation and optimization, (3) Exploratory experiments with an artistic approach and (4) Digital representations and prototypes for communication in the different stages of the design process.*

The first point relates to the research culture of architectural research, where studies of the built include the entire complexity of architecture and engineering as a context to a specifically studied issue. This complexity gives a broader understanding of the question and inspiration for how the question can be processed and how the research results can be reflected and understood in future contexts. This approach aligns with the tradition and culture at the Department of Architecture at Chalmers contributed by Prof. Elias Cornell (1961, 1979) and Prof. Claes Caldenby.

The second point refers to phenomenology, which mixes the research culture of *structural mechanics* at, for instance, Chalmers University of Technology and Lund University and the culture from Bath University through Prof. Chris Williams. While Chalmers has had a vital role in developing the *finite element method* (FEM)[3], Prof.

[3]Chalmers was an early adaptor of matrix methods and FEM in the 1960s. Contributors include Prof. Sven Olof Asplund (1964), Prof. Hans Petersson, who worked both at the University of Lund

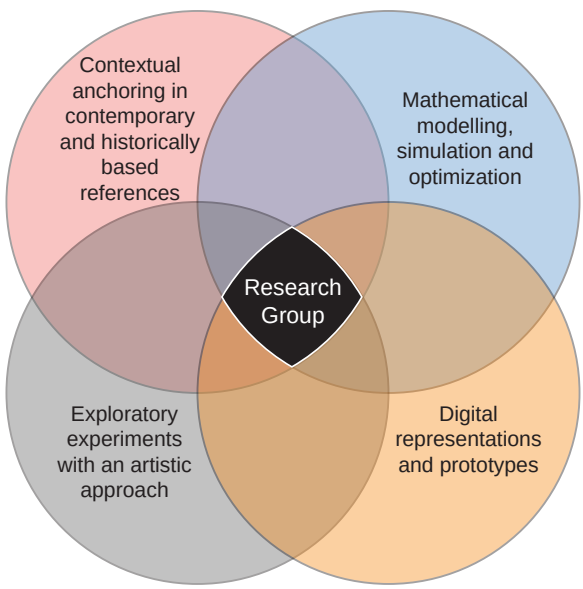

Figure 1.4: *The four elements characterizing the research group.*

Figure 1.5: *A two-day workshop about the geometry and structure of weaving together with artist Alison Martin. The workshop was part of the course Virtual Tools in a Material Culture, 2019. It was organised as a collaboration between researchers and specialists from Chalmers, ETH Zürich, Buro Happold and Core studios at Thornton Tomasetti and artist Alison Martin. Workshop organisers were Emil Adiels, Daniel Jonsson, Sofia Malmsten, Alison Martin, Isak Näslund, Robin Oval, Emil Poulsen and Chris Williams.*

Chris Williams has worked with Alistair Day (Carfrae & Michael, 2019a, 2019b), Prof. Michael Barnes (1977, 1988, 1999) and Prof. Ted Happold (founder of Buro Happold) on developing applications of *dynamic relaxation* for form finding and analysis of shells and grid shells.

The third point is related to the possibility of performing artistic experiments with students in the program of Architecture and Engineering and having the artist Peter Christensson in the research group. It includes similarities to the work of artists such as Andy Goldsworthy (Riedelsheimer, 2001) and Alison Martin (Figure 1.5), exploring phenomena through physical models and experiments that interact with the surrounding environment.

The last point is inspired by research cultures and environments at, for instance, IL (Klaus et al., 1987) and ILEK in Stuttgart, CITA (Thomsen et al., 2015) at the Royal Danish Academy, Smartgeometry (Peters & Peters, 2013) and Block Research Group (Block et al., 2017) at ETH Zürich. The research group formed the core of the organization of Smartgeometry in 2016 (Fig. 1.6) and Architectural Geometry in 2018.

1.6 Thesis structure

The thesis is a compilation thesis consisting of an introductory overview (kappa) and six peer-reviewed conference papers and journal articles. The kappa includes a broader contextualisation of the subject, a discussion on the methodology used, a summary of

and Chalmers, Prof. Alf Samuelssson (Kärrholm & Samuelsson, 1972), Prof. Niels Erik Wiberg and Prof. Kenneth Runesson. In chapter 23 in (Wiberg, 1980) a list of software implementations of the FEM developed in the 1970s for different structural and civil engineering applications.

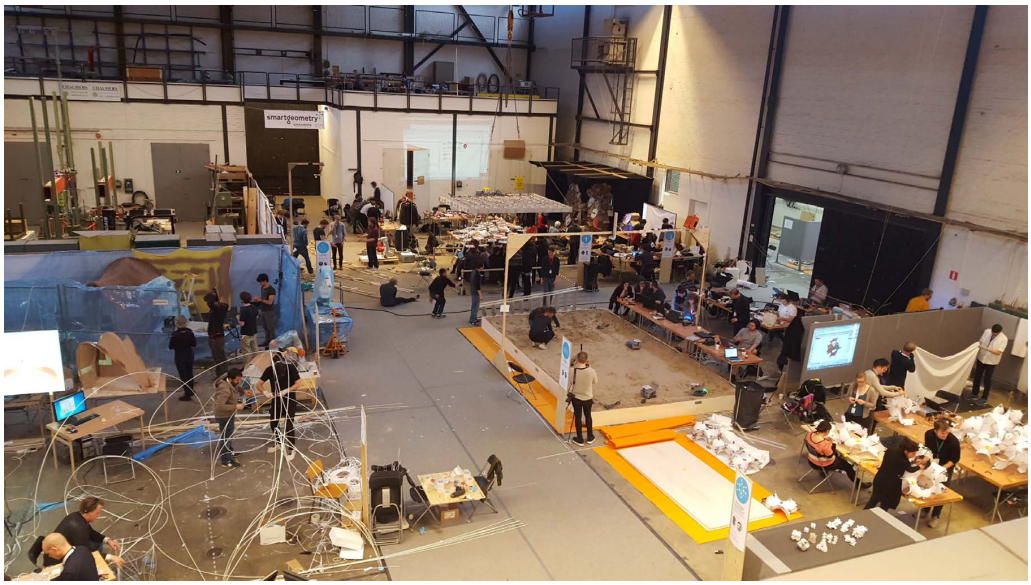

Figure 1.6: *The workshop at Smartgeometry 2016 containing ten different clusters was hosted at Chalmers University of Technology.*

the attached papers and articles, and finally a discussion of the results and some ideas of future research that has evolved from the performed investigations. As a supplement, the design process and execution of design projects are found in Appendices A-C.

The thesis is based on three fields: differential geometry, shell theory and the design and production of shells, and where each of these fields has been given a brief overview.

2 Geometry and architecture

This chapter covers the origins of geometry emerging from two directions: craft and astronomy. Furthermore, the use of geometry in architecture and its importance to the master builder is described. It ends by describing the development and theory of differential geometry.

2.1 Birth of geometry

Heilbron (2020) defines geometry as 'the branch of mathematics concerned with the shape of individual objects, spatial relationships among various objects, and the properties of surrounding space'. It is one of the oldest branches of mathematics and likely came out of the crafts culture. Due to its structural influence, the pattern is an essential part of the craft for weavers and bricklayers. The craft of basket weaving goes back to at least 7000 B.C. (Geib & Jolie, 2008). In old pottery, the form and the pattern also have aspects of pure beauty (Struik, 1987), Figure 2.1. Thus, the mathematician Struik (1987) suggests the connection between the birth of geometry and weaving through the etymology

> The word 'straight' is related to 'stretch', indicating operations with a rope; the word 'line' to 'linen', showing the connection between the craft of weaving and the beginnings of geometry. (Struik, 1987, p. 11)

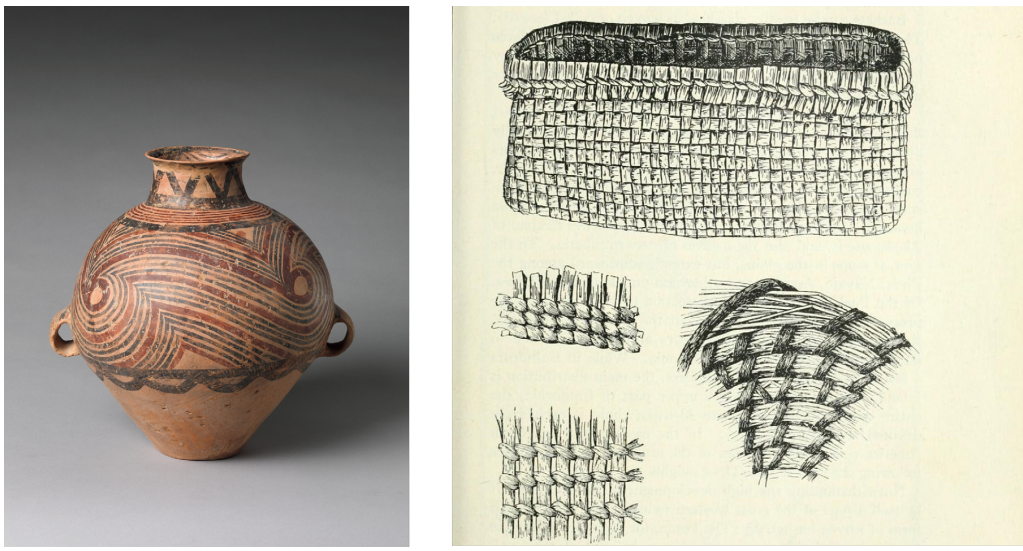

Figure 2.1: *Both decorative and constructive patterns were likely employed in crafts before the development of the mathematical branch of geometry. Left, Chinese Earthenware with decorated with complex patterns, ca 2650–2350 B.C. urn. Right, weaving techniques and patterns used in Native American basketry (Wissler, 1917).*

In Mesopotamia and Egypt, geometry was a tool for solving practical problems. It is believed that geometry in Egypt was needed for surveying tasks such as approximating the size of lands for taxation; a knowledge believed transferred to the Greek scholars. It can be found in writing by the Greek historian Herodotus (ca. 484 – ca. 425 B.C):

> For this reason Egypt was cut up; they said that this king distributed the land to all the Egyptians, giving an equal square portion to each man, and from this he made his revenue, having appointed them to pay a certain rent every year: and if the river should take away anything from any man's portion, he would come to the king and declare that which had happened, and the king used to send men to examine and to find out by measurement how much less the piece of land had become, in order that for the future the man might pay less, in proportion to the rent appointed: and I think that thus the art of geometry was found out and afterwards came into Hellas also. (Herodotus, 440 B.C, para. 109)

However, the best sources for the knowledge of mathematics and geometry in ancient Egypt are the Moscow Mathematical Papyrus and the Rhind Mathematical Papyrus, dating from around 1800 and 1650 B.C, the Rosetta stones of geometry. They contain different problems, some of which are geometrical. Likewise, many of the geometrical problems are of the kind of calculating the area and volume for different objects, such as:

> Problem 50
> Example Of a round field Of diameter 9 khet. What is its area? Take away 1/9 of the diameter, namely 1 ; the remainder is 8. Multiply 8 times 8; it makes 64. Therefore it contains 64 setat of land. (Chace and Mannin, 1927, p. 92)

As described by Herodotus, it is believed that Greek scholars learned geometry in Egypt. Greek mathematicians later excelled over their former teachers. Neither in Mesopotamia nor Egypt was there an interest in the science of geometry or proving the geometrical relations. It was the Greek who found an interest and joy in asking the question *why*. The most influential surviving book from Greece is *Elementa*, consisting of thirteen volumes, by Euclid (ca. 300 B.C.) who systematically organised the mathematical developments in Greece by that time. Another important source is the eight-volume book *Conics* by Apollonius of Perga (262 B.C. – 190 B.C.) on the geometry of conic sections, i.e. the circle, the ellipse, the parabola and the hyperbola.

The first type of non-Euclidean geometry was spherical geometry, concerning geometric objects on the surface of a sphere. The reason for that was also very practical. The ancients called this geometry *Sphaerica*, and it was the study of the heavens and the heavenly bodies. The etymological meaning of geometry is the measurement of the earth. Spherical geometry made it possible to measure the phenomenon of time and the creation of the calendar. The geometers in Egypt had already divided the day into 24 hours (Rosenfeld, 1988). It was to estimate the times to execute different operations linked to agriculture, when to plant and when to harvest. As Scherrer explains:

> Our forbearers followed their sky gods' movements attentively. By marking their appearance & disappearance with great care, they combined religious worship with practical knowledge. The cycle of planting and harvesting crops was regulated by celestial events; important days of celebration and festivity were marked in a celestial calendar. After generations, they learned to predict particular celestial phenomena, such as eclipses, well in advance. (Scherrer, 2015, p. 3)

There are several early books on the subject of Sphaerica by, for instance, Theodosius (ca. 100 B.C.) and Menelaus (ca. 100 A.D.)(Rosenfeld, 1988; Scriba & Schreiber, 2015). The primary and essential difference is to imagine a geometry defined on something curved rather than in the flat plane, as in Euclidean geometry. Menelaus is the first known to define a spherical triangle, bounded by arcs of great circles, and its angles. They are described similarly to the plane triangle by Euclid. However, the best known work is *Almagest* by the astronomer Ptolemy (ca. 100-170 A.D.) written about 150 A.D., which gives a model of ancient astronomy in Babylonian and Greek cultures (Rosenfeld, 1988).

Despite that curved geometries such as arches and domes are also very efficient in carrying loads, known to ancient builders and architects thousands of years before structural theory as defined today. It took, however, many centuries before non-Euclidean geometry would play any significant role in the design, production, or analysis of structures, as will be described in the next section.

2.2 The geometry of the master builder

> Marvel ye not that I said that all sciences live only by the science of Geometry, for there is no artificial or handicraft that is wrought by man's hand but is wrought by Geometry, and a notable cause, for if a man works with his hands he worketh with some manner of tool, and there is no instrument of material things in this world, but it comes of some kind of earth, and to earth it will turn again. And there is no instrument, that is to say a tool to work with, but it hath some proportion more or less, and proportion is measure, and the tool or instrument is earth, and Geometry is said to be the measure of the earth. Wherefore I may say that men live all by Geometry ... Ye shall understand that among all the crafts of the world of man's craft Masonry hath the most notability, and most part of this science of Geometry as it is noted and said in history, and in the Bible, and in the Master of Stories.... (as cited in Yarker, 1909, p. 545)

The above quote is from the Freemasons' ancient charges, believed to be from the 15th century (Yarker, 1909). This text shows that geometry was a valuable tool for architecture and the art of building. Today, it is hard to fathom the difficulties these master builders faced in measuring and setting out such a complex structure as a Gothic cathedral and shaping its stone blocks. Thus, the mason lived and embodied geometry to such an extent that the unknown author states that masonry, in principle, is geometry. Like the Egyptians, the medieval master builder was likely more interested in practical geometry

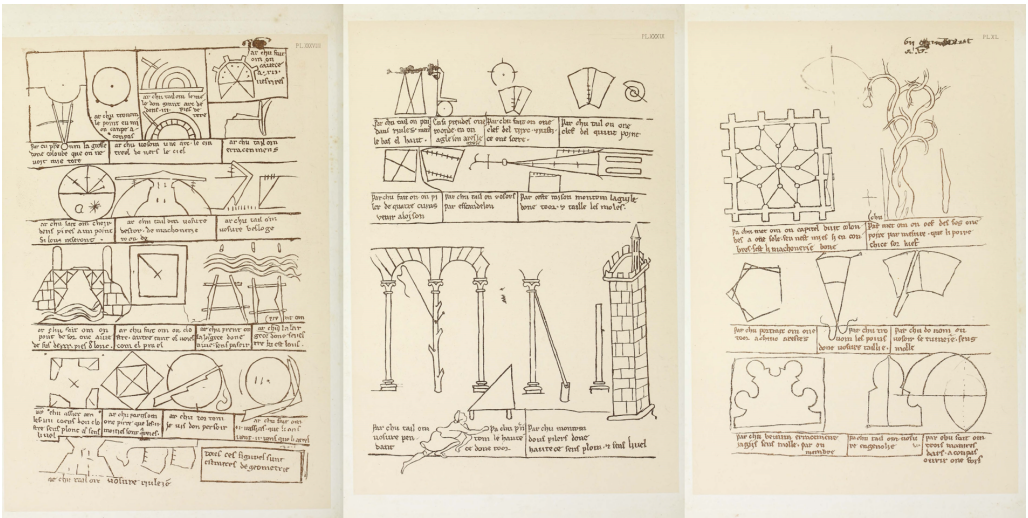

Figure 2.2: *Sketchbook of Villard De Honnecourt (ca. 1230/1859).*

than theoretical geometry. In *The Geometrical Knowledge Of Mediaeval Master Masons* Shelby (1972) describes the profession. Those who aspired to become a master mason probably did not have time to become an academic, possibly they did not even know how to read. As is well known, the early medieval master builders did not have full access to Euclid's geometry, only various fragments that are known to have gathered in the *Codex Arcerianus* from the 6th or 7th century. Their time was likely invested in the more practical school at a construction site, and it was probably through their work or their master that they learned geometry:

> Since the geometry of the masons was an essential part of that technical knowledge, medieval master masons would normally have acquired their geometrical knowledge in the same way that they acquired the rest of their knowledge and skill in building - by mastering the traditions of the craft. (Shelby, 1972, p. 398)

One of the few surviving records of the early medieval masons knowledge and application of geometry is found in the sketchbook of Villard De Honnecourt from the 13th century. Heyman (1995) refer to him as a master builder, but similar to the Roman architect Vitruvius (1914), one of the minor known while active. Villard's book is a practical one as can be seen in Figure 2.2. It gives guidance for geometrical constructions such as: 'How to trace the plan of a five-cornered tower', 'Thus can be drawn three kinds of arches with one opening of the compasses', 'How to find the point in the centre of a circular area', 'How to cut the mold of a great arch in a space of three feet'. During the end of the 15th and beginning of the 16th century handbooks for craftsmen were written, including *Geometria deutsch* (1497) by Matthäus Roritzer and Albrecht Dürer's book *Underweysung der Messung, mit dem Zirckel und Richtscheyt, in Linien, Ebenen unnd*

gantzen corporen (1525). These were written in German instead of Latin, making them more accessible to craftsmen.

Villard's book (ca. 1230/1859) contains elevations and plans but they are not very accurate. However, in Albrecht Dürer's, there are images and instructions on making accurate perspective drawings. The idea of using a vanishing point in linear perspective to represent 3-dimensional spaces and objects on 2-dimensional drawings had been rediscovered by Brunelleschi (1377-1446) around 1415 (Addis, 2007).

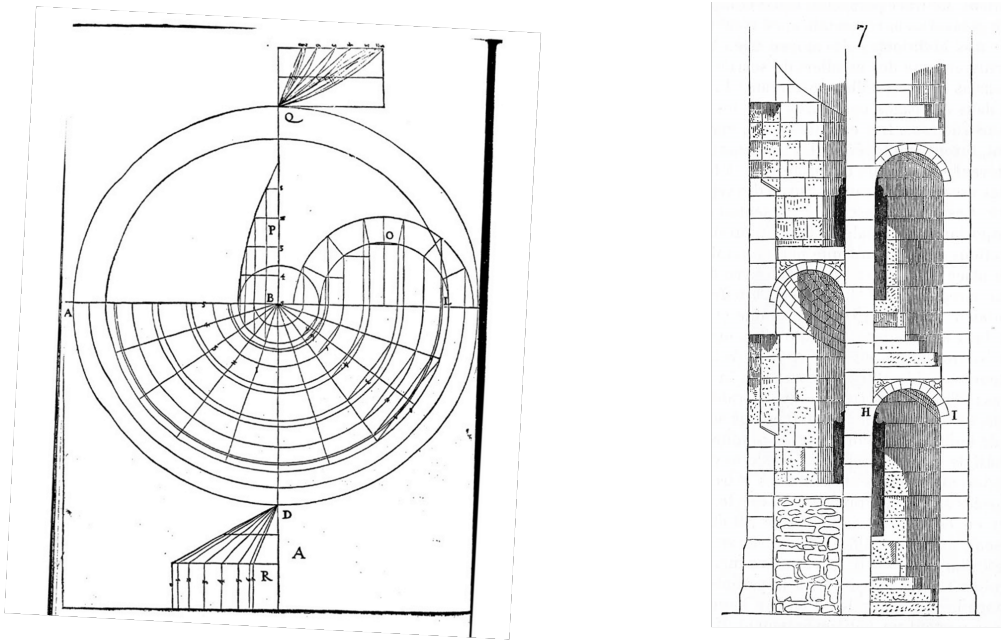

Figure 2.3: *To the left diagram by Philibert de l'Orme of a helical barrel vault (or vis de Saint-Gilles) (Delorme, 1567). Right, Viollet-le-Duc on how such a stair could look like which was typically used in medieval structures in the 11th and 12th-century (Viollet-le-Duc, 1875).*

2.2.1 Stereotomy

The art and geometry of stone cutting, usually referred to as *stereotomy*, was important for designing and constructing vaults and masonry. While there exist some records in the book by Villard (ca. 1230/1859) more advanced treatises in stereotomy include *Le Premier tome de l'Architecture* by Philibert de l'Orme (1567) (Figure 2.3), the architect behind the dome at Château d'Anet. Other important work includes the notebook by Juan de Portor y Castro (Alcaide, 2011) and *Traité de stéréotomie* by Amédée-François Frèzier (1739) (Figure 2.4). Stereotomy is also found in treatises for complex geometries in carpentry (Delataille, 1887), as seen in Figure 2.5. For further information on the history and development of stereotomy, the reader is referred to Calvo-Lopez (2020).

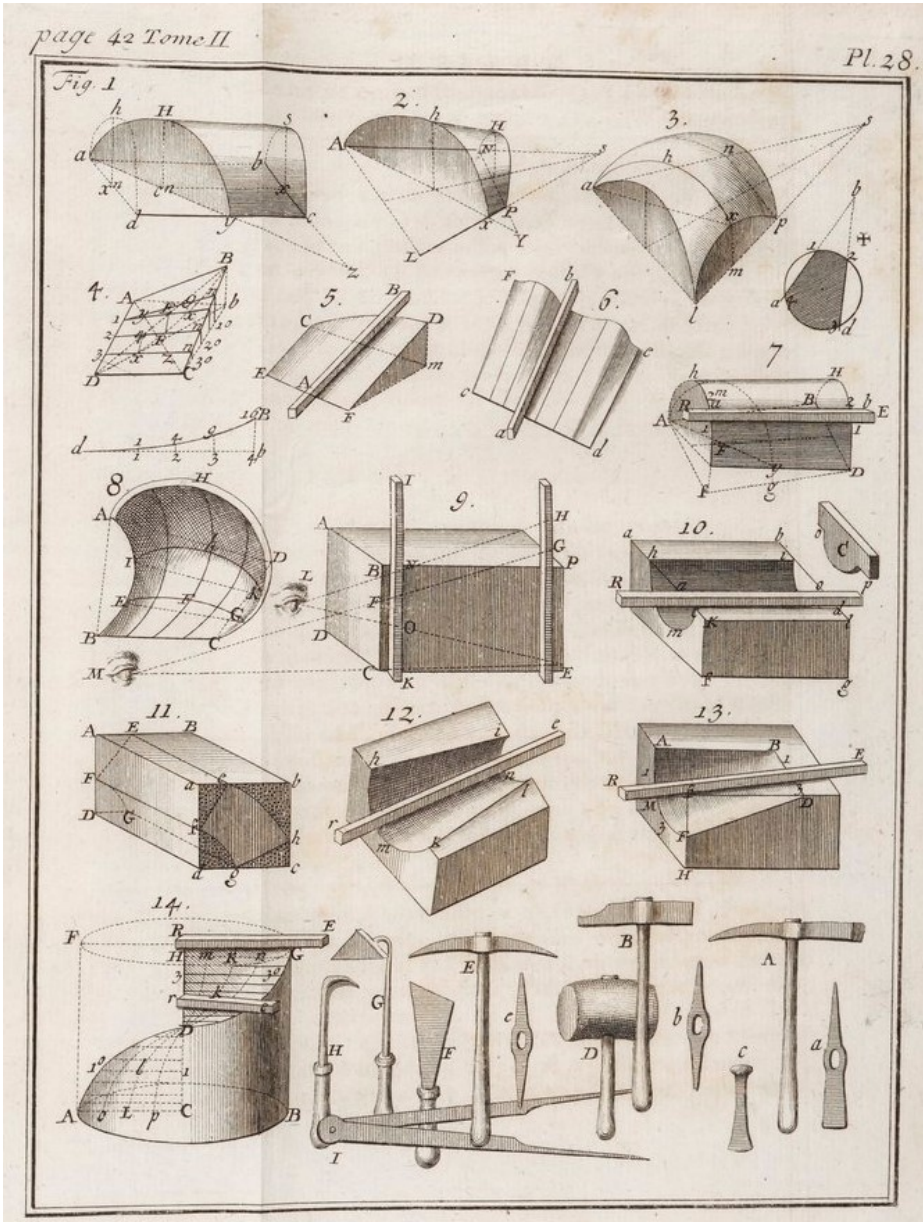

Figure 2.4: *Stereotomy illustraited in Traité de stéréotomie (Frézier, 1739).*

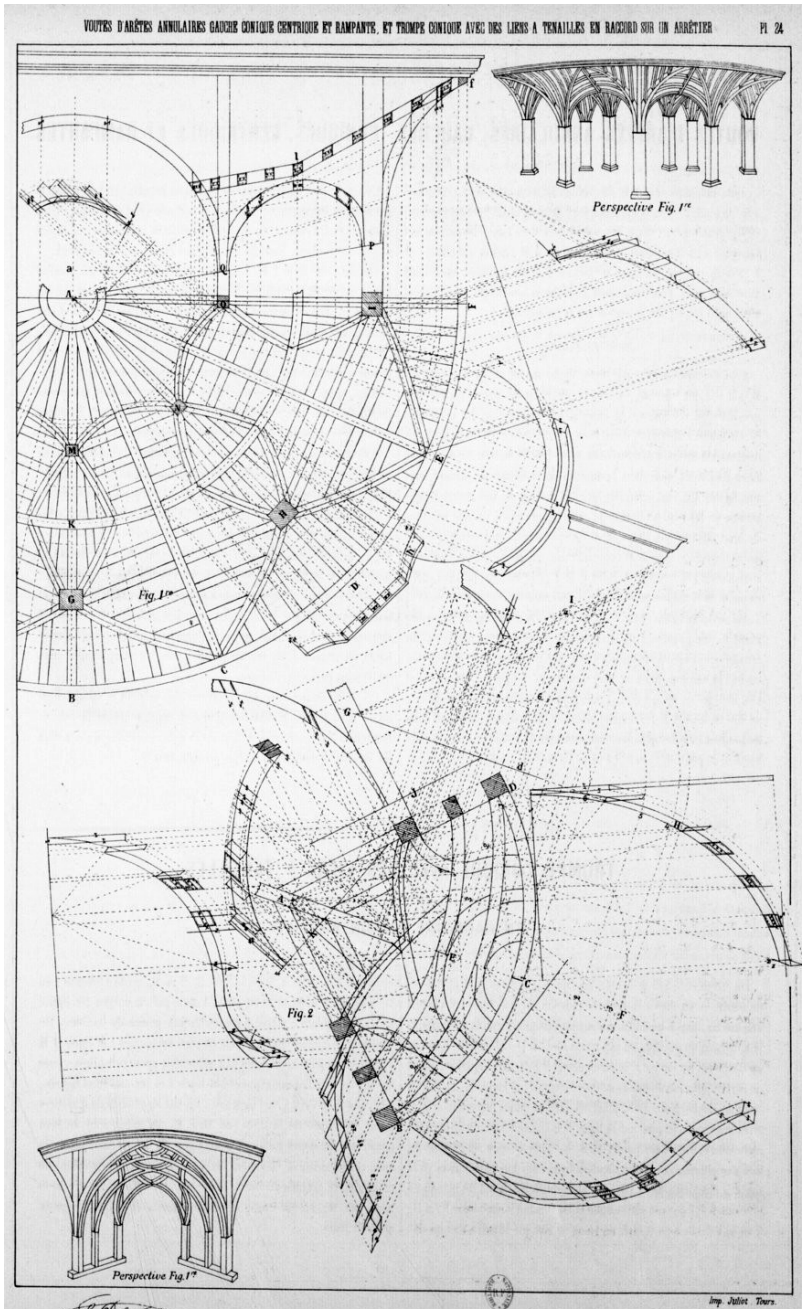

Figure 2.5: *Stereotomy and applied to complex geometries in carpentry (Delataille, 1887).*

Figure 2.6: *Armadillo Vault at the 2016 Venice Biennale. Team: Block Research Group, Ochsendorf DeJong & Block (ODB Engineering) and Escobedo Group.*

The recent emergence of computational tools and digital fabrication techniques has allowed for new opportunities in sterotomy. Fallacara (2016) presents a compilation of recent projects and studies that demonstrate contemporary applications of stereotomy in the design of new masonry structures. The Armadillo Vault (Figure 2.6) is another contemporary example that potentially paves the way for a renaissance of masonry and stereotomy in the digital age.

2.2.2 Geometric rules for structural design

Geometry was also essential in the design to make the structure stable using rules of proportions. Even though no structural theory as we know it existed, the sketches of arches by Leonardo Da Vinci (Addis, 2007; Benvenuto, 1991) and the standing Gothic cathedrals indicate that master builders intuitively understood structural stability and forces. Later sources such as *L'Architecture des voûtes, ou l'Art des traits et coupe des voûtes* by François Derand (1643) contain geometric rules for sizing of abutments based on the form of the arch (Figure 2.7). The reason behind the sizing of abutments and buttresses is that the stresses in masonry structures such as Gothic cathedrals are relatively small in magnitude (Heyman, 1995), and the problem is more related to stability.

Even though the stresses in masonry vaults or arches, in general, are low, the thrust on its supports can be significant. If the abutments fail or collapse due to the thrust, the arch or vault might fall with it. Gothic builders were clever in that sense to add weight on top of the buttresses as a pre-stressing (Addis, 2007). For the dimensional rules of domes, one early source is *Il Tempio Vaticano e sua origine* by Carlo Fontana (1694) (Benvenuto, 1991; Manzanares, 2003).

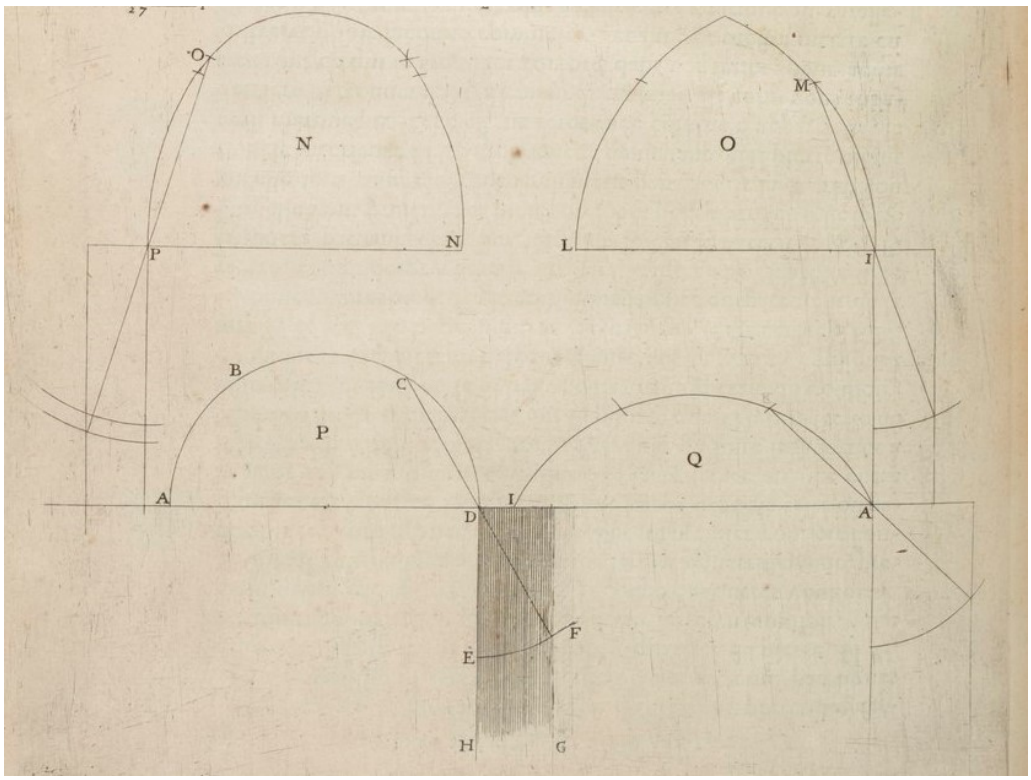

Figure 2.7: *Derand's geometrical rules for the relation between the form of the arch and the width of the abutments (Derand, 1643).*

2.2.3 Graphical analysis

The Spanish and Spanish originating master builders Antoni Gaudí (1852-1926) and Rafeael Guastavino Jr. (1872-1950), used *graphic statics* as a design tool (Collins, 1960; Ochsendorf, 2010). Graphic statics is a method to draw corresponding force diagrams connected to the geometry of the structure (Figure 2.8). Graphic statics originates from the work by Carl Culmann (1866), James Clerk Maxwell (1864) and Luigi Cremona (1872) in the second half of the 19th century. Culmann was inspired by projective geometry,

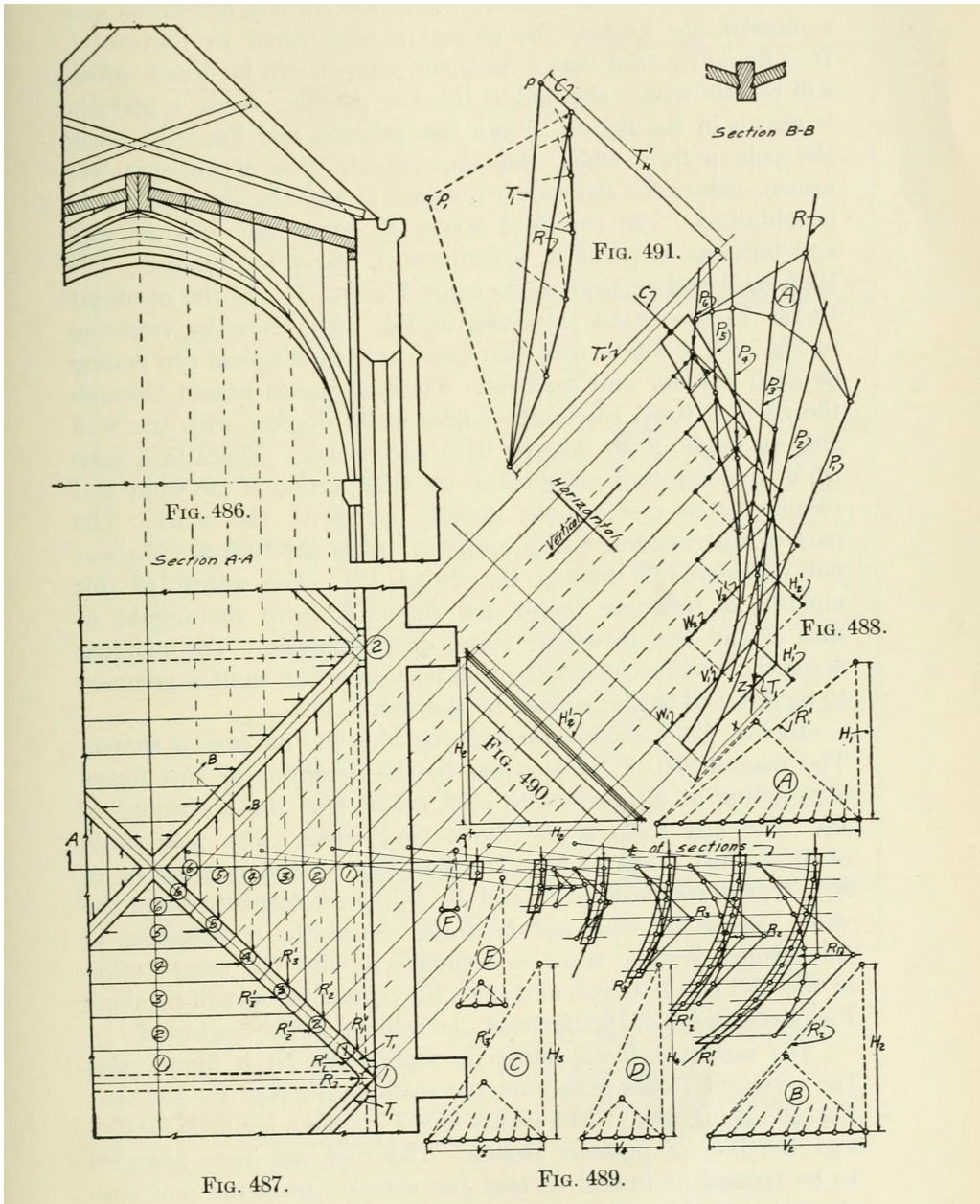

Figure 2.8: *Analysis of a Gothic rib-vault using graphic statics in (Wolfe, 1921).*

what Culmann called *'newer geometry'* (Kurrer, 2008), of Jean-Victor Poncelet's[1] *Traité des propriétés projectives des figures* (Poncelet, 1822). Graphic statics was presented by Culmann as an attempt to *solve the problems accessible to a geometrical treatment from the field of engineering with the help of the newer geometry* (Culmann, 1866).

The use of graphic statics declined in usage during the last half of the 20th century. According to Prof. Philippe Block (personal communication, September 2018), there are several reasons. One is that drafting such diagrams takes time, and it requires skills in drafting. With the development of the theory of elasticity by Navier, it was more convenient and time-efficient for engineers to describe one safe solution by plugging in numbers in a formula. Thus, it comes to the cost of not seeing or describing the wide variety of possible stress states and load paths that inform the designer how to further develop the scheme. However, through new digital tools assisting the time-consuming activity of drawing the diagrams, graphic statics has got a new revival in the 21st century through the work of for instance Allen and Zalewski (2009), Block and Ochsendorf (2007), Williams and McRobie (2016).

To perform modern structural analysis of arches, domes and grid shells, it is convenient with a rigorous theoretical framework for describing and working with the geometry of curves and surfaces. This branch of mathematics is usually called *differential geometry*, which will be covered in the next section.

2.3 Differential geometry

Classical differential geometry is the study of curved lines and surfaces in 3-dimensional Euclidean space. Differential geometry can also be extended to describe geometries of higher dimensions. For instance, in Einstein's general theory of relativity, motions take place along geodesics in space-time.

Differential geometry originates from the development of analytical geometry and differential and integral calculus. Analytical geometry was developed in the 17th century by French mathematicians Fermat and Descartes. The emergence of analytical geometry resulted from a new interest in curves and the mathematical advancement in the theory of equations in the 16th century by Viète (Struik, 1987). This interest in curves was partly based on the texts written by the ancient Greek scholars such as Apollonius and Archimedes and the applications in physics in the field of astronomy, mechanics and optics. The importance of analytical geoemtry, also called Cartesian geometry, is that it 'establishes a correspondence between geometric curves and algebraic equations'(Bix and D'Souza, n.d., Introduction section). Isaac Barrow's *Geometrical Lectures* (1670/1916) is seen as a significant influence for Leibniz and Newton, student of Barrow, in the formulation of the differential and integral calculus, and the fundamental theorem bringing them together. Differential calculus is needed to attain properties such as curvature of geometrical objects, while integral calculus is needed when, for instance, calculating the arc length of a curve.

[1]Poncelet was a pupil of Gaspard Monge (1746-1818). Serving as a military engineer in the Napoleon War, Poncelet was wounded and imprisoned in 1813. During his year in imprisonment, Poncelet had much time to reflect on the teachings of Monge and the study of projective geometry. Poncelet returned to France 1814 and in 1822 he published *Traité des propriétés projectives des figures* (Struik, 1987).

Struik (1988) states that Gaspard Monge and Carl Friedrich Gauss are the founders of the differential geometry of curves and surfaces. Other important contributors to the early development of the theory of differential geometry are Leonard Euler, John Bernoulli, Joseph-Louis Lagrange. Bernoulli showed that curves of shortest distance, geodesics, must only curve in the osculating plane. Euler described the principal curvature lines (Struik, 1988) and Lagrange found the partial differential equations of minimal surfaces (Hyde et al., 1997). One of the big contributions by Gauss was to constitute a framework in which it is possible to work with a globally smooth curved surface (non-Euclidean geometry), which zoomed in on a small area can be locally treated using Euclidean geometry since it is nearly flat (Einstein, 1920). It was also a student of Gauss, Bernhard Riemann (1826-1866), who would later show these concepts for higher dimensions[2], famously indispensable to the general theory of relativity six decades later.

Riemann realised that one of the most important aspects to consider in geometry is how to measure distances. Consider the Cartesian coordinate system, originating from Descartes, and its orthogonal grid in the plane with coordinate axes in x and y. The square distance ds^2 is described using Pythagoras' theorem:

$$ds^2 = dx^2 + dy^2. \tag{2.1}$$

If the coordinates are not orthogonal, the cosine rule needs to be used and (2.1) can be

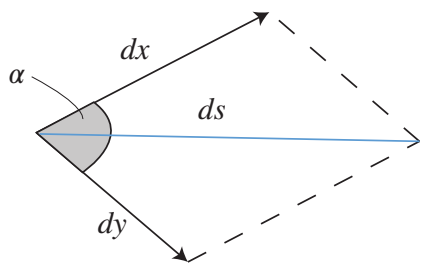

Figure 2.9: *The length of the diagonal of a parallelogram of ds, in which α is the angle between dx and dy.*

rewritten (see Figure 2.9):

$$ds^2 = dx^2 + 2dxdy\cos\alpha + dy^2. \tag{2.2}$$

Consider a net of similar parallelograms as on a smooth two-dimensional surface (Figure 2.10), which can be curved and placed in three-dimensional space, such as the earth. A two-dimensional surface can be locally described by two surface coordinates. Struik

[2]Riemann was to suggest three subjects for the *Habilitation* lecture. Gauss was part of the examination committee, and it was customary to choose the first topic. Gauss, however, chooses the least favourable of Riemann's topics *On the hypotheses that underlie the foundations of geometry*, and Riemann had no choice but to go home and reinvent geometry (Hawking, 2005).

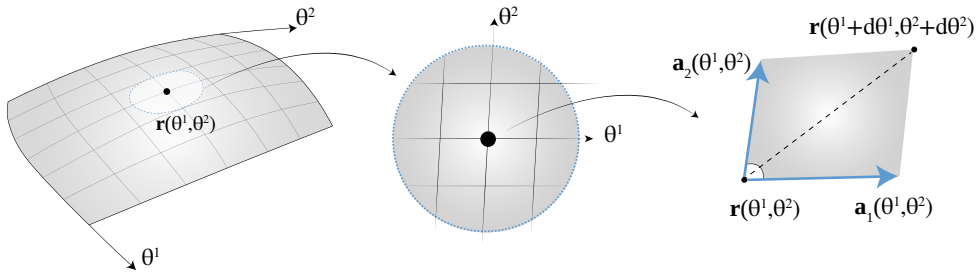

Figure 2.10: *A small region on a curved surface can be interpreted as a flat region where one can apply Euclidean geometry, similar to Figure 2.9.*

(1988) uses u,v to describe these surface parameters, while Green and Zerna (1968) use θ^1, θ^2. Using the latter convention, (2.2) becomes:

$$ds^2 = a_{11}\left(d\theta^1\right)^2 + 2a_{21}\left(d\theta^1\right)\left(d\theta^2\right) + a_{22}\left(d\theta^2\right)^2 \tag{2.3}$$

which gives the square of the distance between the points $\left(\theta^1, \theta^2\right)$ and $\left(\theta^1 + d\theta^1, \theta^2 + d\theta^2\right)$ on the surface. Equation (2.3) is usually referred to as the *first fundamental form* and $a_{\alpha\beta}$ are the components of the *metric tensor*[3]:

$$a_{\alpha\beta} = a_{\beta\alpha} = \mathbf{a}_\alpha \cdot \mathbf{a}_\beta = \begin{bmatrix} a_{11} & a_{12} \\ a_{21} & a_{22} \end{bmatrix} \tag{2.4}$$

The metric tensor is defined as the inner product of the basis vector on the tangent space. Riemann provided a framework for non-Euclidean geometry in higher dimensions for which measuring distances on surfaces or manifolds of higher dimensions would be done in the same manner as (2.3). Thus, for higher dimensions one usually refers to this as the *Riemannian metric*, g_{ij} where $i, j = 1, 2, ..., n$. However, in the general theory of relativity, the metric tensor is not positive-definite (Stoker, 1969).

Tensors[4] describe something real, like measurements of a surface, curvature or stress if it is an elastic surface. Also, the physical properties should be equally true no matter which coordinate system we use to measure it. For instance, transforming the metric tensor in (2.4) to a different coordinate system could be done by

$$\bar{a}_{\alpha\beta} = \frac{\partial\theta^\lambda}{\partial\bar{\theta}^\alpha}\frac{\partial\theta^\mu}{\partial\bar{\theta}^\beta}a_{\lambda\mu}, \tag{2.5}$$

where α, β, μ and λ are dummy indices meaning they are treated as a sum using *Einstein summation convention.*

[3]Struik (1988) uses *E, F, G* instead of a_{11}, a_{12}, a_{22}

[4]The word *tensor* comes from Marcel Grossmann (1878-1936) who introduced Riemannian geometry to Einstein when helping his friend struggling transitioning from special to the general theory of relativity, 'Grossmann, you must help me or else I go crazy!'. Grossmann continued on the work by Gregorio Ricci-Curbastro (1853 - 1925) made accessible through Tullio Levi-Civita (1873 – 1941) in *Méthodes de calcul differéntiel absolu et leurs applications* (Ricci & Levi-Civita, 1900) (eng. The Absolute Differential Calculus (Calculus of Tensors)) (Goodstein, 2018).

The powerful aspect of using tensors is that it enables viewing a quantity or phenomenon from different angles without distorting the entity, which is why tensor analysis is an effective tool combined with differential geometry.

The covariant base vectors $\mathbf{a}_\alpha$ are the vectors tangent to the coordinate curves, the curves on the surface where either θ^1 or θ^2 is constant. They are not necessarily orthogonal to each other but always orthogonal to the normal $\mathbf{a}_3$. Compared to Cartesian coordinates, the surface base vectors change while moving on the surfaces. The covariant base vectors are defined as:

$$\mathbf{a}_\alpha = \frac{\partial \mathbf{r}}{\partial \theta^\alpha} = \frac{\partial x}{\partial \theta^\alpha}\mathbf{i} + \frac{\partial y}{\partial \theta^\alpha}\mathbf{j} + \frac{\partial z}{\partial \theta^\alpha}\mathbf{k} = \mathbf{r}_{,\alpha}\,, \text{for } \alpha = 1, 2, \tag{2.6}$$

where the vector $\mathbf{r}$ is the vector that describes the position in space (Figure 2.11)

$$\mathbf{r}(\theta^1, \theta^2) = x(\theta^1, \theta^2)\mathbf{i} + y(\theta^1, \theta^2)\mathbf{j} + z(\theta^1, \theta^2)\mathbf{k}. \tag{2.7}$$

The square distance ds^2 can now be written in the following way, using Einstein summation

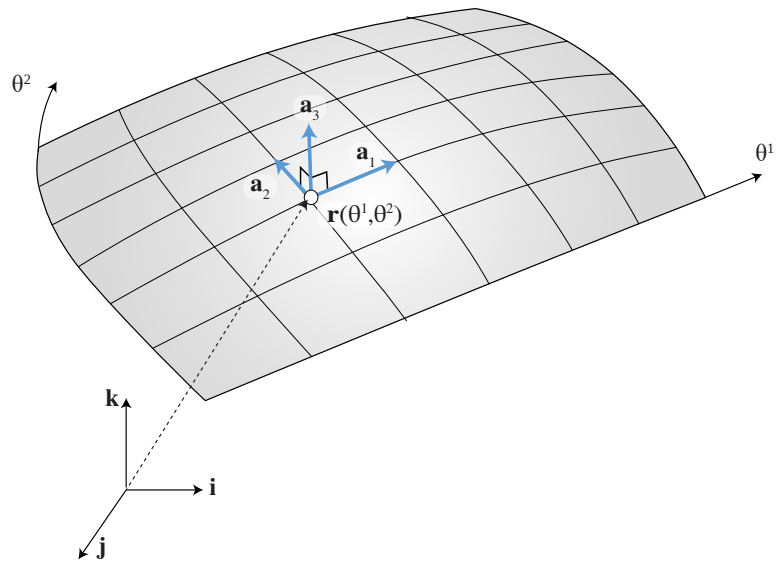

Figure 2.11: *The basis vectors at position* $\mathbf{r}(\theta^1, \theta^2)$ *on the surface.*

.

convention (Green & Zerna, 1968)

$$ds^2 = d\mathbf{r} \cdot d\mathbf{r} = \mathbf{a}_\alpha \cdot \mathbf{a}_\beta d\theta^\alpha d\theta^\beta = a_{\alpha\beta} d\theta^\alpha d\theta^\beta = \sum_{\alpha=1}^{2}\sum_{\beta=1}^{2} a_{\alpha\beta} d\theta^\alpha d\theta^\beta. \tag{2.8}$$

If we want to know the distance s along a curve on the surface $\mathbf{r}\left(\theta^1(t), \theta^2(t)\right)$ it can be expressed as

$$s = \int_{t_0}^{t} \sqrt{\sum_{\alpha=1}^{2}\sum_{\beta=1}^{2} a_{\alpha\beta}\frac{d\theta^{\alpha}}{dt}\frac{d\theta^{\beta}}{dt}}\, dt, \tag{2.9}$$

where the surface parameters are dependent on a curve parameter t.

So far, this section has covered how to measure distances and angles, but how do we measure the surface curvature? Gauss (1825/1827/1902) defines the curvature as the image of the Gauss map, basically taking a small region on the surface and mapping it onto a unit sphere using the normal vectors. The Gaussian curvature, K, is the ratio between the two areas; similar can be done on curves using the unit circle. According to himself, Gauss (1825/1827/1902) found the remarkable connection to the products of the two principal curvatures, κ_1 and κ_2, described earlier by Euler (Euler, 1767; Struik, 1988)

$$K = \kappa_1\kappa_2. \tag{2.10}$$

It is also possible to express the Gaussian curvature in the following form

$$K = \frac{b_{11}b_{22} - (b_{12})^2}{a}, \tag{2.11}$$

where

$$a = a_{11}a_{22} - a_{12}a_{21}, \tag{2.12}$$

and $b_{\alpha\beta}$ are the components of the *second fundamental form*[5], also forming a surface tensor. It is a measure of how much the coordinate curves bend in relation to the normal vector $\mathbf{a}_3$:

$$-d\mathbf{r}\cdot d\mathbf{a}_3 = b_{11}\left(d\theta^1\right)^2 + 2b_{12}d\theta^1 d\theta^2 + b_{22}\left(d\theta^2\right)^2 \tag{2.13}$$

$$b_{\alpha\beta} = b_{\beta\alpha} = \mathbf{a}_3\cdot\mathbf{a}_{\alpha,\beta} = \begin{bmatrix} b_{11} & b_{12} \\ b_{21} & b_{22} \end{bmatrix} \tag{2.14}$$

However, most remarkable Gauss's Theorema Egregium (Latin for 'Remarkable Theorem') proved that the Gaussian curvature is an intrinsic property. Thus, the Gaussian curvature can be expressed only using the components and derivatives of the metric tensor. It means that an ant, living on what it believes to be flatland, can come to the realisation that it lives on a curved surface by measuring distances and angles and calculating its derivatives. These measurements can be done by expressing the Gaussian curvature using the covariant Riemann-Christoffel curvature tensor as eq. 1.13.44 in Green and Zerna (1968)

$$K = \frac{1}{4}\epsilon^{\lambda\alpha}\epsilon^{\beta\gamma}R_{\lambda\alpha\beta\gamma}, \tag{2.15}$$

because the Riemann-Christoffel curvature tensor can be expressed in Christoffel symbols as eq. 11.6 in Dirac (1975)

$$R_{prsi} = \frac{1}{2}\left(g_{pi,rs} - g_{ri,ps} - g_{ps,ri} + g_{rs,pi}\right) + \Gamma_{mpi}\Gamma^m_{rs} - \Gamma_{mps}\Gamma^m_{ri} \tag{2.16}$$

[5]Struik (1988) uses *e,f,g* instead of b_{11}, b_{12}, b_{22}.

where the Christoffel symbmols of the first and second kind are defined in Green and Zerna (1968) as

$$\Gamma_{ijr} = \Gamma_{jir} = \mathbf{g}_r \cdot \mathbf{g}_{i,j} \tag{2.17}$$

$$\Gamma^r_{ij} = \Gamma^r_{ji} = \mathbf{g}^r \cdot \mathbf{g}_{i,j}. \tag{2.18}$$

The components of the psuedo-tensor $\epsilon^{\beta\gamma}$ in (2.15) are

$$\epsilon^{11} = \epsilon^{22} = 0, \quad \epsilon^{12} = -\epsilon^{21} = \frac{1}{\sqrt{a}}, \tag{2.19}$$

and in (2.16) the letter g is used instead of a when describing the metric tensor or base vectors of higher order (2.17) (2.18) as in Dirac (1975) and Green and Zerna (1968). The indices are changed from Greek to Latin letters, as in Green and Zerna (1968) to distinguish between the two-dimensional and the higher order surfaces and (2.8) becomes

$$ds^2 = \mathbf{g}_i \cdot \mathbf{g}_j d\theta^i d\theta^j = g_{ij} d\theta^i d\theta^j = \sum_{i=0}^{n} \sum_{j=0}^{n} g_{ij} d\theta^i d\theta^j. \tag{2.20}$$

For a four-dimensional surface, the Riemann-Christoffel tensor contains 256 components, but due to its symmetry, only 20 components are unique. The geometrical meaning of the Riemann-Christoffel tensor is that it describes the magnitude of the basis vectors' rotation if one parallel transport a vector along a closed loop on a surface. In flatland, the rotation would be zero comparing the start and end vector. Thus, the ant who performed this experiment would return to the starting point but with the vector at a different angle and could conclude that it lives on a curved surface. The Christoffel symbols of the first and second kind can be understood as a measure of the rate of change of the basis vectors (Grøn & Næss, 2011). When using curvilinear coordinates, in comparison to Cartesian coordinates, the base vectors change when moving along the surface. Therefore, in Cartesian coordinates, the Christoffel symbols vanish. For a two-dimensional surface, there are only four components of the Riemann-Christoffel tensor that are not zero, and they have the following relation

$$R_{1212} = -R_{2112} = -R_{1221} = R_{2121} \tag{2.21}$$

and (2.15) becomes

$$K = \frac{R_{1212}}{a}. \tag{2.22}$$

For spherical coordinates, where the coordinate curves cross at right angles, (2.22) can be simplified as in eq. 3-7 in Struik (1988):

$$K = \frac{1}{\sqrt{a_{11}a_{22}}} \left[\frac{\partial}{\partial\theta^1} \left(\frac{1}{\sqrt{a_{11}}} \frac{\partial\sqrt{a_{22}}}{\partial\theta^1} \right) + \frac{\partial}{\partial\theta^2} \left(\frac{1}{\sqrt{a_{22}}} \frac{\partial\sqrt{a_{11}}}{\partial\theta^2} \right) \right] \tag{2.23}$$

From the two surface tensors $a_{\alpha\beta}$ and $b_{\alpha\beta}$, it is tempting to wonder if it is possible to design any surface, and pattern on it, by freely assigning the components of the two tensors. However, this is not possible since in order to make the surface fit together

one needs compatibility equations that relate the lengths, angles and curvature of the surface and its coordinate net (Stoker, 1969), meaning there are some restrictions on the components of $a_{\alpha\beta}$ and $b_{\alpha\beta}$. The first compatibility equation has already been presented in the Gauss equation. The remaining two are the Codazzi or Codazzi–Mainardi equations. Green and Zerna (1968) gives the following definition of the Codazzi equations:

$$\nabla_2 b_{\alpha 1} = \nabla_1 b_{\alpha 2}, \tag{2.24}$$

where ∇_1 and ∇_2 indicates the covariant derivative[6]. Struik (1988) writes them out as

$$b_{11,2} - b_{12,1} = b_{11}\Gamma^1_{12} + b_{12}\left(\Gamma^2_{12} - \Gamma^1_{11}\right) - b_{22}\Gamma^2_{11} \tag{2.25}$$

$$b_{12,2} - b_{22,1} = b_{11}\Gamma^1_{22} + b_{12}\left(\Gamma^2_{22} - \Gamma^1_{12}\right) - b_{22}\Gamma^2_{12} \tag{2.26}$$

Another concept originating from differential geometry that is useful in architecture and engineering is geodesics. Some might have heard about the geodesic domes by Buckminster Fuller (1954). Geodesics are curves on the surface with certain properties. They can be defined in two ways. Either we can define them as the (locally) shortest distance between two points. We can also define them as curves having zero curvature, or vanishing acceleration, in the tangent plane of the surface. A physical interpretation of a geodesic is placing a piece of string on a curved surface while minimising the string length between two fixed points. As a consequence, the acceleration and curvature of the curve will only act in the normal direction of the surface. Using the curvature analogy, it is also possible to construct a geodesic using a piece of tape. Select a starting point and direction, and by applying the tape on the surface with as little wrinkling as possible, the tape will follow a geodesic. With the latter method, the endpoint is unknown, so adding the word locally to the shortest distance in the definition is important.

A geodesic curve can be obtained by taking the second derivative of $\mathbf{r}\left(\theta^1(s), \theta^2(s)\right)$ with respect to the unit speed parameter s, and setting the components in the tangent plane to zero. These considerations lead to the geodesic equation:

$$\frac{d^2\theta^\lambda}{ds^2} + \frac{d\theta^\alpha}{ds}\frac{d\theta^\beta}{ds}\Gamma^\lambda_{\alpha\beta} = 0 \tag{2.27}$$

In flatland, using a Cartesian coordinate system, this is easy to grasp since the Christioffel symbols are zero, leaving

$$\frac{d^2\theta^\lambda}{ds^2} = 0, \tag{2.28}$$

which is only true if it is a straight line. Thus, a geodesic can be seen as the equivalent of a straight line but on a curved surface.

The geodesic equation (2.27) also works in higher dimensions. In the general theory of relativity, motions take place along geodesics in space-time. As Dirac (1975) describes

> We make the physical assumption that the world line of a particle not acted by any force, except gravitational, is a timelike geodesic. This replaces Newton's first law of motion. (p. 15)

[6] Green and Zerna (1968) use $|_\alpha$

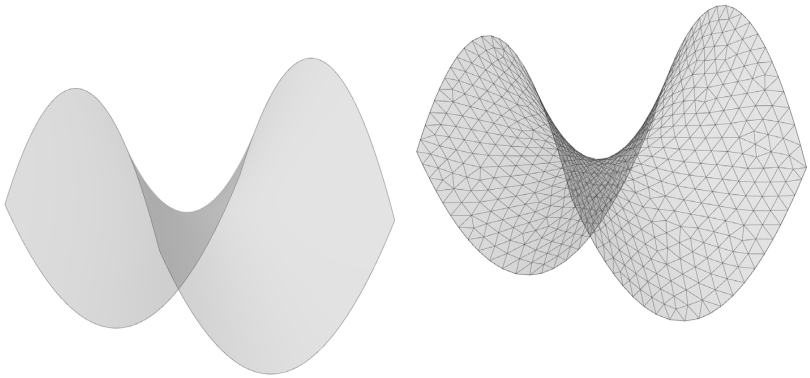

Figure 2.12: *To the left is a smooth version and to the right is a discrete, simplicial surface, approximated from triangles.*

The metric tensor is not positive-definite in general relativity theory, and what *timelike* geodesics means is that the squared distance ds^2 in (2.20) is positive. When the squared distance ds^2 is zero it is a lightlike or null geodesic (Stoker, 1969).

2.3.1 Discrete differential geometry

The classical differential geometry assumes that the difference between $\mathbf{r}(\theta^1, \theta^2)$ and $\mathbf{r}(\theta^1 + d\theta^1, \theta^2 + d\theta^2)$ is very small and that the functions are smooth, meaning that the functions can be differentiated a certain number of times. If this is not the case, the *discrete differential geometry* has to be applied, which is frequently used for geometry processing in computer graphics and architectural geometry.

The advantage of discrete differential geometry is that it is more flexible than classical differential geometry. The disadvantage is that it is not as clear from a theoretical point of view. There are usually several ways to define the discrete counterpart for the theorems described in classical differential geometry. There is no exact translation, and one must evaluate which approach is the most appropriate for each problem. For instance, there are at least four different ways to formulate an equivalent formulation of the curvature of a smooth curve (Crane et al., 2013).

In discrete differential geometry surfaces are discrete versions called *simplicial surfaces* or *simplicial manifolds* (Crane et al., 2013) as seen in Figure 2.12. It consists of a set V of vertices, or points $\mathbf{p}_i$

$$V = \{\mathbf{p}_i, i = 0, 1, 2, ..., n\}. \tag{2.29}$$

To V there are associated subsets, *k-simplices*, describing how the vertices are connected to its neighbouring vertices. A 0-simplex is just a node, while a 1-simplex is an edge and a 2-simplex is a triangle, or mostly called a *face*. Often, one refers to a simplicial surface as a *mesh* in 3D-modelling softwares like *Rhino3d*. There are also meshes consisting

of quadrilateral faces or a combination of quadrilateral or triangular faces[7], but in this section, we describe the theory concerning triangular meshes. The difference between a simplicial surface and a *simplicial complex* is that for a surface they must obey specific rules for its connectivity, meaning the different vertices must not only be associated as k-simplices, but they must also fit together with neighbouring k-simplices geometrically. This is similar to smooth surfaces where the Gauss-Codazzi equations (2.22) and (2.24) make the surface fit together.

The Laplace-Beltrami operator in classical differential geometry is defined as

$$\Delta\phi = \frac{1}{\sqrt{a}}\frac{\partial}{\partial\theta^{\alpha}}\left(\sqrt{a}a^{\alpha\beta}\frac{\partial\phi}{\partial\theta^{\beta}}\right). \tag{2.30}$$

If using Cartesian coordinates[8] it becomes the well-known expression

$$\Delta\phi = \frac{\partial^2\phi}{\left(\partial\theta^1\right)^2} + \frac{\partial^2\phi}{\left(\partial\theta^2\right)^2} = \phi_{,11} + \phi_{,22}. \tag{2.31}$$

The Laplace-Beltrami operator is also connected to the mean curvature vector $H\mathbf{n}$ (Crane et al., 2013) (where $\mathbf{n}$ is the surface normal). Surfaces having zero mean curvature are called *minimal surfaces* and have played a significant role in architecture and engineering in the form finding of fabric structures (see Section 4.1.1). The mean curvature in classical theory is usually expressed using the principal curvatures

$$H = \frac{\kappa_1 + \kappa_2}{2} = \frac{b_{11}a_{22} - 2b_{12}a_{12} + b_{22}a_{11}}{2a}. \tag{2.32}$$

In discrete differential geometry, the Laplace-Beltrami operator applied to coordinate functions x, y, z for point $\mathbf{p}_i$ on the surface (see Figure 2.13) (Hayashi et al., 2021; Meyer et al., 2003) gives

$$\Delta\mathbf{p}_i = \frac{1}{2A_i}\left(\sum_j \frac{1}{2}\left(\cot\gamma_{ij} + \cot\beta_{ij}\right)\right)\left(\mathbf{p}_j - \mathbf{p}_i\right) = 2H\mathbf{n}, \tag{2.33}$$

where the angles γ_{ij} and β_{ij} are defined in Figure 2.13. The equivalent discrete mean curvature H can be calculated from the norm

$$H\left(\mathbf{p}_i\right) = \frac{1}{2}\|\Delta\mathbf{p}_i\|. \tag{2.34}$$

For the same point $\mathbf{p}_i$ on the surface (see Figure 2.13) the equivalent Gaussian curvature could be computed as (Hayashi et al., 2021; Meyer et al., 2003)

$$\int K_i dA_i = 2\pi - \sum_j \alpha_j \tag{2.35}$$

[7]In one sense, the faces can be any polygon, but the issue might be that there is no unique way of representing the face as a local surface since there might not be a unique solution.

[8]In Cartesian coordinates the components of the contravariant metric tensor becomes $a^{11} = a^{22} = 1$ and $a^{12} = a^{21} = 0$, meaning that $a = 1$

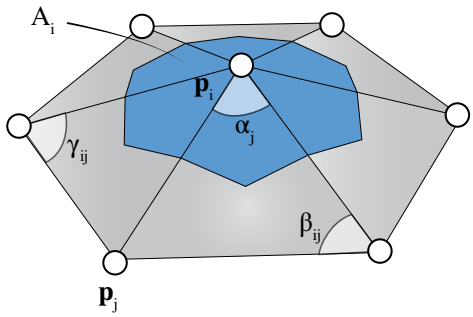

Figure 2.13: *The area and vertices of a vertex are used to calculate the discrete version of the mean and Gaussian curvature.*

$$K_i = \frac{1}{A_i}\left(2\pi - \sum_j \alpha_j\right), \tag{2.36}$$

where A_i is the area of the point or vertex neighborhood at $\mathbf{p}_i$ and α_i are the interior angles at $\mathbf{p}_i$ (see Figure 2.13). The values of the discrete principal curvature can be calculated from

$$\kappa_1(\mathbf{p}_i) = H(\mathbf{p}_i) + \sqrt{(H(\mathbf{p}_i))^2 - K(\mathbf{p}_i)} \tag{2.37}$$

$$\kappa_2(\mathbf{p}_i) = H(\mathbf{p}_i) - \sqrt{(H(\mathbf{p}_i))^2 - K(\mathbf{p}_i)} \tag{2.38}$$

A different approach from the one described above is to approximate a quadratic expression

$$z = ax^2 + 2bxy + cy^2 + fx + gy + h \tag{2.39}$$

for each mesh face, including the vertices from its three neighbouring faces (Crane et al., 2013) (Figure 2.14). Acquiring the constants for the quadratic expression makes it possible to compute different surface properties from classical theory. The best approach will depend on the specific case.

2.3.2 Isotropic differential geometry and projection onto the plane

Before going into the chapter on shell theory, it is worth describing differential geometry in plane coordinates and isotropic differential geometry since both can be advantageous in shell analysis and geometry processing.

Both Green and Zerna (1968, sec. 10.6) and Timoshenko and Woinowsky-Krieger (1959) describe the shell surface in plane coordinates. Green and Zerna describe this more generally and elegantly and let the geometry work, while Timoshenko and Woinowsky-Krieger use Cartesian coordinates, which most engineers are accustomed to. Green and Zerna (1968) refers to the coordinate curves of the surface grid of a middle surface M (the same as in section 2.3) and its plane projection to a plane Π, see Figure 2.15. The position vector in (2.7) can now be expressed as

$$\mathbf{r} = \bar{\mathbf{r}} + z\mathbf{e}_3, \tag{2.40}$$

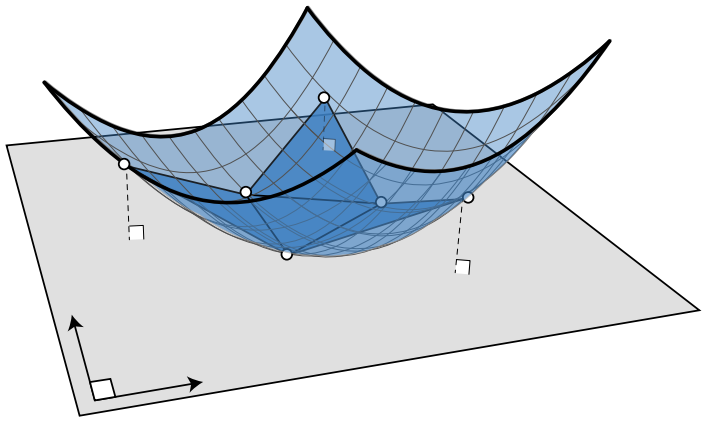

Figure 2.14: *Quadratic approximated from the triangular faces in a mesh.*

where $\mathbf{e}_3$ is the equivalent of the normal $\mathbf{a}_3$ and where $z(\theta^1, \theta^2)$ is

$$z = \mathbf{r} \cdot \mathbf{k}. \tag{2.41}$$

The base vectors of the surface grid on the plane Π can be found in a similar way as on M

$$\mathbf{e}_\alpha = \bar{\mathbf{r}}_{,\alpha}, \tag{2.42}$$

and the components of the first fundamental form on M can be described as

$$a_{\alpha\beta} = \mathbf{e}_\alpha \cdot \mathbf{e}_\beta + z_{,\alpha} z_{,\beta} = e_{\alpha\beta} + z_{,\alpha} z_{,\beta}, \tag{2.43}$$

where $z_{,\alpha} = \mathbf{a}_\alpha \cdot \mathbf{k}$. The components of the second fundamental form on M can be expressed as

$$b_{\alpha\beta} = \sqrt{\frac{e}{a}} \nabla_\alpha \nabla_\beta z, \tag{2.44}$$

where $\nabla_\alpha \nabla_\beta z$ is second covariant derivative and

$$e = e_{11} e_{22} - e_{12}^2, \tag{2.45}$$

which contain the components of the metric tensor in the plane Π defined as

$$e_{\alpha\beta} = e_{\beta\alpha} = \mathbf{e}_\alpha \cdot \mathbf{e}_\beta = \begin{bmatrix} e_{11} & e_{12} \\ e_{21} & e_{22} \end{bmatrix}. \tag{2.46}$$

The formulations so far make it possible to express and transform properties between the actual surface and the plane. However, when using the Airy stress function in shell analysis (see Section 3.2.3), the stresses in the plane coordinates are represented by the *isotropic curvature* of the stress function. The isotropic curvature only corresponds to the actual curvature for shallow surfaces since the distances are only evaluated in the plane as in (2.46). In the same way, the Hessian is only accurate near the peak and the valley

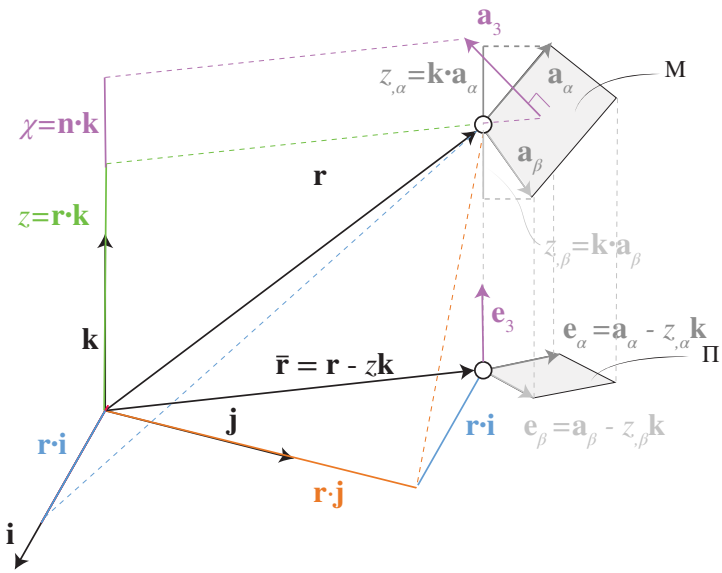

Figure 2.15: *The geometry of a surface element on the middle surface M described in planar coordinates on the plane* Π

of the function. Even so, applications of isotropic differential geometry can also be found in geometry processing of surface patterns of roughly planar panels using the isotropic curvature directions (Tellier et al., 2023).

For simplicity, let's describe our surface using the Cartesian coordinate system such that (2.40) becomes

$$\mathbf{r}(x, y, z) = x\mathbf{i} + y\mathbf{j} + z(x, y)\mathbf{k}, \tag{2.47}$$

as in Pottmann and Liu (2007). In simple terms, the surface properties of *isotropic differential geometry* are evaluated by looking at the surface from the top as if the geometry has been projected on the xy-plane. Thus, the isotropic distance between two points $\mathbf{r}_1(x_1, y_1, z_1)$ and $\mathbf{r}_2(x_2, y_2, z_2)$ is the distance in the xy-plane, removing the z-component

$$ds^i = \| \left((x_1\mathbf{i} + y_1\mathbf{j}) - (x_2\mathbf{i} + y_2\mathbf{j})\right) \|, \tag{2.48}$$

where the superscript i refers to the corresponding isotropic definition.

The isotropic Gaussian curvature can be defined as the determinant of the Hessian matrix of z or the product of its eigenvalues, which are the isotropic principal curvatures κ_1^i κ_2^i

$$K^i = z_{,xx}z_{,yy} - z_{,xy}^2 = \kappa_1^i\kappa_2^i. \tag{2.49}$$

The isotropic mean curvature is the trace of the Hessian matrix

$$H^i = \frac{(z_{,xx} + z_{,yy})}{2} = \frac{\left(\kappa_1^i + \kappa_2^i\right)}{2}. \tag{2.50}$$

The isotropic principal curvature directions are the eigenvectors of the Hessian matrix of z and are orthogonal from the point of view of the top view looking at the xy-plane.

3 Shell theory

This chapter introduces shell theory and some of the different notations used. A general formulation of the equilibrium of forces and moments is shown in Section 3.1. Membrane theory and bending theory of shells are covered in Sections 3.2 and 3.3. The equilibrium equations presented are valid for both thin shells (Kirchhoff-Love theory) and thick shells (Mindlin-Reissner theory). As the possibilities to obtain analytical solutions for shell problems are limited, a brief review of the most common numerical methods is also given in Section 3.4.

A geometric representation of the stress distribution is given through the *Airy stress function* in Section 3.2.3. The membrane stresses are represented by the isotropic curvature (see Section 2.3.2) of the Airy stress function. While the Airy stress function is not commonly used today, likely due to numerical solution techniques, it can be a geometric tool for understanding shell theory and exploring different possible stress states in structural analysis. The Airy stress function is a special case of the *Beltrami stress function*. The Beltrami stress function makes it possible to describe any state of stress in 3D and will be briefly described in Section 3.3.3 in connection to the bending theory of shells.

While this chapter aims to connect different notations in shell theory, it is quite difficult for at least two reasons. Firstly, shell theory is quite a large subject which has been developed from different branches, as Calladine (1982) describes:

> The theory of shell structures is indeed a large subject. It has been actively studied for about 100 yr; and the literature is enormous.
>
> In some large subjects it is possible to discern a main stream of thought, perhaps associated with a succession of dominating personalities. In the field of shell structures there have been, and indeed still are, some dominant figures; but in general they appear to me to be more like the leaders of a collection of schismatic sects than a continuing chain of central authority. The sectarian nature of the subject springs partly from the fact that problems concerning shell structures crop up in many diverse types of engineering practice; and accordingly the stimulus and sponsorship for academic work has come, and still comes, from a wide range of sources. (Calladine, 1982, p. 219)

Secondly, due to the shell's curved surface, shell theory can be difficult to comprehend and performing calculations for structural analysis can be equally challenging. With these two aspects in mind, one can perhaps point out two common approaches used in different shell theory books. The first approach uses tensor notation to formulate general definitions in concise expressions. However, these neat expressions are usually impossible to solve and have little practical use except for theoretical understanding. Thus, the second approach is more applicable to engineering problems but relies on diagrams and specific coordinate systems adapted to specific cases. Flügge (1960) describes this quite well in the commentary of the list of references:

> The following papers use tensor notation and establish sets of basic equations for shells of arbitrary shape...The papers of this group have the merit that

> they provide an extremely general formulation of the theory. However, it is a long way from such general formulations to a solution applicable to a concrete engineering problem. (Flügge, 1960, p. 486)

Thus, this chapter aims to showcase both of these approaches, but we start with a general formulation.

3.1 Equilibrium of forces and moments

The equation for the equilibrium of forces can be written, without any reference to any coordinate system, such that the divergence of the stress tensor $\boldsymbol{\sigma}$ and a body force $\mathbf{p}$ is in balance

$$\mathbf{p} + \nabla \cdot \boldsymbol{\sigma} = 0. \tag{3.1}$$

This is true for membrane shells and shells that can handle bending moments. It is possible to derive this equation. Taking an arbitrary shell body as in Figure 3.1(b), the thickness can vary but is often considered constant. The curve C traced on the shell body is for a homogeneous shell material usually located in the mid-surface of the shell. see Figure 3.1(a). Making a small cut along C (Figure 3.1(a)) at a position $\mathbf{r}$ we can define a vector d$\mathbf{r}$ as from a small increment along the curve C. Integrating through the thickness (the hatched patch in Figure 3.1(a) at d$\mathbf{r}$ we can attain the force $d\mathbf{f}$. The direction of this integration is, to some extent arbitrary, but it is common to use the normal direction. The force $d\mathbf{f}$ is connected to internal stresses tensor $\boldsymbol{\sigma}$ (force per unit length) (Figure 3.2) through the projection on the unit normal upon the outward normal $d\mathbf{r} \times \mathbf{n}$ of the curve C

$$d\mathbf{f} = d\mathbf{r} \times \mathbf{n} \cdot \boldsymbol{\sigma}, \tag{3.2}$$

where, referring to Figure 3.2, $\sigma^{31} = \sigma^{32} = \sigma^{33} = 0$ given by

$$\mathbf{n} \cdot \boldsymbol{\sigma} = 0. \tag{3.3}$$

The total force along the curve is given by taking the curve integral along the curve C

$$\oint_C d\mathbf{f} = \oint_C d\mathbf{r} \times \mathbf{n} \cdot \boldsymbol{\sigma}. \tag{3.4}$$

The divergence theorem states that we can rewrite the curve integral into an area integral as

$$\oint_C d\mathbf{r} \times \mathbf{n} \cdot \boldsymbol{\sigma} = \int_A \nabla \cdot \boldsymbol{\sigma} dA. \tag{3.5}$$

If we have a body load $\mathbf{p}$ per unit area

$$\int_A \mathbf{p} dA \tag{3.6}$$

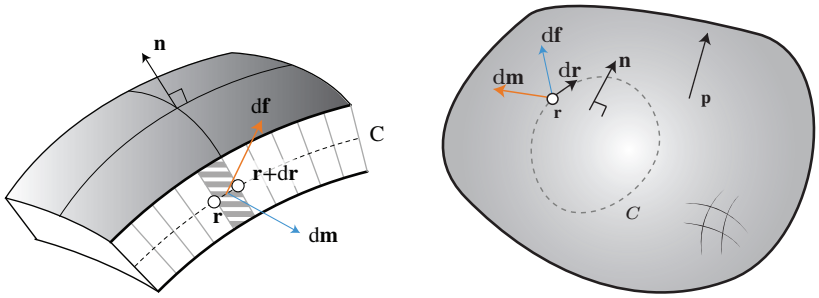

Figure 3.1: (a) *a cut through the shell where the curve C is on the middle surface.* (b) *an arbitrary shell with the arbitrary curve C.*

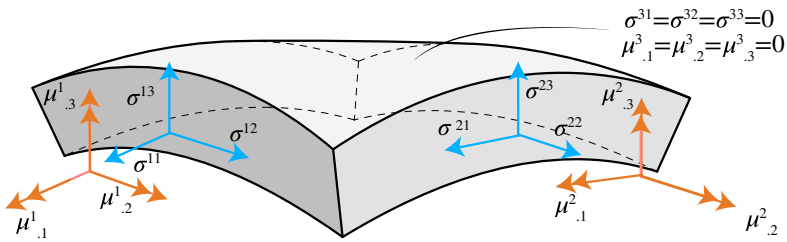

Figure 3.2: *Shell element with the internal stress and moments.*

we can combine the forces and the load

$$\int_A (\mathbf{p} + \nabla \cdot \boldsymbol{\sigma})\, dA \tag{3.7}$$

Thus, reaching the equilibrium of forces in (3.1)

$$\mathbf{p} + \nabla \cdot \boldsymbol{\sigma} = 0. \tag{3.1}$$

For thin and thick shells, the equilibrium of moments must be added to the equilibrium of forces (3.1). Referring to the Figures 3.1 and 3.2, the equilibrium of moments are

$$\mathbf{c} + (\mathbf{r} - \mathbf{o}) \times \mathbf{p} + \nabla \cdot (\boldsymbol{\mu} - \boldsymbol{\sigma} \times (\mathbf{r} - \mathbf{o})) = 0, \tag{3.8}$$

where $\mathbf{c}$ is an applied force couple per unit area, $\boldsymbol{\mu}$ (moment per unit width) are the internal moments and $(\mathbf{r} - \mathbf{o})$ is the lever arm for the internal forces. The moment $d\mathbf{m}$ (Figure 3.1 (a)) can similar to $d\mathbf{f}$, be defined as

$$d\mathbf{m} = (d\mathbf{r} \times \mathbf{n}) \cdot \boldsymbol{\mu}, \tag{3.9}$$

The total moment for the entire curve includes the contribution of the moments from the internal forces taken at $\mathbf{o}$

$$\oint_C (d\mathbf{r} \times \mathbf{n}) \cdot \boldsymbol{\mu} + (\mathbf{r} - \mathbf{o}) \times (d\mathbf{r} \times \mathbf{n}) \cdot \boldsymbol{\sigma}. \tag{3.10}$$

Rearranging (3.10) as

$$\oint_C (d\mathbf{r} \times \mathbf{n}) \cdot (\boldsymbol{\mu} - \boldsymbol{\sigma} \times (\mathbf{r} - \mathbf{o}))\,, \tag{3.11}$$

one can use the divergence theorem to convert the curve integral into an area integral as

$$\oint_C (d\mathbf{r} \times \mathbf{n}) \cdot (\boldsymbol{\mu} - \boldsymbol{\sigma} \times (\mathbf{r} - \mathbf{o})) = \int_A \nabla \cdot (\boldsymbol{\mu} - \boldsymbol{\sigma} \times (\mathbf{r} - \mathbf{o}))\, dA. \tag{3.12}$$

If we have a body load $\mathbf{p}$ per unit area with a lever arm $(\mathbf{r} - \mathbf{o})$ and applied force couple $\mathbf{c}$ per unit area

$$\int_A \mathbf{c} + (\mathbf{r} - \mathbf{o}) \times \mathbf{p}\, dA \tag{3.13}$$

we can combine the external moments with the internal moments

$$\int_A (\mathbf{c} + (\mathbf{r} - \mathbf{o}) \times \mathbf{p} + \nabla \cdot (\boldsymbol{\mu} - \boldsymbol{\sigma} \times (\mathbf{r} - \mathbf{o})))\, dA \tag{3.14}$$

to get the equilibrium of moments in (3.8)

$$\mathbf{c} + (\mathbf{r} - \mathbf{o}) \times \mathbf{p} + \nabla \cdot (\boldsymbol{\mu} - \boldsymbol{\sigma} \times (\mathbf{r} - \mathbf{o})) = 0, \tag{3.8}$$

3.2 Membrane shells

For membrane shells, the internal moments and the transverse shear stresses are neglected. By adding the condition

$$\boldsymbol{\sigma} \cdot \mathbf{n} = 0 \tag{3.15}$$

to (3.3) we assume that all components except $\sigma_{11}, \sigma_{12}, \sigma_{21}$ and σ_{22} to be zero. The equilibrium of forces (3.1) still applies as written. This also means that $\boldsymbol{\mu}$ does not exist, and the shell cannot resist any applied force couples $\mathbf{c}$. Even so, moments around a point $\mathbf{o}$ from the internal forces must still be balanced with the moment from the external load $\mathbf{p}$. Thus, the equilibrium of moments (3.8) must still hold

$$(\mathbf{r} - \mathbf{o}) \times \mathbf{p} = \nabla \cdot \boldsymbol{\sigma} \times (\mathbf{r} - \mathbf{o})\,. \tag{3.16}$$

In the following sections on membrane theory, the equilibrium of forces derived will be expressed using coordinate systems with conventions used in the literature of shell theory.

3.2.1 General membrane theory in curvilinear coordinates

In the previous section, a coordinate-free description of the equilibrium equation was derived. However, one traditionally refers to the cuts along the surface based on some coordinate system on the shell surface. In Green and Zerna (1968) the equilibrium equations for a general membrane element (Figure 3.3) is written:

$$n^{\alpha\beta} b_{\alpha\beta} + p = 0 \tag{3.17}$$

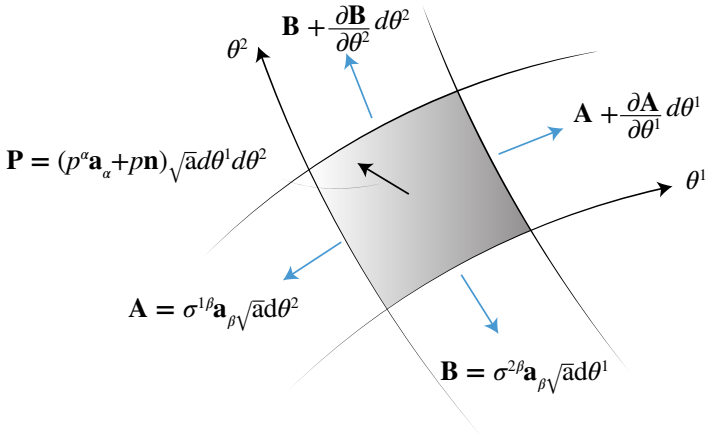

Figure 3.3: *Equilibrium for a general three-dimensional membrane element*

$$\nabla_\alpha n^{\alpha\beta} + p^\beta = 0 \tag{3.18}$$

where $\nabla_\alpha n^{\alpha\beta}$ is the covariant differentiation[1]

$$\nabla_\alpha n^{\alpha\beta} = n^{\alpha\beta}_{,\alpha} + \Gamma^\beta_{\alpha\rho} n^{\alpha\rho} + \Gamma^\alpha_{\alpha\rho} n^{\rho\beta}, \tag{3.19}$$

Remark that (3.18) contains two expressions using the summation convention, describing the equilibrium in the two directions in the plane of the surface. Equation (3.17) refers to the equilibrium in the direction of the normal. The tensor, $n^{\alpha\beta}$, contains the surface stress tensor components of the membrane element and are defined by force per unit length.

$$n^{\alpha\beta} = \begin{bmatrix} n^{11} & n^{12} \\ n^{21} & n^{22} \end{bmatrix}. \tag{3.20}$$

The stress components are connected to $\boldsymbol{\sigma}$ and the force $d\mathbf{f}$ as

$$n^{\alpha\beta} = \sigma^{\alpha\beta}, \text{ for } \alpha, \beta = 1, 2 \tag{3.21}$$

$$d\mathbf{f} = n^{\alpha\beta} \epsilon_{\alpha\lambda} d\theta^\lambda \mathbf{a}_\beta, \tag{3.22}$$

where the components of $\epsilon_{\alpha\lambda}$ are defined as

$$\epsilon_{11} = \epsilon_{22} = 0, \quad \epsilon_{12} = -\epsilon_{21} = \sqrt{a}. \tag{3.23}$$

The load $\mathbf{p} = p\mathbf{n} + p^\alpha \mathbf{a}_\alpha$, is measured in load per unit area. The symbols $\Gamma^\gamma_{\alpha\beta}$ are the Christoffel symbols of the second kind in (2.18). The equilibrium equations, (3.17) and (3.18), are described more in detail in (Adiels, 2016).

[1] Green and Zerna (1968) use $|_\alpha$ and Dirac (1975) $:_\alpha$ for covariant differentiation

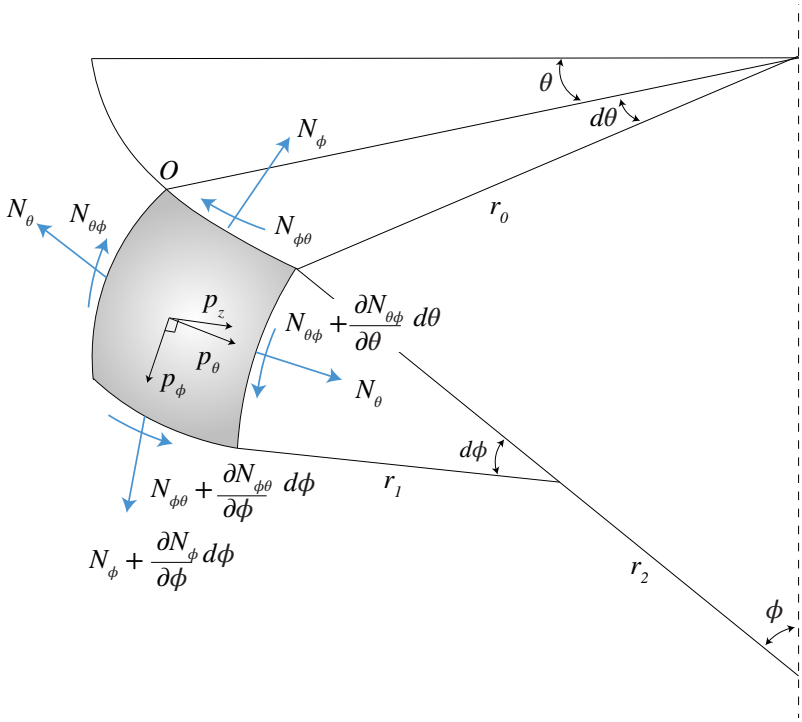

Figure 3.4: *Shell of revolution, redrawn from Billington (1965).*

The equilibrium equations (3.17) and (3.18) are quite difficult to solve. As Williams states, 'Hand calculations for shells are very difficult or impossible. However, some understanding of shell theory will help with the choice of shell shape and interpreting computer and model test results.' (Williams, 2014, p. 31). The most common way of discretising these equations is using the *finite element method*. Other numerical methods include the *finite difference method* and the *discrete element method*. The discrete element method is commonly used for structural analysis of masonry structures, where the structure is modelled as a system of blocks, which can be rigid or undeformable, or particles (Sarhosis et al., 2016). The numerical methods are covered briefly in Section 3.4, while the next section covers how to solve the membrane stresses for analysis of shells of revolution. It is followed by an analytical technique using the Airy stress function (Airy, 1863), which can be used to analyse arbitrary shapes of shells.

3.2.2 Membrane shells of revolution

A common branch of shells linked to traditional shapes applied in architecture and engineering is the shells of revolution. These are shells shaped by a curved profile rotated around a central axis. Thus, special cases of shells of revolution include the dome and the cone. To describe the membrane element ϕ and θ is used as surface parameters, similar to the spherical coordinates as Timoshenko and Woinowsky-Krieger (1959) and

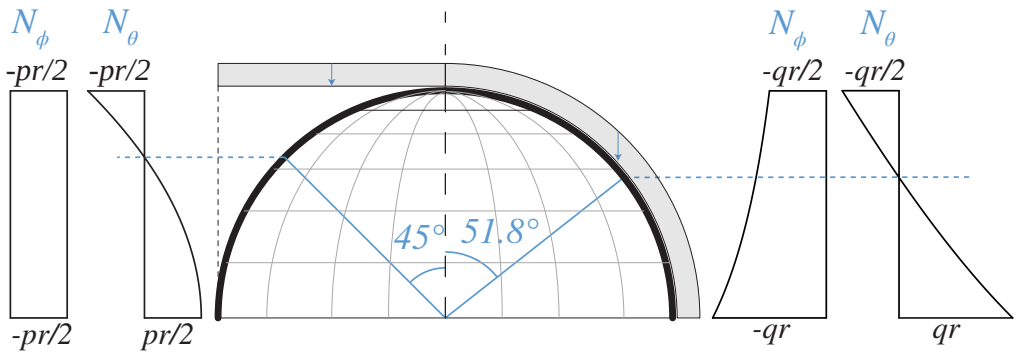

Figure 3.5: *Stresses in a spherical dome. To the left for the projected load and the right for dead weight. The blue lines indicate at what angle the circumferential stress, or hoop stress, changes from compression to tension.*

Billington (1965). Figure 3.4 shows the geometric description of the element where the dotted line on the right is the central axis of rotation. What makes shells of revolution so useful, compared to arches, is the possibility of taking forces in the hoop direction, which is the direction of parallel circles stacked along the central axis or θ direction in Figure 3.4. This is why Pantheon can have a central opening and can also be used as a temporary load path during construction. Under symmetrical loads there exist no shear along any of the coordinate curves (ϕ or θ equals constant). Forces are not applied in the θ direction, which means that the two equations in (3.18) can be reduced to one. It results in the two equilibrium equations for a general shell of revolution under symmetrical load, the first for the normal direction and the second for the ϕ direction (Billington, 1965; S. Timoshenko & Woinowsky-Krieger, 1959). Using the conventions in Billington 1965 those two equilibrium equations are written as:

$$\frac{N_\phi}{r_1} + \frac{N_\theta}{r_2} + p_z = 0 \tag{3.24}$$

$$\frac{d}{d\phi}\left(N_\phi r_0\right) - N_\theta r_1 \cos\phi + p_\phi r_1 r_0 = 0. \tag{3.25}$$

In (3.24) it is clear that stresses are proportional to the curvature, $\kappa = \frac{1}{r}$. For the special case of a spherical dome, r_1 and r_2 are replaced with r

$$\frac{1}{r}\left(N_\phi + N_\theta\right) + p_z = 0 \tag{3.26}$$

$$\frac{d}{d\phi}\left(N_\phi \sin\phi\right) - N_\theta \cos\phi + p_\phi r = 0. \tag{3.27}$$

In the case of a uniform gravity load, it is possible to acquire the stress resultants in (3.26) and (3.27) by solving N_ϕ through its component in the z-direction. Billington (1965) does so for the case dead weight q and for a projected load p, both in load per unit area. The

solutions for both cases are plotted in Figure 3.5. The angle at which the hoop stresses go from compression to tension is indicated, as it is essential for masonry domes that are much sensitive to tension. The results can be compared with the equation $\sigma = \rho r$ for the stresses at the base of the dome used in Section 1.

3.2.3 Airy stress function for analysis of membrane shells

As described in Green and Zerna (1968) it is sometimes useful to have the equilibrium equations projected on the plane surface. If body forces are zero or constant one can reduce the three equations of equilibrium to one differential using a stress function (Airy, 1863; S. P. Timoshenko, 1934). In Green and Zerna (1968) this is described by equation 11.2.11 using ϕ as the stress function:

$$\epsilon^{\alpha\gamma}\epsilon^{\beta\rho}\nabla_\alpha\nabla_\beta z\nabla_\alpha\nabla_\beta\phi = q \tag{3.28}$$

where q contains the loading acting on the shell. The inplane stresses can be obtained from the stress function using equation 7.5.5 in Green and Zerna (1968).

$$n^{\alpha\beta} = \epsilon^{\alpha\gamma}\epsilon^{\beta\rho}\nabla_\gamma\nabla_\rho\phi \tag{3.29}$$

Equation (3.28) contains 16 terms since it has four summation indices. The components of the psuedo-tensor are defined in (2.19). Thus, it is possible to reduce (3.28) to

$$\epsilon^{21}\epsilon^{21}\nabla_2\nabla_2 z\nabla_1\nabla_1\phi + 2\epsilon^{12}\epsilon^{21}\nabla_1\nabla_2 z\nabla_1\nabla_2\phi + \epsilon^{12}\epsilon^{12}\nabla_1\nabla_1 z\nabla_2\nabla_2\phi = q \tag{3.30}$$

Choosing a Cartesian coordinate system, i.e. $\sqrt{a} = 1$, which means (3.30) can be simplified to:

$$z_{,22}\,\phi_{,11} - 2z_{,12}\,\phi_{,12} + z_{,11}\,\phi_{,22} = q \tag{3.31}$$

Equation (3.31) is the same as in Timoshenko and Woinowsky-Krieger (1959, p. 462) and equation (7-8) in Billington (1965), but instead of ϕ they use F

$$\frac{\partial^2 F}{\partial x^2}\frac{\partial^2 z}{\partial y^2} - 2\frac{\partial^2 F}{\partial x\partial y}\frac{\partial^2 z}{\partial x\partial y} + \frac{\partial^2 F}{\partial y^2}\frac{\partial^2 z}{\partial x^2} = q. \tag{3.32}$$

Using Figure 3.6 it is possible to write out the projected in-plane stresses in (3.29) similar to Timoshenko and Goodier (1934)

$$\bar{N}_x = \frac{\partial^2 F}{\partial y^2}, \bar{N}_{xy} = -\frac{\partial^2 F}{\partial x\partial y}, \bar{N}_y = \frac{\partial^2 F}{\partial x^2} \tag{3.33}$$

which is the same as (3.29). The project stresses are represented by the isotropic curvature of the stress function. Specifying the shape, referring to x, y, z in (3.32), it is necessary to find a solution to F such that it satisfies the boundary conditions and equilibrium. As an example, found in Billington (1965) using an elliptical paraboloid, see grey surface in Figure 3.7, which can be described geometrically as (see Figure 3.7),

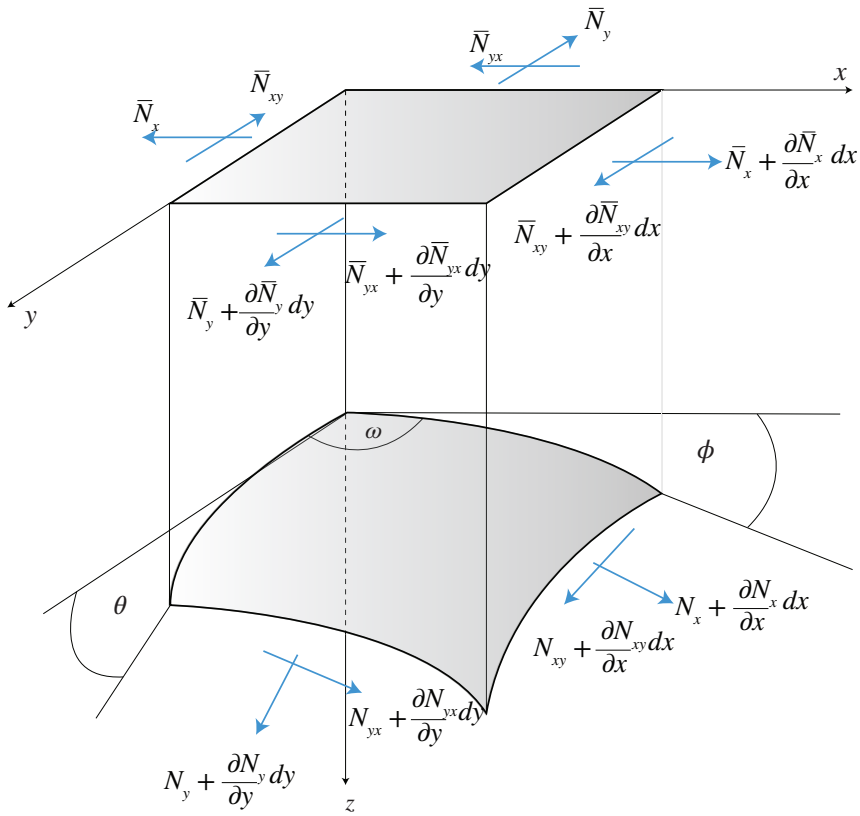

Figure 3.6: *Airy stress function for membrane shells, redrawn from Billington (1965).*

$$z = y^2/h_2 \ + x^2/h_1 \ , h_1 = a^2/c_1 \ , h_2 = b^2/c_2 \tag{3.34}$$

The shell is loaded in the z-direction with a load described by the projected surface area. Several solutions to the stress function F satisfy the boundary conditions. There are two simple solutions in which the load is carried in arch action in either the x- or y-direction, such as

$$F = \frac{1}{4} \bar{p_z} h_1 \left(b^2 - y^2\right). \tag{3.35}$$

However, this is not a very efficient way of using the shell. Timoshenko and Woinowsky-Krieger (1959) and Billington (1965) describe how one could relieve the walls from lateral forces and direct the forces towards the corners, meaning $\bar{N}_x = 0$ at $x = \pm a$ and $\bar{N}_y = 0$ at $y = \pm b$. Since (3.35), which we can call F_0, already fulfils $\bar{N}_y = 0$ at $y = \pm b$, their strategy is to superposition an additional stress function F_1 which does not affect $\bar{N}_y = 0$ but makes $\bar{N}_x = 0$ at $x = \pm a$

$$F = F_0 + F_1 = \frac{1}{4}\bar{p_z}h_1\left(b^2 - y^2\right) + \sum_{n=1,3,5}^{\infty} A_n \cosh\beta x \cos\lambda y, \tag{3.36}$$

where goal is to find a value of A_n fulfilling $\bar{N}_x = 0$. Timoshenko and Woinowsky-Krieger (1959) and Billington (1965) reach the same solution but with slightly different parameters. In Billington (1965) A_n becomes

$$A_n = -\frac{2\bar{p_z}a^2}{c_1\pi n}\frac{1}{\lambda^2}\frac{(-1)^{(n-1)/2}}{\cosh\beta\alpha}, \tag{3.37}$$

where β and λ are defined as

$$\beta = \frac{n\pi}{2a}\sqrt{\frac{c_1}{c_2}}, \lambda = \frac{n\pi}{2b}. \tag{3.38}$$

Even though the solution relieves the walls from lateral forces, it requires the load to be carried by tangential shear along the boundary curves down to the corner support, similar to the umbrella vaults by Candela (Faber, 1963). Thus requiring a stiff edge beam to handle the shear. At the corners, the shear goes to infinity and the stresses in the x- and y-directions vanish, thus requiring some bending moments and transverse shearing forces to balance the load.

Plotting (3.35) and (3.36) with the geometry of the shell, Figure 3.7, it is possible to visualise stress surfaces, similar to the energy and equilibrium surfaces that McRobie (2017) describes poetically

> The structural column that holds the building above your head may be straight, but in the wonderfully imaginative mind of the structural engineer who designed it there live the energy and equilibrium surfaces whose abstract mathematical forms are so sensuously seductive, so beautiful that if they were made solid for you to see them you would want to stroke and caress them. (p. 21)

So far in the presented examples, the geometry or the value of z has been assumed to be fixed while the stresses have been determined by choice of stress functions ϕ. The reverted problem would be to the values of z fulfilling equilibrium when the stress function ϕ is predefined. That is what is generally called *form finding* (Happold & Liddell, 1975), seeking a form that is in equilibrium with the load in a preferable state or stress, usually meaning reducing the amount of bending in favour of the membrane action as described by J. Schlaich and M. Sclaich (2008). More on the topic of form finding is covered later in Chapter 4.

3.2.4 Discrete and discontinuous Airy stress functions

The functions of the Airy stress function in Section 3.2.3 have been considered smooth and continuous for the shell. Williams and McRobie (2016) describe the cases with discontinuous stress functions. One could see the discontinuities as regions of sharp

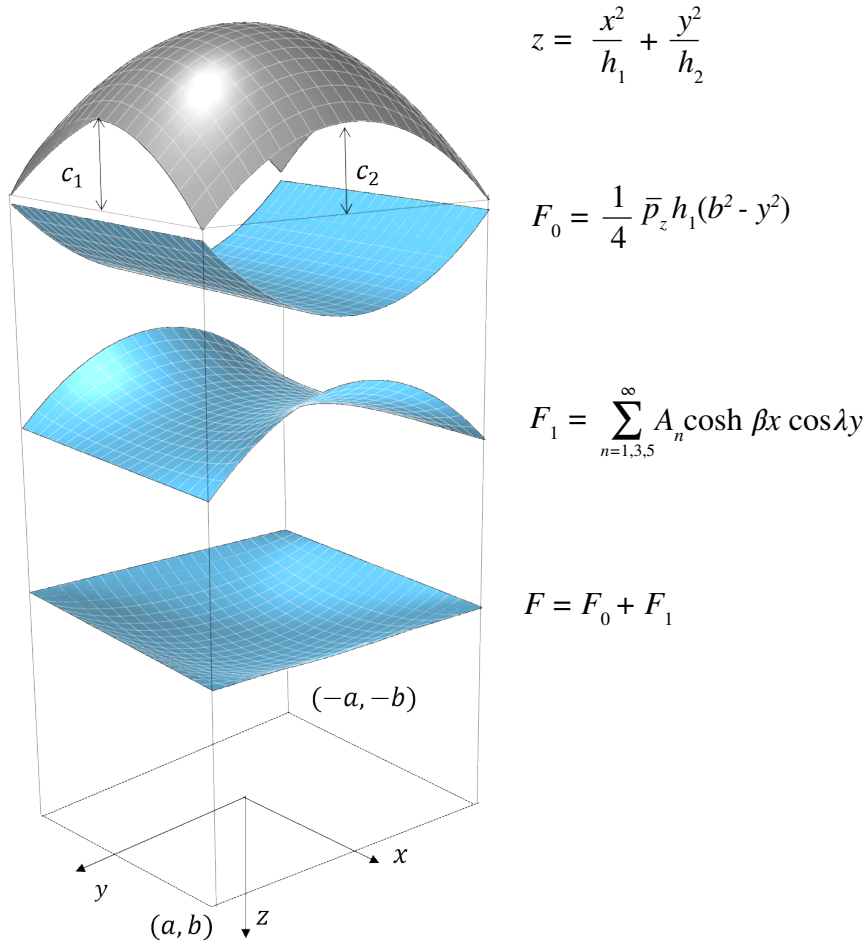

Figure 3.7: *Two solutions for the Airy stress function, blue surfaces, for an elliptical paraboloid shell, in grey.*

curvature increase in the stress function. Thus resulting in contractions of stresses in the discontinuities, similar to the bars or beams in a grid shell.

Williams and McRobie (2016) describe two cases. In the first case, the adjoining stress functions are linear and joined by a smooth function. This can be seen as a discrete or simplicial stress surface having planar faces (Figure 3.8(a)). Since the faces are planar, the face is stress-free and all stresses are concentrated to the edges (the discontinuities). In the second case, the adjoining surfaces are not planar (not stress-free), and thus the bars and beams can be curved. Here the first case will be used, but there are similarities between both cases in that the stresses are found by the discontinuity between two adjoining functions rather than a stress function for the specific region.

For the case of having planar stress functions, Sehlström et al. (2022) describe three

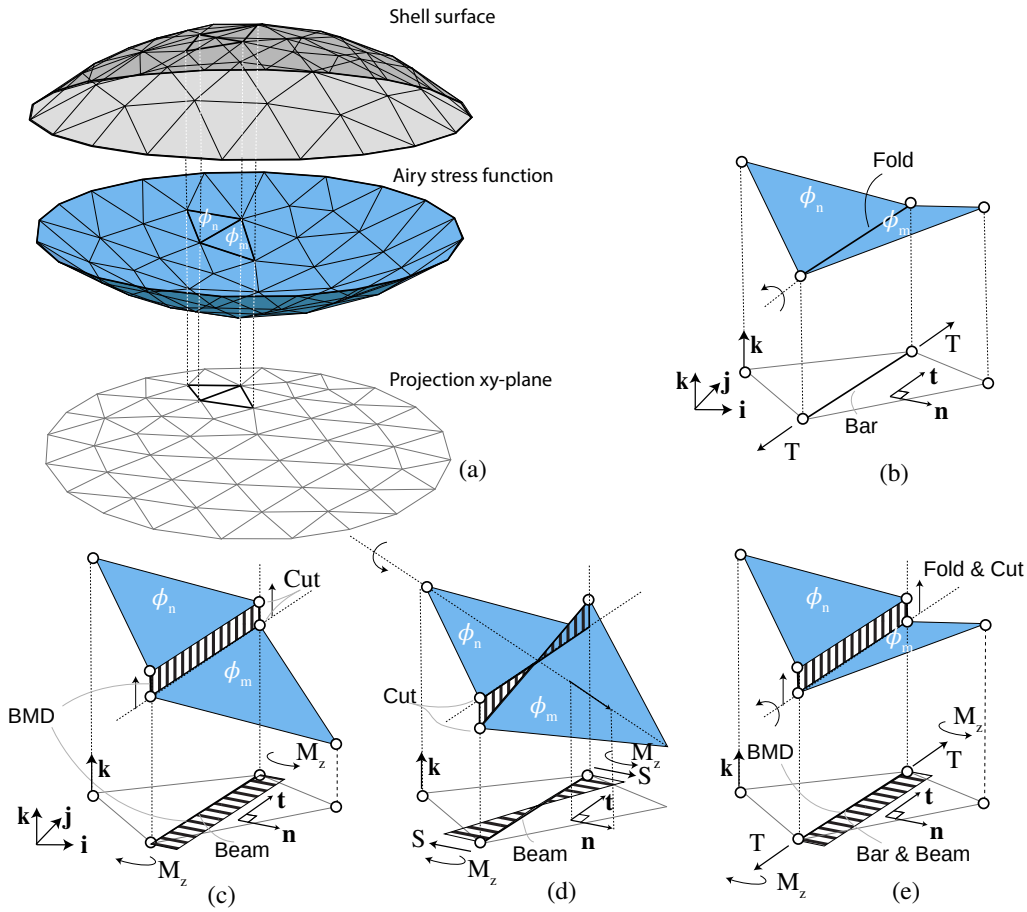

Figure 3.8: *(a) shows a stress discrete Airy stress surface (blue) for a shell geometry (grey) and their projection to the xy-plane. (b)-(e) are different kinds of discontinuities of the stress function. A fold in the Airy stress results in a bar in the xy-plane, of which the force is in tension or compression depending on the fold. (c)-(d) describes two ways a cut in Airy stress functions results in a constant or linear bending moment (BMD) with respect to the vertical axis. In e), the fold and the cut result in a bar and beam in the plane.*

different types of discontinues as (1) folds, (2) cuts and (3) folds and cuts (see Figure 3.8). The folds are two planar panels connected, and the change in the slope of the stress function represents a concentrated force T in tension

$$T = \left(\left(\frac{\partial \phi_m}{\partial x} - \frac{\partial \phi_n}{\partial x} \right) \mathbf{i} + \left(\frac{\partial \phi_m}{\partial y} - \frac{\partial \phi_n}{\partial y} \right) \mathbf{j} \right) \cdot \mathbf{n}, \tag{3.39}$$

where ϕ_m and ϕ_n are stress function patches and $\mathbf{n} = \mathbf{t} \times \mathbf{k}$ (see Figure 3.8(b)). The cut

represents when there is no slope but a height difference. The height difference of the stress function represents a moment in the plan with respect to the z-axis

$$M_z = \phi_n - \phi_m. \tag{3.40}$$

A constant height difference gives a constant moment (Figure 3.8 (c)). The planar panels are allowed to rotate with respect to the axis perpendicular to the edge giving a linear height difference, which results in a linearly varying movement and a constant shear force S (Figure 3.8 (d))

$$S = \left(\left(\frac{\partial \phi_n}{\partial x} - \frac{\partial \phi_m}{\partial x} \right) \mathbf{i} + \left(\frac{\partial \phi_n}{\partial y} - \frac{\partial \phi_m}{\partial y} \right) \mathbf{j} \right) \cdot \mathbf{t}. \tag{3.41}$$

Combining the fold and cut results in both bar and beam action in the plane (Figure 3.8 (e)). However, to describe any state of stress in 3D, it would require something like the *Beltrami stress function* (McRobie & Williams, 2018; Sadd, 2020), (see Section 3.3.3). Thus, this last example serves as a transition to a more rigorous description of shells that can work both through membrane and bending action in the next section.

3.3 Bending theory of shells

The equations for the equilibrium of forces and moments have already been covered in Section 3.1, without taking any reference to a coordinate system. It is important to note that additional conditions used in treating the membrane shells are now reverted. Similarly, as for the membrane shells, the equilibrium equations derived will be connected to the conventions used in established books on shell theory.

3.3.1 Bending theory of shells in curvilinear coordinates

In general curvilinear coordinates, the equilibrium equations for the bending theory of shells are written in Green and Zerna (1968) as

$$b_{\alpha\beta} n^{\alpha\beta} + \nabla_\alpha q^\alpha + p = 0 \tag{3.42}$$

$$\nabla_\alpha n^{\alpha\beta} - b^\beta_\alpha q^\alpha + p^\beta = 0 \tag{3.43}$$

$$\nabla_\alpha m^{\alpha\beta} - q^\beta + \tilde{p}^\beta = 0 \tag{3.44}$$

$$\epsilon_{\lambda\beta} n^{\lambda\beta} - \epsilon_{\lambda\beta} m^{\alpha\beta} b^\lambda_\alpha = 0, \tag{3.45}$$

where they assume that $m^{12} = m^{21}$.

Equation (3.42) is similar to (3.17), with the addition of the contribution of shear forces q^α. For the in-plane equilibrium equations (3.43), one must take into account that the curvature of the shell causes a component shear forces to appear in the plane, similar to out-of-plane components of the axial and shear stress in (3.42). The mixed surface tensor in (3.43) is defined as

$$b^\alpha_\beta = -\mathbf{a}^\alpha \cdot \mathbf{n}_{,\beta} = \mathbf{n} \cdot \mathbf{a}^\alpha_{,\beta}, \tag{3.46}$$

describing the change of the normal with respect to the contravariant base vectors.

Equation (3.8) is the same as (3.44) and (3.45), where (3.44) says that the moment divergence is equal to the negative shear forces. Neglecting the applied force couple $\tilde{p}^{\beta}$ it has the same meaning as equations 99 (b-c) in Timoshenko and Woinowsky-Krieger (1959), which looks rather strange due to the unorthodox definition of the twisting moment.

$$\frac{\partial M_{yx}}{\partial y} + \frac{\partial M_{xx}}{\partial x} - Q_x = 0$$
$$\frac{\partial M_{xy}}{\partial x} - \frac{\partial M_{yy}}{\partial y} + Q_y = 0$$

Like most books, Green and Zerna (1968) define the shell's moments to be similar to those in plate theory. The internal moments $\mu^{\alpha}_{.\beta}$ and $m^{\alpha\lambda}$ in Green and Zerna (1968) are related as

$$\boldsymbol{\mu} = \mathbf{m} \times \mathbf{n} \tag{3.47}$$
$$\mu^{\alpha}_{.\beta} = m^{\alpha\lambda}\epsilon_{\beta\lambda} \tag{3.48}$$
$$\mu^{\alpha}_{.\beta}\mathbf{a}_{\alpha}\mathbf{a}^{\beta} = m^{\alpha\lambda}\mathbf{a}_{\alpha}\mathbf{a}_{\lambda} \times \mathbf{n}. \tag{3.49}$$

Figure 3.9: *The British Museum Great Court roof by Foster and Partners, Buro Happold and Waagner Biro.*

3.3.2 Stretching and bending surfaces

In structural analyses, it is common to refer to *statically determinate* and *statically indeterminate* structures. In statically determinate structures, the sectional forces can be solved using statics alone. In statically indeterminate structures, the equations of statics are insufficient to determine sectional forces and knowledge about the material and cross-sectional properties and the rigidity of the supports are required for the solution.

For the shell element described in Figure 3.2, there are 12 unknown components, whereas the equilibrium of forces and moments are only 6 in total. Thus, most shells are statically indeterminate, meaning that there are different possible ways for the structure to carry the load. Unless you have a membrane shell, assuming $\sigma_{12} = \sigma_{21}$, and where the boundary conditions allow a statically determinate solution.

One could argue that a shell or a grid shell should work as much as possible through membrane action for the dominant load case and use bending capacity to handle other load cases and prevent buckling (the more efficient the shell becomes, the more likely it is to suffer from buckling). However, in some cases, this is not possible, as shown in the example of the elliptical paraboloid shell in Secion 3.2.3 where the shear forces go to infinity in the corners, requiring bending and transverse shear to balance the load. Another example is the British Museum Great Court roof (Figure 3.9), where roller supports along the perimeter require forces to go towards the stiffer corners, thus making it difficult to find a shape in equilibrium with the load using membrane action alone.

Calladine (1977, 1983) presents a geometric interpretation of the static–geometric analogy for *shallow shells* for such cases where he splits the shell into what he calls a stretching surface (S-surface) and a bending surface (B-surface). The S-surface contains stress resultants N_x, N_y and N_{xy}, assuming $N_{xy} = N_{yx}$. The B-surface contains the stress resultants Q_x, Q_y, M_x, M_y and M_{xy}, assuming $M_{xy} = M_{yx}$. The B-surface cannot handle in-plane forces, Calladine describes its behaviour using a model for a beam seen in Figure 3.11. However, the in-plane load q_{xB} and q_{yB} are needed due to in-plane component of the shear force Q_x and Q_y due to curvature, as in (3.43). Calladine assumes the edges follow the principal curvature directions in Figure 3.10 follows the x- and y-direction in a Cartesian coordinate system.

The S-surface and B-surface are coupled through an interface stress or pressure, p_b. Where the load p is defined as $p = p_s + p_b$. The distortions of the surfaces are also coupled through

$$g_s = g_b \tag{3.50}$$

$$\frac{\partial^2 \epsilon_y}{\partial x^2} - \frac{\partial^2 \gamma_{xy}}{\partial x \partial y} + \frac{\partial^2 \epsilon_x}{\partial y^2} = \frac{\kappa_y}{R_1} + \frac{\kappa_x}{R_2}. \tag{3.51}$$

Calladine perhaps illustrates the analogy best when he arranges the equations for the two surfaces in two columns

$$\frac{N_x}{R_1} + \frac{N_y}{R_2} = p_s \quad \text{(S1)} \qquad\qquad \frac{\kappa_y}{R_1} + \frac{\kappa_x}{R_2} = g_b \quad \text{(B1)}$$

$$\left.\begin{aligned} \partial N_x/\partial x + \partial N_{xy}/\partial y &= 0 \\ \partial N_y/\partial y + \partial N_{xy}/\partial x &= 0 \end{aligned}\right\} \quad \text{(S2)} \qquad\qquad \left.\begin{aligned} \tfrac{\partial \kappa_y}{\partial x} - \tfrac{\partial \kappa_{xy}}{\partial y} &= 0 \\ \tfrac{\partial \kappa_x}{\partial y} - \tfrac{\partial \kappa_{xy}}{\partial x} &= 0 \end{aligned}\right\} \quad \text{(B2)}$$

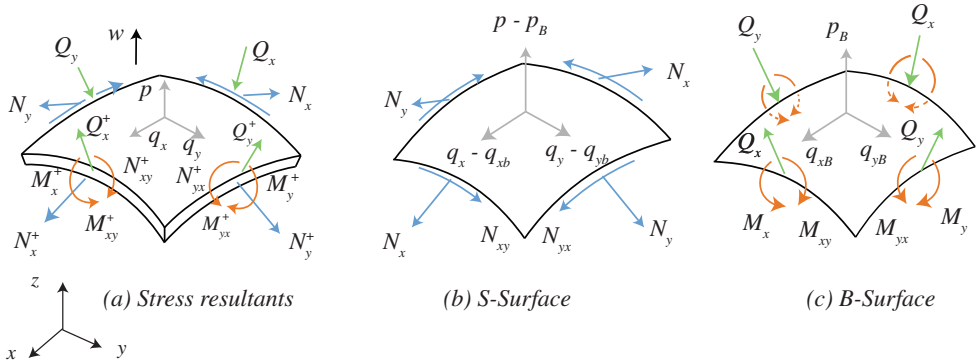

Figure 3.10: *Shallow shell element redrawn from Calladine (1983).*

$$\left.\begin{aligned} N_y &= \frac{\partial^2\phi}{\partial x^2} \\ N_{xy} &= -\frac{\partial^2\phi}{\partial x\partial y} \\ N_x &= \frac{\partial^2\phi}{\partial y^2} \end{aligned}\right\} \quad \text{(S3)} \qquad \left.\begin{aligned} \kappa_x &= -\frac{\partial^2 w}{\partial x^2} \\ \kappa_{xy} &= -\frac{\partial^2 w}{\partial x\partial y} \\ \kappa_y &= -\frac{\partial^2 w}{\partial y^2} \end{aligned}\right\} \quad \text{(B3)}$$

$$\frac{\partial^2\epsilon_y}{\partial x^2} - \frac{\partial^2\gamma_{xy}}{\partial x\partial y} + \frac{\partial^2\epsilon_x}{\partial y^2} = -g_s \quad \text{(S4)} \qquad \frac{\partial^2 M_x}{\partial x^2} + 2\frac{\partial^2 M_{xy}}{\partial x\partial y} + \frac{\partial^2 M_y}{\partial y^2} = -p_b \quad \text{(B4)}$$

$$\left.\begin{aligned} \epsilon_x &= (N_x - \nu N_y)/Et \\ \epsilon_y &= (N_y - \nu N_y)/Et \\ \gamma_{xy} &= 2(1+\nu)N_{xy}/Et \end{aligned}\right\} \quad \text{(S5)} \qquad \left.\begin{aligned} M_y &= D(\kappa_y + \nu\kappa_x) \\ M_x &= D(\kappa_x + \nu\kappa_y) \\ M_{xy} &= D(1-\nu)\kappa_{xy} \end{aligned}\right\} \quad \text{(B5)}$$

where ϕ is the Airy stress function, w is the normal component of displacement and $D = Et^3/12(1-\nu^2)$ being the bending stiffness. The variables are connected in the analogy as follows

$$\begin{aligned} N_x &\leftrightarrow \kappa_y & \epsilon_x &\leftrightarrow M_y & \phi &\leftrightarrow -w \\ N_y &\leftrightarrow \kappa_x & \epsilon_y &\leftrightarrow M_x & g_s &\leftrightarrow p_b \\ N_{xy} &\leftrightarrow -\kappa_{xy} & \gamma_{xy} &\leftrightarrow -2M_{xy} & p_s &\leftrightarrow g_b. \end{aligned}$$

Returning to the initial discussion of trying to work as much as possible through membrane action. Using the analogy of Calladine, we could instead say that the designer should aim to design his or her shell such that it works as little as possible with the B-surface. Having $p_b = 0$ means that the shell works only through the S-surface, which is equal to a membrane shell.

3.3.3 Beltrami stress functions

In Section 3.2.3, it was described how the Airy stress function could describe different stress distributions in a membrane shell and in Section 3.2.4, it was shown how shear forces

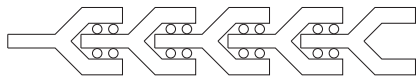

Figure 3.11: *A straight beam illustration describing the physical characteristics of the B-surface, being unable to work through membrane action. Redrawn from Calladine (1983).*

and moments in plan can be represented as discontinuities of the Airy stress function. This limitation could be overcome using several stress functions formulated by the *Beltrami stress function* $\mathbf{\Psi}$, which is a second-order tensor with nine components through which one could describe any state of stress in 3D (McRobie & Williams, 2018). The components of the stress tensor are defined as

$$\sigma^{ij} = \epsilon^{imp}\epsilon^{jkl}\nabla_p\nabla_l\,\Psi_{mk}, \tag{3.52}$$

where the ϵ is the Levi-Civita tensor.

Two common representations of the Beltrami stress function are the *Maxwell stress function representation* and *Morrera stress function representation* (Sadd, 2020). In the former, all components except Ψ_{11}, Ψ_{22} and Ψ_{33} are zero, thus the stresses are

$$\begin{aligned}
\sigma^{11} &= \nabla_2\nabla_2\,\Psi_{33} + \nabla_3\nabla_3\,\Psi_{22}\\
\sigma^{22} &= \nabla_3\nabla_3\,\Psi_{11} + \nabla_1\nabla_1\,\Psi_{33}\\
\sigma^{33} &= \nabla_1\nabla_1\,\Psi_{22} + \nabla_2\nabla_2\,\Psi_{11}\\
\sigma^{12} &= -\nabla_1\nabla_2\,\Psi_{33}\\
\sigma^{23} &= -\nabla_2\nabla_3\,\Psi_{11}\\
\sigma^{31} &= -\nabla_3\nabla_1\,\Psi_{22}.
\end{aligned} \tag{3.53}$$

The Airy stress function is a special case of the Maxwell stress function where $\Psi_{33} = \phi(x, y)$ and all other entries are zero. In the Morrera stress function representation Ψ_{11}, Ψ_{22} and Ψ_{33} are zero, thus the stresses are

$$\begin{aligned}
\sigma^{11} &= -2\nabla_2\nabla_3\,\Psi_{23}\\
\sigma^{22} &= -2\nabla_3\nabla_1\,\Psi_{31}\\
\sigma^{33} &= -2\nabla_1\nabla_2\,\Psi_{12}\\
\sigma^{12} &= -\nabla_3\nabla_3\,\Psi_{21} + \nabla_3\nabla_1\,\Psi_{23} + \nabla_2\nabla_3\,\Psi_{31}\\
\sigma^{23} &= -\nabla_1\nabla_1\,\Psi_{32} + \nabla_1\nabla_2\,\Psi_{31} + \nabla_3\nabla_1\,\Psi_{12}\\
\sigma^{31} &= -\nabla_2\nabla_2\,\Psi_{13} + \nabla_2\nabla_3\,\Psi_{12} + \nabla_1\nabla_2\,\Psi_{23}.
\end{aligned} \tag{3.54}$$

There is a point where some of these concepts of stress functions or graphic statics can go from helping understanding to becoming quite complicated to imagine. Thus, some might find it more convenient to use numerical analysis methods, which will be covered shortly in the next section.

3.4 Numerical methods for shell analysis

The two most common numerical techniques to solve the partial differential equations associated with plates and shells are *finite difference method* and the *finite element method*. The finite difference method takes its starting point from the differential equation (3.1), while the finite element method originates from the differential equation expressed in integral form.

3.4.1 Finite difference method

The history of the calculus of finite differences goes back to the birth of differential calculus, and one of the earliest accounts is by Brook Taylor (1685-1731) in *Methodus Incrementorum Directa et Inversa* (eng. Direct and Indirect Methods of Incrementation)(1715). The finite difference method is in the simplest sense rather easy, having a square or rectangular grid, thus suitable for solving for the bending of plates. Timoshenko and Woinowsky-Krieger (1959) show the well-known scheme for representing the process of obtaining the approximated partial derivatives, and in sec. 83, they apply it on a simply supported plate. The method can similarly be applied to simple shapes of shells, such as shells of revolution as done by Edmondson (1970) and Nodargi et al. (2022). More elaborate shapes or coordinates will introduce difficulties in the interpolation between the points.

3.4.2 Finite element method

The finite element method is the dominant numerical method in structural analysis today. Depending on what field you come from, the origin might be considered different. According to Oden (1987), most mathematicians refer to the appendix of the paper *Variational methods for the solution of problems of equilibrium and vibrations* (Courant, 1943). However, engineers might attribute the origins to the work of John Argyris (1913–2004), who developed the matrix displacement method for aircraft design during World War II (Tenek & Argyris, 1998). Further development was done in the aircraft industry by Turner et al. (1956) at Boeing, where the co-author Ray William Clough (1920-2016) later in 1960 gave the numerical technique its current name in the paper *The Finite Element Method in Plane Stress Analysis*. The finite element method gained in popularity with textbooks such as Zienkiewicz and Cheung (1967) during the 1960s and 1970s (Oden, 1987), followed by the two-volume series by Zienkiewicz and Taylor (1987, 1991).

According to Ottosen and Petersson (1992) there are four basic steps in the finite element formulation:

1. Establish the strong form of the problem
2. Obtain the weak form of the problem
3. Make an elementwise approximation over the entire boundary of the unknown function.
4. Choose the weight function in accordance with the Galerkin method.

The strong form is here represented by the differential equation in Section 3.1 as

$$\mathbf{p} + \nabla \cdot \boldsymbol{\sigma} = 0. \tag{3.1}$$

This equation is valid both in 3D and for a membrane shell. By use of the Green-Gauss Theorem, a virtual increment of displacement $\delta\mathbf{u}$, and a virtual increment of strain $\delta\boldsymbol{\gamma}$, we obtain

$$\int_V \boldsymbol{\sigma} : \delta\boldsymbol{\gamma} dV = \int_V \mathbf{p} \cdot \delta\mathbf{u} dV + \int_A (\mathbf{n} \cdot \boldsymbol{\sigma}) \cdot \delta\mathbf{u} dA, \tag{3.55}$$

which is the weak form that can be interpreted as the principle of virtual work. In (3.55) the $\delta\mathbf{u}$ is the equivalent to the weighting function in the Galerkin method. The double dots indicate

$$\boldsymbol{\sigma} : \delta\boldsymbol{\gamma} = \sigma^{\alpha\beta}\delta\gamma_{\alpha\beta}, \tag{3.56}$$

and the relationship between $\delta\mathbf{u}$ and $\delta\boldsymbol{\gamma}$ is

$$\delta\boldsymbol{\gamma} = \frac{1}{2}\left(\nabla(\delta\mathbf{u}) + (\nabla(\delta\mathbf{u}))^{\mathrm{T}}\right). \tag{3.57}$$

Rewriting the differential equation or the strong form (3.1) to an integral or weak form (3.55) allows for a numerical procedure where an arbitrary global domain can be divided into smaller and well-defined subdomains (finite elements). With the two final steps listed by Ottosen and Petersson (1992): 3. Introducing one for the physical problem and the chosen element geometry suitable approximation, and 4. Minimising the residual function arising from the approximation, by use of the Galerkin method - an equation system with a symmetric system matrix is obtained.

4 Design and production of shells

While the previous chapters have focused on the geometry of shells and the theory of how to analyse them, this chapter gives a brief background with some key references to the art of shaping and erecting curved structures. This chapter is divided into two parts. The first part covers form finding, with the aim to reduce the bending behaviour in the shell. The second covers surface patterns for simple manufacturing, ending with combining the two parts. First, a brief description of how form finding is defined and applied in the architectural design.

4.1 Form finding

The design of shells and grid shells is often connected to the concept of *form finding*. Form finding goes back to the discussion, or competition, among scholars during the 17th century and early 18th century on finding the most optimal shape for the structural stability of arches. In May 1690, James Bernoulli posed a challenge in the Acta Eruditorum

> And now let this problem be proposed: To find the curve assumed by a loose string hung freely from two fixed points. I assume also that the string is a line which is easily flexible in all its parts, (as cited in Truesdell, 1960, p. 64)

The list of scientists involved in this competition includes Robert Hooke (1635-1703), Pierre Varignon (1654-1722), Philippe de La Hire (1640-1718), David Gregory (1659 -1708), Gottfried Wilhelm von Leibniz (1646 -1716) and James Bernoulli (1654-1705). While heuristic and practical methods existed, as shown in Section 2.2.2, the scientists formulated research challenges such as Bernoulli 'Problem of the curvature of an arch whose parts support each other by their own weight, without the use of mortar.' (as cited in Truesdell, 1960, p. 83).

In fact, Robert Hooke had already found the solution in his anagram from 1675 'as hangs the flexible line, so but inverted will stand the rigid arch', but Hooke did not give any mathematical proof or inform his colleagues of his finding. The relationship between geometry and structural form is likely best depicted by Varignon in his posthumously published *Nouvelle mécanique, ou Statique* (1725), seen in Figure 4.1.

Already here, the distinction between structural analysis and form finding becomes difficult. David Gregory formulated a powerful statement '...an arch of any form can only be in equilibrium if we can draw a catenary curve which passes through it.' (as cited in Benvenuto, 1991, p. 327), which Giovanni Poleni (1685 - 1761) used in his analysis of St. Peter's dome (Figure 4.2). The hanging chain was used as an analysis tool for a long time. The one who deliberately started to use the hanging chains to derive funicular shapes as part of the exploration of the architectural design process was Antoni Gaudí (1852 - 1926) during the design process of Colonia Güell (Rubió i Bellver, 1913).

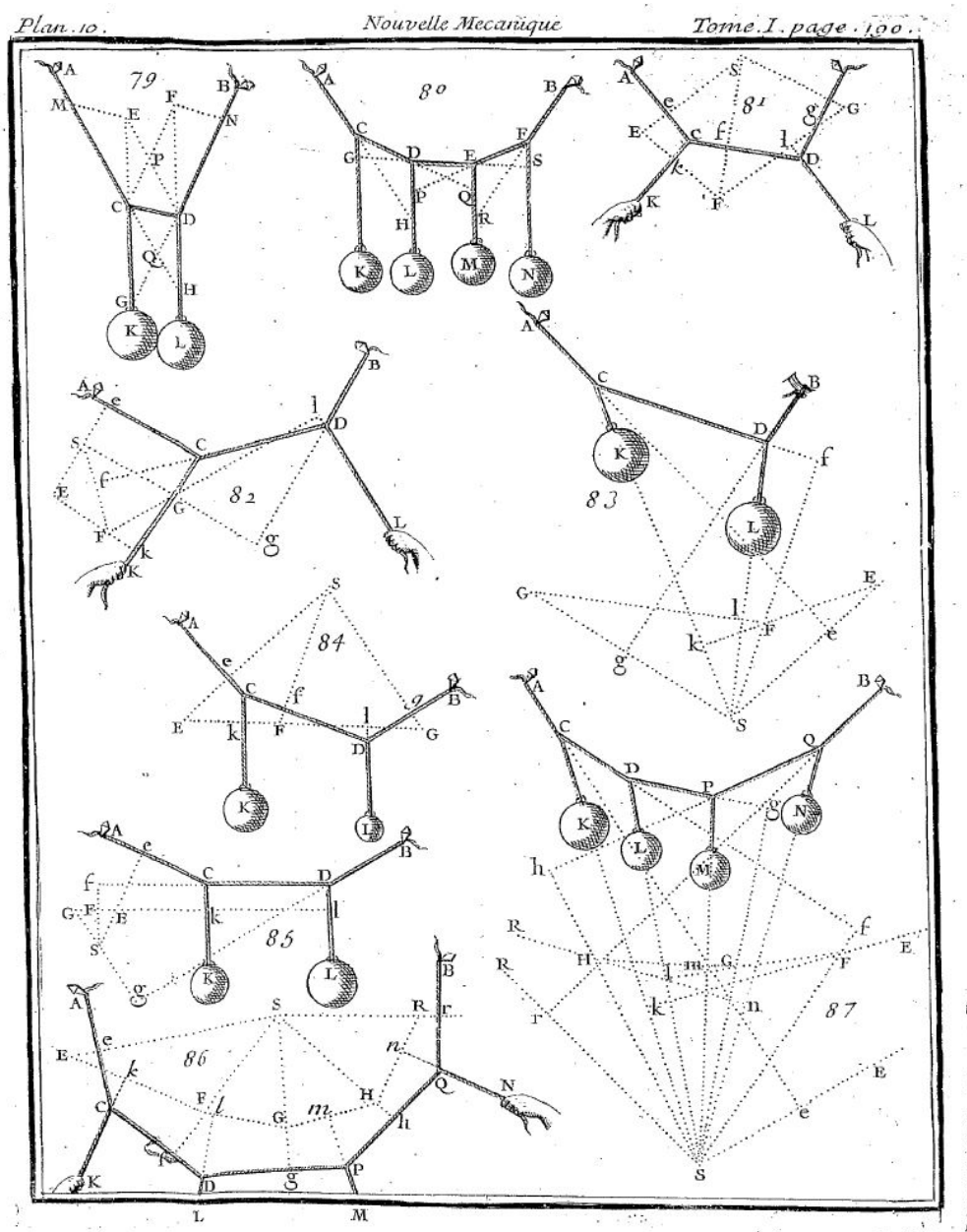

Figure 4.1: *Funicular shapes illustrated Nouvelle mécanique, ou Statique, dont le projet fut donné en M. DC. LXXXVII. (Varignon, 1725).*

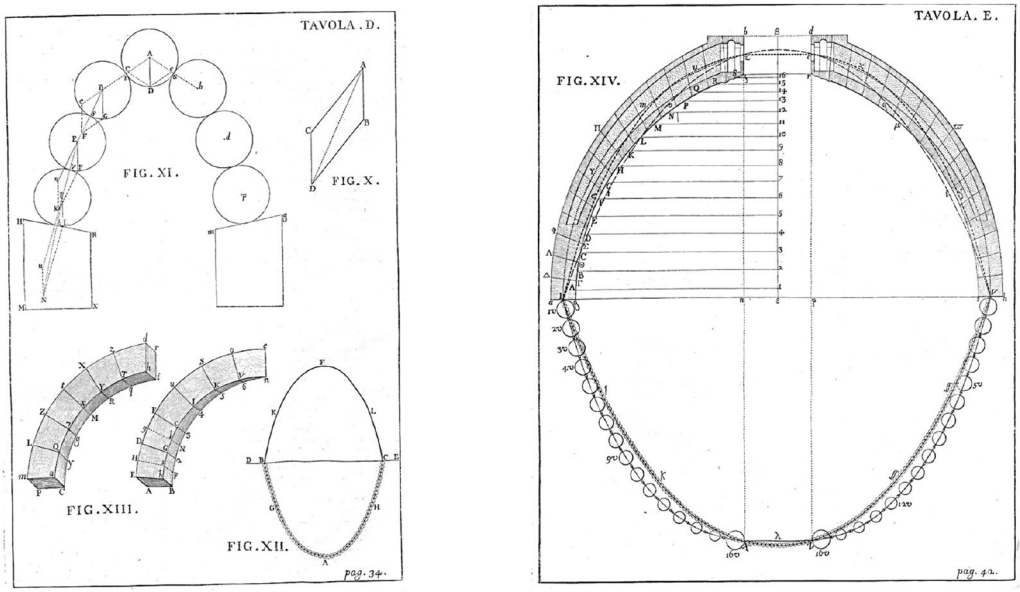

Figure 4.2: *The hanging chain used in the analysis of St. Peter's dome, from Memorie Istoriche della Gran Cupola del Tempio Vaticano (Poleni, 1748).*

While there can exist different opinions on the exact meaning of form finding Adriaenssens et al. (2014) provide a possible definition

> Form finding is a forward process in which parameters are explicitly/directly controlled to find an 'optimal' geometry of a structure which is in static equilibrium with a design load. (p. 2)

Of which the parameters to control that Adriaenssens et al. refer to are in three categories: (1) Boundary conditions, supports, external loads. (2) Topology of the model. (3) Internal forces, and their relationship to the geometry. The evaluation criteria in 'optimal' will be specific for each situation and architectural design project.

The architectural design process consists of two parallel and intertwining tracks (Figure 4.3). One that refers to the building design, or architecture, which includes the design of the space, the structure (including its design and structural efficiency) and other important functions. The other part refers to the realisation of the project, including the manufacturing and construction. In both of these tracks, the initial form finding plays a crucial role.

In form finding an interplay between spatial qualities and an efficient stress distribution is sought. However, the form finding process could also create a better starting point for economical and simple production and manufacturing. Zawisny et al. (2017) describe such considerations by Guastavino Jr. when designing the dome Cathedral of St John the Divine:

> The geometrical features of the cathedral dome are based on the original geometry of the cathedral, the forces in a dome structure, and constructability considerations. Each of these factors greatly influenced the final shape of the dome. (2017, p. 9)

In Figure 4.4, the main working drawing of the dome of St John the Divine shows the form finding process, which includes graphical analysis alongside drawings of details.

Form finding is normally followed by a preliminary structural analysis with different load cases to assess the risk of instability behaviour, such as buckling. The sizing is connected to the structural analysis and a production strategy. Usually, the design process is not linear but iterative, where the results at each stage can be fed back in a loop, as illustrated in Figure 4.3.

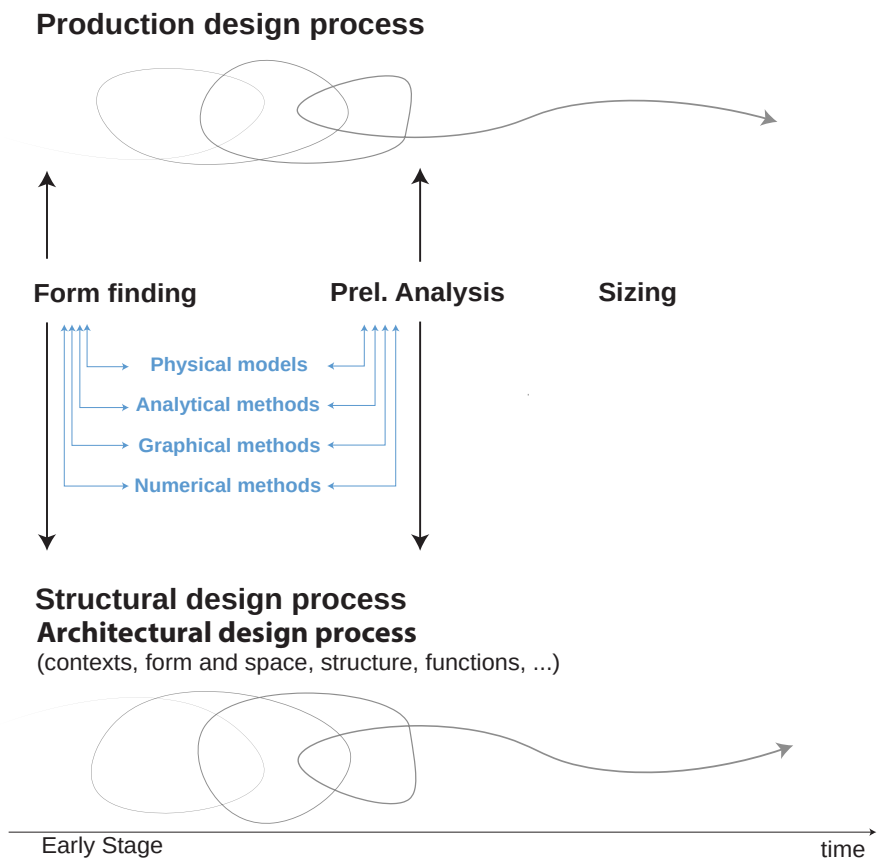

Figure 4.3: *A conceptual image of the design process where form finding is placed in the early stage feeding into both the architectural design process and the production design process.*

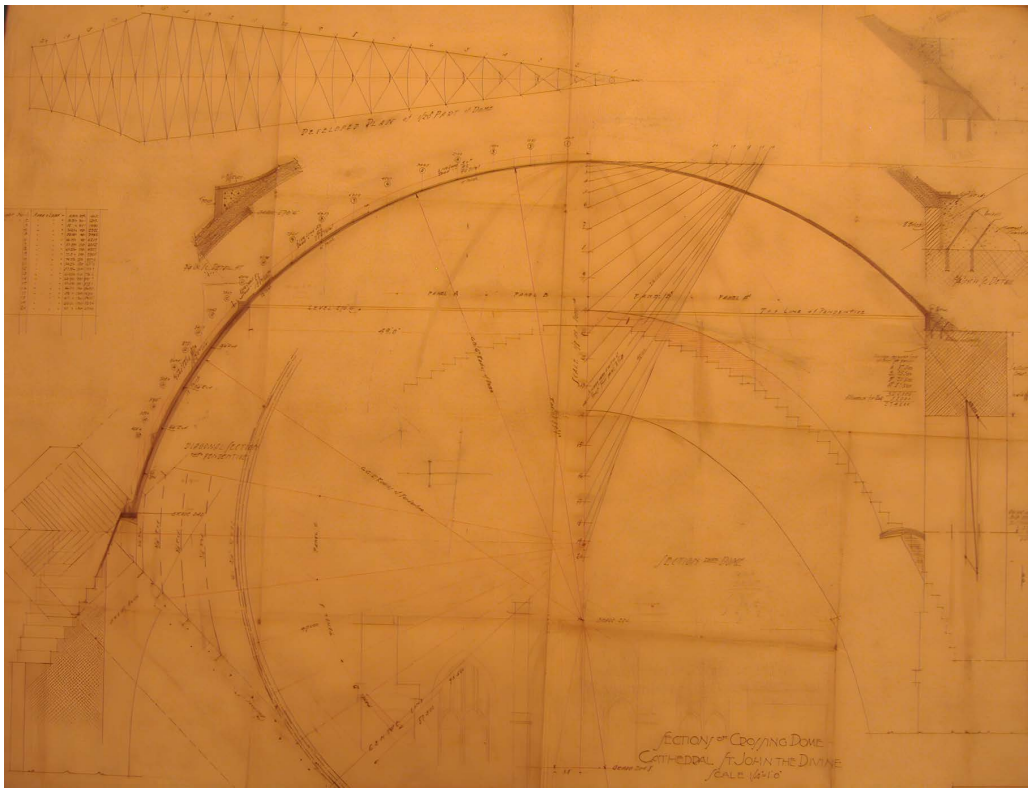

Figure 4.4: *Main working-drawing for the dome of the Cathedral of St. John the Divine (Avery Library) that illustrates a form finding process, which includes structural analysis aswell construction and manufacturing considerations.*

Form finding comprises a set of possible techniques[1][2] in the categories of *physical models, graphical methods* and *numerical methods*. Graphical methods have already been covered to some extent since graphic statics in Section 2.2.3 can easily be adapted to find the shape instead, as done by Guastavino Jr. (Ochsendorf, 2010). Thus, the following sections will cover the physical and numerical methods in more detail.

4.1.1 Physical models

During the design process of Colonia Güell, Gaudí had ten years of exploration from 1898 until 1908, when the construction started. During this time, he performed experiments using the famous hanging chain model seen in Figure 4.6(a)-(b). One of Gaudí's collaborators Joan Rubió Bellver (1913), expresses the relationship between form and structure and

[1]Many of the methods for form finding could also be used for structural analysis.

[2]One could perhaps argue that form finding methods also include analytical methods or geometric concepts typically used by shell designers and builders such as Felix Candela (1910-1997) (Faber, 1963), Eladio Dieste (1917-2000) (Anderson, 2003) and Eduardo Torroja (1899-1961) (Torroja, 1958).

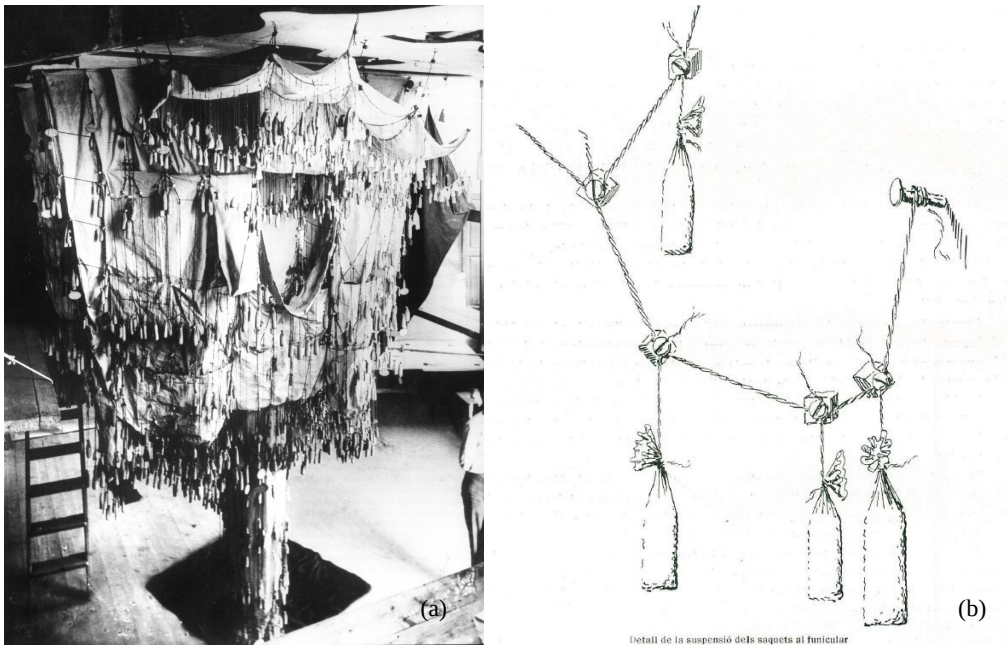

Figure 4.5: (a) *Gaudí's hanging chain model used in the design of the Church at Colonia Güell.* (b) *illustrations from Rubio (1913) of the poaches of sand attached to the model.*

shows images from the mechanical models used along with drawings of how the interior space would look like. The church was never finished, and after ten years of construction, the project was stopped, and now only the crypt exists. Similar models were later used in the design of the grid shell in Mannheim described in Section 1.3 (Figure 1.3).

One who was much inspired by the work of Gaudí was Frei Otto, who is mostly known for his research work at the Institute for Lightweight Structures (IL) and his work on tensile structures. His design projects include the Olympic stadium in Munich as well as the timber grid shell in Mannheim. Otto famously used soap film models to approximate suitable shapes for his tent structures (Klaus et al., 1987). Otto should have been aware of the experiments of Joseph Plateau (1801-1883), who used soap films to approximate forms of minimal surfaces, through works such as *On growth and form* (1917) by D'Arcy Wentworth Thompson (Escher, 2017). Soap films were also used in the design of the Viadotto dell'Industria by Sergio Musmeci (1926-1981) (Ingold & Rinke, 2015).

Heinz Isler (1926-2009) is mostly known for his thin concrete shells such as Deitingen Service Station. Isler developed a specific form finding technique using a piece of cloth that was dipped into gypsum that later hardened (Addis, 2014). The advantage of such models is that they could also be used for analysis, considering the scale effects. The disadvantage is that they can be tedious to make. Thus, numerical methods can, in those cases, be preferable. Also, it offers opportunities to simulate some phenomena or cases that can be fictitious, which can also be a drawback since the physical model never lies. However, both approaches involve evaluating whether the phenomena will occur in the

Figure 4.6: *Soap film model similar to those used by Frei Otto and Sergio Musmeci, among others.*

real structure. The following section will briefly describe the numerical methods for form finding.

4.1.2 Numerical methods

In general, numerical methods aim to mimic the behaviour of physical objects, like hanging chains and soap films. However, there are other techniques, such as topology optimisation, that would be difficult but not impossible to do physically. Veenendaal and Block (2012) provide a historical overview of the development of the numerical form finding techniques and one possible categorisation: *stiffness matrix methods*, *geometric stiffness methods* and *dynamic equilibrium methods*.

The common features of most numerical form findings methods are the need for predefined external and internal loading, topology, support conditions, and in the case of iterative methods, a tolerance for convergence (Veenendaal & Block, 2014).

The *stiffness matrix methods* relies on the connection to the finite element method where the differential equations are captured in an equation system with an explicit stiffness matrix. While the finite element method is standard in structural analysis, it can also be used as a form finding technique in structural optimisation, for example, topology optimisation (Bendsøe, 1995).

The *geometric stiffness methods* include the force density method and thrust network analysis (Block & Ochsendorf, 2007). The force density method was developed in the early seventies by Linkwitz and Schek (Linkwitz & Schek, 1971; Schek, 1974) and applied in the design of the Munich Olympic roofs. The method is suitable for structures where the

prestressing is significant, meaning the geometric stiffness is the dominating stiffness. The geometric stiffness is expressed as forces densities q, sometimes called tension coefficients (Southwell, 1933), containing the two unknowns, the force and the stressed length. The equilibrium for a vertex $\mathbf{x}_i$ with neighbouring nodes $\mathbf{x}_j$ and a load $\mathbf{p}_i$ can be written:

$$\sum_{j=0}^{n} \left((\mathbf{x}_j - \mathbf{x}_i) \frac{F_{ij}}{l_{ij}} \right) + \mathbf{p}_i = 0, \tag{4.1}$$

where the forces F_{ij} in the bar and the stressed length l_{ij} are replaced by the force density q_{ij}

$$q_{ij} = \frac{F_{ij}}{l_{ij}}. \tag{4.2}$$

The equilibrium at a node i can now be written as

$$\sum_{j=0}^{n} \left((\mathbf{x}_j - \mathbf{x}_i) \, q_{ij} \right) + \mathbf{p}_i = 0, \tag{4.3}$$

thus the non-linear system becomes a linearized system, which is much easier to solve the unknown vertex positions (Linkwitz, 2014).

Dynamic equilibrium methods include relaxation methods such as *dynamic relaxation*. Dynamic relaxation originated from Alistair Day (1965), and it can be equally used in structural analysis or form finding since it is just a numerical procedure to solve a set of non-linear equations.

The formulation of dynamic relaxation usually starts from Newton's second law. Using the notation in (Adriaenssens, Barnes, Harris, & Williams, 2014) it is formulated for a node i as

$$\mathbf{R}_i^t = M_i \dot{\mathbf{v}}_i^t, \tag{4.4}$$

where $\mathbf{R}_i^t$ is the residual force at a time t and $\dot{\mathbf{v}}_i^t$ is the acceleration. M_i is the lumped fictitious mass and is defined as

$$M_i = \frac{\Delta t^2}{2} S_i, \tag{4.5}$$

where S_i is a scalar representing the stiffness of a node, assuming the surrounding nodes are fixed.

Adriaenssens et al. rewrite the acceleration in (4.4) using finite differences to attain the velocity

$$\mathbf{v}_i^{t+\Delta t/2} = \mathbf{v}_i^{t-\Delta t/2} + \frac{\Delta t}{M_i} \mathbf{R}_i^t. \tag{4.6}$$

In a similar fashion, they find the new positions for $\mathbf{x}_i^{t+\Delta t}$

$$\mathbf{x}_i^{t+\Delta t} = \mathbf{x}_i^t + \Delta t \cdot \mathbf{v}_i^{t+\Delta t/2}. \tag{4.7}$$

This procedure is the same as the Leapfrog integration, which is similar to the Verlet integration. With the new updated positions, the new lengths l_{ij} and the new forces F_{ij}

in the links can be computed. The updated residual force $\mathbf{R}_i^{t+\Delta t}$ becomes

$$\mathbf{R}_i^{t+\Delta t} = \mathbf{p}_i + \sum_{j=1}^{n} \left[\left(\frac{F_{ij}}{l_{ij}} \right) (\mathbf{x}_j - \mathbf{x}_i) \right]^{t+\Delta t}, \tag{4.8}$$

with a load $\mathbf{p}_i$. Equation (4.8) can be compared to (4.1) in the force density formulation.

For more information regarding the dynamic relaxation formulation, the reader is referred to Barnes (1999). More information about Alistair Day and the history of dynamic relaxation can be found in two articles by Carfrae and Michael (2019a,b).

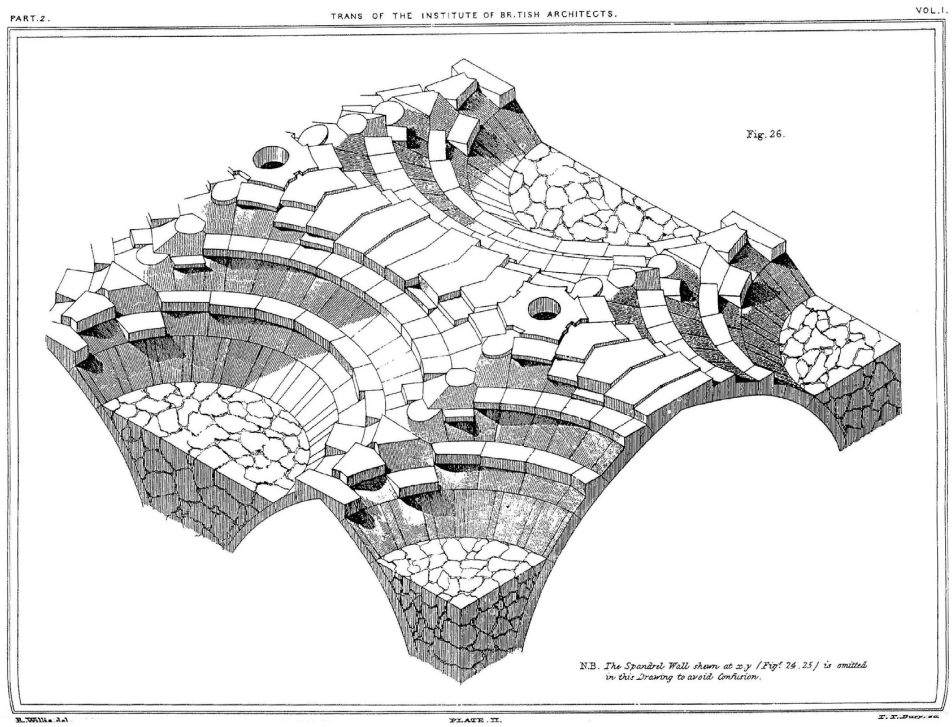

Figure 4.7: *The complex construction of the fan vaults in Peterborough Cathedral illustrated by Willis (1842).*

4.2 Geometry and rational production of shells

In the previous section, it was shown why geometry is a most important factor to achieve structural efficiency. What is then the drawback? One drawback is connected to the cost or complexity of manufacturing the building elements, as Gehry describes: 'Flat pieces cost one dollar, single curvature pieces cost two dollars; double curvature pieces cost ten dollars.' (Zaera, 1995, p. 36). J. Schlaich and M. Schlaich (2008) also describe the manufacturing and construction of double-curved surfaces as complex:

> Expensive formwork and complicated cutting patterns are required for the manufacture of these double-curved surfaces. The details of tensile structures and membranes are complicated and have to be manufactured with extreme precision. (p. 5)

This is valid for both curved tensile and compressive structures, as shown in Section 2.2. Heyman (2015) claims that only four large cathedrals were constructed with fan vaults, as seen in King's College in Cambridge or Peterborough Cathedral (Figure 4.7) since they were so complicated to build and expensive to manufacture. Fitchen (1961) describes and emphasises the difficulty in constructing falsework during medieval times and that it has not got enough attention when evaluating these structures. Fitchen argues that the rib vaults in the Gothic Cathedrals had an essential contribution to lowering the cost of labour in terms of easier connections and less timber work than the Romanesque groin vaults. The complexity of constructing scaffolding is witnessed in the only preserved medieval centring in the tower of the Lärbro church in Sweden from the 13th century (Frankl, 1962).

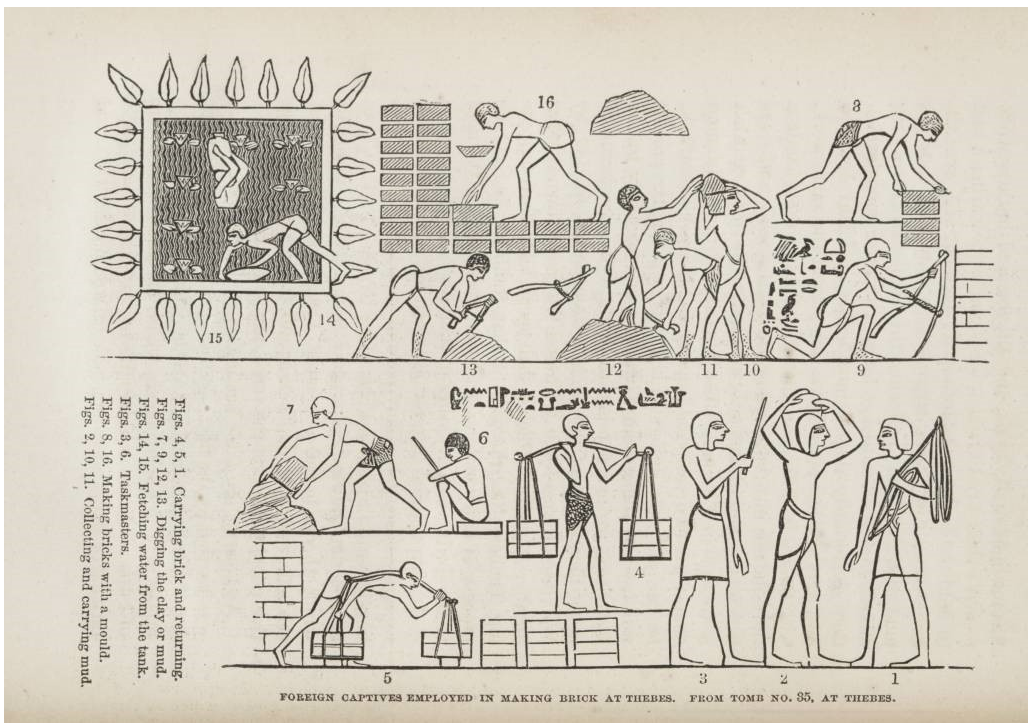

Figure 4.8: *Illustration made from wall painting in the tomb of Rekh-mi-Re (1450 B.C) illustrating the process of manufacturing bricks of mud and straw using brick moulds, (Prime, 1860).*

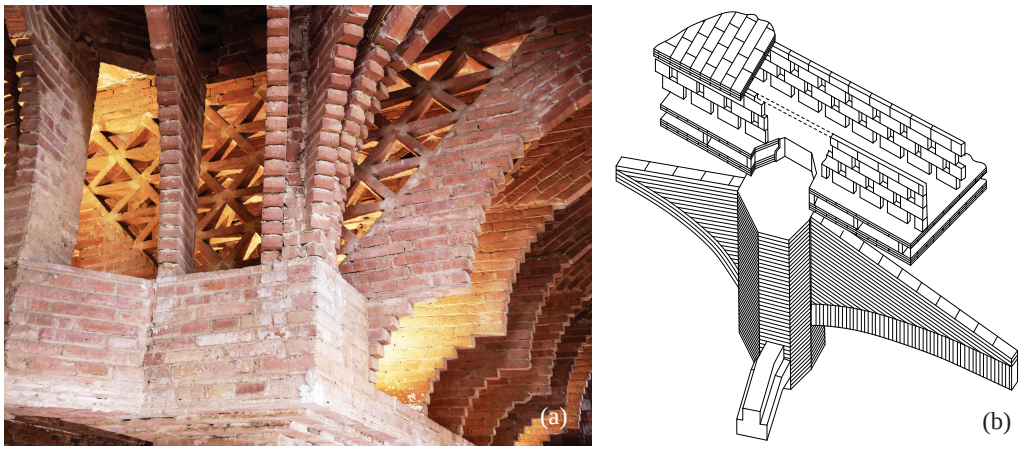

Figure 4.9: (a) *Brick arches from the attic in Bellesguard,* (b) *detail of the floor structure at the Crypt at Colonia Güell, redrawn from Balagué and Moreno-Navarro (1990).*

4.2.1 Simple building elements

Throughout history, different strategies for manufacturing and construction have been developed and applied based on the use of simple building elements and the wish for an economically efficient erection of the building. The brick mould can be seen in wall paintings from Egyptian tombs dating to ca 1450 B.C (Figure 4.8), but it was likely invented much earlier and not in Egypt, maybe as early as around 5900-5300 B.C (Campbell, 2003). Rottlaender (1977) presents tables of measurements from masonry buildings in the ancient cities of Tepe Yahya (5-4 millennium B.C) and Uruk (4 millennium B.C.) where the building blocks are standardised, having a mean value of a cubit. Spanish-originating architects and master builders such as Antoni Gaudí, Lluis Domenech, Eduardo Torroja, Rafael Guastavino Sr. and Rafael Guastavino Jr. mastered designing using the brick and the brick tile. Using thin tiles in combination with fast setting gypsum mortar they could build vaults using little or no formwork (Collins, 1968; Ochsendorf, 2010), a technique traditionally common in Spain and the region of Roussillon in France (Bannister, 1968). Gaudí used the brick tiles in creative ways, such as the attic in Bellesguard (Figure 4.9(a)), Casa Vicens and the Crypt at Colonia Güell (Figure 4.9(b)). Rafael Guastavino Sr., seen standing on an arch in Figure 4.10, and Rafael Guastavino Jr. built many vaults and domes in iconic public buildings in America during the end of the 19th century and the first half of the 20th century. In the Sancti Petri Bridge, Eduardo Torroja used steel-reinforced brick shells as form-work for the foundations, as seen in Figure 4.11 (Ochsendorf & Antuña Bernardo, 2003).

Other examples of bridge design using simple building elements include the timber arch bridges Mathematical bridge in Cambridge and the Old Walton Bridge (Queens' College Cambridge, n.d.).

The use of simple building elements can also be a driving concept in the design and the construction of grid shells as shown in projects such as the House for Hippopotamus,

Figure 4.10: *Master builder Rafael Guastavino Sr. standing on a recently finished arch during the construction of the Boston Public Library, 1889.*

Zoo Berlin (Figure 4.12) (J. Schlaich & Schober, 1996; J. Schlaich & Schober, 2005) and Mannheim Multihalle. Schlaich Bergermann Partner designed grid shells such that they could be covered with planar glass panels. The form is described as translational surfaces that give the possibility to define the two boundary curves, the directrix and the generatrix, arbitrarily — offering a wide variety of shapes where the surface grid can be manufactured from planar quadrangular panel sheets. Master builder Rafael Guastavino Sr. also used translational surfaces in his tile vaults. First, his craftsmen built the edge arches and to later disassemble the centering, letting it slide along the arches as a temporary falsework while filling the void (see Figure 4.10). In the double-layer timber grid shell in Mannheim (Figure 4.13) by Frei Otto, Ian Liddell and Edmund Happold, the grid is an equal mesh net built out of straight timber laths. The grid was built flat on the ground and erected and locked into place, giving the shell action.

4.2.2 Surface patterns and the production of shells

As mentioned in Section 1.3, equal mesh nets are nets where the lengths of the edges of each cell in the grid are of the same length, also called Chebyshev nets after the

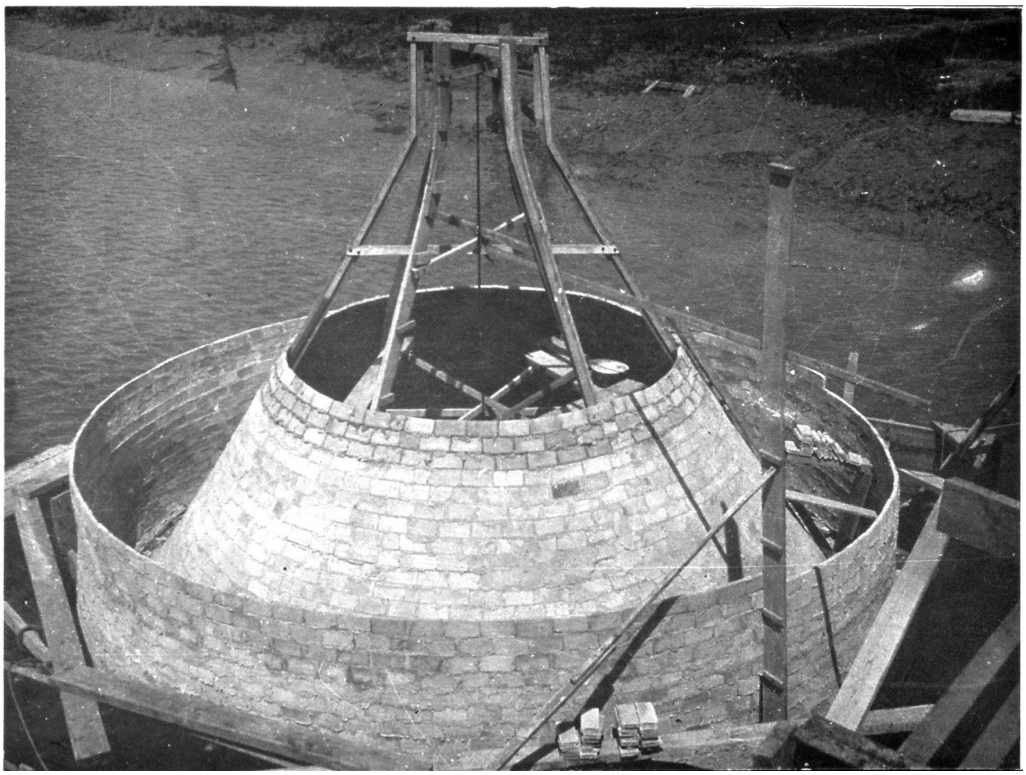

Figure 4.11: *Eduardo Torroja using thin brick shells as form-work for the foundations of the Sancti Petri Bridge, 1927.*

Russian mathematician Chebyshev (1887/1946). Chebyshev applied, what he called the mathematics by Gauss, to solve the matter of cutting patterns on clothes. This can be seen as a purely mathematical problem of dressing a surface with a certain pattern. As mentioned in section 2.3, it is not possible to decide the properties of the form and the pattern using the components of the metric tensor, $a_{\alpha\beta}$, and the components of the surface tensor $b_{\alpha\beta}$ completely arbitrarily. That is due to the three compatibility equations, usually referred to as the Gauss-Codazzi equations (Stoker, 1969). Since there exist six independent components and there are three compatibility equations, there are three unknowns that one can specify. In a Chebyshev net one specifies the metric tensor components (Williams 2014):

$$a_{11} = L^2 \tag{4.9}$$

$$a_{22} = L^2 \tag{4.10}$$

$$a_{12} = L^2 \cos\omega, \tag{4.11}$$

Figure 4.12: *Steel grid shell at the House for Hippopotamus at Berlin Zoo was designed such that it could be covered by planar quad panels. Schlaich Bergermann Partner, 1996.*

where the length L is constant and ω is the angle between the two basis vectors. The Guass theorem becomes (Williams 2014):

$$K = -\frac{1}{L^2 \sin\omega} \frac{\partial^2 \omega}{\partial\theta^1 \partial\theta^2}. \tag{4.12}$$

If the angle ω is constant, the surface must have zero Gaussian curvature, meaning that it is either flat or something that can be formed from a flat sheet of paper without deforming it, such as rolling it into a cylinder. So for other types of curved surfaces, this angle must be allowed to vary. However, it is possible to combine these geometrical properties with the physical properties described in membrane theory, as in form finding. The three tensors, $a_{\alpha\beta}, b_{\alpha\beta}$ and $n^{\alpha\beta}$ has nine unique components and there are six equations; the Gauss-Codazzi equations (2.22), (2.25), (2.26), and the three equilibrium equations (3.17), (3.18). Thus, a solution require three choices which can be used to describe the sought properties of the form, pattern or state of stress. For the Mannheim grid shell (Figure 4.13) the choise was an equal mesh net that is (Adiels et al., 2017):

$$a_{11} = L^2 \tag{4.13}$$

$$a_{22} = L^2 \tag{4.14}$$

$$n^{12} = 0 \tag{4.15}$$

Equation (4.15) sets the shearing to zero, constraining the state of stress to follow lines in the grid, meaning the structure can be treated as a pin-jointed structure. Having these three constraints, it is possible to solve the remaining six unique components of the three

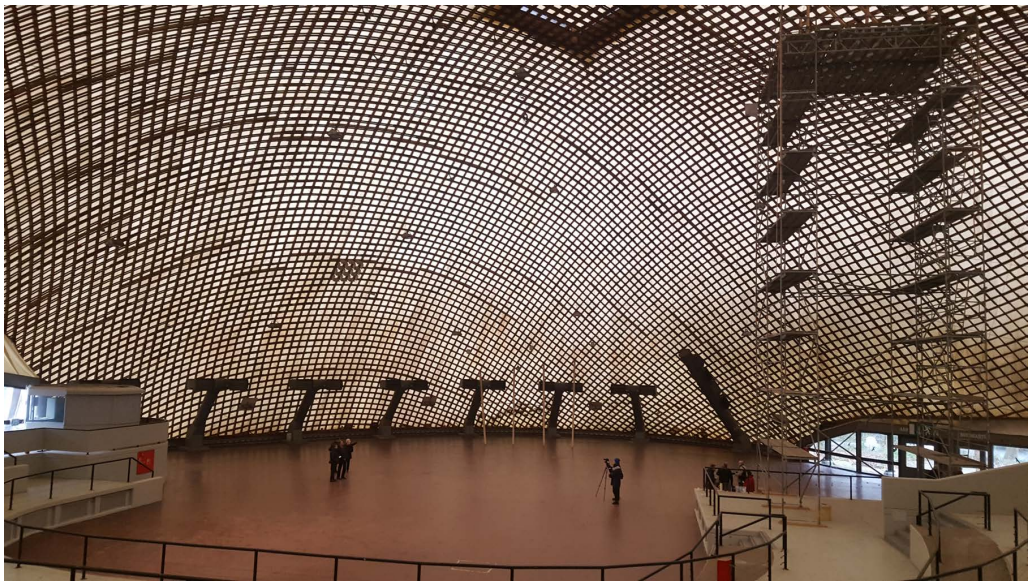

Figure 4.13: *Timber grid shell in Mannheim (1975) by Frei Otto (1925-2015) together with structural engineers Ted Happold (1930 – 1996), Ian Liddell and Chris Williams from Structures Group 3 at Arup.*

tensors using numerical methods such as those described in Section 4.1.2. Williams (1980) uses a similar approach to cutting patterns of inflated membrane structures by the use of geodesic coordinates.

This last example ties back to the beginning of chapter 2 with the weaver, of which Struik (1987) describes gave birth to geometry, described with the same type of equations that also describe the space-time fabric of the universe.

5 Methodology

Before describing the methodologies used in this thesis a brief overview of research in art and design is given in Section 5.2. However, to put these arguments in a historical context, a short note about James Clerk Maxwell's review of the work by the blind visual scientist Joseph-Antoine Plateau begins this chapter.

5.1 The blind visual scientist blowing bubbles

> Here, for instance, we have a book, in two volumes, octavo, written by a distinguished man of science, and occupied for the most part with the theory and practice of bubble-blowing. Can the poetry of bubbles survive this? Will not the lovely visions which have floated before the eyes of untold generations collapse at the rude touch of Science, and 'yield their place to cold material laws'? (Maxwell, 1874, p. 119)

Figure 5.1: *To the left is Belgian scientist Joseph Plateau, and to the right is 'Soap Bubbles' by Jean-Jacques de Boissieu.*

James Clerk Maxwell (1831-1879), a distinguished man of science himself, posed this question in his review of *Statique expérimentale et théorique des liquides soumis aux seules forces moléculaires* by the blind Belgian physicist Joseph-Antoine Plateau (1801 - 1883).

Plateau was the son of a flower painter who desired his son to be an artist (Thirion, 1914), but most mathematicians know him through the *Plateau problem* as finding a minimal surface based on a defined boundary curve in space. It is possible to find the partial differential equation under which conditions a surface has a minimal surface area using the calculus of variation (Strauss, 2008). Joseph-Louis Lagrange (1736 - 1813) showed this already in 1762 (Hyde et al., 1997). The issue is to find a function $z = f(x, y)$

such that it fulfils the requirement:

$$\left(1+\left(\frac{\partial f}{\partial y}\right)^2\right)\frac{\partial^2 f}{\partial x^2}-\frac{\partial f}{\partial x}\frac{\partial f}{\partial y}\frac{\partial^2 f}{\partial x \partial y}+\left(1+\left(\frac{\partial f}{\partial x}\right)^2\right)\frac{\partial^2 f}{\partial y^2}=0 \tag{5.1}$$

Plateau proved in 1849 that the solution could be found experimentally using a soap-film that spans the void of a closed curve formed using a steel-wire.

Plateau became blind eight years prior, in 1841, which is believed to have been due to an experiment in which he gazed into the sun for a long time in 1829. The tragic fate of Plateau placed him in a similar contradicting situation, being 'the blind visual scientist' similar to Beethoven being the deaf composer (Verriest, 1990). Thus, Plateau had to teach and instruct his friends and fellow researcher to perform the experiments described in his book (Maxwell, 1874). Still, Plateau describes the beauty and charm of his experiments he could no longer see.

> All these experiments are extremely curious; there is a particular charm to contemplate these thin shapes, almost reduced to mathematical surfaces, which are adorned with brilliant colours, and which, in spite of their extreme brittleness, persist for so a long time. (Plateau, 1873/2005, p. 83)

> The beauty of the film shapes of glyceric liquid naturally inspires the desire to have the same shapes completely permanent. (1873/2005, p. 254)

Plateau's work has been important in understanding the forms of nature through physics and mathematics. Zoologist D'Arcy W. Thompson (1917) refereed to Plateau in *On growth and form*. Thompson believed that, in general, no organic forms existed that did not live in compliance with ordinary physical laws. Thompson's work influenced architect Frei Otto and structural engineer Edmund Happold (Walker & Addis, 1997), designing lightweight tent structures, making the shapes Plateau wished permanent.

Before Maxwell (1874) goes into the review of Plateau's work, Maxwell gives this comment on Plateau's research process: 'But we must now attempt to follow our author [Plateau] as he passes from phenomena to ideas, from experiment to theory' (p.119). An artist working very close to the phenomena through experiments is the artist *Andy Goldsworthy*. Goldsworthy creates ephemeral sculptures using natural building blocks, such as straws, icicles or stone rubble. Often these structures or experiments are performed outdoors or in nature where an essential aspect of these sculptures or experiments is the interplay and interaction with the surrounding environment. In the documentary *Rivers and Tides*, Goldsworthy is observed creating these fragile sculptures in a tense atmosphere, where collapse is perilously close. It can be structures made from sticks or straws that collapse under the slightest touch or slight wind, making the phenomena naked, exposed and visible. Goldsworthy says: 'When I make a work I often take it to the very edge of its collapse, and that is a very beautiful balance.' (Riedelsheimer, 2001, 57:00). Similar to Antoine de Saint-Exupéry's view of the perfect design, 'In anything at all, perfection is finally attained not when there is no longer anything to add, but when there is no longer anything to take away, when a body has been stripped down to its nakedness.'(1939, p. 66).

Going back to the first question posed by Maxwell, regarding if science ruins the poetry bubble blowing Maxwell answers:

> No, we need to go further than this book and its author [Plateau] to learn that the beauty and mystery of natural phenomena may make such an impression on a fresh mind open mind that no physical obstacle can ever check the course of thought and study which it has once called forth.

However, Maxwell ends his introduction with a new question he does not answer:

> Which, now, is the more poetical idea—the Etruscan boy blowing bubbles for himself, or the blind man of science teaching his friends how to blow them, and making out by a tedious process of question and answer the conditions of the forms and tints which he can never see? (Maxwell, 1874, p. 119)

5.2 Research in art and design

A suggestion for a research structure in the field of art and design has been given by Frayling (1993). This section takes departure in his article *Research in Art and Design* often cited by researchers in the field. Frayling (1993) describes three different categories of research in art and design: *research into art and design*, *research for art and design* and *research through art and design*

Research into art and design is the most straightforward, or uncomplicated, and includes historical research and various theoretical aspects of art and design. This is the most common category of research of the three.

Research for art and design is probably the less clear one, or as Frayling states, research with a small 'r'. It is where the research is manifested within the artefact.

> Research where the end product is an artefact - where the thinking is, so to speak, embodied in the artefact, where the goal is not primarily communicable knowledge in the sense of verbal communication, but in the sense of visual or iconic or imagistic communication. (Frayling, 1993, p. 5)

Frayling has a reference to an interview with Picasso in which the artist does not think his work is research. Frayling, however, opens for, or at least see a possibility, that it might be classified as research. What Picasso calls a gathering of reference material used to in his preparation might have similarities with research. Both Frayling and Arlander (2014) refers to the expressive art like dance and film for this type of research: 'And yet many of the preparations for a production involve activities that are similar to research – such as archive research and experimentation. It is only a question of degree that separates them from more formal research processes.' (Arlander, 2014, p. 33).

Research through art and design is the second most common research category, even though not as frequent. He refers to three groups within this category: *materials research, development work* and *action research.* In the first group, Frayling refers to titanium sputtering and colourisation of metals and jewellery. Sputtering is a physical method in which energetic electrons are blasted onto a target surface to remove some of the

metal atoms to compose a vapour. The vapour can then be applied as a thin film onto a substrate. The second group Frayling exemplifies as customising technology that enables some sort of novelty, where the results are communicated. The third group is related to the design process. The researcher documents her or his practical experiments performed in a studio or laboratory, and the resulting report contextualises it.

In the paper *The Debate on Research in the Arts* Borgdorff (2007) elaborates on the categories by Frayling (1993) but instead use the terms in a modified manner (in the same order as Frayling): *research on the arts*, *research for the arts* and *research in the arts*. Borgdorff refers to the last category, *research in the arts*, as the most controversial and adds a connection to Donald Schön's description of 'reflection in action' (Schön, 1992).

Frayling (1993) also has a hypothesis that the creative artist and the experimental scientist has much in common, mentioning the work of David Gooding (1985) regarding the scientist Michael Faraday (1791-1867), but also the book *Double Helix* by Dr James Watson:

> Where the artist has difficulty persuading people of the connection of art with research, the scientist (whose research expertise has until recently been taken for granted) has exactly the same problem with creativity - which is generally seen as the prerogative of the artist rather than the scientist. This is partly why the process of discovering has been virtually ignored until recently, and why the activity of fine art is of increasing interest to historians of science. Look at The Double Helix: it could almost be an artist's autobiography. (Frayling, 1993, p. 3)

The Double Helix is Watson's memoir on discovering the spiral structure of DNA, describing the work by him, Cricket, Wilkins and Franklin. At the beginning of the book, Watson (1968/2010) states that research rarely is a linear process as outsiders often perceive it. Much of the progress is often based on human interactions in which personalities and cultural traditions are essential. The book illustrates a research process where theory development is closely integrated with performing experiments and building physical models (Figure 5.2).

One of the major problems with research in art is distinguishing where the line goes between art and research. As both Frayling and Borgdorff state, everything that is art is not research. Borgdorff (2007) comes to this conclusion on when art practice becomes research:

> Art practice qualifies as research if its purpose is to expand our knowledge and understanding by conducting an original investigation in and through art objects and creative processes. Art research begins by addressing questions that are pertinent in the research context and in the art world. Researchers employ experimental and hermeneutic methods that reveal and articulate the tacit knowledge that is situated and embodied in specific artworks and artistic processes. Research processes and outcomes are documented and disseminated in an appropriate manner to the research community and the wider public. (Borgdorff, 2007, p. 14)

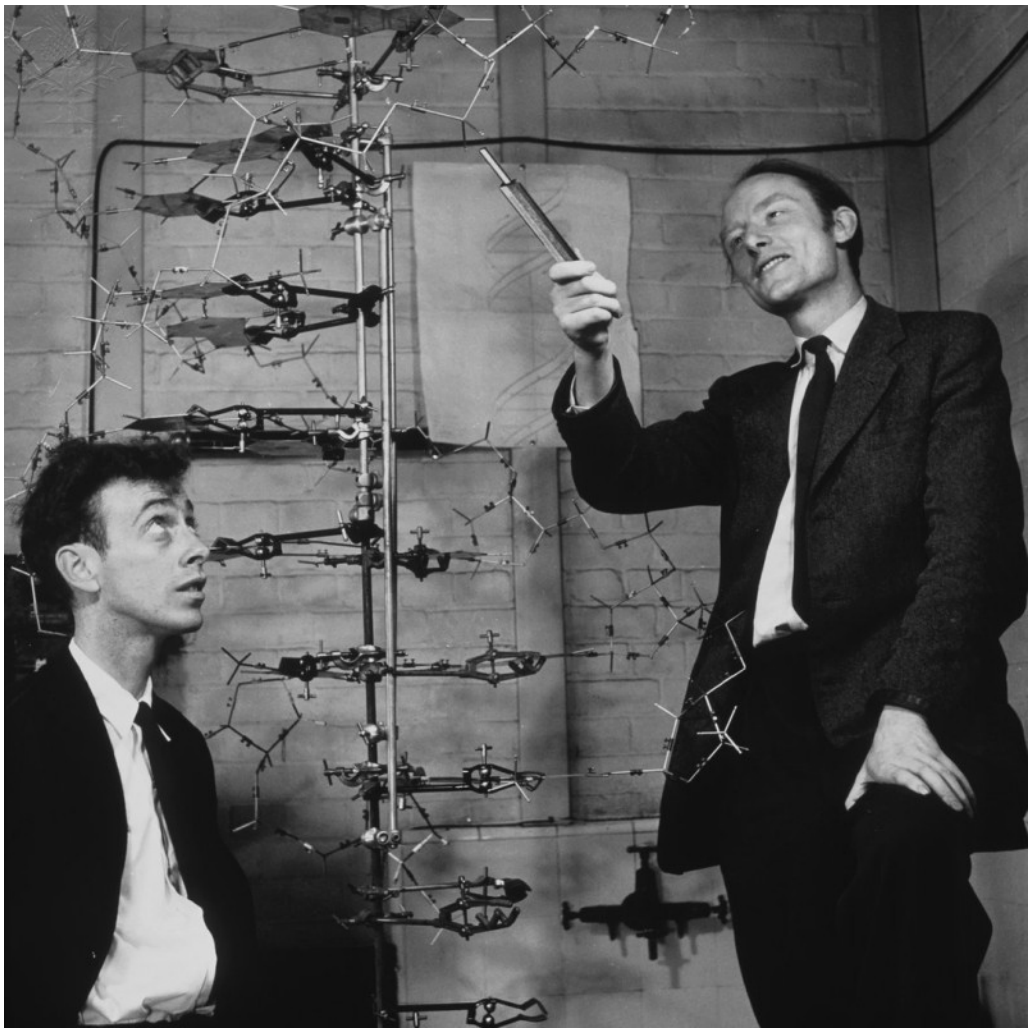

Figure 5.2: *Watson and Crick standing next to their model describing the helical structure of DNA*

Adding another layer to the proposals for a research structure in Frayling (1993) and Borgdorff (2007) is what in Hauberg (2011) refers to as *Research by design*. It has been used in the context of architectural research. It has some similarities to *research through art and design* (Frayling, 1993) but it is more practised based and the design and the research are further closely integrated. Furthermore, the knowledge is generated while designing. Hauberg (2011) describes research by design as:

> Research by design is any kind of inquiry in which design is a substantial part of the research process. In research by design, the architectural design

process forms a pathway through which new insights, knowledge, practices and products come into being. Research by design generates critical inquiry through design work that may include realised projects, proposals, possible realities and alternatives. Research by design produces forms of output and discourse proper to disciplinary practice, verbal and non-verbal that make it discussable, accessible and useful to peers and others. Research by design is validated through peer review by panels of experts who collectively cover the range of disciplinary competencies addressed by the work. (p. 51)

5.3 Research methodology

The research methods used in this thesis can be divided into five main categories: *literature review, theory development, simulations, design inquiries, and documentation.* The methods have been chosen from the traditional scientific approach as well as from an artistic research process (see Section 5.2).

In this section, it's shown how the literature studies have been set up and carried out. Thereafter a review is given of how the various research methods have been combined to investigate the respective research question.

5.3.1 Literature review

The literature review is primarily an investigation of four important aspects of shells in architecture. Initially, built examples were studied and evaluated from four different points of view: *geometry, structural theory, design tools* and *production technology*, as illustrated in Figure 5.3. These aspects were later refined into three specific literature studies found in the three chapters of the contextualization (see Chapters 2 - 4).

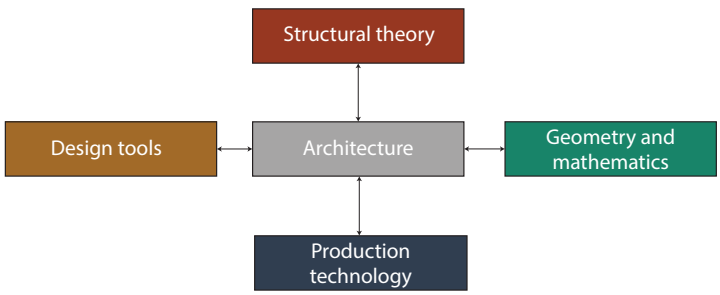

Figure 5.3: *The literature review emphasised how architecture has been linked to design tools, structural theory, production technology and geometry.*

The built examples have served as a tool or test bed for such investigation by being assessed through the four aspects, as shown in Figure 5.4. The examples were also put into a broader context by using a timeline to show their relation to the developments in geometry, structural theory and the design tools around that period as illustrated in the matrix in Figure 5.5. This approach has been inspired by the method used by Addis

(2007). The examples were chosen based on their relevance to the research questions and their impact, novelty or influence in the development of architecture, structural engineering and construction.

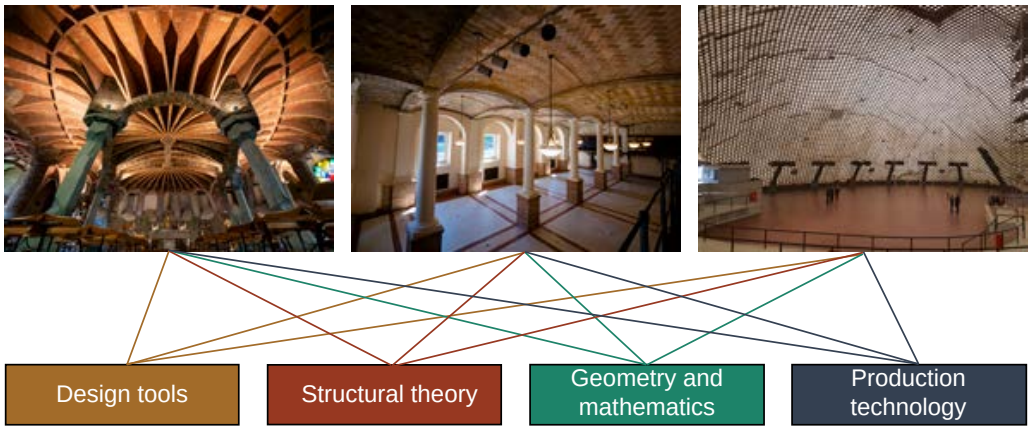

Figure 5.4: *In the literature review, various built examples were examined using the various parameters.*

The theory of geometry has been reviewed mainly in the field of classical differential geometry, from Gauss to the geometry used by Einstein in the general theory of relativity. The literature has been chosen based on classical and established books and authors in the field of mathematics such as Struik (1988), Stoker (1969), Pressley (2009) and Carmo (1976).

For the shell theory, classical books including Timoshenko and Woinowsky-Krieger (1959), Calladine (1983), Billington (1965) was studied, and for the link between differential geometry and shell theory the work of Green and Zerna (1968) have been used.

Design tools and production technology have been studied through the works of well-known shell builders and designers such as Eladio Dieste (Anderson, 2003), Eduardo Torroja (1958), Antoni Gaudí (Collins, 1963), Frei Otto (Vrachliotis, 2018), Jörg Schlaich (2005) Rafael Guastavino Sr. and Rafael Guastavino Jr (Ochsendorf, 2010). There were also studies of structures on a smaller scale, such as the Inside Out Pavilion (Schling et al., 2018) and projects that combine digital tools and low-tech construction, including the Almond Pavilion (Soriano, 2017) and the UWE Research Pavilion (Harding et al., 2017). To get an overview of the field of computational methods for form finding *Shell structures for architecture: Form finding and optimization* (Adriaenssens, Barnes, Harris, & Williams, 2014) has been a great help.

Figure 5.5: *A matrix has been used in literature review of the development in architecture and mathematics through history, based on a set of parameters. This particular matrix is connected to the developments in connection to the Colonia Güell by Antoni Gaudi*

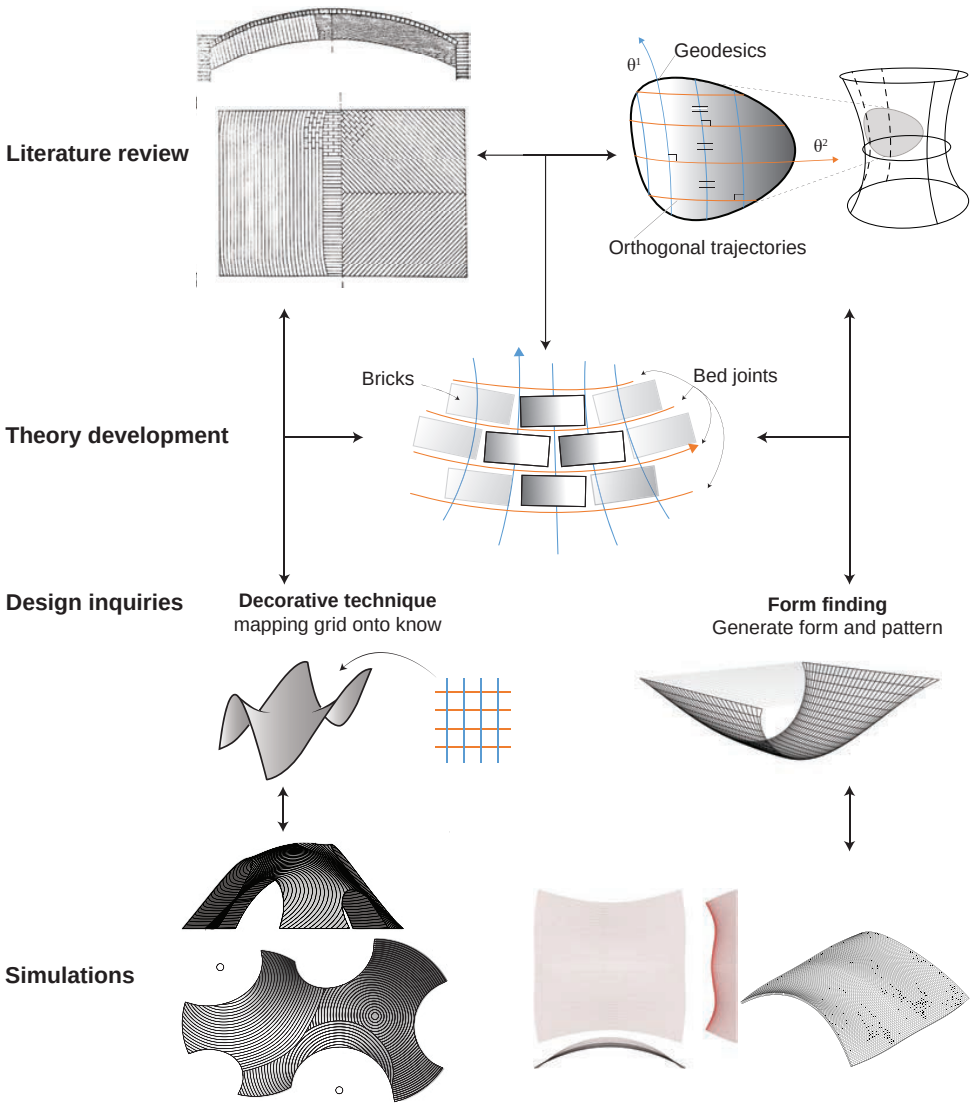

Figure 5.6: *Conceptual image of the methodology research question 1, using the investigation from paper A as an example. At the top shows the literature review in both fields of architecture and the field of mathematics and geometry. The theoretical framework in geometry is developed to explain or create new insights into these historic structures with the possibility of applying them in contemporary projects. The last step is to evaluate the theory and the possibility of using it in the architectural design process.*

5.3.2 Research question 1

How can differential geometry be used to design structurally efficient shells and shells with surface patterns for simple production? The investigation of this question include four methods: *literature review*, *theory development design inquiries* and *simulations*. As illustrated in Figure 5.6, these parts are not necessarily used in linear succession but can influence and go into each other in an iterative process, similar to the view of Watson (1968/2010).

Theory development has a central role in the research methodology and is influenced and steered by findings in the literature in architecture, mathematics and shell theory, as well as speculative architectural applications and experience of experiments and tests using computer simulations. Thus, the parts inflicting the theory development are described as follows.

The design inquiry serves as a hypothesis or a speculative idea of how the theory can be used as a new design technique or method during a design situation. There are multiple ways in which the mathematical theory can be implemented into a design technique, which also informs the choice of the proper simulation technique.

The simulation involves numerical methods to solve partial differential equations as well as geometrical programming packages such as *Rhinocommon* in the commercial software Rhinoceros3d. The evaluation is based on the digital experiments and various digital models generated in the simulations, where it is compared to the theoretical hypothesis through the digital model's geometrical properties and measurements. It also evaluates the application of the design technique. Unexpected results or phenomena from the simulation can help develop the theory as well as the architectural application during the research process.

This methodology has been used in the different types of inquiries described in Paper A, Paper D, Paper E and Paper F. Paper F differs from the other mentioned papers since it is the most recent work and it is more focused on theory development, and while it's driven by a design application, it is more speculative than defined at this stage.

5.3.3 Research question 2

How can differential geometry be applied in a design process supporting the quick production of a grid shell? This research question is strongly process-oriented and investigated through a set of case studies or design inquiries. Figure 5.7 shows the general character of the process connected to the case studies.

A *research through design* approach has been used, where the case studies have been used as a challenge where the constraints and limitations in the design process force new ideas to be developed. The challenge was formulated such that a structure would be constructed during a two-day workshop. The participants were approximately 35 undergraduate students in the Architecture and Engineering program. The group, in general, did not have prior experience in building and construction.

The input in a research based on case studies involved both external and internal constraints (Lawson, 2006). The external constraints involve those one cannot change or control, which in these cases were the limited time of two days to manufacture and assemble the structure, the group size, the budget and the site conditions. The internal

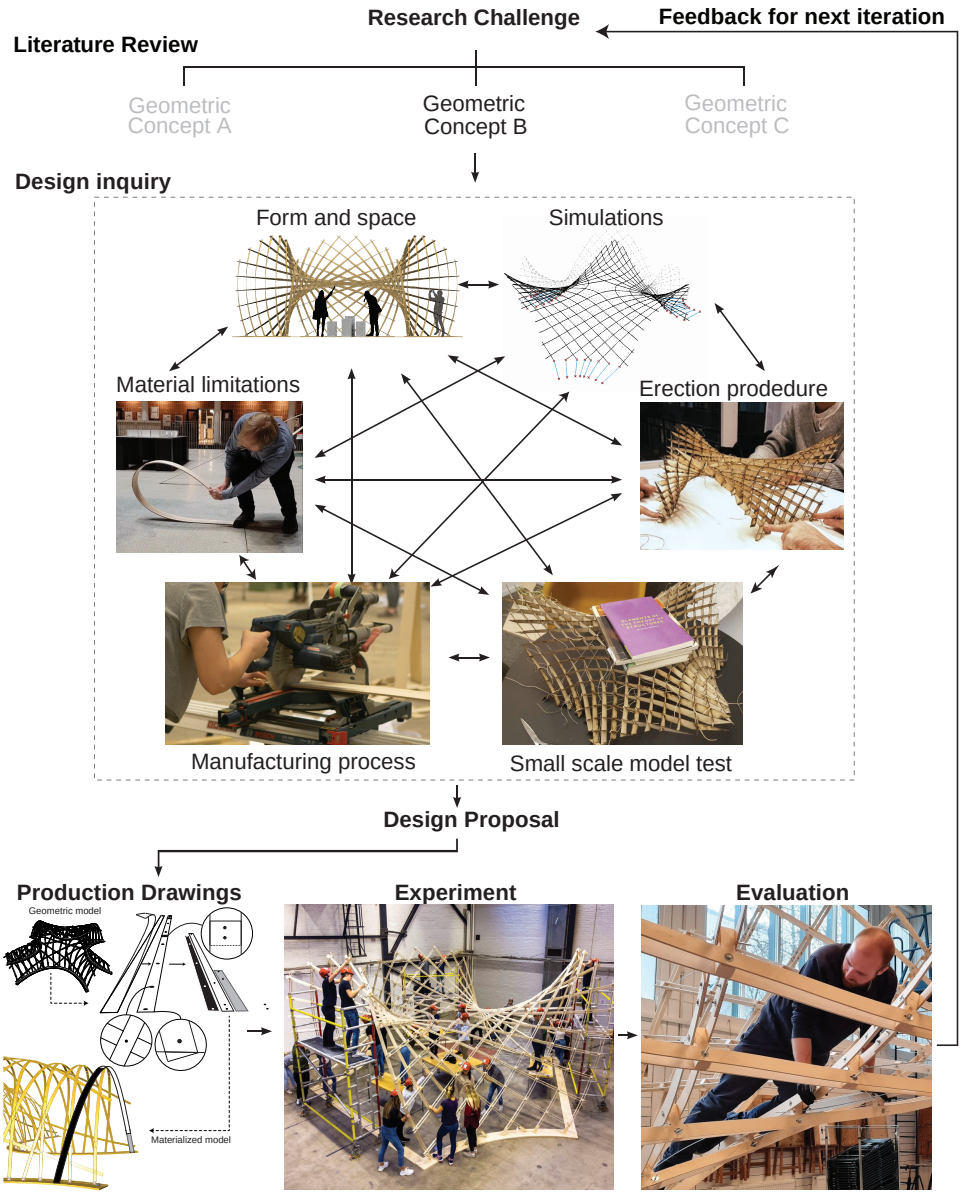

Figure 5.7: *Conceptual image of the methodology in question 2.*

constraints are more flexible and more under the designer's control. In these cases, the internal constraints were the geometric constraints of the building blocks which were chosen to be straight planar laths. Another chosen constraint was to primarily use manual manufacturing techniques to activate and utilize the group more efficiently.

Documentation through film and moving pictures has played a consistent role in the following stages. The design process has been recorded, including the experiments and tests and the final experiment or test during the workshop. The reasons have been several. One important use was to evaluate the time efficiency of the manufacturing techniques. At other times, the recordings of the model tests were analysed and discussed with team members based in different countries. The recording during the workshop was made to capture the process.

The design inquiry started with a range of theoretically viable geometric concepts. A rough evaluation was done to narrow the selection. The evaluation was based on time and feasibility to construct the elements, structural performance, economy, safety, time and feasibility to assemble and erect the structure. These criteria were applied in an iterative non-linear design process where digital drawings and models were tested against smaller and larger physical models and material parameters. This was an iterative process in which the model tests and the manufacturing methods informed and challenged the design. The outcome of this process was a design proposal with a set of associated manufacturing strategies.

The following stage was to create the final digital model. The purpose was to create a digital twin where final adjustments could be made and to generate the necessary production drawings and data to communicate the fabrication procedure to the participants (and digitally controlled machines such as the CNC when necessary) during the experiment. The information from the digital model could also be used to generate a structural analysis model for more detailed analysis.

One day before the experiment, participants were informed about the design, the design process, the mathematics behind the concept, and the code used to model the structure. The group was presented with various tasks associated with the production drawings and was free to organise smaller units. Each unit was responsible for structuring its working process and deciding how to use assigned production drawings and tools, with possible assistance from the design team.

After the structures were manufactured, assembled and erected and the exhibition was over, the design and design process was evaluated based on how well it responded to and handled the external constraints, the choices of internal constraints before the design process and the criteria set up during the design process. The predicted structural behaviour and analysis were tested by loading and pushing the structure. Rough measurements were made to check for similarity with the digital model or the expected difference.

In addition to our investigations, an open seminar was arranged before the structure was taken down to create an environment for a joint evaluation. Students, researchers and professionals were invited to a discussion where participants could give their opinions regarding improvements, new research questions and new insights.

From the input from the seminar, recordings and our investigations, the decisions made during the design process were assessed, and areas of improvement were identified for the next design iteration.

The methodology has been used in the case studies described in the appended Papers B and C. The methodology has been in successive case studies having similar constraints as in Paper C to gain knowledge and improve the design. While not published in any paper, the case studies are included in Appendices A and B.

6 Summary of papers and other important works

6.1 Papers

6.1.1 Paper A

Brick patterns on shells using geodesic coordinates

Emil Adiels, Mats Ander, Chris J. K. Williams

IASS Annual Symposium 2017 "Interfaces: Architecture. Engineering. Science"

It is a common desire to build a curved shell using a standardised building block, such as a brick, from a rational and economic perspective. However, generating brick patterns on a curved shell surface is not trivial. There exist heuristically developed patterns for traditional shapes (Figure 6.1 (a)), but no strategy applies to new designs of shells for more complex situations. We present two strategies for generating brick patterns on free-form shells and vaults using geodesic coordinates where the orthogonal trajectories separated by constant distance define the bed joints (Figure 6.1 (b))

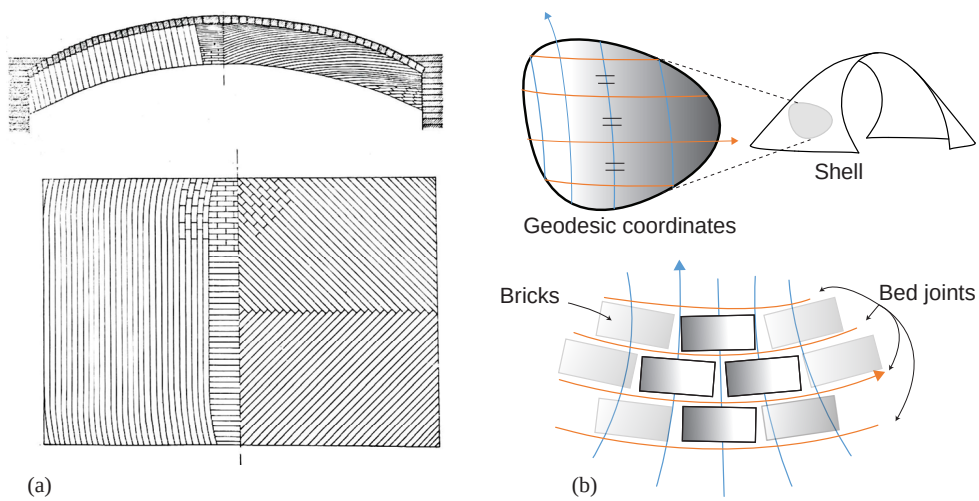

Figure 6.1: (*a*) *Brick patterns seen in (Paulsson & Granholm, 1953) where the brick patterns are described through the bed joints.* (*b*) *The idea presented in paper A is to use geodesic coordinates on a shell surface to describe the bed joints of brick patterns.*

The first strategy integrates the generation of the geodesic coordinates in a form finding procedure derived from the geometric and mechanical properties of a membrane shell. The geometric and structural equations are solved using dynamic relaxation. The second strategy can be applied on an arbitrary surface, separating the form finding and

brick pattern generation, enabling adaption to different constraints in the design process.

While it is structurally desirable to align the bed joints perpendicular to the principal stress as in the first strategy, the second strategy might be more desirable in actual projects since it can be combined with a structurally efficient shape while still offering flexibility for construction constraints.

Contributions by Emil Adiels

Emil Adiels, was the primary author of this paper and developed the code, implemented the method and generated the results of the second strategy in the paper. The idea was developed by Chris Williams and Emil Adiels during his master thesis. This paper extends those investigations but with further developed numerical methods. The paper was presented by Emil Adiels at the IASS 2017 symposium in Hamburg.

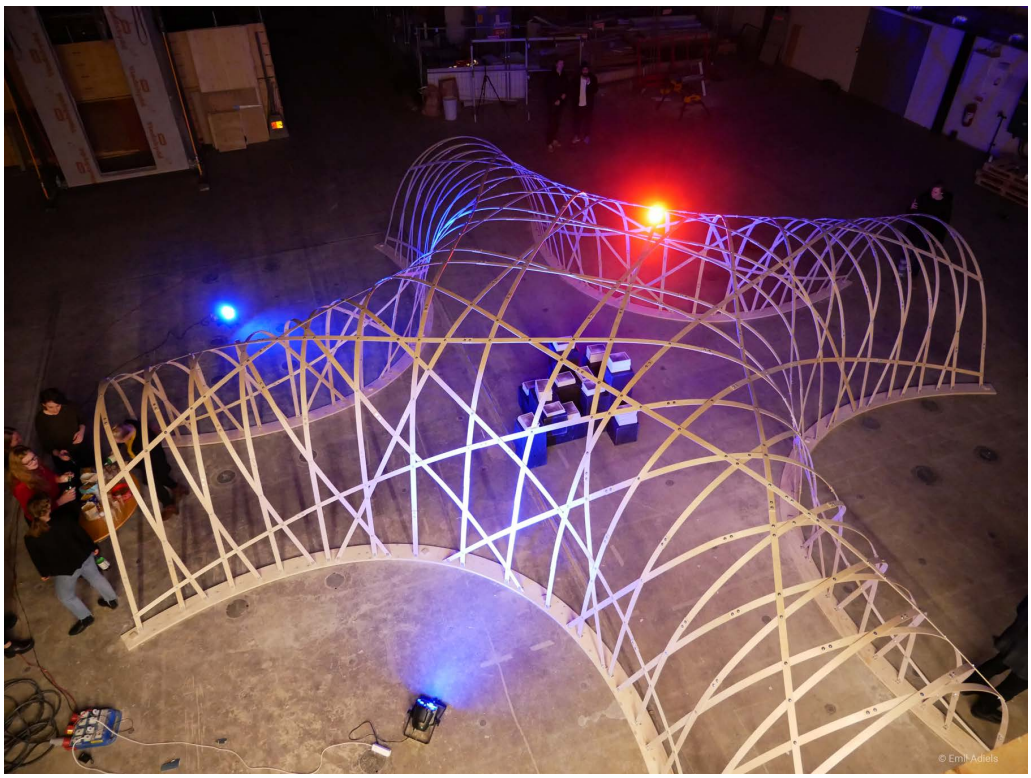

Figure 6.2: *The geodesic timber grid shell described in paper B.*

6.1.2 Paper B

Design , fabrication and assembly of a geodesic gridshell in a student workshop

Emil Adiels, Nicolo Bencini, Cecilie Brandt-Olsen, Al Fisher, Isak Näslund, Robert Otani, Emil Poulsen Emil, Puria Safari, Chris J. K. Williams

IASS Annual Symposium 2018 “Creativity in Structural Design”

Can concepts from differential geometry be used in designing a grid shell, integrating architectural qualities, structural requirements, rapid and material-efficient production and the use of techniques and skills in a local context? This paper describes how such a question was investigated during a two-day workshop. The specific concept investigated utilized geodesics, which are curves on a surface analogues with straight lines on a plane, allowing the grid shell to be made from straight planar plywood laths.

The proposal was to build an 11x11m grid shell that would be manufactured, constructed and assembled during a two-day workshop by undergraduate students. This paper describes the process of going from a geometric concept to production utilizing digital and computational tools. The design was incorporated in a fully parametric model, including automated design checks and the generation of all necessary production. Further, a description of manufacturing, which was made using primarily manual tools, and construction during the workshop is given. The final structure seen in Figure 6.2 was used for a book release party.

During the construction, two laths broke. The first had a knot in the middle layer, and the second broke near a connection in the finger joints of the plywood. To few material tests were performed to catch such possible defects in the plywood, and due to the small width of 50mm, the laths were extra sensitive. The spliced connection could also have been constructed to be less stiff to avoid stress concentrations and the second failure. However, since all production was done on-site, manufacturing and replacing the element was easy and quick.

While the structure was a temporary pavilion for indoor use, it still highlights and proves the possibility of using differential geometry early in the architectural design process together with digital tools to achieve the benefits of rapid production anchored in the local context.

Contributions by Emil Adiels

Emil Adiels, was the primary author and presented the paper at the IASS 2018 symposium at MIT in Boston. The preparation of the experiment including the design, building models and prototypes, acquiring materials and tools, writing code, informing the participants and generating production drawings was performed by Emil Adiels together with the other authors.

6.1.3 Paper C

The design , fabrication and assembly of an asymptotic timber gridshell

Emil Adiels, Cecilie Brandt-Olsen, Johanna Isaksson, Isak Näslund, Karl-Gunnar Olsson, Chris J. K. Williams

Proceedings of the IASS Annual Symposium 2019 - Structural Membranes 2019

The research question, equivalent to Paper B, concerns how geometry can be a tool in the architectural design process to develop a sustainable design that integrates space and structure with rational and time-efficient manufacturing and construction adapted to the local context. This was investigated by designing a grid shell 35 students could build in

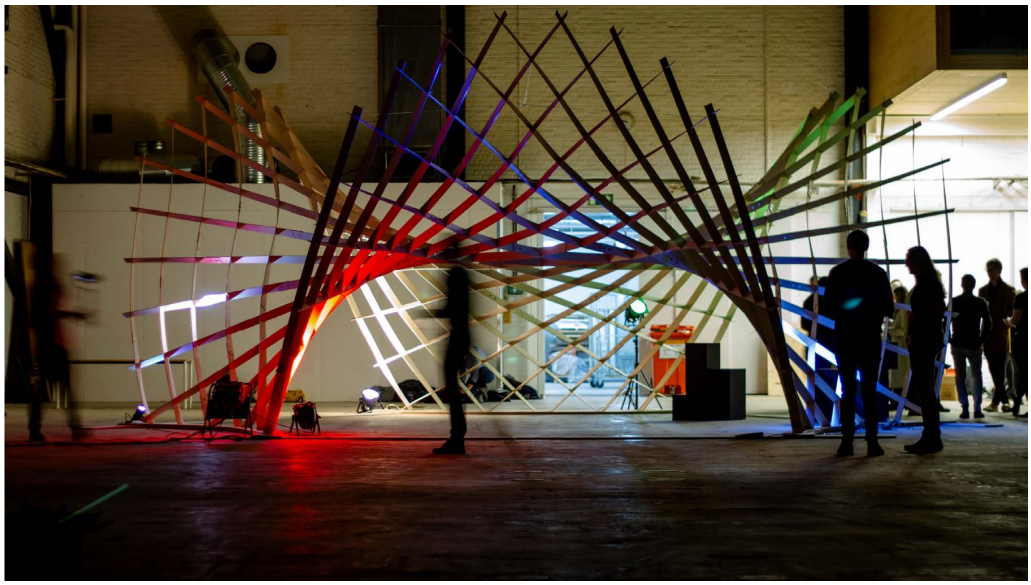

Figure 6.3: *The asymptotic timber grid shell described in paper C.*

two days, using simple building elements of straight plywood laths and simple on-site manufacturing techniques and tools. The design proposal was tested during a two-day workshop, with students (without prior construction experience) taking ownership of the manufacturing and construction based on drawings and instructions from the design team.

The shape of the grid shell was based on an Enneper surface of three-fold rotational symmetry with a boundary baseplate inscribed within a circle of 4.5m radius. Utilizing the concept of asymptotic curves, which are surface curves whose osculating plane coincides with the tangent plane of the surface, the structure was built using planar straight laths of plywood made using manually operated drills and saws. Using the mechanisms in the grid shell, the structure was assembled flat and erected to its final shape, achieving stability by anchoring it to the baseplate.

The structure would have benefited from locking the mechanism in the erected state to make it less flexible. Future work includes designing a structural node that is still easy and time-efficient to manufacture while allowing it to be assembled flat and erected but locking the mechanisms in the erected state.

Contributions by Emil Adiels

Emil Adiels, was the primary author of this paper and presented the paper at the IASS 2019 symposium in Barcelona. The preparation of the experiment including the design, building models and prototypes, acquiring materials and tools, writing code, informing the participants and generating production drawings was performed by Emil Adiels together with the other authors.

6.1.4 Paper D

The construction of new masonry bridges inspired by Paul Séjourné

Emil Adiels, Chris J. K. Williams

IASS Annual Symposium and Spatial Structures Conference: Inspiring the Next Generation

It is estimated that 40% of existing rail network bridges in Europe are masonry arches and many of them carry much higher loads than initially intended and require relatively little maintenance compared to modern bridges. What is unique about masonry bridges is that they contain a considerable amount of fill that is an integral part of their structural behaviour and performance. The fill spreads the load on the arch, and the weight makes the sensitive load combinations have less impact on the arch.

One issue of traditional masonry bridges is the lateral pressure on the wing walls. The concept presented in this paper combines the arch and the wing walls into a hydrostatic shell in compression in three dimensions. The single-span bridge also has a surface grid of geodesic coordinates enabling rational construction using bricks, as described in Paper A.

The form finding method for a single-span bridge takes its starting point from membrane theory. The equilibrium equations are derived such that the principal stresses follow geodesic coordinates. Examples are presented of how such a bridge could look, see Figure 6.4.

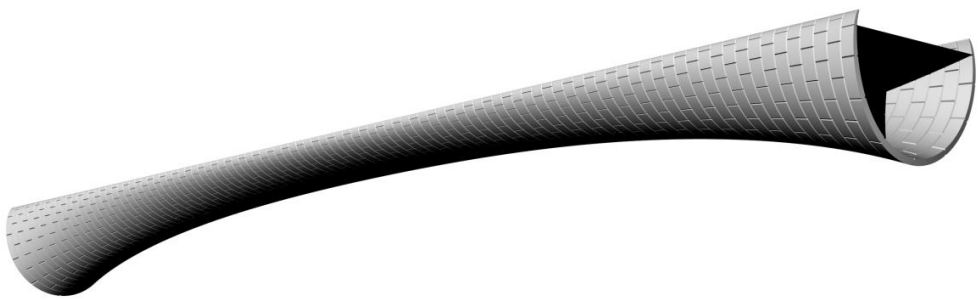

Figure 6.4: *Hydrostatic shell single-span masonry bridge from paper D.*

The presented method does not include the masonry's weight or the soil interaction. Further studies, including more detailed numerical analysis complemented by physical model tests, are needed to ensure how to improve the method and choose its parameters to better support the design of an actual bridge.

Contributions by Emil Adiels

Emil Adiels was the primary author of this paper and presented the paper at the IASS 2021 symposium in Surrey. Chris Williams and Emil Adiels developed the concept. The video presentation is publicly available online

6.1.5 Paper E

The architectural application of shells whose boundaries subtend a constant solid angle

Emil Adiels, Mats Ander, Chris J. K. Williams

Surface geometry plays a central role in the design of bridges, vaults and shells, using various techniques for generating a geometry which aims to balance structural, spatial, aesthetic and construction requirements. In this paper, we propose the use of surfaces defined such that given closed curves subtend a constant solid angle at all points on the surface and form its boundary.

Constant solid angle surfaces enable one to control the boundary slope and hence achieve an approximately constant span-to-height ratio as the span varies, making them structurally viable for shell structures. In addition, when the entire surface boundary is in the same plane, the slope of the surface around the boundary is constant and thus follows a principal curvature direction. Such surfaces are suitable for surface grids where planar quadrilaterals meet the surface boundaries. They can also be used as the Airy stress function in the form finding of shells having forces concentrated at the corners.

Our technique employs the Gauss-Bonnet theorem to calculate the solid angle of a point in space and Newton's method to move the point onto the constant solid angle surface. We use the Biot-Savart law to find the gradient of the solid angle. The technique can be applied in parallel to each surface point without an initial mesh, opening up for future studies and other applications when boundary curves are known but the initial topology is unknown. We show the geometrical properties, possibilities and limitations of surfaces of constant solid angle using examples in three dimensions.

It is possible to generate surfaces having multiple boundary curves positioned and angled in different planes with individually tuned currents in the wires. One drawback is that the principal curvatures no longer follow the boundary curves. However, it is possible to rotate the slope around each curve independently by varying the current in the equivalent wire. Thus, the shapes can still be useful, and they can be used for other surface grids and possibly in other fields where one needs to generate surfaces without an initial mesh.

The paper is currently under review but can be accessed as preprint https://arxiv.org/abs/2212.05913

Contributions by Emil Adiels

Emil Adiels, in dialogue developed the idea and theory behind the paper, with Chris Williams. Emil Adiels and Chris Williams wrote the paper together. Emil Adiels made the code to run the simulations and the images from the simulations.

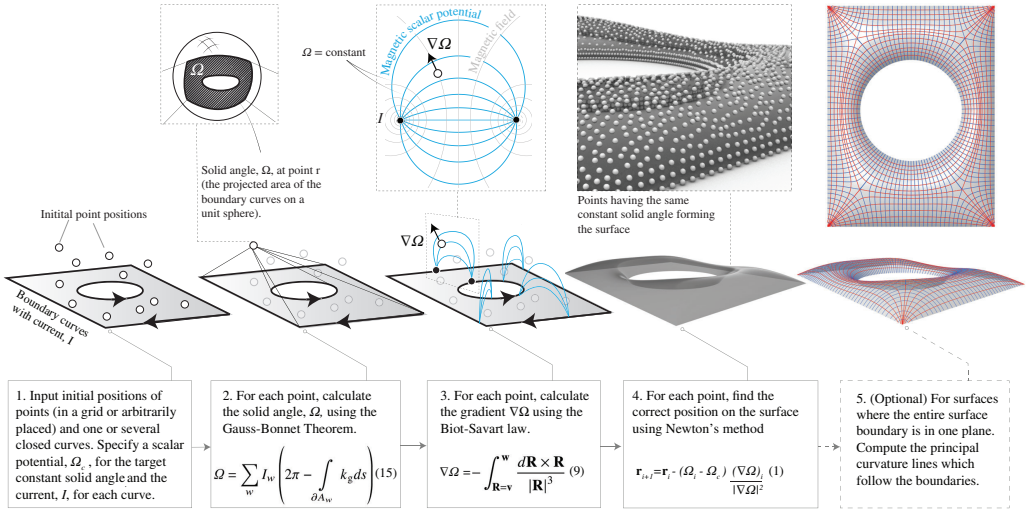

Figure 6.5: *The steps of our method for generating surfaces of constant solid angle, as described in paper E. The first four steps are necessary while the last step is optional and specifically interesting for surfaces where the entire boundary is in the same plane.*

6.1.6 Paper F

Internal force and moment surfaces for shells

Emil Adiels, Chris Williams

Shell and Spatial Structures: Proceedings of IWSS 2023

Shells are generally statically indeterminate structures, which means that there are different ways for them to carry a load. Form finding methods for shells traditionally concentrate on obtaining a geometry that can work primarily by membrane action. There are, however, certain situations where the boundary conditions make this impossible.

A technique in structural analysis is to imagine a statically determinate set of internal forces and moments in equilibrium with the externally applied loads together with a set of *redundant* statically indeterminate internal forces and moments in equilibrium with redundant support reactions, but zero loads. Thus, it is possible to superimpose redundant stresses and moments on those carrying loads to control the state of stress in the shell by modifying its stiffness properties.

We present a method to visualise the redundant forces and moments as vectors forming two surfaces in a shell only loaded at the boundaries (Figure 6.6). The surfaces can be used to produce desired stresses and internal moments.

Contributions by Emil Adiels

Emil Adiels was part of the dialogue and discussion that developed the idea and theory behind the paper with Chris Williams. Emil Adiels and Chris Williams wrote the paper together.

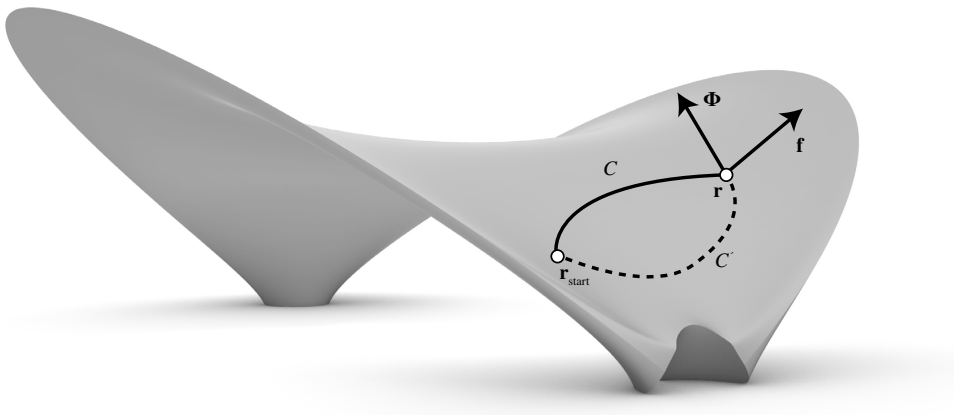

Figure 6.6: *The vectors* $\mathbf{\Phi}$ *and* $\mathbf{f}$ *represent the redundant moments and forces, forming two surfaces in a shell only loaded at the boundaries. These surfaces could be used to produce desired stresses and internal moments on the unloaded shell.*

6.2 Other publications

6.2.1 The historical and technological development of masonry structures

This work aims to study the technical development of masonry and brickwork structures in relation to architecture. Masonry buildings can remain for several hundred and sometimes over a thousand years. Therefore, a considerable part of the historic buildings and important cultural buildings that still exist are of masonry. Thus, masonry structures have much cultural value, but due to their long life spans they can also be important for sustainable construction in the future. The method is based on selecting built examples and parameters related to the knowledge and tools at the time of design and construction. The chosen parameters are used to evaluate the current ability and idioms regarding *geometry and mathematics, structural theory, design tools, production methods, material development,* and *architecture.* This work is centred around five examples from different periods: the cathedral of Saint-Denis, the dome of Santa Maria del Fiore, the third lighthouse of Eddystone by John Smeaton, the Boston public library and the unfinished crypt in Colonia Güell by Antoní Gaudí. Each example is placed within its historical context and evaluated based on the chosen parameters.

This work is expected to be published in 2024 and has been funded by ARQ, a research foundation by White architects, www.arqforsk.se.

Contributions by Emil Adiels

Emil Adiels is the sole author of this work.

6.2.2 The composition of matter, space and structure in shells and grid shells

The structural benefits of shells and grid shells are well known, but they also possess unique architectural and spatial qualities that are difficult to quantify. They are often a result of an architectural aspiration idea that, in the best examples, exists in an interplay with the load-bearing structure. The difficulty is communicating the architectural experience and qualities, such as materiality, spaciousness and light. Traditionally it is done through text and pictures, but is it the best way? It led to the research question of *how to communicate the spatial experience and spatial qualities of these spaces?* An experience that is both personal and subjective, so the challenge is to portray that feeling embodied in the architecture. The chosen method was using motion pictures accompanied by music. During trips worldwide, chosen objects were filmed and later edited with added music.

At the moment of writing, the result is eleven movies of eleven different buildings, which are 1.5 - 3 minutes long (Figure 6.7). A public viewing was held during the conference *Advances in Architectural Geometry* in 2018. The videos are also publicly available online at the webpage of Prof. Sigrid Adriaenssens' research group *Form finding lab* at Princeton University (2019). An interview concerning the work and purpose accompanies the videos.

The videos are published at: https://vimeo.com/showcase/5361926 and https://formfindinglab.wordpress.com/2019/02/28/what-i-am-thinking-movie-maker-and-masonry-specialist-emil-adiels/

Contributions by Emil Adiels

Emil Adiels is the sole contributor to this work. This includes preparing the shooting of the films, including trips and equipment. The movies were made by Emil Adiels including the shooting, editing and distribution.

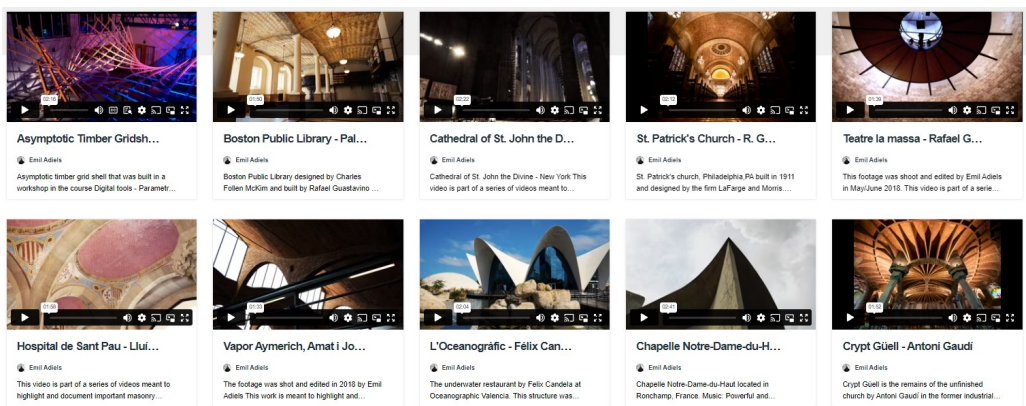

Figure 6.7: *Films capturing the architectural experience of shells and grid shells.*

6.3 Additional workshops

A set of exploratory workshops has been performed as a red thread through the investigations of geometry and shell structures. Two of the workshops are presented in Papers B and C. In addition, three of them have been of particular importance for the development of the thesis work: The further development of the concepts *Asymptotic timber grid shells* and the *Hydrostatic masonry bridges*, both themes illustrating the attempts to elaborate with the geometry of simple building elements to establish structurally efficient and spatial usable 3D shapes. A more comprehensive description of the implementation of these workshops is attached in Appendices A - C.

Summary of workshops:
2016-04 Smart Geometry (organiser), www.emiladiels.com/smartgeometry2016gotheburg
2017-04 Tensegrity and cable-stay structures, www.emiladiels.com/tensegrity
2017-08 The crafts and structural behaviour of masonry, www.vimeo.com/254638151
2017-12 Geodesic timber grid shell, Paper A.
2018-04 Minimal surfaces and fabric structures, www.vimeo.com/278508841
2018-12 Asymptotic timber grid shell, Paper B.
2019-04 Weaving and architecture, www.emiladiels.com/weavingworkshop2019
2019-12 Asymptotic timber grid shell 2019, Appendix A.
2021-12 Asymptotic timber grid shell 2021, Appendix B.
2022-04 Hydrostatic masonry bridges, https://www.emiladiels.com/hydrostatic
2022-12 Hydrostatic masonry bridges, Appendix D.
2023-12 Prestressed cable netw for concrete casting, www.emiladiels.com/cablestay-form

6.3.1 Asymptotic timber grid shells

Workshop 2019: Emil Adiels, Johanna Isaksson, Isak Näslund, Habiba Moubarak, Chris J. K. Williams

Chalmers University of Technology

Workshop 2021: Emil Adiels, Isak Näslund, Emil Poulsen, Puria Safari, Chris J. K. Williams

Chalmers University of Technology

These two workshops are further iterations based on the same concept of asymptotic timber gridshells described in Paper C. Thus, the main question and method are the same: how can geometry be a tool in the architectural design process to develop a sustainable design that integrates space, structure and rational and time-efficient manufacturing and construction adapted to the local context? The question is reformulated as a research challenge: design a structure 35 students can build in just two days, using simple building elements of straight plywood laths and simple on-site manufacturing techniques and tools. The design proposal is tested during a two-day workshop, with students (without prior experience of construction) taking ownership of the manufacturing and construction based on drawings and instructions from the design team.

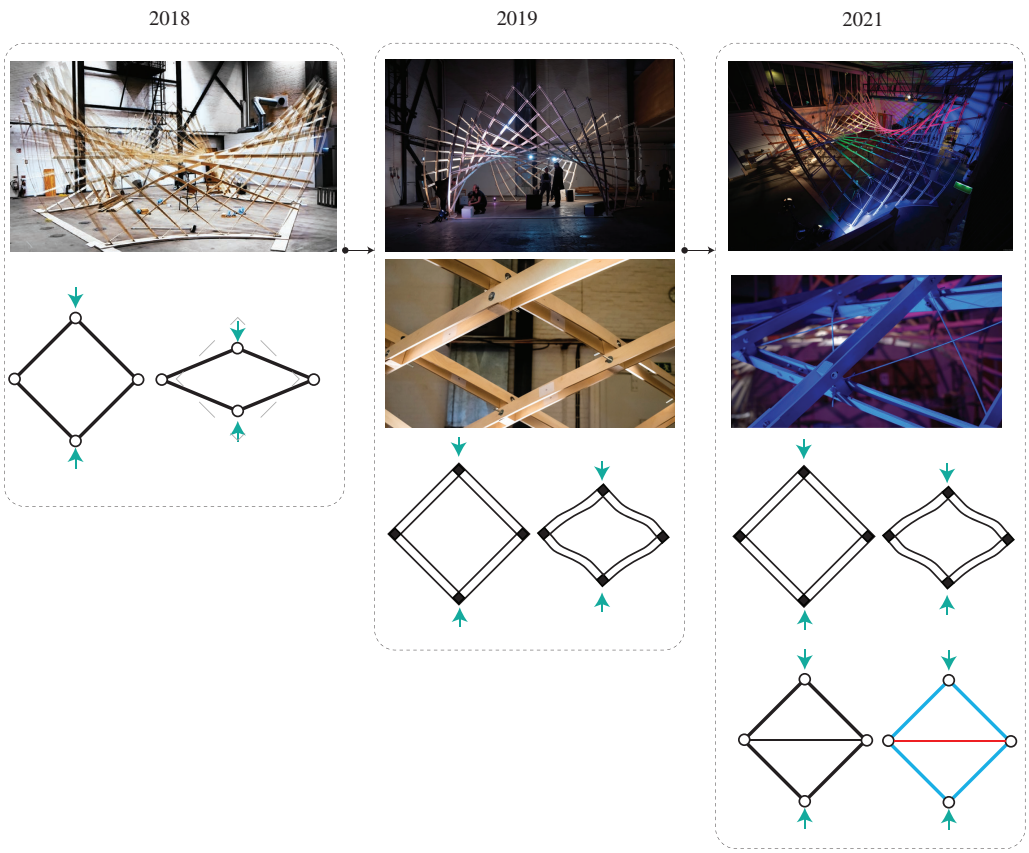

Figure 6.8: *The evolution and iterations of the design of the asymptotic timber gridshell. In 2019 the nodes were developed to handle the mechanism visible in the 2018 design through Viereendel action. In 2021 the node design was further refined to incorporate both bracing and Vierendeel action.*

Appendices A and B cover the design process behind the design proposals, describing how the design team tackled the complexity of converting a geometric concept into a functioning space and structure where all aspects must also be tested against the main constraints of simple and time-efficient manufacturing and construction. The same methodology as in Papers B and C was used, described in Section 5.3.3 and in Figure 5.7, incorporating geometric modelling and structural analysis and building physical models and prototypes.

The 2019 and 2021 designs both utilised the same surface and geometric idea of straight planar laths following the asymptotic lines, as well as the idea of assembling the structure flat and erect into its intended form. However, apart from the main objective, the specific objectives in both 2019 and 2021 were to iterate further and develop the nodal connections

from the grid shell in 2018 so that the mechanism utilized in the erection could be locked (see Figure 6.8), while still maintaining simple manufacturing and construction.

In 2019 (see Appendix A) the idea was to develop the node so that the mechanism was handled through Vierendeel action by stiffening the nodes. In 2021 (see Appendix B), the idea was to utilize a combination of Vierendeel action and bracing to make the structure even stiffer and be able to handle even bigger loads.

The resulting design and structure and the design process must be evaluated based on the fact that all parts were designed and executed with the simplicity of manufacturing and time efficiency as a top priority. While further improvements can be made in the future, much of it was a success since it is an example of the qualities in terms of space, structure and rapid manufacturing adapted to a local context, which can be achieved if concepts from differential geometry are applied early in the design process. A simple but efficient improvement of the design adjustment of the node designed in 2021 would be to move the bracing from the middle layer to the top or bottom of the grid. Removing the gap between the laths hinders the timber blocks from rotating, similar to the node design in 2019.

Contributions by Emil Adiels

The preparation of the experiment including the design, building models and prototypes, acquiring materials and tools, writing code, informing the participants and generating production drawings was performed by Emil Adiels together with the other members of the design team.

6.3.2 Hydrostatic masonry bridges

Emil Adiels, Fredrik Boman, Erik Wigh, Chris J. K. Williams

Chalmers University of Technology

Figure 6.9: *Physical model of a single-span hydrostatic masonry bridge built during a workshop in 2022.*

The objective of this case study and workshop was to design and build a model based on the concept of hydrostatic shells for masonry bridges covered in paper D. While paper D covers the historical context and the theory behind the form-finding, the purpose was to make a proof of concept model of a single span masonry bridge. The specific areas of interest were investigating how well the form finding could work in the design process and relating the design and dimensions to built masonry arch bridges.

The model was made from 3D-printed gypsum blocks assembled without any glue or mortar based on the assumptions from plasticity theory (Heyman, 1995) that the results are scalable. Similarly, the scale effects of the soil were removed by using dry sand, a cohesionless soil, for the fill.

The workshop resulted in the fabrication and assembly of two models with different cross-sectional profiles during the form finding, seen in Figure C.1 and Figure C.11.

Future work includes further analysis of these structures using numerical methods such as the discrete element method and comparing it with load tests on the models, as well as further evaluation if the normality condition is violated.

Contributions by Emil Adiels

The preparation of the experiment including the design, building models and prototypes, acquiring materials and tools, writing code, informing the participants and generating production drawings was performed by Emil Adiels together with the other members of the design team.

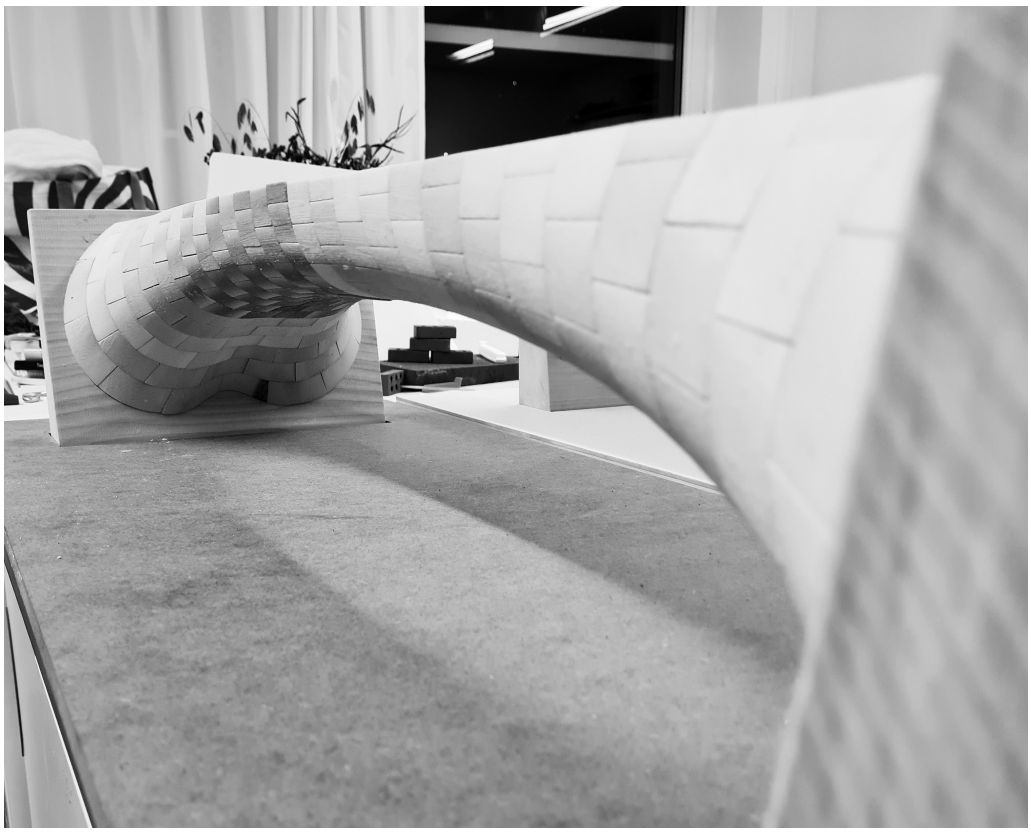

Figure 6.10: *Close-up of a physical model of a single-span hydrostatic masonry bridge built during a workshop in 2022, where the cross-section at mid-span is a superellipse or Lamé curve.*

7 Discussion and conclusion

This section contains reflections on the results and insights provided in the thesis as well as possible directions for future work.

7.1 Research question 1

How can differential geometry be used to design structurally efficient shells and shells with surface patterns for simple production?

Four studies related to this question have been performed and are found in Paper A, D, E and F. The key findings from these papers include four geometric concepts for the design of shell structures:

- A development of the use of *geodesic coordinates* for describing brick patterns on shells.
- *Surfaces of constant solid angle* subtended by surface boundaries, suitable for surface grids with planar panels or as Airy stress function when having planar boundaries.
- *Hydrostatic shells* for the design of more structurally efficient masonry bridges.
- *Internal force and moment surfaces* for the design of statically indeterminate shells.

Brick patterns on shells can be described through their bed joints using *geodesic coordinates*. In Paper A, we present two different techniques for implementing this in the design of new brick vaults. The first is a form finding technique generating a geodesic coordinate in compression. The second technique can be applied to free-form and form-found shells. The limitation that only bed joints are generated can be seen as an opening to interpret the design for a craftsman or craftswoman so they can use their skills and judgement to solve the details best since bricks can be easily managed and adapted on-site. Techniques meant to solve all problems could potentially restrict possible interpretations or adaptations on site, which can be difficult to foresee during the design phase. It is, therefore, a balancing act in creating a design technique that is an aid and can also be combined with the sound judgement and skills of other professions. In that sense, the second technique presented gives more freedom to elaborate and play with different patterns for production since it can be applied on a structurally viable surface in compression with the load generated using other form finding techniques. Papers published afterwards by Motamedi et al. (2020) and Carneau et al. (2019) have applied our concept in the context of 3D printing, where the bed joints represent each extruded layer instead. Thus, there might be other technologies and new applications in the future using the concept presented in Paper A.

One issue with traditional masonry arch bridges is the lateral pressure from the fill on the wing walls. In Paper D, we present a novel approach to designing modern masonry bridges such that the arch and wing wall are combined into a more structurally efficient *hydrostatic shell* in compression interacting with the load from the fill. In the case of

the single-span bridge, the principal stress follows the geodesics in a geodesic coordinate net such that the bridge can also be built using bricks based on the idea presented in Paper A. However, the technique and concept must not be restricted to brickwork. In some circumstances, it would perhaps be more appropriate to build it using stone cut with precision using digital fabrication techniques such as in the Armadillo Vault (Block et al., 2017) or Hyparvault (Fallacara, 2016), similar to the models we have built using 3D printed blocks assembled without mortar (see Appendix C). The bridges could also be made as concrete shells. Still, the technique opens up the possibility of creating sustainable infrastructure that can last centuries in areas lacking expensive fabrication but where bricks can be easily manufactured. As McKibbins (2006) states,

> Masonry arch bridges can be viewed as among the most sustainable structures ever to have been built. Many have already been in service for hundreds of years without significant repair or strengthening works — exceeding the design life requirements of modern structures. By contrast, many of the steel and concrete bridges built in the last century have required considerable expenditure on maintenance and repair or even replacement within the first 30—40 years of service. (p. 25)

Surface grids of planar panels aligned with the boundary can be achieved using *surfaces of constant solid* angle subtended by surface boundaries in the same plane, presented in Paper E. This is because one of the principal curvature directions follows the surface boundaries, and thus, a principal curvature net is consistent on the surface, which is a rare occurrence if one chooses a surface arbitrarily. From my experience working with geometry for grid shells and shells in real projects, the client, architect and manufacturer usually dislike cutting the panels off at the boundary due to clashes in the aesthetics and the manufacturing of specially made components. However, since the net is consistent, the panel dimensions may vary between small and large spans, which may or may not be a problem. An unusual and interesting aspect of the technique is that it does not require any topology in their generation. Each point can find its position on the surface and evaluate the surface curvature at the same position independently. Even though it is a purely geometric concept, the surfaces it produces are still structurally viable. However, more work would be needed to make it more stable for complex boundary curves in different planes. Constant solid angle surfaces can be used not only for the geometry of the actual shell surface but also for the Airy stress function. Having a constant slope along the edges, the forces are directed towards the corners of the boundary curve. Applicable to situations similar to the British Museum Court Roof, where the horizontal thrust is taken at the corners. This would be an alternative to Equation 3.36 used by Timoshenko and Woinowsky-Krieger (1959) and Billington (1965). Our method does not rely on any shear along the boundary but can be seen as a concentrated force along the edges, like a tension cable.

Shells are generally statically indeterminate structures, and in an unloaded shell, the redundant forces and moments can be represented by *internal force and moment surfaces*. The redundant forces and moments are the unknowns to be solved using the force method to analyse statically indeterminate structures. Thus, a speculative application of the concept can be in a case similar to the British Museum Court Roof, where relieving the

surrounding walls from lateral thrust makes it challenging to find a solution only using membrane action alone. Using the force method, fictitious supports can be added to make the shell statically determinate. The fictitious support reactions are then added as boundary loads to an unloaded shell where the *internal force and moment surfaces* can be used to produce desired stresses and internal moments to be superimposed on the statically determinate solution, as depicted in Figure 7.1. This speculative application of the geometric concept in Paper F could potentially be used to design a more elaborate use of the redundant stresses and moments to achieve a structurally and production-efficient solution. This could be a way to reintroduce the force method and its advantages in structural design and analysis, which might have been overshadowed due to the dominance of the displacement method used in computational methods like the finite element method.

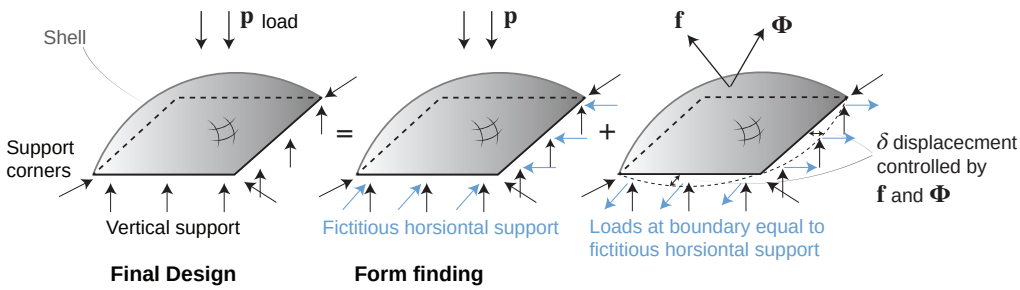

Figure 7.1: *Possible application of the internal force and moment surfaces* **f** *and* **Φ** *presented in paper F using the force method.*

7.2 Research question 2

How can differential geometry be applied in a design process supporting the quick production of a grid shell?

The question was studied through a series of case studies of geodesic and asymptotic timber grid shells presented in Papers B and C and Appendices A and B. The key findings from these studies are:

- Differential geometry in combination with simple building elements is a useful combination for rapid production and assembly making it possible to adapt to the constraints in a situation.
- Using symmetry greatly helped to increase the repetition of elements which increased the efficiency of manufacturing as well as a quicker assembly with less confusion.
- For such complex geometries, digital tools and parametric modelling environments are essential to assist the design process. Such tools are also critical for controlling

and checking the final design, accommodating changes and automatically generating the production drawings.

- Physical models and prototypes were essential to gain further understanding of the translation from geometry to a structure and how to improve the design.

There was a significant difference between the geodesic grid shell and the asymptotic grid shell in the flexibility during the design process. For the geodesic grid shell, the designer had much more freedom to shape the form and pattern, while the orientation of the laths gives less structural depth. For the asymptotic grid shell, the shape and the pattern are not separable. In our case studies, we were constrained to using minimal surfaces where the asymptotic lines intersect at right angles to achieve the simple construction. It was challenging to find a minimal surface that would also be suitable for the space as well as the structural form. In summary, whatever geometric concept chosen to achieve desirable features for manufacturing it will come with some cost or restrictions. The designer must find ways to deal with these restrictions to balance manufacturing with the spatial aspects and functional requirements during the design process.

In all the case studies, there was a limitation in that they were built and assembled indoors, meaning that to make the structures outdoors, a more detailed structural analysis would be needed to include wind and snow loads. However, in our case studies, the primary constraint was time, which required us to use manual tools since a CNC was too slow. Under other circumstances, having more time for manufacturing and with different manufacturing techniques, the possibility of handling the external loads would differ. One example of this is the Inside Out pavilion by Eike Schling, Denis Hitrec and Jonas Schikore (Schling et al., 2018). It also highlights the strengths and drawbacks of using case studies in research. Each situation is different, forcing new solutions and raising new insights, but it is sometimes also difficult to compare apples and oranges. Every project or design must be evaluated against how well it handles and responds to the constraints and limitations of each situation.

7.3 Future research

There are several directions in which the work can continue from this thesis, and I will mention a few:

Surfaces of constant solid angle subtended by the surface boundaries have some interesting properties. Since they do not require any information about internal connectivity, they could be helpful for various design situations. Thus, future work could improve the method's stability for more complex boundary curves situated in different planes. Most benefits come when these surfaces have boundary curves in the same plane. Therefore, future work could include implementing a varying current in the boundary such that the same benefits could be attained when having boundary curves at different levels.

The studies performed of *hydrostatic shells* have mainly concerned form finding. In the case of multi-span bridges, it is more complicated than single-span bridges. More studies would be needed on how to treat the free edges on top of the bridge, which are sensitive. While there exists much work and understanding of traditional arch bridges

interacting with fill, more studies are needed to understand the structural behaviour of hydrostatic shells. Soil and structure interaction is relatively complicated, and such investigation would ideally involve physical model tests and computer simulations. The results from the model tests and simulations could inform how to improve the shape and what considerations to include in or improve the form finding technique.

Since shells are generally, to a high degree, statically indeterminate structures the ability to steer or redirect forces and moments to achieve more elaborate use of the shell is intriguing. The geometric concept of representing the redundant forces and moments as *internal force and moment surfaces* could be the first step to developing a theoretical framework for such a technique. Still, the technique and application are currently speculative as described in Section 7.1. Thus, future work would be to develop further the theory and a method or technique implementing these ideas that can applied in the design process.

In the workshops (Papers B and C and Appendices A and B), design inquiries were used within a framework that one might refer to as *a workshop culture*. These workshops have four characteristic features: *simple building elements*, *student participation*, *collaboration with external partners* and *short construction time*. It would be interesting to investigate further the value and benefits of using design inquiries in a workshop culture. One such aspect to be further developed could be to build the structures outdoors while still temporarily for a year. It would require more detailed structural analysis, but it could also generate other insights being exposed to other conditions and used by the public.

7.4 Conclusion

While shells have been used less in structural and architectural design over the last hundred years, they still have a huge potential for tackling the sustainability challenges of the built environment we are facing now. Their structural efficiency makes it possible to work with materials with low embodied carbon. They can also be used with highly durable materials like stone or bricks in bridges that can stand for hundreds of years and possibly carry heavier trains or loads than we can possibly imagine today, like previous generations of bridge builders and designers.

Still, one of the great complexities with shell structures is understanding their structural behaviour and construction. My studies confirm that knowledge of differential geometry and skills in implementing digital tools or computational tools enables one to handle constraints such that the building blocks are adapted to the available local resources and technology. However, it is important to be humble since most shells have likely been built with little or no knowledge of shell theory or differential geometry. Many shell builders were practical people like Gaudí and Guastavino Sr. Even today, one can still see clips of brick vaults being built without falsework (Priske, 2013), which is difficult to explain or analyse using shell theory, but rather through an intuitive understanding based on experience from practically working with these structures. Ideally, you would need to exercise both theory and practice which have been the case in this thesis. That is the joy of shell structures. Their structural behaviour is both so simple and so complex that you cannot really answer what you need to know before taking up a brick and starting to

build a structure that can stand several lifetimes. Returning to the quote by Christopher Alexander et al. (1977)

> The central problem of materials, then, is to find a collection of materials which are small in scale, easy to cut on site, easy to work on site without the aid of huge and expensive machinery, easy to vary and adapt, heavy enough to be solid, longlasting or easy to maintain, and yet easy to build, not needing specialised labor, not expensive in labor, and universally obtainable and cheap. (p.956)

Is it an imaginary material, or is it possibly, as Carolyn Haynes (2019) say, just a good description of a brick? Hopefully, the work described in this thesis can help bring bricks, masonry and timber laths back to their place as load-bearing structures in buildings and bridges.

References

Addis, B. (2007). *3,000 Years of Design, Engineering, and Construction*. Phaidon Press;

Addis, B. (2014). Physical modelling and form finding. In S. Adriaenssens, P. Block, D. Veenendaal, & C. J. K. Williams (Eds.), *Shell structures for architecture: Form finding and optimization*. Routledge.

Adiels, E. (2022a). Bracing options for asymptotic gridshell 2021. https://vimeo.com/710266727

Adiels, E. (2016). *Structural influence of the geometry of masonry vaults: Brick tiling patterns for compression shells using geodesic coordinates* [MSc Thesis]. Chalmers University of Technology. https://doi.org/10.13140/RG.2.2.23041.71521

Adiels, E. (2018). Fabrication and assembly of an actively bent plywood geodesic gridshell - student workshop, 2017. https://www.youtube.com/watch?v=cTRvXiK9dK8

Adiels, E. (2019a). Making the slots - asymptotic timber gridshell 2.0. https://vimeo.com/376146710

Adiels, E. (2019b). Modal analysis of asymptotic gridshell ii. https://vimeo.com/338759055

Adiels, E. (2019c). Prototype of asymptotic timber gridshell 2.0. https://vimeo.com/373409998

Adiels, E. (2019d). Simulating the erection procedure of the Asymptotic gridshell on Vimeo. Retrieved May 23, 2019, from https://vimeo.com/312943826

Adiels, E. (2020a). Asymptotic timber gridshell 2.0 - timelapse. https://vimeo.com/385822144

Adiels, E. (2020b). Disassembly of asymptotic timber gridshell 2.0 - timelapse. https://vimeo.com/395064638

Adiels, E. (2022b). Asymptotic timber gridshell 2.5 - timelapse day 1 and day 2. https://vimeo.com/738990590

Adiels, E. (2022c). The design and construction of a hydrostatic masonry bridge model. https://vimeo.com/738324107

Adiels, E., Ander, M., & Williams, C. J. K. (2023). *The architectural application of shells whose boundaries subtend a constant solid angle* [Under review (first revision, October 2023)].

Adiels, E., Ander, M., & Williams, C. J. K. (2017). Brick patterns on shells using geodesic coordinates. *IASS Annual Symposium 2017 "Interfaces: Architecture. Engineering. Science"* (September) (2017), 1–10.

Adiels, E., Bencini, N., Brandt-Olsen, C., Fisher, A., Näslund, I., Otani, R. K., Poulsen, E., Safari, P., & Williams, C. J. K. (2018). Design , fabrication and assembly of a geodesic gridshell in a student workshop. *IASS Annual Symposium 2018 "Creativity in Structural Design"* (2018), 1–8.

Adiels, E., Brandt-Olsen, C., Isaksson, J., Näslund, I., Olsson, K.-G., Poulsen, E., & Williams, C. J. K. (2019). The design , fabrication and assembly of an asymptotic timber gridshell. *Proceedings of the IASS Annual Symposium 2019 - Structural Membranes 2019* (October) (2019), 1–8.

Adiels, E., & Williams, C. J. K. (2021). The construction of new masonry bridges inspired by Paul Séjourné. *IASS Annual Symposium and Spatial Structures Conference: Inspiring the Next Generation* (August) (2021).

Adiels, E., & Williams, C. J. K. (2024). Internal force and moment surfaces for shells. In S. Gabriele, A. Manuello Bertetto, F. Marmo, & A. Micheletti (Eds.), *Shell and spatial structures* (pp. 118–128). Springer Nature Switzerland.

Adriaenssens, S., Barnes, M., Harris, R., & Williams, C. J. (2014). Dynamic relaxation. In *Shell structures for architecture: Form finding and optimization*. Routledge.

Adriaenssens, S. (2019). What I am thinking: movie maker and masonry specialist Emil Adiels. Retrieved July 7, 2020, from https://formfindinglab.wordpress.com/2019/02/28/what-i-am-thinking-movie-maker-and-masonry-specialist-emil-adiels/

Adriaenssens, S., Barnes, M., Harris, R., & Williams, C. J. K. (2014). Designed of a strained timber gridshell. In *Shell structures for architecture: Form finding and optimization* (pp. 89–102). Routledge.

Airy, G. B. (1863). On the Strains in the Interior of Beams. *Philosophical Transactions of the Royal Society of London* **153** (1863), 49–79. https://www.jstor.org/stable/108789

Alcaide, R. C. (2011). Stairs in the Architecture Notebook of Juan de Portor y Castro: An Insight into Ruled Surfaces. *Nexus Network Journal* **13**.(3) (2011), 631–648. https://doi.org/10.1007/s00004-011-0084-2

Alexander, C., Ishikawa, S., Silverstein, M., & Jacobson, M. (1977). *A pattern language : towns, buildings, construction.* Oxford U.P.
Accession Number: clc.ff99e3c4.bd8b.4fc2.9430.f76ce23bbfaa; Publication Type: Book; Physical Description: xliv, 1171 s. ill.; Language: English.

Allen, E., & Zalewski, W. (2009). *Form and Forces: Designing Efficient, Expressive Structures*. WILEY.

Anderson, S. (Ed.). (2003). *Eladio Dieste: Innovation in Structural Art*. Princeton Architectural Press. http://archnet.org/library/documents/one-document.jsp?document%7B%5C_%7Did=4784

Arlander, A. (2014). On Methods of Artistic Research. In *Method - process - reporting: Articles, reviews and reports of the ongoing development on artistic research* (pp. 26–39).

Asplund, S. O. (1964). *Matrix formulation of structural analysis for electronic computations.*

Balagué, A. C., & Moreno-Navarro, J. L. G. (1990). Gaudí y el misterio de la encarnacíon (las incógnitas de la cripta de la colonia Güell). *Informes de la Construcción* **42**.(408) (1990), 63–76.

Bannister, T. C. (1968). The Roussillon Vault : The Apotheosis of a " Folk " Construction The Roussillon Vault The Apotheosis of a " Folk " Construction. *Journal of the Society of Architectural Historians* **27**.(3) (1968), 163–175.

Barnes, M. R. (1977). *Form finding and analysis of tension space structures by dynamic relaxation.* [Doctoral dissertation, City University London].

Barnes, M. R. (1988). Form-Finding and analysis of prestressed nets and membranes. **30**.(3) (1988).

Barnes, M. R. (1999). Form finding and analysis of tension structures by dynamic relaxation. *International Journal of Space Structures* **14**.(2) (1999), 89–104. https://doi.org/10.1260/0266351991494722

Barrow, I. (1670/1916). *The geometrical lectures of Isaac Barrow (child, j. m, trans.)* [(Original work published 1670)]. https://archive.org/embed/geometricallectu00barr

Bendsøe, M. P. (1995). *Optimization of Structural Topology, Shape, and Material*. https://doi.org/10.1007/978-3-662-03115-5

Benvenuto, E. (1991). *An Introduction to the History of Structural Mechanics. Part II: Vaulted Structures and Elastic Systems*. Springer New York.

Billington, D. P. (1965). *Thin shell concrete structures*. McGraw-Hill.

Bix, R. A., & D'Souza, H. J. (n.d.). Analytic geometry. Retrieved 2020, from https://www.britannica.com/science/analytic-geometry

Block, P., & Ochsendorf, J. (2007). Thrust network analysis: A new methodology for three-dimensional equilibrium. *Journal of the International Association for Shell and Spatial Structures* **48**.(155) (2007), 167–173.

Block, P., Van Mele, T., Rippman, M., & Paulson, N. (2017). *Beyond Bending: Reimagining Compression Shells*. Detail Busniness Information GmbH.

Borgdorff, H. (2007). The Debate on Research in the Arts. *Dutch Journal of Music Theory* **12**.(1) (2007), 1–17.

Bosch. (n.d.). Bosch gcm12sd dual-bevel glide miter saw. https://boschtools.com/us/en/boschtools-ocs/miter-saws-gcm12sd-33969-p/

Box, G. E. P., & Draper, N. R. (1987). *Empirical Model-Building and Response Surfaces*. Wiley. https://books.google.se/books?id=QO2dDRufJEAC

Brandt - Olsen, C., & Solly, J. (n.d.). K2engineering. https://github.com/CecilieBrandt/K2Engineering

Brencich, A., & Morbiducci, R. (2007). Masonry arches: Historical rules and modern mechanics. *International Journal of Architectural Heritage* **1** (2 2007, May), 165–189. https://doi.org/10.1080/15583050701312926

Caldenby, C., Borgström, O., Olsson, K.-G., Jansson, U., Lund, M., Dahlberg, J., & Isaksson, J. (2017). *Architecture and engineering - 10 years anniversary book*. https://research.chalmers.se/publication/247048

Calladine, C. R. (1977). The static-geometric analogy in the equations of thin shell structures. *Mathematical Proceedings of the Cambridge Philosophical Society* **82**.(2) (1977), 335–351. https://doi.org/10.1017/S0305004100053974

Calladine, C. R. (1982). The theory of shell structures Aims and methods. *International Journal of Mechanical Sciences* **24**.(4) (1982), 219–230. https://doi.org/10.1016/0020-7403(82)90076-5

Calladine, C. R. (1983). *Theory of Shell Structures*. Cambridge University Press. https://doi.org/10.1115/1.3167758

Calvo-López, J. (2020). *Stereotomy: Stone construction and geometry in Western Europe 1200–1900*. Birkhäuser Cham. https://doi.org/https://doi.org/10.1007/978-3-030-43218-8

Campbell, J. (2003). *Brick: A world history*. Thames & Hudsaon Ltd.

Carfrae, T., & Michael, D. (2019a). Alistair day and the origins of dynamic relaxation. Part 1: Bringing an idea to life. *Structural Engineer* (June) (2019), 20–26.

Carfrae, T., & Michael, D. (2019b). Alistair day and the origins of dynamic relaxation. Part 2: A practice viewed through projects. *Structural Engineer* (July) (2019), 12–18.

Carneau, P., Mesnil, R., Roussel, N., & Baverel, O. (2019). An exploration of 3d printing design space inspired by masonry. *IASS Symposium 2019, "Form and Force"* (October) (2019). https://doi.org/10.5281/zenodo.3563672

Chace, A. B., & Mannin, H. P. (1927). *The Rhind Papyrus Volume 1: British Museum 10057 and 10058*. Mathematical Association of America.

Chebyshev, P. L. (1887/1946). On the cutting of garments. *Uspekhi Mat. Nauk* **1**.(Issue 2(12)) (1887/1946), 38–42. https://doi.org/10.18287/0134-2452-2015-39-4-459-461.

college Cambridge, Q. (n.d.). Mathematical bridge (). https://www.queens.cam.ac.uk/visiting-the-college/history/college-facts/mathematical-bridge

Collins, G. R. (1960). *Antonio Gaudí*. George Braziller Inc.

Collins, G. R. (1963). Antonio Gaudi : Structure and Form. *Perspecta* **8** (1963), 63–90.

Collins, G. R. (1968). The transfer of thin masonry vaulting from Spain to America. *Journal of the Society of Architectural Historians* **27**.(3) (1968), 176–201.

Cornell, E. (1961). Humanistic enquiry into architecture. *Architectural Science Review* **4** (1 1961), 25–41[1] E. Cornell, "Humanistic enquiry into arch. https://doi.org/10.1080/00038628.1961.9696015

Cornell, E. (1979). *Byggnadstekniken : Metoder och idéer genom tiderna*. Byggförl.

Courant, R. (1943). Variational methods for the solution of problems of equilibrium and vibrations. *Bulletin of the American Mathematical Society* **49** (1943), 1–23.

Crane, K., de Goes, F., Desbrun, M., & Schröder, P. (2013). Digital Geometry Processing with Discrete Exterior Calculus. *ACM SIGGRAPH 2013 courses* **30664** (2013), 126.

Cremona, L. (1872). *Le figure reciproche nella statica grafica*. Tipografia di Giuseppe Bernardoni. https://doi.org/10.3931/e-rara-18757

Culmann, C. (1866). *Die graphische Statik*. Meyer & Zeller. https://doi.org/10.3931/e-rara-20052

Day, A. S. (1965). An introduction to dynamic relaxation. *The Engineer* (219) (1965), 218–221.

Delataille, É. (1887). Art du trait pratique de charpente / par Émile Delataille ... (1887). https://gallica.bnf.fr/ark:/12148/bpt6k8505503/f2.item.langFR%7B%5C#%7D

Delorme, P. (1567). Le Premier tome de l'Architecture de Philibert de L'Orme ... (1567). http://www.mdz-nbn-resolving.de/urn/resolver.pl?urn=urn:nbn:de:bvb:12-bsb10195337-1

Derand, F. (1643). *L'Architecture des voûtes, ou l'Art des traits et coupe des voûtes... par le R. P. François Derand,...* S. Cramoisy.

Dirac, P. A. M. (1975). *General theory of relativity*. Wiley.

Dirac, P. (1975). *General Theory of Relativity*.

do Carmo, M. (1976). Differential geometry of curves and surfaces. https://doi.org/10.1007/978-3-319-39799-3

Dürer, A. (1525). Underweysung der Messung, mit dem Zirckel und Richtscheyt, in Linien, Ebenen unnd gantzen corporen. https://digital.slub-dresden.de/werkansicht/dlf/17139/1/0/

Edmondson, A. J. (1970). Solution of shell problems by finite difference method. *Nuclear Engineering and Design* **11**.(2) (1970), 208–216. https://doi.org/10.1016/0029-5493(70)90144-5

Einstein, A. (1920). *Relativity; the special and general theory* (R. W. Lawson, Trans.). Hentry Holt; Company. https://archive.org/embed/cu31924011804774

Escher, C. (2017). Model-experiment-environment. In G. Vrachliotis, J. Kleinmanns, M. Kunz, & P. Kunz (Eds.), *Frei otto: Thinking by modelling*. Spector books.

Euler, L. (1767). Recherches sur la courbure des surfaces. *Mémoires de l'academie des sciences de Berlin* **16** (1767), 119–143.

Faber, C. (1963). *Candela: The Shell Builder*. Reinhold Publishing Corporation. https://catalog.hathitrust.org/Record/000452039

Fallacara, G. (2016). *Architectural stone elements: Research, design and fabrication*. Presses des Ponts.

Fitchen, J. (1961). *The construction of gothic cathedrals: A study of medieval vault erection*. Oxford University Press.

Flügge, W. (1960). *Stresses in shells*. Springer-Verlag.

Fontana, C. (1694). *Il Tempio Vaticano e sua origine : con gl'edifitii più cospicui, antichi e moderni, fatti dentro e fuori di esso*. In Roma : Nella stamparia di Gio. Francesco Buagni. https://archive.org/details/gri%7B%5C_%7D33125008467413/page/n11/mode/2up

Forest Plywood. (n.d.). Grades of plywood. https://forestplywood.com/blog/about-plywood/grades-of-plywood/

Frankl, P. (1962). *Gothic Architecture*. Penguin Books.

Frayling, C. (1993). Research in art and design. *Royal College of Art Research Papers* **1**.(1) (1993), 1–5.

Frézier, A. (1739). *La théorie et la pratique de la coupe des pierres et des bois pour la construction des voûtes et autres parties des bâtiments civils & militaires, ou Traité de stéréotomie, à l'usage de l'architecture. Tome 3*. https://gallica.bnf.fr/ark:/12148/bpt6k85688q

Fuller, R. B. (1954). Building Construction [U.S. Patent 2,682,235]. pdfpiw.uspto.gov/.piw?docid=02682235

Gauss, K. F. (1825/1827/1902). General Investigations of Curved Surfaces of 1827 and 1825. Translated by Morehead J. C. and Hiltebeitel A. M. [(Original work published 1825 and 1827)]. *The Mathematical Gazette* **2**.(35) (1825/1827/1902), 215. https://doi.org/10.2307/3604249

Geib, P. R., & Jolie, E. A. (2008). The role of basketry in early holocene small seed exploitation: Implications of a ca. 9,000 year-old basket from Cowboy Cave, Utah. *American Antiquity* **73**.(1) (2008), 83–102. https://doi.org/10.1017/S0002731600041299

Gooding, D. (1985). 'In Nature's School': Faraday as an Experimentalist. In D. Gooding & F. A. J. L. James (Eds.), *Faraday rediscovered: Essays on the life and work of michael faraday, 1791-1867*. THE MACMILLAN PRESS LTD.

Goodstein, J. R. (2018). *Einstein's italian mathematicians: Ricci, Levi-Civita, and the birth of general relativity*. American Mathematical Society.

Green, A. E., & Zerna, W. (1968). *Theoretical elasticity* (2nd). Oxford University Press.

Green, A., & Zerna, W. (1968). *Theoretical elasticity* (2nd). Oxford University Press.

Grøn, Ø., & Næss, A. (2011). *Einstein's Theory : a rigorous introduction for the mathematically untrained*. https://doi.org/https://doi-org.proxy.lib.chalmers.se/10.1007/978-1-4614-0706-5

Hammond, M., & Wellington, J. (2021). *Research Methods; The Key Concepts; Second Edition*. Routledge.

Happold, E., & Liddell, W. I. (1975). Timber Lattice Roof for the Mannheim Bundesgartenschau. *Structural Engineer* **53**.(3) (1975), 99–135.

Harding, J. E., Hills, S., Brandt-olsen, C., & Melville, S. (2017). The UWE Research Pavilion 2016. *Proceedings of the IASS Annual Symposium 2017 "Interfaces: architecture.engineering.science"* (2017).

Hauberg, J. (2011). Research by Design - a research strategy. *AE... Revista Lusófona de Arquitectura e Educação* **5** (2011), 46–56. https://revistas.ulusofona.pt/index.php/revlae/issue/view/213

Hawking, S. (2005). *God created the integers: The mathematical breakthroughs that changed history*. Penguin Books.

Hayashi, K., Jikumaru, Y., Ohsaki, M., Kagaya, T., & Yokosuka, Y. (2021). Discrete Gaussian Curvature Flow for Piecewise Constant Gaussian Curvature Surface. *CAD Computer Aided Design* **134** (2021), 102992. https://doi.org/10.1016/j.cad.2021.102992

Haynes, C. (2019). *Brick: A Social History*. The History Press.

Herodotus. (440 B.C). The History of Herodotus (G. Rawlinson, Trans.). **2** (440 B.C). http://classics.mit.edu/Herodotus/history.2.ii.html

Heyman, J. (1972). *Coulomb's memoir on statics: An essay in the history of civil engineering*. Cambridge University Press.

Heyman, J. (1982). *The masonry arch*. Ellis Horwood Ltd.

Heyman, J. (1995). *The Stone Skeleton: Structural Engineering of Masonry Architecture*. Cambridge University Press.

Heyman, J. (1998). *Structural analysis: A historical approach*. Cambridge University Press.

Heyman, J. (2015). Jacques Heyman, The membrane analysis of thin masonry shells. https://www.youtube.com/watch?v=DI-leSI68dM%7B%5C&%7Dfeature=youtu.be%7B%5C&%7Dab%7B%5C_%7Dchannel=BibliothecaMechanico-Architectonica

Hyde, S., Ninham, B. W., Andersson, S., Larsson, K., Landh, T., Blum, Z., & Lidin, S. (1997). The Mathematics of Curvature. In *The language of shape* (pp. 1–42). https://doi.org/10.1016/b978-044481538-5/50002-2

IEA. (2019). *Global Status Report for Buildings and Construction 2019* (tech. rep.). Paris. https://www.iea.org/reports/global-status-report-for-buildings-and-construction-2019

Ingold, L., & Rinke, M. (2015). Sergio musmeci's search for new forms of concrete structures. *Fifth International Construction History Congress* (2015).

Kärrholm, G., & Samuelsson, A. (1972). Analysis of a prestressed cable-roof anchored in a space-curved ring beam. *IABSE congress report* (9) (1972).

Klaus, B., Berthold, B., & Frei, O. (1987). *Seifenblasen - Forming bubbles, IL 18*. Institut für leichte Flächentragwerke.

Kurrer, K.-E. (2008). *The history of the theory of structures - From arch analysis to the computational mechanics*. Ernst & Sohn Verlag für Architektur und technische Wissenschaften GmbH & Co.

Lawson, B. (2006). *How designers think: The design process demystified* (Fourth). Architectural Press.

Liddell, I. (2015). Frei Otto and the development of gridshells. *Case Studies in Structural Engineering* **4** (2015), 39–49. https://doi.org/10.1016/j.csse.2015.08.001

Linkwitz, K. (2014). Force density method: Design of a timber shell. In *Shell structures for architecture: Form finding and optimization* (pp. 59–69). Routledge.

Linkwitz, K., & Schek, H. J. (1971). Einige Bemerkungen zur Berechnung von vorgespannten Seilnetzkonstruktionen. https://doi.org/10.1007/BF00532146

Manzanares, G. L. (2003). The XVIIth century: Carlo Fontana's expertises. *First International Congress on Construction History* (January) (2003).

Maxwell, J. C. (1874). PLATEAU ON SOAP-BUBBLES. *Nature* **X**.(242) (1874), 119–121.

Maxwell, J. C. (1864). XLV. On reciprocal figures and diagrams of forces. *The London, Edinburgh, and Dublin Philosophical Magazine and Journal of Science* **27**.(182) (1864), 250–261. https://doi.org/10.1080/14786446408643663

McKibbins, L. D., Melbournce, C., Sawar, N., & Gaillard, C. S. (2006). *Masonry arch bridges: condition appraisal and remedial treatment* (tech. rep.). CIRIA.

McRobie, A. (2017). *The seduction of curves: The lines of beauty that connect mathematics, art, and the nude*. Princeton University Press.

McRobie, A., & Williams, C. (2018). Discontinuous Maxwell–Rankine stress functions for space frames. *International Journal of Space Structures* **33**.(1) (2018), 35–47. https://doi.org/10.1177/0266351118763500

Meyer, M., Desbrun, M., Schröder, P., & Barr, A. H. (2003). Discrete differential-geometry operators for triangulated 2-manifolds. In *Visualization and mathematics iii*. Springer-Verlag Berlin Heidelberg.

Motamedi, M., Oval, R., Carneau, P., & Baverel, O. (2020). Supportless 3D Printing of Shells: Adaptation of Ancient Vaulting Techniques to Digital Fabrication. In *Impact: Design with all senses*. https://doi.org/10.1007/978-3-030-29829-6

Nodargi, N. A., & Bisegna, P. (2022). A finite difference method for the static limit analysis of masonry domes under seismic loads. *Meccanica* **57**.(1) (2022), 121–141. https://doi.org/10.1007/s11012-021-01414-3

Ochsendorf, J. (2010). *Guastavino Vaulting: The Art of Structural Tile*. Princeton Architectural Press.

Ochsendorf, J., & Antuña Bernardo, J. (2003). Eduardo Torroja and ≪Cerámica Armada≫. *Proceedings of the First International Congress on Construction History* (January) (2003).

Oden, J. T. (1987). Historical comments on finite elements. *Proceedings of the ACM Conference on History of Scientific and Numeric Computation, HSNC 1987* **1987-January** (1987), 125–130. https://doi.org/10.1145/87252.88083

Olsson, K.-G. (2005). *Strukturmekanik & arkitektur : Om strukturmekanisk förståelse i gestaltningsprocessen.* Chalmers tekniska högskola. https://search.ebscohost.com/login.aspx?direct=true&db=cat09075a&AN=clpc.oai.edge.chalmers.folio.ebsco.com.fs00001000.89988b0f.fb7f.412c.8feb.695cae0797ed&site=eds-live&scope=site&authtype=guest&custid=s3911979&groupid=main&profile=eds

Olsson, K.-G., Janson, U., Persson, M., Caldenby, C., Madjarova, J., Lund, M., Christensson, P., Crona, K., Wahlgren, P., Ander, M., & Williams, C. (2019). Architecture and engineering-education of form and force. *Proceedings of IASS Annual Symposia, IASS 2019 Barcelona Symposium: Contributions in Memory of Mike Barnes, pp. 1-8(8)* (2019, October).

Ottosen, N., & Petersson, H. (1992). *Introduction to the finite element method*. Pearson Education.

Paulsson, G., & Granholm, H. (1953). *Hantverkets bok. Mureri* (3., omarb. uppl.). Lindfors.

Peters, B., & Peters, T. (Eds.). (2013). *Inside Smart Geometry: Expanding the Architectural Possibilities of Computational Design*. John Wiley & Sons.

Piker, D. (n.d.). Kangaroo physics. https://www.food4rhino.com/en/app/kangaroo-physics

Plateau, J. (1873). Statique expérimentale et théorique des liquides soumis aux seules forces moléculaires (1873).

Plateau, J. (1873/2005). Experimental and theoretical statics of liquids subject to molecular forces only (K. A. Brakke, Trans.) [(Original work published 1837)] (1873/2005).

Poleni, G. (1748). *Memorie Istoriche della Gran Cupola del Tempio Vaticano*. https://www.e-rara.ch/zut/wihibe/content/titleinfo/4079847

Poncelet, J. V. (1822). *Traité des propriétés projectives des figures: ouvrage utile à ceux qui s'occupent des applications de la géométrie descriptive et d'opérations géométriques sur le terrain*. Bachelier, Libraire. https://doi.org/10.3931/e-rara-55268

Pottmann, H., & Liu, Y. (2007). Discrete surfaces in isotropic geometry. *Lecture Notes in Computer Science (including subseries Lecture Notes in Artificial Intelligence and Lecture Notes in Bioinformatics)* **4647 LNCS**.(1) (2007), 341–363. https://doi.org/10.1007/978-3-540-73843-5_21

Pressley, A. (2009). *Elementary Differential Geometry*. Springer London Ltd.

Prime, W. C. (1860). *Boat life in Egypt and Nubia*. Harper & Brothers. https://archive.org/embed/boatlifeinegyptn00prim

Priske, C. (2013). Impressively skilled bricklayers, vault construction. https://youtu.be/PB8TWMKHHMQ?si=iPmtnvACYY_gT-xI

Rankine, W. (1895). *A manual of applied mechanics* (14th ed.). C. Griffin; Co., Limited. https://archive.org/details/cu31924031285384

Ricci, M. M. G., & Levi-Civita, T. (1900). Méthodes de calcul différentiel absolu et leurs applications. *Mathematische Annalen* **54**.(1) (1900), 125–201. https://doi.org/10.1007/BF01454201

Riedelsheimer, T. (2001). Rivers and Tides.

Roritzer, M. (1497). Geometria deutsch (1497). https://daten.digitale-sammlungen.de/0004/bsb00040191/images/index.html?fip=193.174.98.30&seite=1&pdfseitex=

Rosenfeld, B. (1988). *A History of Non-Euclidean Geometry - Evolution of the Concept of a Geometric Space* (G. Toomer, Ed.). Springer Science+Business Media.

Rottlaender, R. C. (1977). On the mathematical connections of ancient measures of length. *Acta Praehistorica and Archaeologica* (1977), 49–51.

Rubió i Bellver, J. (1913). Dificultats per a arribar a la sintessis arquitectònica. *Anuario de la Asociación de Arquitectos de Cataluña* (1913), 63–79.

Sadd, M. H. (2020). *Elasticity: Theory, Applications, and Numerics*. Elsevier Inc.

Saint-Exupéry, A. (1939). *Wind Sand And Stars*. Reynal & Hitchcock. https://archive.org/embed/in.ernet.dli.2015.264850

Sarhosis, V., Bagi, K., Lemos, J. V., & Milani, G. (2016). *Computational modeling of masonry structures using the discrete element method* (Vol. 1). Engineering Science Reference (an imprint of IGI Global). https://doi.org/10.4018/978-1-5225-0231-9

Schek, H. J. (1974). The force density method for form finding and computation of general networks. *Computer Methods in Applied Mechanics and Engineering* **3**.(1) (1974), 115–134. https://doi.org/10.1016/0045-7825(74)90045-0

Scherrer, D. (2015). Ancient Observatories - Timeless Knowledge (2015), 1–43.

Schlaich, J., & Schlaich, M. (2008). Lightweight structures (2008).

Schlaich, J., & Schober, H. (1996). Glass-covered grid-shells. *Structural Engineering International: Journal of the International Association for Bridge and Structural Engineering (IABSE)* **6**.(2) (1996), 88–90. https://doi.org/10.2749/101686696780495716

Schlaich, J., & Schober, H. (2005). Freeform Glass Roofs. (March) (2005), 25–27.

Schling, E., Kilian, M., Wang, H., Schikore, J., & Pottman, H. (2018). Design and construction of curved support structures with repetitive parameters. In L. Hesselgren, A. Kilian, S. Malek, K.-G. Olsson, O. Sorkine-Hornung, & C. J. K. Williams (Eds.), *Advances in architectural geometry* (pp. 140–165). Klein Publishing GmbH (Ltd.)

Schön, D. A. (1992). Designing as reflective conversation with the materials of a design situation. *Knowledge-Based Systems* **5**.(1) (1992), 3–14. https://doi.org/10.1016/0950-7051(92)90020-G

Scriba, C. J., & Schreiber, P. (2015). *5000 years of geometry: Mathematics in history and culture*. https://doi.org/10.1007/978-3-0348-0898-9

Sehlström, A., Olsson, K. G., & Williams, C. J. (2022). Design of tension structures and shells using the airy stress function. *International Journal of Space Structures* **37** (2 2022, June), 94–106. https://doi.org/10.1177/09560599211064104

Shelby, L. R. (1972). The Geometrical Knowledge Of Mediaeval Master Masons. *Speculum* **47**.(3) (1972), 395–421. https://doi.org/10.2307/2856152

Soriano, E. (2017). Low-Tech Geodesic Gridshell: Almond Pavilion. (February) (2017).

Southwell, R. V. (1933). On the calculation of stresses in braced frameworks [doi: 10.1098/rspa.1933.0032]. *Proceedings of the Royal Society of London. Series A, Containing Papers of a Mathematical and Physical Character* **139** (839 1933), 475–507. https://doi.org/10.1098/rspa.1933.0032

Stoker, J. J. (1969). *Differential Geometry*. Wiley-Interscience.

Strauss, W. A. (2008). *Partial Differential Equations : An Introduction* (2nd). John Wiley & Sons Inc.

Struik, D. J. (1987). *A concise history of mathematics* (4 Revised). Dover Publications Inc.

Struik, D. J. (1988). *Lectures on classical differential geometry* (2nd). Dover.

Swiss federal Office of Culture (Ed.). (2018). Davos Declaration 2018. Towards a high quality Baukultur for Europe (2018). https://davosdeclaration2018.ch/

Tellier, X., Douthe, C., Baverel, O., & Hauswirth, L. (2023). Designing funicular grids with planar quads using isotropic linear-weingarten surfaces. *International Journal of Solids and Structures* **264** (2023, March). https://doi.org/10.1016/j.ijsolstr.2022.112028

Tenek, L. T., & Argyris, J. (1998). A brief history of FEM. In *Finite element analysis for composite structures* (pp. 17–25). Springer Dordrecht. https://doi.org/10.1007/978-94-015-9044-0_2

Thirion, J. (1914). Plateau, Joseph-Antoine (16th ed.). https://archive.org/details/V16CatholicEncyclopediaKOfC/page/67/mode/2up

Thompson, D. W. (1917). *On growth and form*. Cambridge University press. https://archive.org/details/ongrowthform1917thom

Thomsen, M. R., Tamke, M., Ayres, P., & Nicholas, P. (2015). *CITA works*. Riverside Architectural Press.

Timoshenko, S., & Woinowsky-Krieger, S. (1959). *Theory of plates and shells* (2nd). McGraw-Hill.

Timoshenko, S. P. (1934). *Theory of elasticity* (1st). McGraw-Hill book company, inc.

Torroja, E. (1958). *The Structures of Eduardo Torroja: An Autobiography of Engineering Accomplishment*. F. W. Dodge Corporation.

Truesdell, C. (1960). *The rational mechanics of flexible or elastic bodies 1638 - 1788: Introduction to Vol. X and XI*.

Turner, M., Clough, R., Martin, H., & Topp, J. (1956). Stiffness and deflection analysis of comlex strucutres.pdf. *Journal of the aeronautical sciences* **23**.(9) (1956), 805–823.

Varignon, P. (1725). *Nouvelle mécanique, ou Statique, dont le projet fut donné en M. DC. LXXXVII*. Jombert, C. https://gallica.bnf.fr/ark:/12148/bpt6k5652714w/f4.item

Veenendaal, D., & Block, P. (2012). An overview and comparison of structural form finding methods for general networks. *International Journal of Solids and Structures* **49**.(26) (2012), 3741–3753. https://doi.org/10.1016/j.ijsolstr.2012.08.008

Veenendaal, D., & Block, P. (2014). Comparison of form-finding methods. In *Shell structures for architecture: Form finding and optimization* (pp. 115–129). Routledge.

Verriest, G. (1990). Life, eye disease and work of Joseph Plateau. In H. E. Henkes & C. Zrenner (Eds.), *History of ophthalmology: Sub auspiciis academiae ophthalmo-*

logicae internationalis (pp. 9–20). Springer Netherlands. https://doi.org/10.1007/978-94-009-0641-9_2

Villard, d. H., Willis, R. ; Quicherat, J. É. J., Darcel, A., & Lassus, J. B. A. (ca. 1230/1859). *Facsimile of the sketch-book of Wilars de Honecort, an architect of the thirteenth century : illustrated by commentaries and descriptions* [(Original work published ca. 1230)]. https://hdl.handle.net/2027/gri.ark:/13960/t87h41r7h

Viollet-le-Duc, E.-E. (1875). *Dictionnaire raisonné de l'architecture française du XIe au XVIe siècle*. Paris : A. Morel. https://archive.org/details/raisonnedelarchi01viol

Vitruvius. (1914). *Vitruvius : The ten books on architecture* (M. H. Morgan, Trans.). Cambridge : Harvard university Press. https://archive.org/details/vitruviustenbook00vitruoft

Vrachliotis, G. (2018). *Frei Otto, Carlfried Mutschler: Multihalle*. Spector Books.

Walker, D., & Addis, B. (1997). *Happold: The Confidence to Build*. Happold Trust Publications Limited.

Watson, J. D. (1968/2010). *The Double Helix: A Personal Account of the Discovery of the Structure of DNA* [(Original work published 1968)]. Orion Publishing Co.

Wiberg, N.-E. (1980). *Finita elementmetodens tillämpningar inom olika teknikområden.* Studentlitt.

Williams, C., & McRobie, A. (2016). Graphic statics using discontinuous Airy stress functions. *International Journal of Space Structures* **31**.(2-4) (2016), 121–134. https://doi.org/10.1177/0266351116660794

Williams, C. J. K. Form finding and cutting patterns for air-supported structures. In *Air-supported structures: The state of the art*. London: The Institution of Structural Engineers, 1980, 99–120.

Williams, C. J. K. (2014). What is a shell? In S. Adriaenssens, P. Block, & C. J. Williams (Eds.), *Shell structures for architecture: Form finding and optimization* (pp. 21–31). Routledge.

Willis, R. (1842). On the Construction of the Vaults of the Middle Ages. *Transactions of the Royal Institute of British Architects* (1842), 1–69.

Wissler, C. (1917). *The American Indian; an introduction to the anthropology of the New World*. D.C. McMurtrie.

Wolfe, W. (1921). *Graphical analysis; a text book on graphic statics*. New York McGraw-Hill. https://archive.org/details/graphicalanalysi00wolf

Yarker, J. (1909). *The arcane schools : a review of their origin and antiquity; with a general history of Freemasonry and its relation to the theosophic, scientific, and philosophic mysteries*. Belfast : W. Tait. https://archive.org/details/b24886002

Zaera, A. (1995). Conversations with Frank O. Gehry. In *Frank gehry 1991-1995 (el croquis 74/75)*. El Croquis.

Zawisny, N., Fivet, C., & Ochsendorf, J. (2017). Guastavino design of the 1909 thin brick dome of the Cathedral of St John the Divine. *Construction History* **32**.(2) (2017), 39–65.

Zienkiewicz, O. C., & Cheung, Y. K. (1967). *The finite element method in structural and continuum mechanics : numerical solution of problems in structural and continuum mechanics.* McGraw-Hill.

Zienkiewicz, O. C., & Taylor, R. L. (1987). *The Finite Element Method; Volume 1: Basic Formulation and Linear Problems* (4th ed.). McGraw-Hill Book Company Inc.

Zienkiewicz, O. C., & Taylor, R. L. (1991). *The finite element method; Volume 2: solid and fluid mechanics, dynamics and non-linearity* (4th ed.).

Picture credits

Unless nothing else is stated, the pictures are either the authors or under public domain. This thesis has licensed several images under the public domain or Creative Commons. Information regarding the different licenses can be found here:

1.0: https://creativecommons.org/publicdomain/mark/1.0/deed.en
CC0 1.0:https://creativecommons.org/publicdomain/zero/1.0/
CC BY 2.0 2.0:https://creativecommons.org/licenses/by/2.0/
CC BY-SA 3.0:https://creativecommons.org/licenses/by-sa/3.0/
CC BY-SA 4.0:https://creativecommons.org/licenses/by-sa/4.0/
CC BY-ND 2.0:https://creativecommons.org/licenses/by-nd/2.0/
CC BY-NC-ND 2.0:https://creativecommons.org/licenses/by-nc-nd/2.0/
CC BY-NC-ND 4.0: https://creativecommons.org/licenses/by-nc-nd/4.0/deed.en/

Figure 1
over a bed of pins (ii), photo by Ciro Mondueri licensed under CC BY 2.0, https://flic.kr/p/yVJC1

Figure 1.2a
Vue du Limpopo en Afrique du Sud, photo by South African Tourism licensed under CC BY 2.0 https://commons.wikimedia.org/w/index.php?curid=67747409

Figure 1.2b
Mapungubwe, Limpopo, South Africa, photo by South African Tourism licensed under CC BY 2.0 https://flic.kr/p/xg6B8y

Figure 1.3
Final Hanging chain model for Mannheim. Photo by Ian Lidell licensed under CC BY-NC-ND 4.0 https://www.researchgate.net/publication/283164806_Frei_Otto_and_the_Development_of_Gridshells/figures

Figure 2.1a
Jar (Hu), licensed under CC0 1.0 by The Metropolitan Museum of Art. https://www.metmuseum.org/art/collection/search/44723

Figure 2.6
Armadillo Vault, photo by Iwan Baan licensed under CC BY-NC-ND 2.0, https://flic.kr/p/Mdvmih

Figure 3.9
The Great Court in the British Museum, Photo by Andrew Stawarz, licensed under CC BY-ND 2.0 DEED https://www.flickr.com/photos/stawarz/4736547190

Figure 4.4
Main working-drawing for the dome of the Cathedral of St. John the Divine from Avery Library, https://findingaids.library.columbia.edu/ead/nnc-a/ldpd_3463538. Photo of the drawing taken by Assistant Professor David López López.

Figure 4.6a
Maqueta polifunicular de la iglesia de la Colonia Güell, de Antoni Gaudí (1898-1908), distributed under Public Domain, https://commons.wikimedia.org/w/index.php?curid=4524156

Figure 4.10
Rafael Guastavino stands on recently laid tile arch along Boylston Street, construction of the McKim Building, photo by Boston Public Library licensed under CC BY 2.0 https://flic.kr/p/4D3P2Y

Figure 4.11
Construcción de uno de los cajones para el Puente de Sancti Petri. I-ETM-018-07_02, photo used with permission from the Archivo Torroja, http://www.cehopu.cedex.es/etm/pict/I-ETM-018-07.htm

Figure 4.12
House for Hippopotamus at Berlin Zoo, photo used with permission from Berlin Zoo©.

Figure 5.1
Retouched version of the original picture of Joseph Plateau by Albert Callisto, licensed under CC BY-SA 4.0 https://quest.eb.com/search/132_1256566/1/132_1256566/cite

Figure 5.2
Watson and Crick with their DNA model. [Photography]. Retrieved from Encyclopædia Britannica ImageQuest. https://quest.eb.com/search/132_1256566/1/132_1256566/cite

Appendix A

Asymptotic timber grid shell 2019

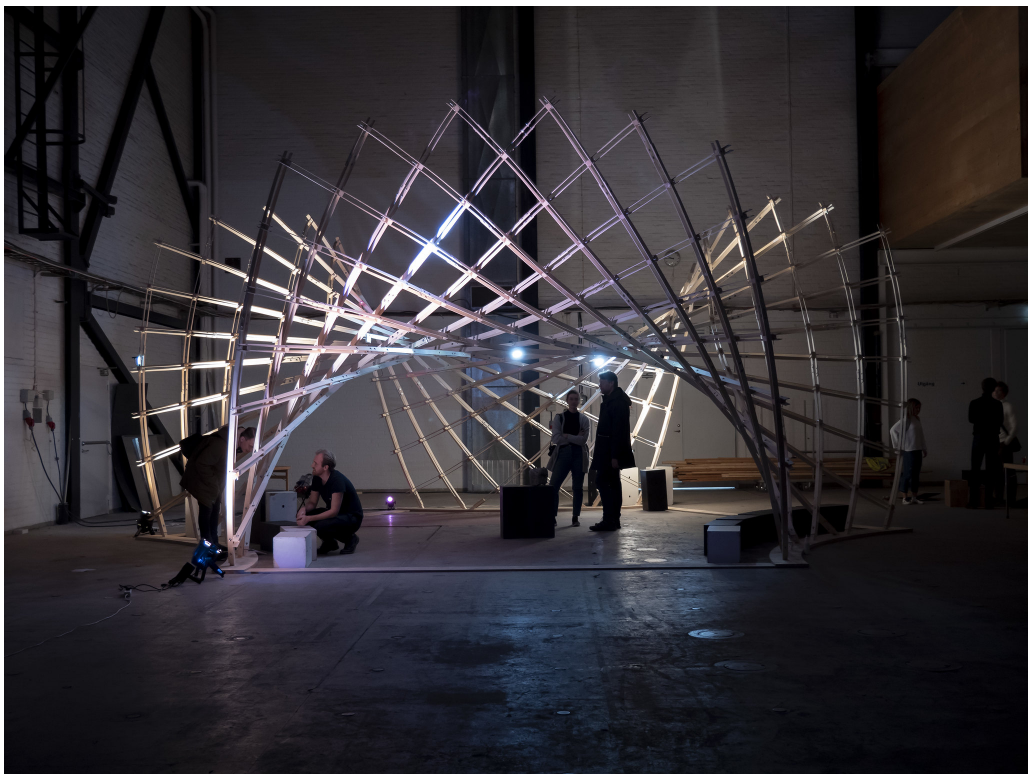

Figure 2: *The exhibition of the asymptotic timber grid shell built during the 2019 workshop.*

The 2019 Asymptotic timber grid shell workshop took place on December 19th and 20th. The workshop was part of an introductory course in parametric design for 35 undergraduate students in the architecture and engineering program. The course is 3 ECTS, consisting of 8.5 days in total, where the workshop is the two final days as an ending segment.

The research challenge and the design objective were to, similar to Papers B and C, design an indoor pavilion for an exhibition that could be manufactured and built during a two-day workshop together by our students. The purpose was to examine how differential geometry can be applied early in the architectural design process to develop design concepts that enable rapid production adapted to a specific context using simple building elements produced by simple manufacturing methods.

The methodology and the design process are summarized in Figure 5.7, where physical models, prototypes, digital tools and simulations are used to evaluate the feasibility of the design so that it can be manufactured and constructed in just two days. The chosen

proposal is further refined and tested during the two-day workshop.

The design proposal and the resulting structure, seen in Figure 2, was a double-layer grid shell spanning seven meters. The geometric idea behind the concept was to utilize asymptotic lines on a minimal surface, which in this case was an Enneper surface. Thus, the laths could be made from straight 50mm wide and 6mm thick plywood strips connected with timber blocks (Figure A.1).

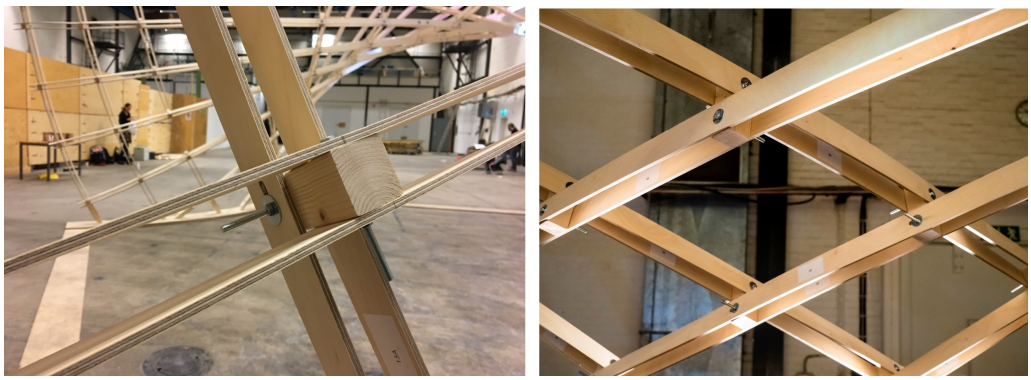

Figure A.1: *The nodes of the asymptotic timber grid shell built during the 2019 workshop. The timber blocks connect the laths in two layers, making it possible to lock the mechanism in the erected state. It requires a slot to accommodate the transformation from flat to erected state, as seen in the left picture.*

The main challenge was to design an improved nodal connection, which compared to 2018, could be locked in the erected state. The challenge included the manufacturing procedure and the geometric modelling of the slots necessary for a node. Thus, the reading order for those already familiar with the asymptotic lines can go straight to Sections A.2 and A.3 describing the lessons learned from the gridshell in 2018 and the design process and considerations behind the improved nodal connection. The geometric modelling is described in Section A.4 followed by Section A.5 describing the resulting production drawings and data for the manufacturing and assembly during the workshop. In Section A.6 the structural model and analysis are described. The workshop is described in Section A.7 followed by the disassembly in Section A.8 and an ending evaluation in Section A.9.

A.1 Asymptotic lines on a surface

Asymptotic lines are curves on the surface which has zero normal curvature. Meaning the curves only bend in the surface plane.

Asymptotic lines appear only on surfaces with negative Gaussian curvature. This can be explained visually using Mohr's circle of curvature as in (Adiels et al., 2019). Another way is to use the Dupin indicatrix, which can be seen as an intersection of a slightly offset surface tangent plane. In Figure A.2, one can see the Dupin indicatrix to the left and a tangent plane intersection on an Enneper surface to the right. The orange lines are the

asymptotes to the blue hyperbolas, hence the name asymptotic lines. On the surface, one can see that the asymptotes are in the same direction as the black curves, which follow the asymptotic direction.

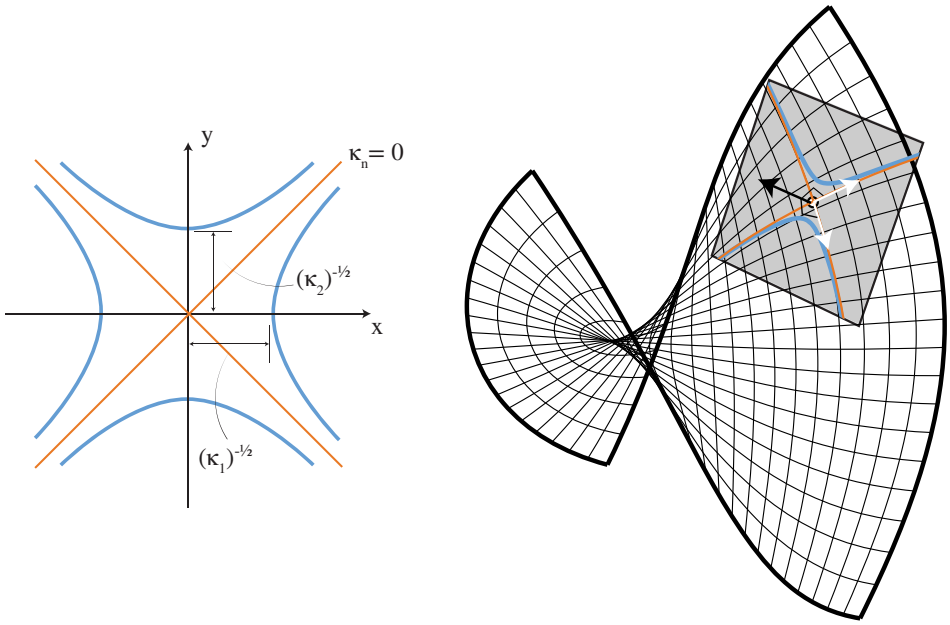

Figure A.2: *Left the Dupin indicatrix for a minimal surface, where the asymptotic directions are given by the orange asymptotes. Taking an intersection using a slightly offset tangent plane in the normal direction at a minimal surface, one can see the dupin indicatrix. Right, only one plane was used. A second plane offset in the opposite direction is needed to get an exact representation. The black curves follow the asymptotic direction on the Enneper surface.*

For the particular case of minimal surfaces, the asymptotic lines intersect at right angles and are angled 45 degrees to the principal curvature directions. If you create a ruled surface from lines following the surface normals, you get a surface that roughly can be unrolled as flat straight laths. This is the basic geometric idea behind the design to simplify the fabrication of the building elements.

A.2 Lessons learned from 2018

The design of the asymptotic timber grid shell for the workshop of 2019 (Figure 2) took its starting point from that grid shell built in 2018 and is described in Paper C (Adiels, 2019d). It was challenging in 2018 to design a simple node that could be manufactured quickly, which also locked the structures' mechanisms when erected. Thus, at a certain point close to the workshop, it was necessary to accept that the structure would be

pretty flexible and focus on ensuring that the flexibility would not result in a collapse. Thus, structural analysis models, physical models and other instruments were used to ensure there would be no collapse. As can be seen in Figure A.3 (a) and (Adiels, 2019b), it was indeed a much flexible structure, but it did not break even under quite heavy motion. While each cell of the grid worked as a mechanism, Figure A.3 (b), the supports added stability, which can be seen in the blue triangle in Figure A.3 (a). However, in the following year, 2019, there was an eagerness to improve the design by directing attention to how to utilize the mechanism in the erection and lock it in the erected state. Thus, a similar geometry was used, i.e. an Enneper surface. Paper C describes the theory of asymptotic lines and their specific application on minimal surfaces.

A.3 Improved node design and prototype

There are two common approaches to removing or handling the mechanisms in a structure, as seen in Figures A.3 (a)-(b). The most obvious from a theoretical point of view is adding bracing as in Figure A.4 (a), where a tension tie is applied to Figure A.3 (b), removing the mechanism. The other option is to stiffen the nodes and work with a force couple to handle the moment, i.e. Vierendeel action as in Figure A.4 (b). While the second option is less efficient than bracing, it can still reduce the mechanism.

The second alternative using Vierendeel action, was chosen since forcing the angle with a timber block would be relatively easy due to the asymptotic lines intersecting at a right angle on a minimal surface. Instead of having interlocking laths in the 2018 grid shell, the laths were seperated into two layers of 6mm birch plywood (B-BB)[1] connected

[1]The quality of the plywood is graded on a scale from A-D. You have two grades for the front and

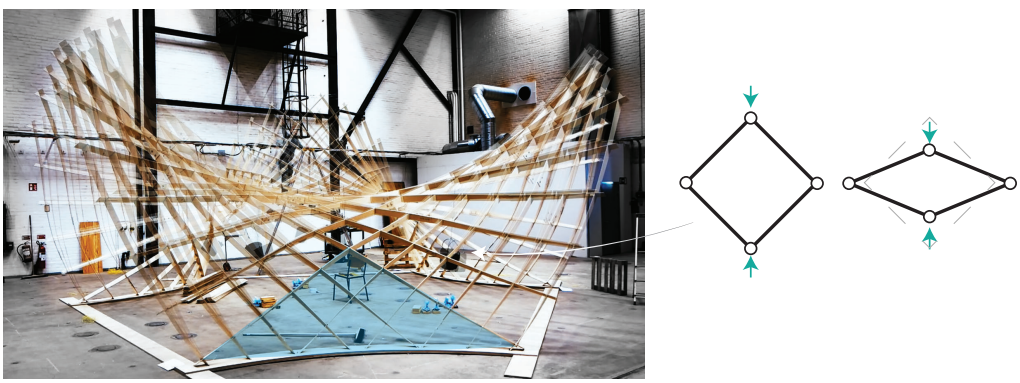

(a) Gridshell built in 2018 (b) mechanism in each cell

Figure A.3: *In* (a)*, the structure of 2018 was essentially a mechanism that got its stability from the attachment to the boundary. Applying load to the structure, one can see by interpolating the images the stiff triangle in blue from the supports.* (b) *represents a cell in the surface grid, which can be seen as a pin-jointed structure, which is a mechanism in the plane of the surface.*

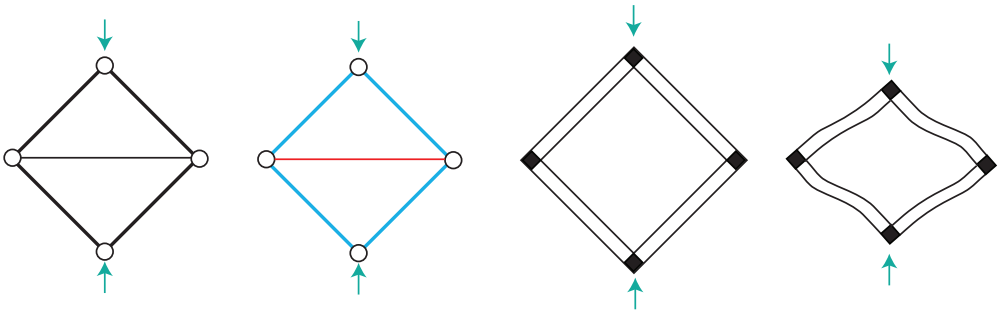

(a) Add tension tie, no mechanism by members working in tension (red) and compression (blue)

(b) Stiffening the nodes and work with force couple to handle the moment, i.e Vierendeel action. Mechanism still exist but not as prominent.

Figure A.4: *Two different techniques to handle the mechanism in the pin-jointed structure representing each cell in the grid Figure A.3. In* (a)*, a tension tie is used (red tension and blue compression). In* (b)*, stiffening the joints and working with force couples, i.e. typically referred to as Vierendeel action.*

by a timber block of pine with a cross-section of 45x45 mm^2, see Figure A.1. Two parallel laths in each layer are connected to the node, providing the necessary force couple. Each layer is offset from the middle surface, a distance of half the lath width. The bigger the offset from the middle surface, the further the lath deviates from a straight line in the plane. However, the deviations calculated were considered within tolerance for the achievable precision for this type of project, where students make the elements using manual machines. Most deviations were around 0.5- 1%, while some had around 1.5%, from a straight line. The measurement was made by unrolling the laths and measuring the maximum deviation of the longest edges compared to a straight line. The percentage is given by dividing the deviation by the length of the lath.

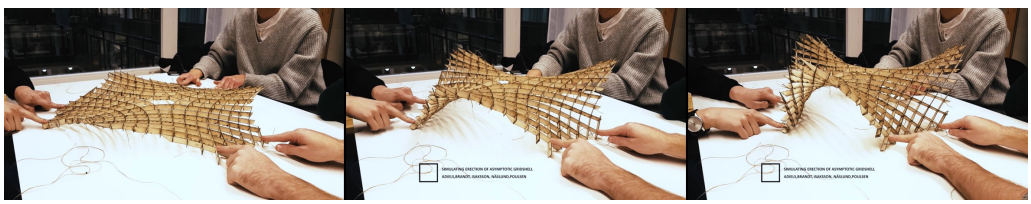

Figure A.5: *A physical model showcasing the erection procedure of the grid shell. Assembling it flat and then push it into shape.*

Like the grid shell in 2018, the intention was to assemble the structure flat and erect it

back of softwood plywood boards (Forest Plywood, n.d.).

[2]The timber stud with a cross-section 45x45mm is standard dimension and is both cheap and easy to find off the shelf.

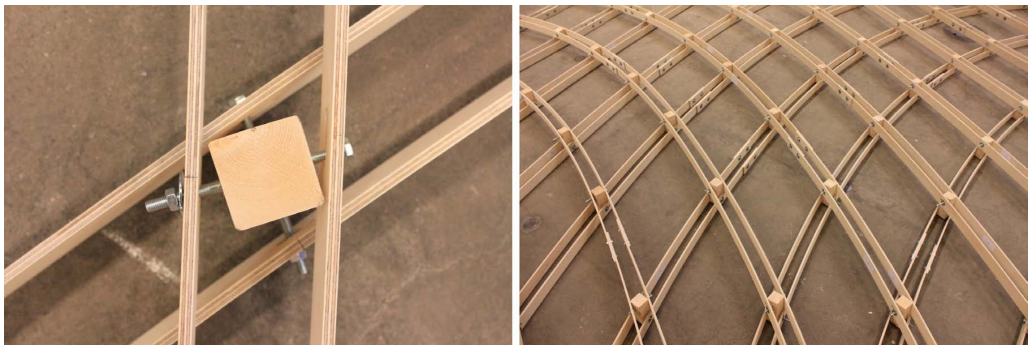

Figure A.6: *The angles of the grid will change between the flat state and the erected state. In the flat state, the laths will not intersect at right angles, and a slot in the laths is necessary to accommodate that change.*

to its intended form (Figure A.5). Thus, one issue with having two parallel laths would be accommodating the uncoordinated movement between the two layers when transforming the structure from flat to erected form. This can be seen in Figure A.6 where the cells take a rhombus shape in the flat state, compared to the approximately right angles in the erected state seen in Figure A.1, and the timber block and its connectors to the laths need to rotate. Thus, there must be a slot in the middle of the laths, similar to the node design of the Mannheim grid shell, which was also assembled flat before erection (Happold & Liddell, 1975; Liddell, 2015; Vrachliotis, 2018).

The main issue with the node design was creating the slot in the middle in a time-efficient manner. It could be done using the CNC, but it would take too long time. Thus, it was necessary to find a method using manual tools. With the help from the carpenters in the wood workshop, it was suggested to use a 'biscuit joiner' for making slots for 'biscuits' (without using the actual 'biscuits'). The biscuit joiner had three possible widths for the slot. Since there are many slots for each lath, a rig was built to calibrate the machine's height to make the slots precisely in the middle of the lath. After calibration, it was straightforward to slide the laths and make slots at each location. Each location was marked with the correct width setting on the machine. If a wider slot was needed than the machine setting allowed, two marks separated with extra width necessary could be used for specific locations. The process is shown in Figure A.7 (Adiels, 2019a). The rig in Figure A.7 was made for one lath, but adjusting the rig to take several identical laths simultaneously was easy.

The fabrication of the timber blocks was straightforward, chopping 100 mm lengths from a 2000-4000 mm timber stud. A rig was designed for a stationary drill in the wood workshop to make the holes in a time-efficient manner for the threaded 100mm M6 bolts connecting the laths. The extra length was sufficient to allow the rotation of the timber block, as seen in Figure A.6.

A prototype was made to measure the time for fabrication and ensure that the kinematics of the nodes would allow the structure to transform from the flat to the erected state. The relatively simple shape of a double Enneper was chosen as the surface. The

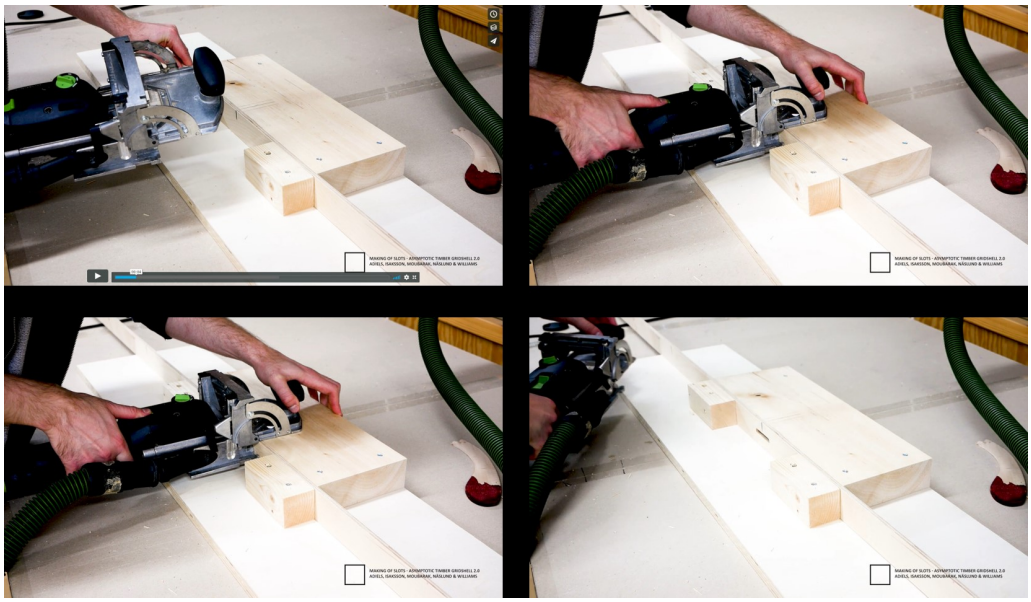

Figure A.7: *The process of making the slots for allowing movement between two parallel laths. The slots were made using a 'biscuit joiner' machine. The locations and necessary width were marked on the lath. Using a rig, it was straightforward to set up the correct height and right position.*

geometry and the asymptotic lines were generated from the analytic expression with a principal curvature parametrization (do Carmo, 1976)

$$\mathbf{r}(\theta^1, \theta^2) = x(\theta^1, \theta^2)\mathbf{i} + y(\theta^1, \theta^2)\mathbf{j} + z(\theta^1, \theta^2)\mathbf{k} \tag{A.1}$$

$$x = \theta^1 - \frac{1}{3}(\theta^1)^3 + \theta^1(\theta^2)^2 \tag{A.2}$$

$$y = -\theta^2 + \frac{1}{3}(\theta^2)^3 - \theta^2(\theta^1)^2 \tag{A.3}$$

$$z = \left((\theta^1)^2 - (\theta^2)^2\right), \tag{A.4}$$

which is easy to rotate 45 degrees to get the asymptotic lines. At this stage, the slot width was chosen based on a conservative value. The finished prototype can be seen in Figure A.8, and a video of the process can be viewed (Adiels, 2019c). The fabrication, assembly and erection gave enough confidence that it was possible to produce enough laths during the workshop and the kinematics of the nodes allowed for assembling flat and erecting to the final shape. A key takeaway was that getting the right geometry in the erected state would be much easier if the slot lengths were more elaborately calculated.

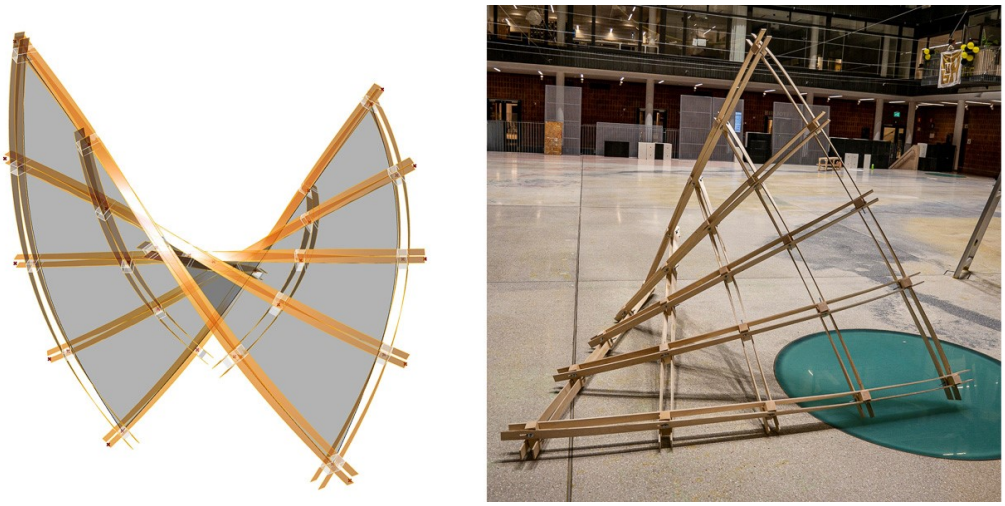

Figure A.8: *Left the digital model of the prototype. Right, the prototype as built in 2019.*

A.4 Geometric modelling

The main objective of the geometric modelling was to incorporate it into a parametric model that would allow changes and still produce all the production drawings and data presented in Section A.5. The four specific objectives were: generate the surface and the asymptotic lines forming the surface grid (see Section A.4.1), calculate the required sloth lengths on the laths (see Section A.4.2), model the interface between the laths and the base plate (see Section A.4.3), and model the base plate geometry (see Section A.4.4).

A.4.1 Surface and the surface grid

The surface geometry for the pavilion was chosen to be Enneper of 3-fold symmetry. While different minimal surfaces were evaluated initially, having the same shape as in 2018 was considered beneficial for comparison. With the shape known, generating the asymptotic lines on the surface that formed the surface grid was necessary. Since the analytic expression for an Enneper of 3-fold symmetry ($k = 3$) was known,

$$\begin{aligned} x(\theta^1, \theta^2) &= \theta^1 \cos(\theta^2) - \frac{\left(\theta^1\right)^{(2k-1)}}{(2k-1)} \cos((2k-1)\theta^2) \\ y(\theta^1, \theta^2) &= -\theta^1 \sin(\theta^2) - \frac{\left(\theta^1\right)^{(2k-1)}}{(2k-1)} \sin((2k-1)\theta^2) \\ z(\theta^1, \theta^2) &= \frac{2}{k} \left(\theta^1\right)^k \cos(k\theta^1), \end{aligned} \tag{A.5}$$

it is straightforward using *Euler's theorem*

$$\kappa_n = \kappa_1 \cos(\phi)^2 + \kappa_2 \sin(\phi) \tag{A.6}$$

to find the angle ϕ for which to rotate the principal curvature directions to obtain the asymptotic directions by assuming the normal curvature κ_n to be zero. While eq. 2 in Paper C worked, it was bit naughty from a mathematical point of view, and the correct expression should be

$$\phi = \arccos\left(\pm\sqrt{\frac{1}{1+\frac{-\kappa_1}{\kappa_2}}}\right), \tag{A.7}$$

where the κ_1 and κ_2 are the principal curvatures. Finding the asymptotic direction at a given starting point makes it possible to trace the asymptotic lines by repeatedly updating the asymptotic directions at each new point on the surface. The resulting surface grid following the asymptotic lines can be seen in black in Figure A.9.

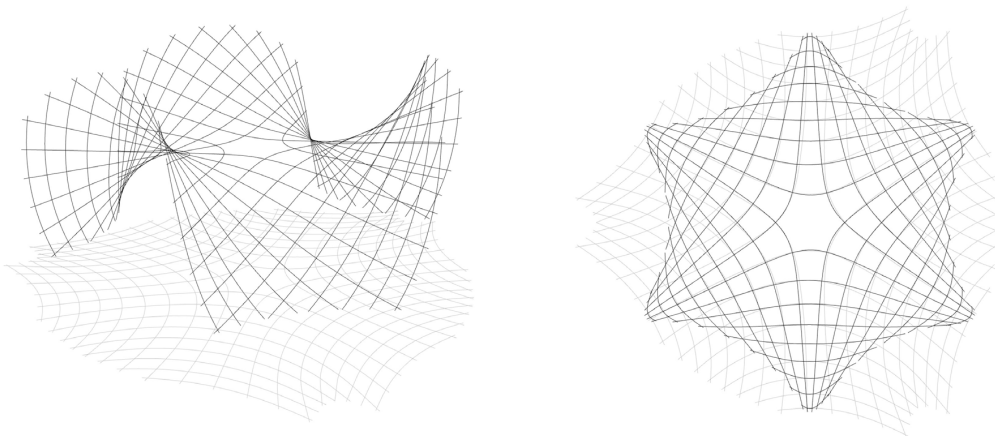

Figure A.9: *The grid on the surface is in black, and the flat grid in the xy-plane is in grey. To the right, the grids are seen from the top view. The main objective of the mapping was to preserve the lengths at the expense of the angles changing.*

A.4.2 Calculating the slot lengths

To calculate the necessary slot lengths, it was necessary to map the asymptotic grid to the flat xy-plane, preserving the lengths while minimising the angle changes as much as possible.

To find the flat grid a combination of *Kangaroo2* (Piker, n.d.) and *K2Engineering* (Brandt - Olsen & Solly, n.d.) in Grasshopper3d was used. To get an initial approximation, the surface grid was projected onto the xy-plane, and a relaxation was performed to preserve the surface grid's lengths and minimise the angle changes to the surface using Kangaroo2. Subsequently, the solution was fine-tuned using K2Engineering, incorporating the material properties of the timber laths, and relaxation was performed by modelling the laths as a combination of bars and elastic rods having bending stiffness. While several solutions exist to this problem, a solution was found in which the flat geometry had lengths very close to the grid on the surface.

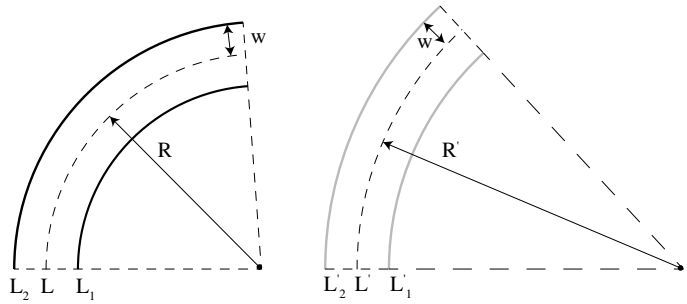

Figure A.10: *Left, circle segment of the laths on the erected grid shell and to the right a circle segment of the flat grid.*

Having the flat grid, it was possible to calculate the slot length necessary. Splitting up the continuous centre line of both the flat and the grid on the surface into small segments was assumed to have constant curvature. The length L' of the flat curve and the length L of the corresponding curve on the surface are the same. However, the laths are the offsets of a length of w from the centre line. Calling the interior lengths L_1' and L_1 on the flat and the curve on the surface, the lengths will not be the same since the curvature radii R_1' and R_1 are not equal. The objective was to find the length difference ΔL_1 and ΔL_2 defined as

$$\begin{aligned} \Delta L_1 &= L_1 - L_1' \\ \Delta L_2 &= L_2 - L_2'. \end{aligned} \tag{A.8}$$

These lengths were calculated as

$$\begin{aligned} \Delta L_1 &= Lw\left(\frac{1}{R'} - \frac{1}{R}\right) = Lw\left(\kappa' - \kappa\right) = -\Delta L_2 \\ \Delta L_2 &= Lw\left(\frac{1}{R} - \frac{1}{R'}\right) = Lw\left(\kappa - \kappa'\right). \end{aligned} \tag{A.9}$$

From (A.9) the total length difference of each curve was calculated by integrating over the entire curve. The length of the individual slots was calculated from the middle of the curve. This means there will be no slot in the middle of the curve, just a drill hole for the bolt, with increasing slot length from the middle to the ends of the laths. Thus, the lengths of the slots are smaller than if starting at the end of the curve.

Although the calculations (A.9) were straightforward, two important observations were made. The first observation was that for some laths the curvature changes direction between the flat grid and the surface grid. For those cases, the intrados laths will be longer than the extrados laths in the flat assembly. This seems intuitively wrong when assembled, and clear instructions and drawings were required to avoid mistakes during the workshop. Thus, drawings for the order and starting point of the laths would be necessary, as seen in Figure A.15. The second observation was realised that the timber blocks with the steel bolts would need to rotate. And the question was whether this

would be in the same or opposite direction of the slots. Thus, visual inspections were carried out at the most extreme locations at the ends of the laths and some more regular locations. As seen in Figure A.12 the block rotates in such a way that the bolts (black lines indicate directions) are within the calculated slot opening (white). Even though the timber block intersects the laths (red lines) in this picture, in the actual assembly, the timber blocks separate the laths in the flat state, as seen in Figure A.6

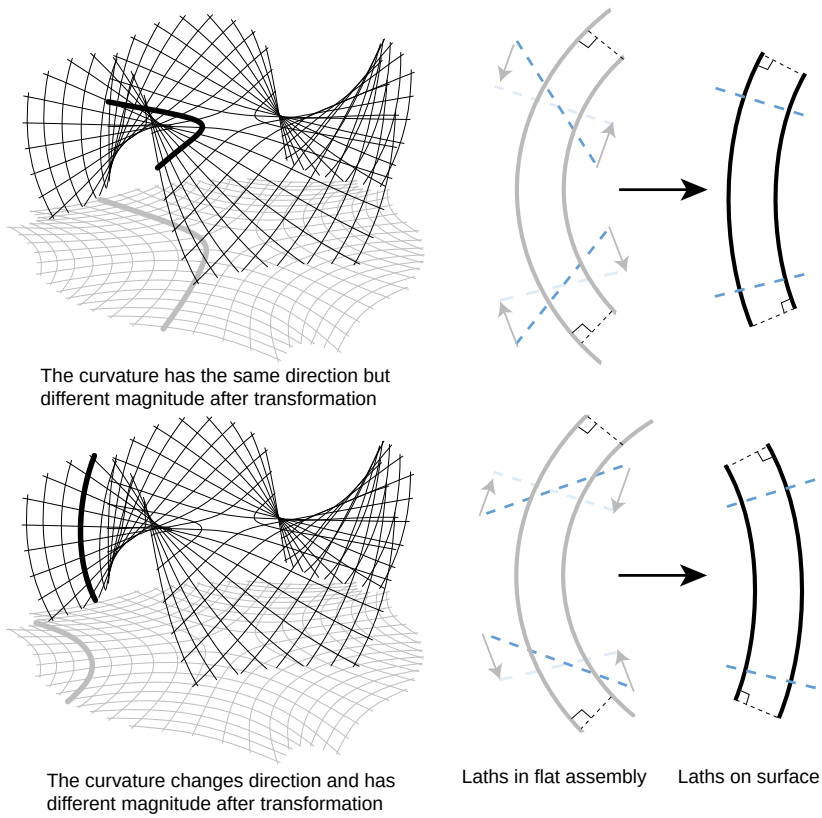

Figure A.11: *The top image shows the transformation of the lath pairs where the curvature has the same direction. The bottom shows the transformation of the lath pairs when the curvature changes direction between the flat and the erected state.*

A.4.3 Connecting the laths to the base plate

The main constraint in designing the connection or interface between the base plate and the grid shell was to ensure simple and quick manufacturing. The tools available were double-bevel miter saws (Bosch, n.d.), which has two angles aligning the blade. The first is the miter angle ϕ that rotates the blade in the xy-plane. The angle of the bevel cut θ tilts the blade. Thus, the challenge was to design and model solely on those two angles, ϕ

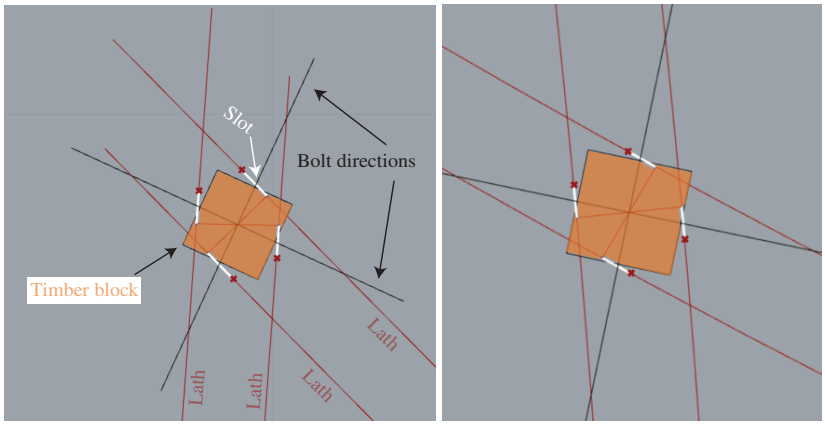

Figure A.12: *A plan drawing of the laths and timber block in the flat state at two different locations. It was necessary to check if it was sufficient to only calculate the slot length based on curvature change (white) or if it was necessary to include the rotation of the timber block. The exaggerated black bolts show that the timber block's rotation fits within the calculated slots (white).*

and θ and length for simple production drawings to be produced.

It was decided to use a timber stud from the same material as the timber blocks: pine with a 45x45mm cross-section. The timber stud was to have the same direction as the laths and cut in the xy-plane by the base plate. A hole in the timber stud was for attaching to the laths, and the stud was to be drilled and screwed into the base plate (Figure A.13).

It was possible from the geometric model to solve the intersection to the base plate to attain the geometry of the timber stud. From the intersection plane spanned by **a** and **b** (see Figure A.13), it was possible to find the miter and bevel cut angles.

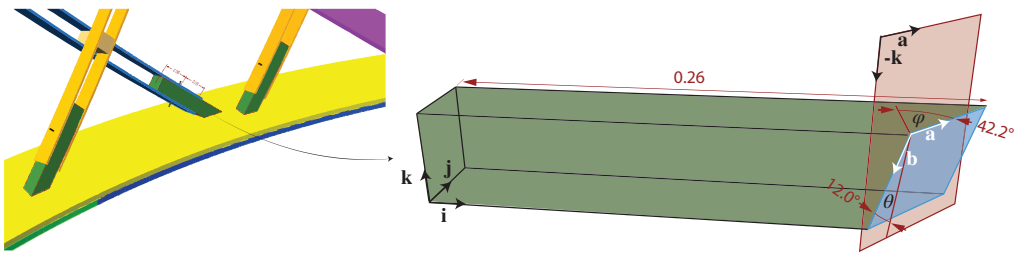

Figure A.13: *The timber studs connecting the base plate were designed to be manufactured with double-bevel miter saw and its two angles ϕ and θ aligning the blade.*

To get the correct angles, the following approach was used. Assume the uncut sides of the timber studs follow vectors **i**, **j**, **k** (cf. Figure A.13). The miter cut angle ϕ is just the

angle between **a**, from the cutting plane, and **j**

$$\phi = \arccos\left(\frac{\mathbf{a}\cdot\mathbf{j}}{|\mathbf{a}|\,|\mathbf{j}|}\right). \tag{A.10}$$

To get the bevel cut angle θ, a plane spanned by vectors **k** and **a** from the cutting plane was created and projected the normal, **n**, $\left(\frac{\mathbf{a}\times\mathbf{k}}{|\mathbf{a}\times\mathbf{k}|}\right)$ onto the cutting plane spanned by vectors **a** and **b**.

$$\text{proj}_{\mathbf{b}}\mathbf{n} = \frac{\mathbf{b}\cdot\mathbf{n}}{\mathbf{n}\cdot\mathbf{n}}\mathbf{n} \tag{A.11}$$

$$\text{oproj}_{\mathbf{b}}\mathbf{n} = \mathbf{b} - \text{proj}_{\mathbf{b}}\mathbf{n} \tag{A.12}$$

$$\theta = \arccos\left(\frac{\text{oproj}_{\mathbf{b}}\mathbf{n}\cdot\mathbf{b}}{|\text{oproj}_{\mathbf{b}}\mathbf{n}|\,|\mathbf{b}|}\right) \tag{A.13}$$

After attaining the angles ϕ and θ, it was possible to produce the production drawings seen in Figure A.15.

A.4.4 Geometry of the base plate

The base plate was necessary since it was impossible, nor desired, to attach the structure directly to the floor. Thus, the shape was given based on the three curves from the intersection of the surface with the xy-plane, which were connected with straight segments to work as one unit. The baseplate was made from two layers of 18 mm birch plywood cut using the CNC and thus needed to be assembled from smaller segments. The most important aspect behind the design was to reduce the time spent operating the CNC so that the base plates would be cut on time on the first day. Thus, the design was based on reducing the number of unique drawings since the operator needed to calibrate the machine between new drawings.

The final design of the base plates only needed three .dwg files (Figure A.16). The CNC would need to run the bottom and top layers of the curved segments three times each and the straight segments only once. This meant that one could reduce the time of the CNC since the operator only needed to calibrate the machine three times.

A.5 Production data and drawings

The final design resulted in the following number of elements. The structure required 300 hundred timber blocks of size 45x45x100 mm, meaning 600 bolts (M8x100mm, threaded the entire length), 600 nuts and 1200 washers (one on each side) were needed for the nodes. The total length of the timber needed was at least 30 m. The structural grid consisted of 16 unique laths that, due to the dimensions of the 6mm birch plywood boards (1250x2500), needed to be split up into 58 unique elements. These elements were, due to symmetry, repeated six times. Thus, 96 laths of 348 elements were needed to be produced.

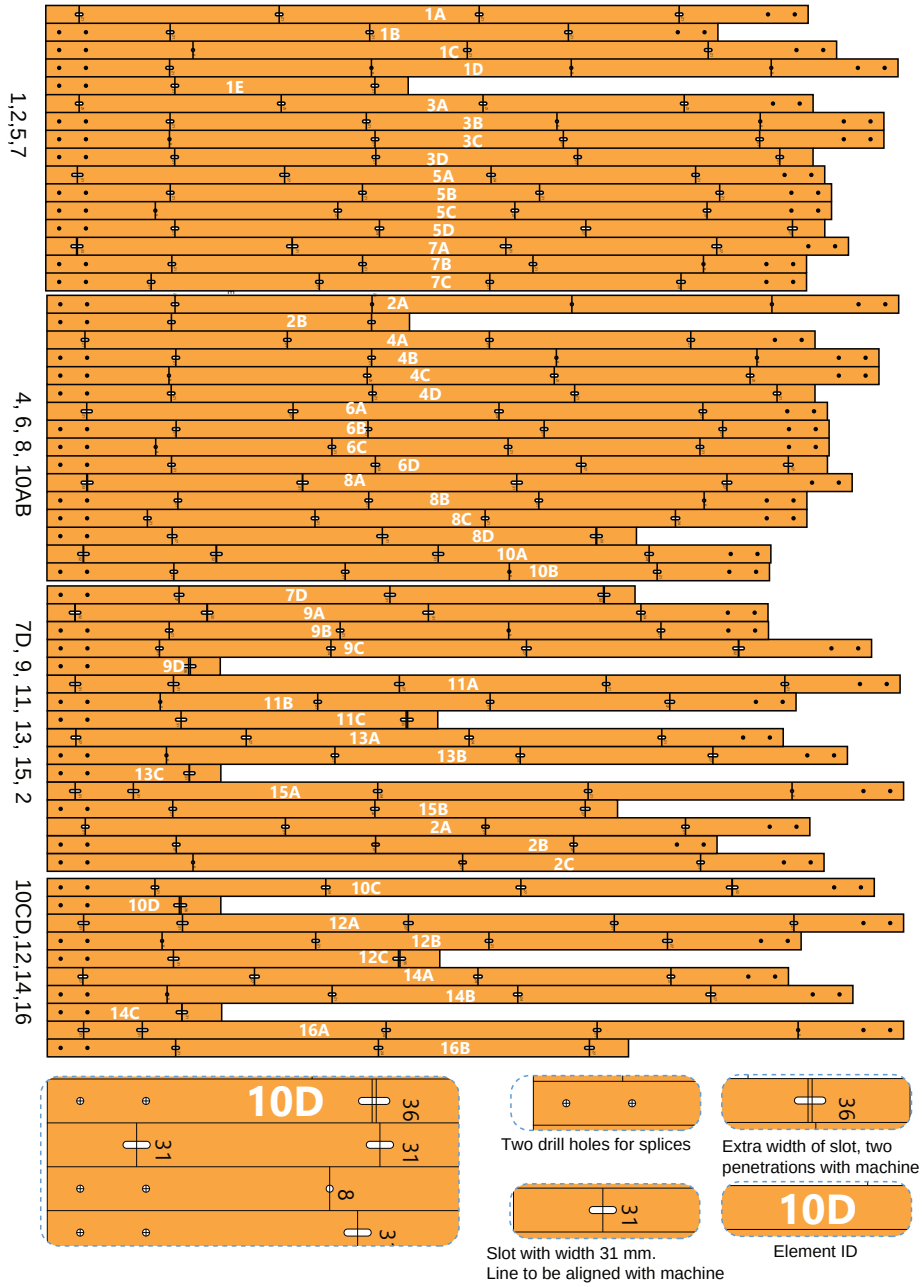

Figure A.14: *The drawings for all the lath elements, which were printed out in 1:1 scale and mounted on the plywood laths.*

The timber laths required 120 splices, needing 240 bolts (M8x25mm) and nuts, and 480 washers (one on each side) for the connections.

The production drawings for the laths to be printed 1:1 on a printer can be seen in Figure A.14. Each lath element contained an ID describing the lath number and element order in which it should be assembled to full length. On the drawings were markings for placement and width of the slot for the biscuit joiner, as well as locations for drill holes for splices.

Schematic drawings were made to obtain the correct order and direction of the laths during the assembly (Figure A.15), overcoming the potential confusion of the lath pairs described in Figure A.11. The drawing indicated the lath pairs, e.g. '1-2', the first number on the inside, and the ball indicated the starting direction where element 'A' should be.

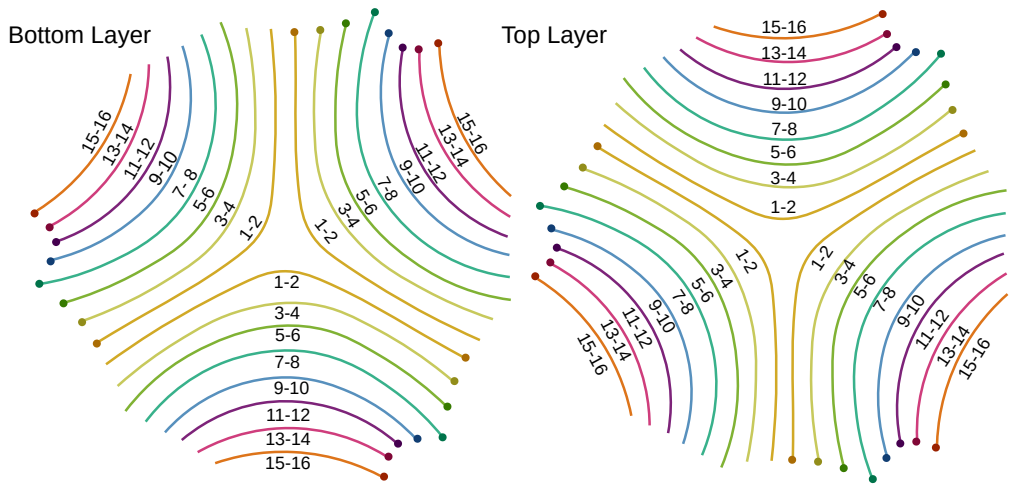

Figure A.15: *Illustrations necessary for the grid assembly showing the two laths forming pairs and their direction, with a sphere signalling the start.*

The base plates only required three dwg files (Figure A.16), where the bottom and top layers of the curved segments require three runs on the CNC and the straight segments only once. The instruction for the timber studs attached to the base plate were drawings with the indicated cutting angle of the miter and bevel cut, as well as the cut length (Figure A.16). Due to symmetry, only eight unique studs were repeated three times. Thus, 24 M8x100 bolts and nuts, 48 washers, and around 8 meters of the same timber as the blocks were needed.

A.6 Structural analysis

The structural analysis aimed to ensure the structure's safety, not its serviceability, since it was temporary and indoors in a controlled environment. Thus, the considerations regarding safety were evaluated based on this context. Had it been a permanent structure

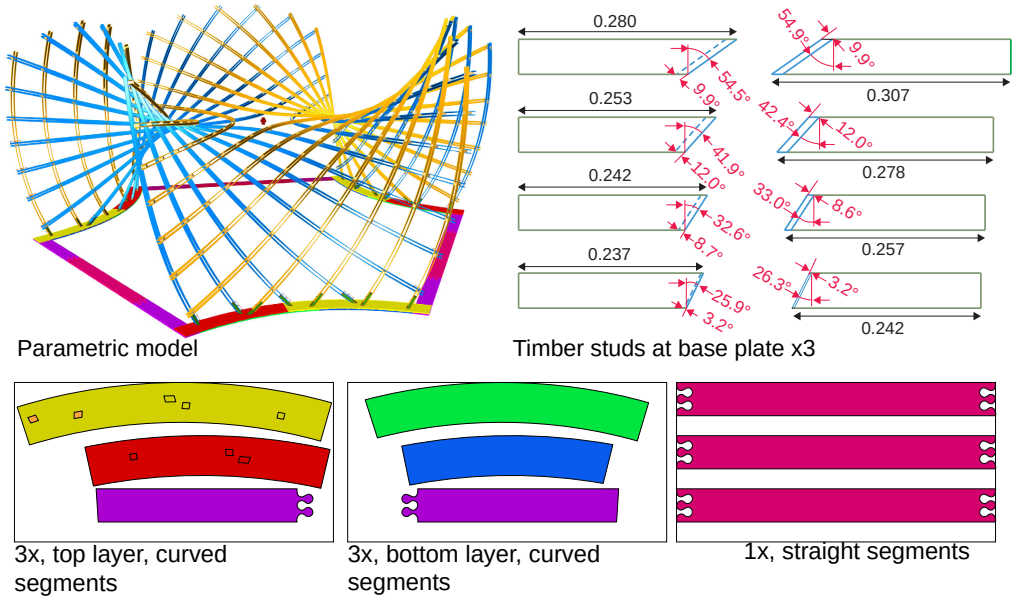

Figure A.16: *Top left, the visual output of the final parametric model. On the top right are the production drawings of the timber studs connecting the laths to the base plate. Black numbers are the cut lengths, and the red numbers are the miter and bevel cut angles described in Figure A.13. The bottom shows the three base plate drawings for the CNC.*

outdoors, other types of considerations must be considered.

The structural model was analysed using *Robot Structural Analysis*. The model was generated using BHoM, making it possible to transfer the information from the parametric model to the analysis software. The model consisted of beam elements with six degrees of freedom in each node (Figure A.17 (a)). The interface between the two layers can be seen in Figure A.17 (b). The timber block and the laths are connected by dummy elements, for which the nodes connected to the laths have the rotation along the local axis released. This is to simulate the possible rotation of the timber blocks along the axis of the bolts connecting the timber blocks and the laths (this mechanism is visualised later in Figure B.11).

The results from the analysis model should be treated and evaluated with caution, as will be explained later. Figure A.18 (a), shows the axial forces in the axis in the direction along the laths (beam elements) based on the dead weight of the structure. The analysis shows that the laths work as force couples (Vierendeel action) as intended. This can also be verified in the exaggerated deformation plot Figure A.18 (b) where the members act following the expected pattern in Figure A.4 (b). Thus, the model seems to depict the behaviour as initially intended. The analysis also gave a rough idea of the magnitude of the forces, where the maximum compression force is 0.5 kN near the supports and a possibility that those laths might buckle. Thus, two questions were asked: Is it likely to occur? What will happen if the member buckles?

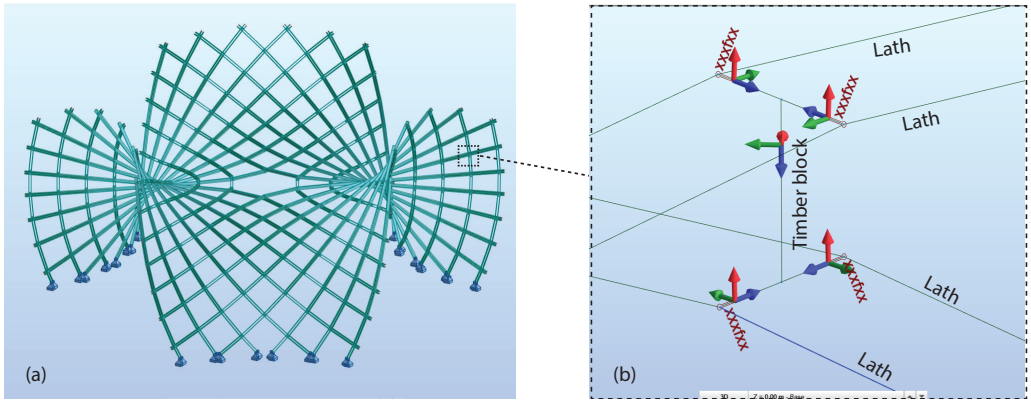

Figure A.17: *The structural analysis model in Robot Structural Analysis.* (a) *shows the entire geometry which was modelled and imported using BHoM in Grasshopper3d.* (b) *shows how the nodes have been modelled to consider the rotation of timber blocks. Dummy elements are added which are released to allow such rotation.*

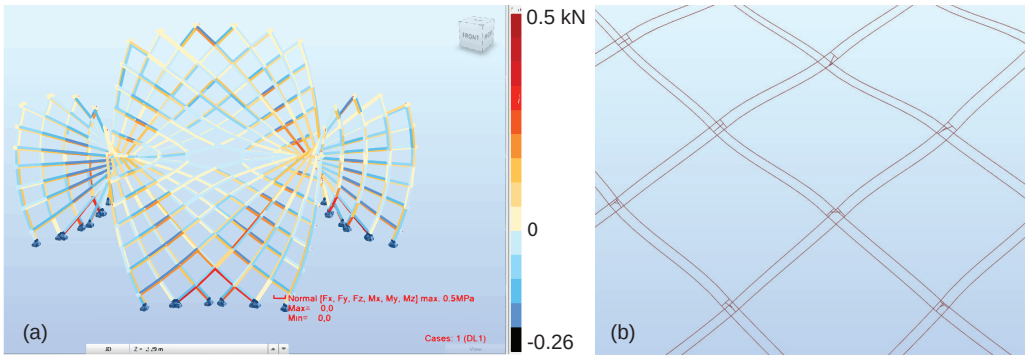

Figure A.18: (a) *The magnitude of the axial forces in the direction of the laths. In Robot, the compressive forces are red, and the ones in tension are blue. In* (b)*, the deformation pattern of the laths, which resembles Vierendeel action depicted in Figure A.4, which was the expected behavior.*

Going to the first question, is it likely for buckle to occur? It was argued that the force distribution in the structure is a hypothetical case since the shape analysed is the idealised geometric shape. This is because the structural analysis does not consider the erection procedure, and the structure needs to be pushed and forced into the idealised shape. Even though the nodes were locked using the bolts, it was believed to be likely that the structure would have some flexibility to redistribute its internal forces and, in doing so, find a more relaxed state and more even force distribution. Since it is a statically indeterminate structure, it was believed there to be many ways the structure could carry the load.

Still, what will happen if the lath would buckle? Similarly, it was believed and argued

that there would be many ways the structure could carry the load and thus redistribute the forces in the grid shell. And even a lath did buckle, the member would likely have some capacity to carry some load. Thus, there was a strong belief that it would not be dangerous to build with respect to our conditions, i.e., a temporary indoor structure where the total weight was around 200 kg.

To summarize, the structural analysis was not believed to be entirely accurate since it would assume that the structure had been forced into the geometric idealised form. Ideally, the structural analysis would include the erection procedure and the relaxation of the structure. However, getting that accurate would still be difficult for many reasons, including the necessary information about the procedure and the order of locking the nodes. Still, the structural analysis provided an overall notion of the magnitude of the forces and displacements so that the height could be adjusted for the party. With the inbuilt possibility of the structure adjusting to a more comfortable position and redistributing its forces due to the nodes, there was a strong belief it would not be in any danger. As pointed out by Box and Draper, 'Essentially, all models are wrong, but some are useful.' (1987, p. 424).

A.7 Workshop

A.7.1 Workshop day zero - Preperations

Before the two days of the workshop, there were four hours to prepare the students for the workshop and teach them the geometric concept that is the core idea behind the design. The first hour was a lecture on differential geometry and its application during the design process. This was followed by going through the script in the Grasshopper3d file. Since this was part of the course in parametric design, it was important to relate it to the prior parts of the course. Subsequently, the different tasks in the manufacturing process were described. The goal was to perform all fabrication and manufacturing on day one, and on day two, the structure would be assembled and erected. The students then assigned themselves to different tasks during the morning and afternoon of day one. It was important that they had enough information and instructions to start and enough freedom to find their best method of executing the task. This way, they would take ownership of the design and not see it as only the teacher's and the workshop leaders' design. The afternoon ended with a tour of the wood workshop where some of the fabrication would be made, such as the CNC milling of the base plates, cutting and drilling of the timber blocks, and cutting plywood board into laths. The preparations ended with a visit to the main manufacturing area and space for the assembly, the old lab facility for concrete research, and safety instructions for the machines to be operated.

A.7.2 Workshop day one - Manufacturing

The workshop day one started with one group cutting up all the 6 mm plywood bards into straight laths of 50 mm width (Figure A.19 (a)). In parallel, a group printed paper templates of the laths on a scale of 1:1 on the printer. These were cut and mounted on top of the wood laths (Figure A.19 (b)). The drawings had marks for making the

Figure A.19: *Making the laths from 6mm birch plywood board.* (a) *The boards were cut in the wood workshop using a wall-mounted saw to cut the board into straight laths of 50 mm width.* (b) *Paper templates were printed in scale 1:1 and mounted on the cut laths. With the templates, the groups responsible could use the markings for cutting the laths to correct lengths* (c) *and making the slots and drilling the holes for connections* (d).

slots using the biscuit joiner and where to cut the length using a chop saw. These first laths became the wooden templates for the rest of the identical elements. The groups making the laths could then stack several laths to make the process more time-efficient (Figure A.19 (d)). Similarly, the group cutting the lengths of the laths could tape them together and cut across all the laths (Figure A.19 (c)). Three biscuit joiner machines were available, meaning three workstations ran simultaneously, making the slots. The same number of cut saws was available and assigned to lath making.

To make the holes for the connections between the lathes, drills with a 7mm drill head for the m6 bolt were used. This gives some tolerance when assembling them to full length to avoid the mistake in 2017 (Paper B) when it was necessary to disassemble the laths and widen the holes to straighten them out.

Simultaneously, as the laths were being processed, all identical finished elements were grouped to ease the assembly process.

To make the timber blocks which connect the laths at the nodes, a table saw was used in the wood workshop to cut the blocks to the correct length of 100 mm using a fixed distance. A jig was made for a mounted drill to push the cut timber blocks against an angle to make the first drill hole for the top layer of the laths (Figure A.20). Thus, no measuring was needed for each drill hole. Then, one could rotate the block and push against the angle to drill the second hole for the bottom layer of the laths. In Figure A.20 it is possible to see all the finished blocks, and in the top of the right image one can

Figure A.20: *To the left, the timber blocks are being drilled using a mounted drill in the wood workshop utilising a jig to avoid measurements each time. To the right, the finished timber blocks and the timber studs connecting the laths to the base plate are seen.*

see the timber studs that connected the laths to the base plate. These were cut to the correct angle using a chop saw, based on the instructions with the different angles from the geometric model (Figure A.16).

The elements for the base plate were cut into the correct shapes using the CNC in the wood workshop (Figure A.21) (a). The base plate was made out of 18 mm birch plywood. Carvings were made with the CNC for where the timber studs were to be attached (Figure A.21 (b)).

Since the base plate was made of two layers of 18 mm plywood, it was necessary to assemble parts of it on the first day. Thus, the three curved segments of the base plate were glued and screwed together such that the glue would be set to the following day.

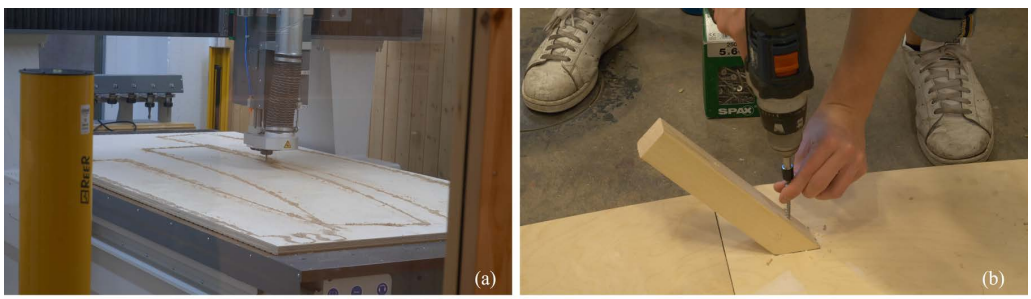

Figure A.21: (a) *The elements for the base plate were cut using a CNC in the wood workshop, which can operate on full-size plywood boards. To make the attachment of the timber studs easier, markings were made for the correct position* (b).

A.7.3 Workshop day two - Assembly and erection

The final base plate assembly was relatively straightforward due to precise cutting of the CNC. The three curved segments assembled on the first day were attached to the three

straight segments using screws.

The assembly for the grid starts with assembling the laths at full length since the elements are limited to the length of the plywood board. Afterwards, the laths that worked as pairs in the bottom layer were grouped and connected with the timber blocks. All the lath pairs were laid out according to the diagrams made to assemble the bottom layer (Figure A.15). It was important since one could easily make a mistake as described in Figure A.11. The laths for the top layer were attached to the bottom layer, using the diagram for the top layer (Figure A.15).

Figure A.22: *The laths in the bottom layer are connected to the timber blocks during the 2019 workshop. Left, a closeup of the process and to the right the connected laths are laid out before connecting the top layer.*

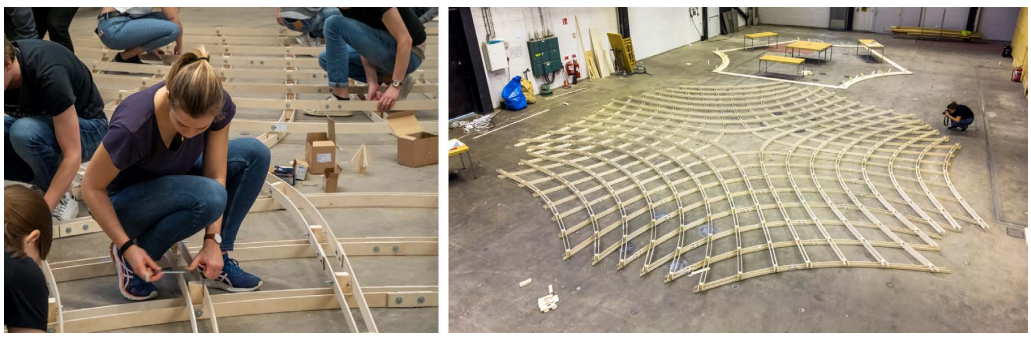

Figure A.23: *Left, the laths of the top layer are attached to the bottom layer assembled in Figure A.22 during the 2019 workshop. Right the entire grid is assembled in the flat configuration, to be compared with Figure A.9.*

The erection sequence of the structure is described in Figures A.24 (a)-(d) and can be seen as timelapse in Adiels (2020a). First, the grid was lifted such that it was placed above the assembled base plate. Tables were placed in the middle such that the center of the structure was elevated slightly (Figure A.24 (a)). This would make it easier to push the grid. Then, the students on the outside started to push parts to be attached to the base plate inwards (Figure A.24(b)). The first goal was to push and lift the structure

enough such that the grid could be attached to the base plate (Figure A.24 (c)). With the grid attached to the base plate, the structure was given enough stiffness that students could lift and push the structure from the inside. The process of reducing the mechanisms of the structure by activating the Vierendeel action by looking the laths against the timber blocks using wrenches (Figure A.24 (d)). The grid gained more stiffness continuously as more nodes were locked. It was, however, important to ensure that the grid looked proper before locking the nodes. At some locations, we had to loosen and relax the grid and possibly push it to a more correct positon before locking it again.

Figure A.24: *The erection sequence of the asymptotic timber grid shell built during the 2019 workshop.* (a) *the grid is placed on tables over the baseplate to get the initial curvature such that it can be pushed from the boundary* (b). *The first objective was to push it to be attached to the base plate* (c), *giving the necessary stability to push the rest of the structure into the desired shape. In* (d), *the nodes are being locked to remove the mechanism in the structure.*

A.8 Disassembly for reuse

It was decided to test whether the structure could be dissembled so that the laths could be reused and the structure could be reassembled at a future opportunity.

The disassembly worked well (see timelapse in Adiels (2020b)), although it would have been easier to have had as many people as during the erection. All identical lathes were grouped together and placed on two pallets (see figure A.25) and could easily have been fitted into a car for assembly somewhere else.

Figure A.25: *The grid shell was disassembled after the workshop, and the timber laths were grouped together and could easily it on two pallets for storage and possible resuse.*

A.9 Evaluation

Overall, the design and the construction during the two days of the workshop turned out very well. The improved nodes made the structure much stiffer and made it possible to get closer to the reference minimal surface. What could be improved was having a more elaborate strategy for the order of when to lock the nodes. It was necessary to loosen some of the nodes, push the structure into a better shape, and lock it again. It is, however, tricky during the quite tense erection sequence to have complete control and perhaps more semi-objectives are necessary to achieve such control.

The key outcome is that this project showcases the possibilities and benefits of utilising concepts from differential geometry from an early stage in the design process. Even though asymptotic lines was used in this case, the specific geometric concept should be adapted to the specific context and functions in mind.

Acknowledgements

The design team 2019 included Emil Adiels, Isak Näslund, Johanna Isaksson, Habiba Moubarak and Chris Williams. The work presented should be seen as a common effort, and many of the observations described are also based on discussions before and after the workshop. The project would not been built without the participation and engagement of Architecture and Engineering students in year 2. The support from Cramo for sponsoring with machines and equipment was greatly appreciated.

Appendix B

Asymptotic timber grid shell 2021

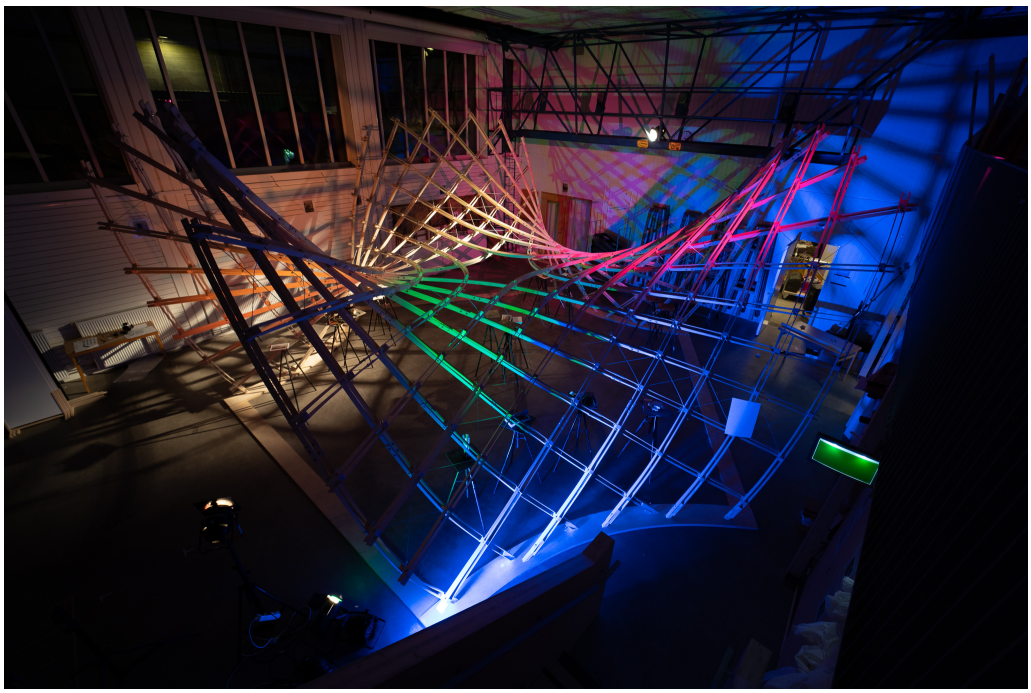

Figure B.1: *The exhibition of the asymptotic timber grid shell built during the 2021 workshop.*

The 2021 asymptotic timber grid shell workshop took place on the 16-17th of December. The research challenge and the design objective were the same as in 2019, as described in Appendix A, designing an indoor pavilion for an exhibition that our students could fabricate and build in just two days. The context was the same regarding the course and the students. The only difference was the space, which was smaller than in 2019.

Due to the COVID-19 restrictions, which meant it was uncertain if the workshop would take place and restricted possibilities to meet during the design stage, it was decided to reuse the laths from the 2019 workshop and improve or modify the design. The specific design objective was to add bracing to fully reduce the mechanisms in the erected state, making the structure stiffer than in 2019. Thus, combining strategies in Figure A.4 (a) and (b). The resulting structure is shown in Figure B.1.

The main challenges and difficulties during the design process were how to design the node (see Section B.1), choosing a bracing pattern for the structure (see Section B.2), and geometric modelling related to the practical aspects of bracing assembly (see Section B.3) to generate all the necessary instructions for the workshop (see Section B.4).

The final test of implementing and executing the manufacturing and construction during the workshop in just two days is described in Section B.5.

B.1 Nodal design and prototype

There were different approaches discussed for the nodal design. Using a similar timber block as in 2019, one could extend it to the bottom or top to add bracing. The other alternative was to slightly separate the laths to place the bracing in the middle surface. The second alternative was chosen to avoid eccentric forces in the bracing, and we were afraid that the timber blocks would need to extend quite far for the drill holes not to splinter the wood.

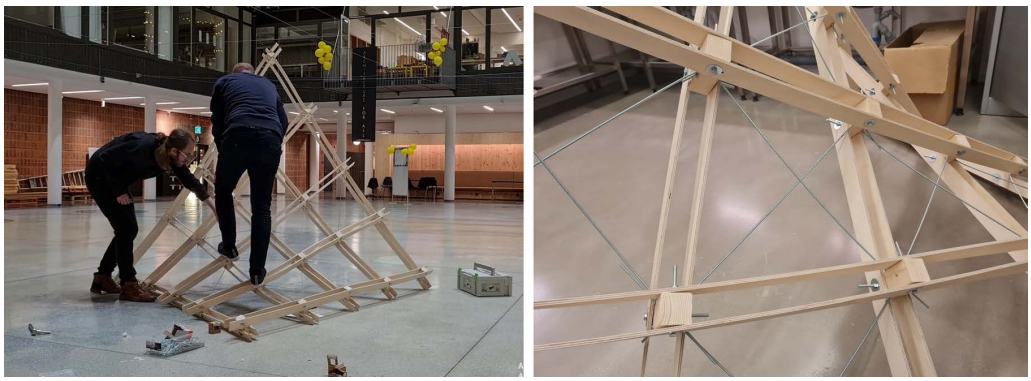

Figure B.2: *The prototype built prior to the actual structure in 2021. Left the load test to see if the bracing was activated. Right, a closer look at the details.*

However, it was necessary to examine how that would affect the laths to separate them further from the middle surface. It did not affect it very much. Most laths had a deviation around 0.5-1.8% and some between 2% - 2.5% from a straight line. This was slightly larger than the 2019 grid shell. However, from a practical point of view and experience, this is within tolerance when assembling the laths to full length since there will be a tolerance in the spliced connections. These laths will never be entirely straight with manual fabrication and drilling (Adiels, 2018, 0:35-0:42). It was also believed that such a small magnitude of deviations could, to some extent, be handled through elastic deformation and tolerances in the splices.

A similar prototype was made using the same geometry as in 2019 (Figure A.8). The bracing was applied in the two directions of the surface parameters, similar to stiffening a plate in two dimensions (Figure B.2). Since it would be difficult practically and expensive to tension real cables, it was decided to use threaded steel rods (M4x1000mm) going through the timber blocks, which could be tensioned by adjusting the nut against the timber block.

Before making the prototype, it was thought only four timber blocks were needed, i.e. no bracing, one tension tie, two tension ties and three tension ties. However, the first

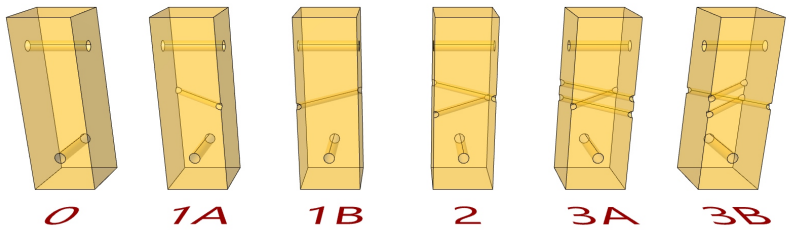

Figure B.3: *From the building of the prototype in Figure B.2, it was clear that it was necessary to have two versions of the blocks having one and three bracing elements attached. Thus, it was necessary to have six different types of timber blocks.*

important realisation was that it was necessary to have two versions of the ones with one and three tension ties (Figure B.3). The second realisation was that it was quite difficult to attach the threaded rods in the timber blocks after erecting the structure. Thus it would be easier to apply in the flat state. However, one would then need to know which direction of that would be on top and bottom. Otherwise, they would tangle themselves in the erected state, which was the third realisation from the prototype.

The final test was to climb the structure to see if the bracing was activated as intended, which it did and could handle quite a substantial load.

B.2 Design of bracing pattern using canonical stiffness

While the design of the nodal connection was decided, the question was how to choose the cells to apply the bracing, and there are numerous approaches that one could take. Three approaches were discussed, of which the first was to choose a dominant load case and design a system which transfers the load most efficiently to the supports. The second alternative was to think of the structure as a mechanism and try to find the most efficient way to remove all mechanisms. The third option was to perform an optimization using one or more criteria.

A combination of the second and third approaches was chosen. It was carried out using a combination of drawing and reasoning, physical model tests, and structural analysis using the canonical stiffness of the system (Olsson, 2005) as the chosen evaluation parameter (Figure B.4).

Evaluation of the canonical stiffness can be formulated as an eigenvalue problem

$$\det\left(\mathbf{K} - \lambda\mathbf{I}\right) = \mathbf{0}, \tag{B.1}$$

where $\mathbf{K}$ is the stiffness matrix. The higher the value of the lowest eigenvalue λ_0, the higher the overall stiffness of the structure. In mathematical terms, a design that maximizes λ_0 is sought.

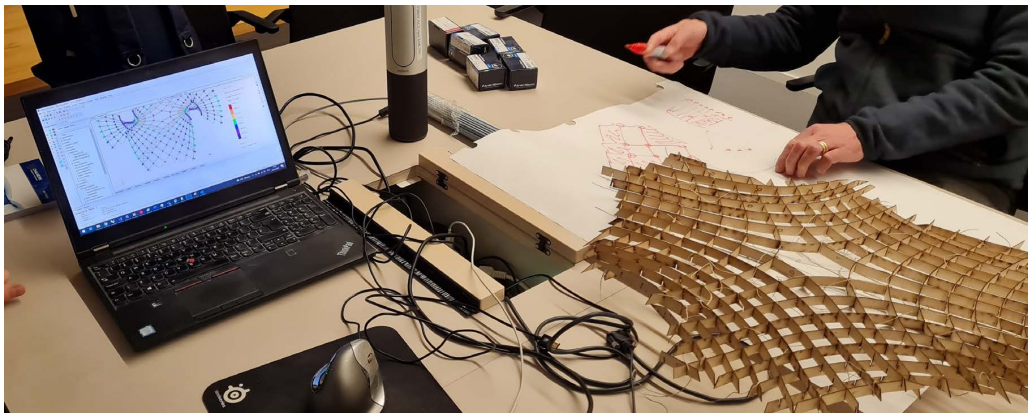

Figure B.4: *Design process of the bracing pattern using a combination of drawing and reasoning, physical model tests, and structural analysis.*

Structural reasoning originated from Figure A.3 (a) of the grid shell built in 2018, there was a stiff triangle, coloured blue, given by the fixation along the boundary. It was observed that if the blue triangle were seen as a fixed boundary, the cells would be locked between an offset v-shaped bracing (Figure B.5 (b)). This can be compared to the case of a regular 2D grid where the cells along the boundary are not locked in Figure B.5 (a). Thus, the v-shaped bracing in Figure B.5 (b) was a promising starting point for different pattern designs.

The different options generated through sketches were transformed into the parametric model where the canonical stiffness could be calculated and evaluated, as seen in Figure B.6 (Adiels, 2022a). The most promising option chosen is seen in Figure B.6.

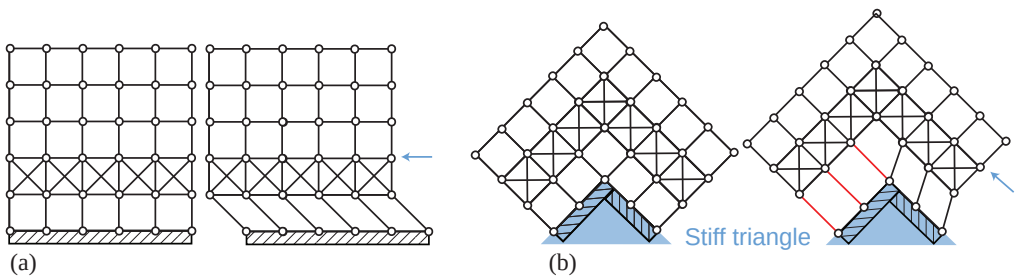

Figure B.5: *Left, a grid only braced along the grid lines in one direction is still sensitive for a load in the same direction. However, due to the stiff triangle from the supports (Figure A.3), a bracing pattern following the grid locks hinders the mechanism for the members inbetween.*

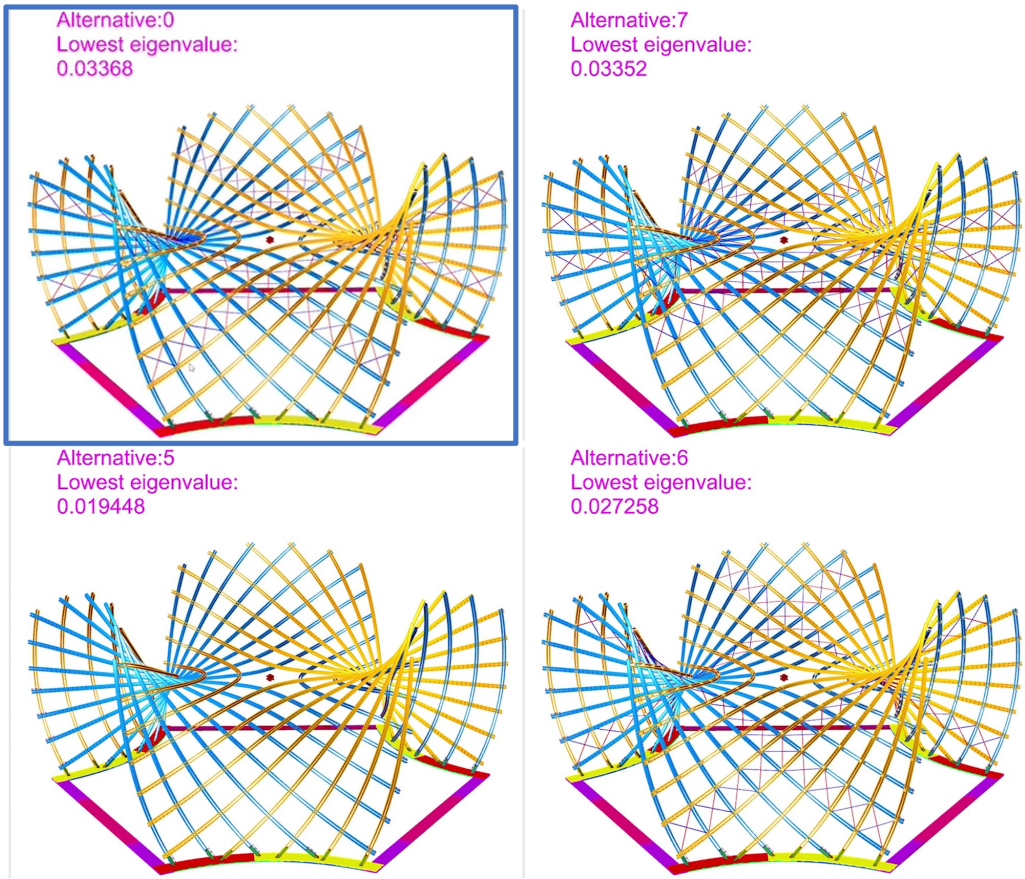

Figure B.6: *Evaluation of some of the alternatives of bracing patterns based on canonical stiffness. The highlighted alternative in blue was the one used in the final design.*

B.3 Geometric modelling

Much of the modelling was reused since the design was identical to the 2019 gridshell, except for the node details. Thus, the reader is directed to Section A.5 for further details not covered here.

The specific objectives for the modelling in 2021 were based on the three observations from the prototype (see Section B.1) and the desire to automatically generate the production drawings for different options for bracing patterns (see Section B.2) as seen in Figure B.6. The first objective was automatically detecting which of the two ties would be below or above a given bracing pattern. The second objective was to find the positions for the different versions of the timber blocks for the ties to be attached to (Figure B.3). The third objective was to find the proper cut lengths of the ties, which needed to be decided based on the flat and the erected grid.

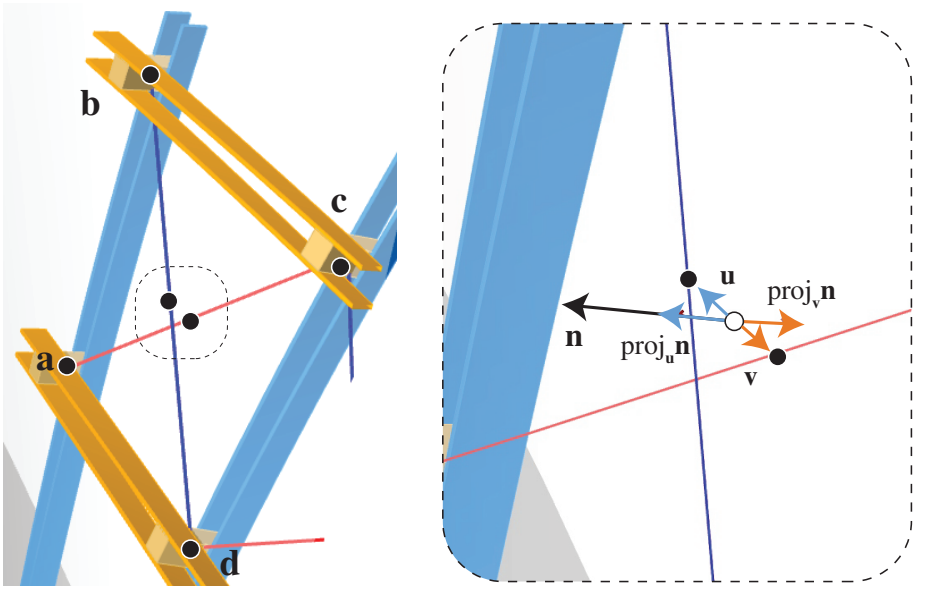

Figure B.7: *It was possible to categorize the tension ties acting as bracing automatically based on the position, blue on top and red below, using the normal* $\mathbf{n}$ *of the middle surface.*

There are several ways to solve the first objective detecting the top and bottom tension ties. In this case, it was solved using the four points ($\mathbf{a}$, $\mathbf{b}$, $\mathbf{c}$, $\mathbf{d}$ in Figure B.8) of each face and the normal $\mathbf{n}$ of the surface. The normal is taken at the point $(\mathbf{a}+\mathbf{b}+\mathbf{c}+\mathbf{d})/4$. The vector $\mathbf{v}$ is found by

$$\mathbf{v} = \left(\frac{\mathbf{a}-\mathbf{c}}{2}+\mathbf{a}\right) - \frac{(\mathbf{a}+\mathbf{b}+\mathbf{c}+\mathbf{d})}{4}. \tag{B.2}$$

To know whether it is below or on top, the vector is projected onto the normal given and the given a colour based on its direction

$$f(\mathbf{n},\mathbf{v}) = \begin{cases} \text{blue}, & \text{if } \dfrac{\text{proj}_{\mathbf{v}}\mathbf{n}\cdot\mathbf{n}}{|\text{proj}_{\mathbf{v}}\mathbf{n}|\,|\mathbf{n}|} = 1 \\ \text{red}, & \text{otherwise .} \end{cases}$$

The same process is done for the tension tie between $\mathbf{b}$ and $\mathbf{d}$. The result can be seen on the left of Figure B.8.

With the information regarding the position (red or blue) of the tension ties, it was possible solve the second objective, which was to find the position of timber blocks 1A, 1B, 3A and 3B (Figure B.3) in the grid, as shown in Figure B.8.

The third objective was to calculate the actual cut lengths of the threaded rods acting as tension ties. Since they were to be attached in the flat state and adjusted in the erected state, information about the diagonals ($(\mathbf{a}-\mathbf{c})$ and $(\mathbf{b}-\mathbf{d})$ in Figure B.7) in the flat and

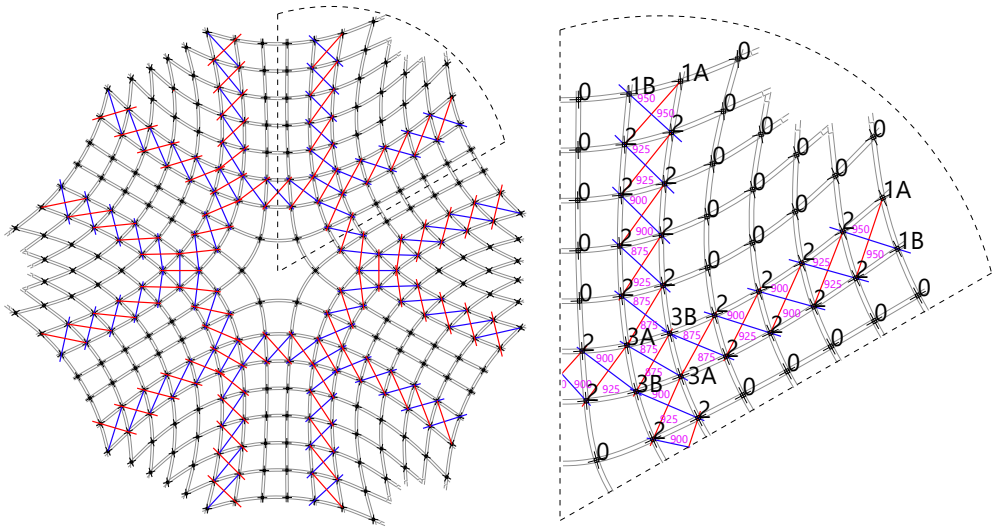

Figure B.8: *The production drawings show the bracing's placement and position (blue on top and red below). The lengths of the bracing are also written in purple. The black numbers indicate the type of timber block as seen in Figure B.3.*

erected state was necessary. The necessary cut length $l_{bracing}$ was the maximum value of

$$l_{bracing} = d_{block} + \max\left(\left(l_{flat} + e_{flat}\right), \left(l_{surf} + e_{surf}\right)\right), \tag{B.3}$$

where the length of the bracing l_{surf} and l_{flat} is the distance $|\mathbf{a} - \mathbf{c}|$ or $|\mathbf{b} - \mathbf{d}|$ on the surface and in the plane respectively. The variables e_{surf} and e_{flat} minimal allowed extension allowing for screwing the nuts on the rods in the erected and flat state. These values were chosen based on the experience from the prototype. In this case, $e_{surf} = 80mm$ and $e_{flat} = 30mm$ were chosen. The lesser value in the flat was motivated by the fact that the friction alone would hold it in threaded rods in place during erection. And d_{block} is the diagonal of the timber block cross-section, which in this case was $45\sqrt{2}mm$.

To reduce the number of unique lengths of the ties, the cut lengths $l_{bracing}$ grouped in categories at certain intervals, which in this case was a step size of 25 mm. The results can be seen in the right of Figure B.8, where the lengths are in purple, and it is possible to observe that the red and blue lines extend beyond the nodes.

B.4 Production data and drawings

Since the base plate, laths and timber studs for the base plate were the same as in 2019, much of the production drawings and data were similar to the grid shell in 2019 (see Section A.5). In addition to the drawings and data in Figures A.23 and A.16, the drawing of the grid and bracing shown in Figure B.8 was needed.

Bracing	
Rod length [mm]	Quantity
875	36
900	60
925	42
950	30
Nodes	
Node type	Quantity
0	132
1A	12
1B	12
2	120
3A	12
3B	12

Table B.1: The quantity of the different bracing lengths as well as the different timber blocks for the nodes.

The number of the different cut lengths of the threaded rods (M4x1000mm) can be seen in Table B.1, which would need 168 nuts and 336 washers. The number of different types of nodes (Figure B.3) are described in Table B.1. The amount of bolts (M6x100mm), nuts and washers was the same as in 2019 Section A.5.

B.5 Workshop

Like the workshop in 2019 (see Section A.5), an afternoon before the workshop was used to prepare and instruct the students so that the starting process on the first day would be more time efficient. The preparation was done similarly in 2021 with a few adjustments. Thus, the reader is directed to Section A.5 for more information regarding the preparation.

Since all the laths were reused from 2019, the manufacturing was simpler. However, the assembly was more complicated due to the bracing. Thus, it was desirable to start the assembly as soon as possible.

There were four different areas of manufacturing: base plate, timber studs at the base plate[1], timber blocks for the nodes, and threaded rods. In parallel, the laths needed to be assembled to full length. The bottleneck would be manufacturing the timber blocks since the assembly of the flat grid could not start without them. Thus, it was essential that it would be a fast process.

The timber blocks for the nodes were a bit more complicated than in 2019 due to the bracing. Thus, an additional jig to the one used in 2019 was made to drill the diagonal holes to make the process faster. To make the process even faster, two parallel workstations were drilling the holes for the bolts and the ones for the bracing, see Figure B.9.

[1]The base plate and the timber studs were manufactured in the same fashion as in 2019, and the reader is directed to Section A.5 for this procedure.

Figure B.9: *Left, the jig used to drill the holes for the bracing. Right, a different jig to drill the holes for bolts connecting the laths.*

When the timber blocks were finished, the assembly of the lath pairs of the bottom layer started. This was similar to 2019 (Figure A.22), except for the need for the right node type at the right place. Thus, the drawing of the bracing and the nodes (Figure B.8) was essential. This also meant that the flat grid assembly took longer time than in 2019. However, the assembly started earlier. The assembly of the bottom and top layers of the grid was almost finished at the end of the first day.

The second day started with attaching the threaded rods (Figure B.10) cut to the correct lengths the first day, working as bracing using the drawing in Figure B.8. This was finished just before lunchtime, and the erection could start directly after lunch.

One of the difficulties with the erection was that the space was much smaller and tighter than in 2019, and the flat grid did not fit. Thus, it was necessary to start in a position which was not optimal. Otherwise, the process was very similar to 2019, but the

Figure B.10: *The threaded rods, acting as bracing, are added in the assembled structure on the ground before the erection. On the left, the printed drawing in Figure B.8 is used for the correct placement.*

tighter space made adjusting to the right position more challenging. It was also more difficult to transport and fit the scaffolding towers for the locking of the nodes. This could be the reason one of the timber studs broke during the erection, and it was also tricky to get it properly into position before the locking of the nodes started. This can affect the regularity of the grid if not coordinated correctly. Afterwards, it was possible to locate some areas that were better than others, but it was quite difficult to adjust due to space restrictions and the repair of the timber studs. Another issue not considered was that the spacing between the laths allowed the node to rotate slightly (Figure B.11), which it did not in 2019, making the procedure more difficult. There was also a hurry to be finished on time for the exhibition, making it more difficult to loosen and readjust some parts of the structure.

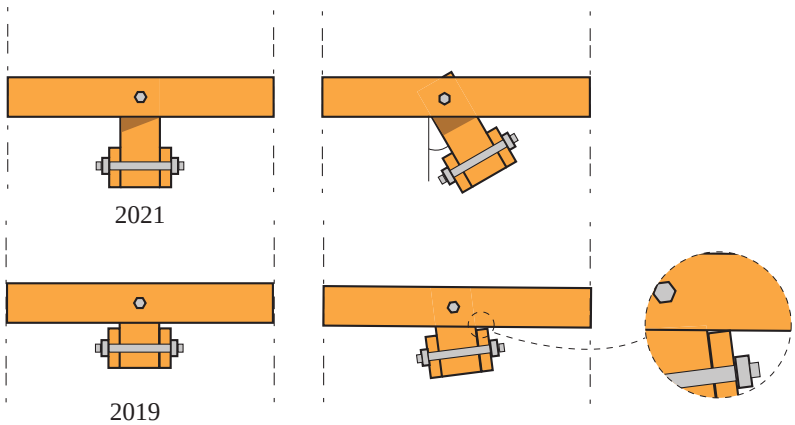

Figure B.11: *Top showing a mechanism (exaggerated) where the timber block can rotate. This rotation was hindered in the 2019 node below since there was little or no distance between the laths.*

After the grid was locked, the adjustment of the bracing started. The goal was not to add any pretension but to be the correct length to be activated with added loads. This took quite a long time, as the threaded rods were quite long, and the nuts needed to be screwed quite far to come into contact with the timber blocks. The final adjustments to the structure were made just before the party at 6 o'clock.

The entire assembly and erection of the grid shell (Figure B.12) can be seen as a timelapse in Adiels (2022b).

B.6 Evaluation

Even though there were great similarities between this design and the one in 2019, it was a much trickier assembly where more things could go wrong, such as the right timber block at the right location and the proper placement (top or below) of the bracing. Even so, there were no mistakes during assembly, meaning the instructions and the material

Figure B.12: *Erection procedure of the grid shell in 2021.*

provided were good and sufficient.

It was a mistake separating the laths and placing the bracing in the middle surface. It was based on the notion that the forces in the bracing would be eccentric with respect to the middle surface. However, as described in the Figure B.11, the allowed rotation had more disadvantages. Thus, it would have been better to place bracing on top or below, where the former would have been easy during the flat assembly.

The structure was load-tested using the bodies of the design team. Two members, with a combined weight of around 180 kg, could hang in the middle of the structure. The bracing was activated, and the structure could handle a load similar to its weight. Thus, even though the placement in the mid-surface between the top and bottom layer was a mistake, since it allowed rotation of the timber blocks, the bracing clearly added stiffness to the structure. Overall, the design and the execution of the experiment during the workshop were considered a success.

Acknowledgement

The design team 2021 included Emil Adiels, Isak Näslund, Emil Poulsen, Puria Safari and Chris Williams. The work presented should be seen as a common effort, and many of

the observations described are also based on discussions before and after the workshop. The workshop also relied on contributions by Johanna Isaksson and Habiba Moubarak in 2019. The project would not been built without the participation and engagement of Architecture and Engineering students in year 2. The support from Cramo for sponsoring machines and equipment was greatly appreciated.

Appendix C

Hydrostatic masonry bridges

Figure C.1: *Physical model of a single-span hydrostatic masonry bridge built during a workshop in 2022.*

The objective of this case study and workshop was to design and build a model based on the concept of hydrostatic shells for masonry bridges covered in paper D. While paper D covers the historical context and the theory behind the form-finding, the purpose was to make a proof of concept model of a single-span bridge seen in Figure C.1. The specific areas of interest were investigating how well the form finding could work in the design process and relating the design and dimensions to built masonry arch bridges.

The assumptions of the scale effects are described in Section C.1. The form finding of hydrostatic single-span shells is described in Section C.2 and its application in Section C.3. The geometric modelling for the fabrication and the fabrication is covered in Sections C.4 and C.5.

C.1 Scale effects of masonry models

Structural analysis of masonry arches and vaults is usually not a question of strength but stability. This is because the stresses are relatively low in the architectural scale of, for instance, cathedrals, as Heyman (1995) describes. Hence, Heyman states three key postulates that translate the plastic theorems from steel to masonry: masonry has no tensile strength, stresses are so low that masonry has effectively an unlimited compressive strength, and sliding failure does not occur. As long as a solution of the line of thrust, or an inverted 'hanging chain', can be found within the structural thickness, the structure is safe (see the analysis by Poleni Figure 4.2). This means structural stability is a question of equilibrium, and the behaviour and the results from the masonry model can be scaled

to the actual structure since it is a question of proportions. Compared to the case of a grid shell, such as in the design process in Mannheim, dimensional analysis must be performed to scale and interpret the results from the model test to the actual structure (Happold & Liddell, 1975). Models have historically been used to verify masonry theory where early studies include Danyzys experiments (Frézier, 1739) (Figure C.2) with masonry arches to verify the masonry arch theory by Couplet (Heyman, 1998). A theory in which Couplet, in fact, formulated the postulates by Heyman.

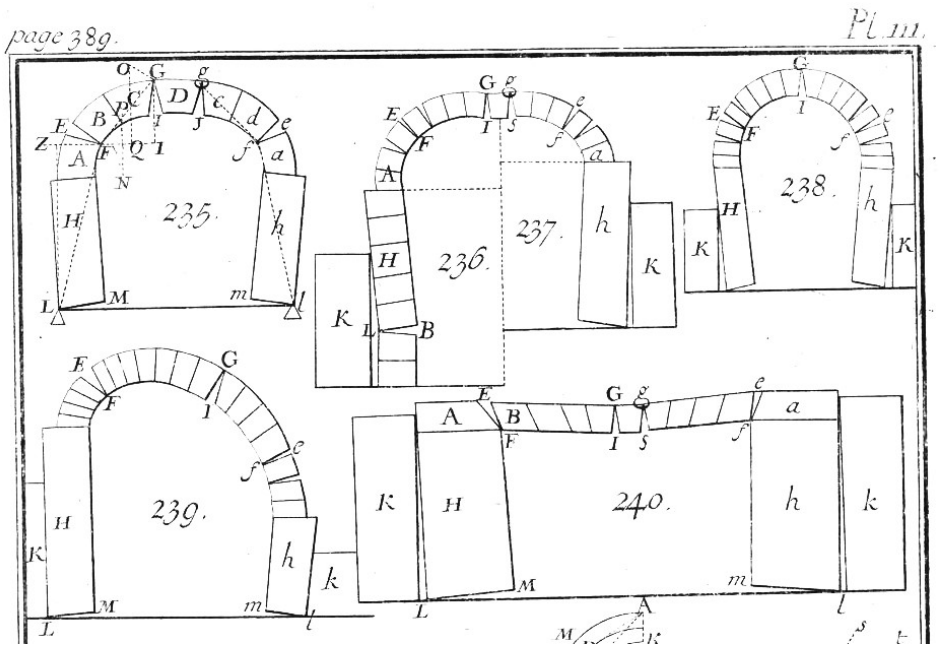

Figure C.2: *Depictions of Danyzy's experiments of masonry arches in La théorie et la pratique de la coupe des pierres et des bois pour la construction des voûtes et autres parties des bâtiments civils & militaires, ou Traité de stéréotomie, à l'usage de l'architecture. Tome 3 (Frézier, 1739).*

It is known that traditional masonry structures designed based on gravity are not affected by scaling effects (assuming an architectural scale). Masonry bridges often contain a considerable amount of fill material (which is the foundation behind the idea of the design concept of using hydrostatic shells presented in Paper D). The question is how well a model of a masonry bridge scales.

Looking at the scaling of the fill or soil. From the Mohr-Columb criterion

$$\tau = c' + \sigma' \tan \phi', \tag{C.1}$$

where τ is the shearing stress acting on the plane of failure and σ' is the effective normal stresses to the same plane. The effective stress is the total stress minus the pore water pressure. For a fill that is a granular soil that allows water and air to penetrate through

the soil, the pore water pressure has less influence. The cohesion and friction angle are the material constants c' and ϕ', respectively.

The cohesion c' should be affected by scaling. However, using dry sand as the fill could be seen as cohesionless soil (Heyman, 1972), meaning $c' = 0$ in (C.1). In such cases, the soil is purely frictional and only the ratio between the shear and normal stresses matters.

If the fill is purely frictional, one could imagine that it would be a conservative assumption and that real fill would be safer. These are the assumptions made for making these models, even though one must consider if the three postulates from plasticity theory still hold.

C.2 Form finding hydrostatic single-span bridge

The equilibrium equation for a membrane shell can be written as

$$\frac{1}{\sqrt{a}}\left(\sigma^{\alpha\beta}\sqrt{a}\mathbf{a}_\beta\right)_{,\alpha} + p^\beta \mathbf{a}_\beta + p\mathbf{n} = 0. \tag{C.2}$$

Green & Zerna use $n^{\alpha\beta}$ instead of $\sigma^{\alpha\beta}$ for the membrane stress tensor and $\mathbf{a}_3$ instead of $\mathbf{n}$ for the normal. For a hydrostatic shell, i.e only having a hydrostatic load excluding gravity one assumes

$$p = -\rho g z \tag{C.3}$$

$$\rho g = \text{weigth per unit volume} \tag{C.4}$$

$$p^\beta = 0. \tag{C.5}$$

In form finding, the stresses and loading are known, and the geometry is unknown. For this problem, one can use the already mentioned techniques, such as dynamic relaxation and force density method, see, for instance, (C. J. K. Williams, 1980). However, for the special case of a single-span bridge, assuming a grid of geodesic coordinates and where the forces flow along the geodesics, it can be much simpler. Rewriting (C.2) to

$$T_b\mathbf{b} - T_a\mathbf{a} + \frac{\rho g z}{4}(\mathbf{a}+\mathbf{b}) \times \mathbf{c} = 0, \tag{C.6}$$

where $z \leq 0$. Vector $\mathbf{a}$ is $\mathbf{r}_{i,j} - \mathbf{r}_{i-1,j}$, $\mathbf{b}$ is $\mathbf{r}_{i+1,j} - \mathbf{r}_{i,j}$ and $\mathbf{c}$ is $\mathbf{r}_{i,j+1} - \mathbf{r}_{i,j-1}$ for a grid as in Figure C.3. T_a and T_b are the force densities at $\mathbf{a}$ and $\mathbf{b}$. The unknown in this case is $\mathbf{b}$.

Geodesic coordinates mean that one of the coordinate curves follows geodesics, and the other coordinate curves intersect at a right angle and have a constant spacing. We only need to impose two of these conditions since the third results from the other two. In this case, it is assumed that the spacing is constant $|\mathbf{a}| = |\mathbf{b}| = L^2$. The condition of orthogonality comes from the set boundary conditions, blue in Figure C.3, which is the transverse section profile to the span of the bridge at mid-span. Thus, the geometry is found by integrating along the geodesics (coming from the two other conditions), finding $\mathbf{b}$ to get the new position of $\mathbf{r}_{i+1,j}$.

The expression (C.6) can be simplified by assuming $T_a = T_a = T$

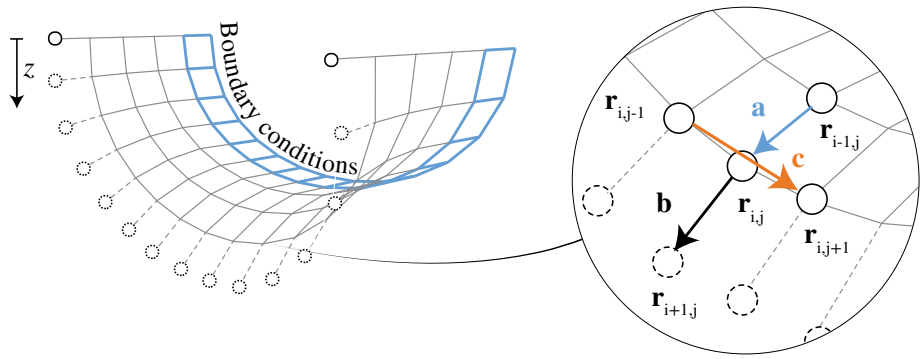

Figure C.3: *Form finding of hydrostatic shell with geodesic coordinates. Left, the right angles are given by the set boundary conditions. Right, the vectors* $\mathbf{a}$ *and* $\mathbf{b}$ *are the direction of the geodesics. The vector* $\mathbf{c}$ *is the direction of the orthogonal trajectories.*

$$\mathbf{b} - \mathbf{a} + \frac{\rho g z}{4T} (\mathbf{a} + \mathbf{b}) \times \mathbf{c} = 0. \tag{C.7}$$

One can find the expression for $\mathbf{b}$ as a linear combination of $\mathbf{a}$, $\mathbf{c}$ and $\mathbf{a} \times \mathbf{c}$

$$\mathbf{b} = \alpha \mathbf{a} + \beta \mathbf{c} + \gamma \mathbf{a} \times \mathbf{c}, \tag{C.8}$$

which is then plugged in into C.7. After solving the constants α, β and γ one can get an expression for $\mathbf{b}$ as

$$\mathbf{b} = \frac{(1 - \mathbf{q} \cdot \mathbf{q})\, \mathbf{a} + 2\, (\mathbf{a} \cdot \mathbf{q})\, \mathbf{q} - 2\mathbf{a} \times \mathbf{q}}{1 + \mathbf{q} \cdot \mathbf{q}}, \tag{C.9}$$

where $\mathbf{q} = (\rho g z / 4T)\, \mathbf{c}$.

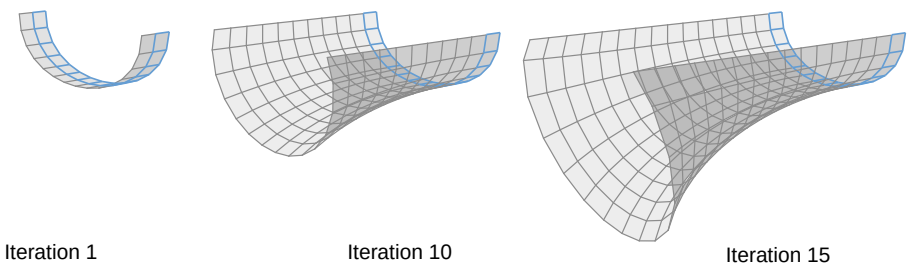

Figure C.4: *Form finding in progress at iteration 1, 10 and 15. The blue lines are the set boundary conditions.*

The form finding is illustrated in Figure C.4. The left part of the image shows the first iteration, and the following two parts shows the simulation at iterations 10 and 15. Depending on the choice of force density and the starting profile (blue) one get different

results. After a certain amount of iterations, the surface will fold in on itself, similar to the case of a hydrostatic arch (Rankine, 1895).

C.3 Shape of the bridge

The form finding technique presented requires the designer to specify force density and the transversal section at mid-span of the bridge. Force density affects the span-to-rise ratio, where a lower force density will require higher curvature of the geodesics. The specified profile's shape and curvature affect the cross-section's stiffness. More curvature should give more stiffness and thus attract forces, similar to the fold in a piece of paper. In Figure C.5 and Figure C.6 are different examples of the mid-span profile, showing the magnitude of the curvature in red and how it affects the overall shape of the bridge. This is most visible on the *superelipse* or *Lamé curve* to the right in Figure C.5 and Figure C.6.

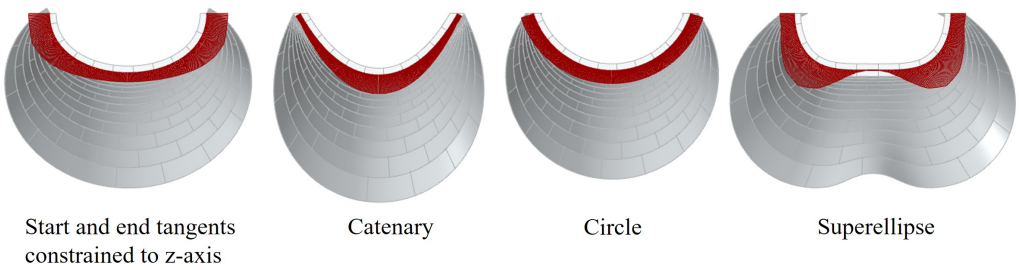

Figure C.5: *Front view of alternatives that generated having different on the starting profile at mid-span during form finding. The red graph shows the magnitude of curvature of the profile curve.*

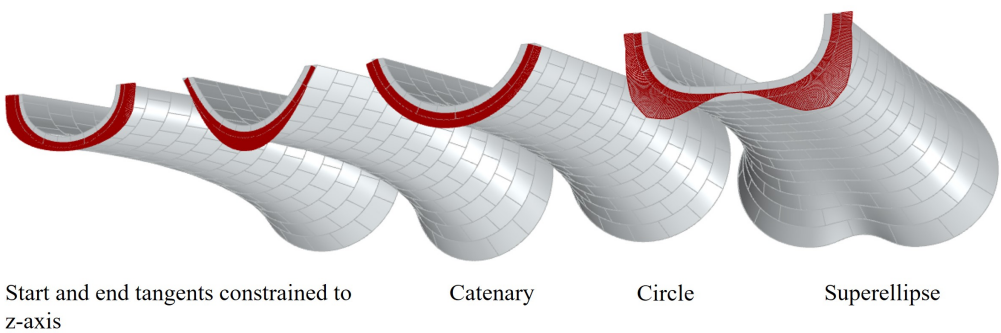

Figure C.6: *Perspective view of alternatives that generated having different on the starting profile at mid-span during form finding. The red graph shows the magnitude of curvature of the profile curve.*

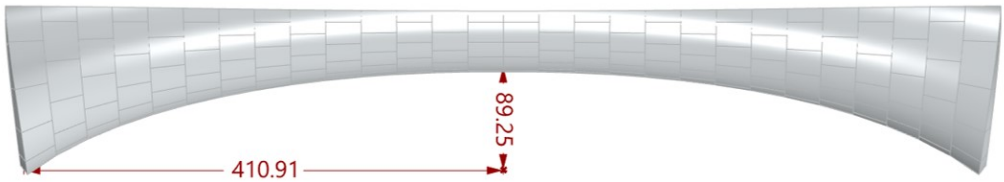

Figure C.7: *Elevation of the bridge, the left alternative in Figure C.5, showing the span to height dimensions.*

For this particular bridge model, the left profile was chosen to find a reasonable smooth curve where its tangents at the end and the start were vertical to simplify construction. One could have chosen a circle, but the fill depth was considered too deep. For this design, the fill depth to span ratio at the crown was 0.045, which is quite normal compared to other masonry arch bridges where it is common to lie between 0.04-0.06 (Figure 8 in (Brencich & Morbiducci, 2007)).

The span-to-rise ratio was chosen to be 0.11 (Figure C.7), considered a shallow bridge for masonry arch bridges. Shallow arch bridges are considered between 0.15 and 0.30, where the average value is 0.20 in historic and contemporary bridges (Brencich & Morbiducci, 2007). As a reference, the Maidenhead Railway Bridge by Brunel has a span-to-rise ratio of 0.19, which was considered very shallow when built. However, since this bridge is not an arch but a shell, it is difficult to compare directly.

The thickness of the bridge model was chosen to be 10 mm, giving it a ratio between the thickness in the crown and the span to be 0.012. This is considered low compared to other masonry arch bridges in the survey by Brencich and Morbiducci (2007), where most lie in the span 0.05-0.07.

C.4 Geometric modelling

The geometry for the model was modelled in Grasshopper3d. This included the building blocks, abutments, the base plate, and the falsework supporting the blocks during the assembly (Figure C.8).

The blocks were modelled such that the bed joints followed the orthogonal trajectories. Spherical groves and bulges were modelled on each block to work as male and female connectors during the assembly. The spherical geometry was chosen such that the connector would not transfer any moment or inflict any bending capacity when assembled.

C.5 Fabrication and assembly

The masonry bridge was manufactured and assembled by students during a two-day workshop in a voluntary course in computational design called *Virtual tools in a material culture*. The video (Adiels, 2022c) shows the entire process described.

The abutments, which had grooves for the first course of blocks, and the falsework were milled using a CNC machine.

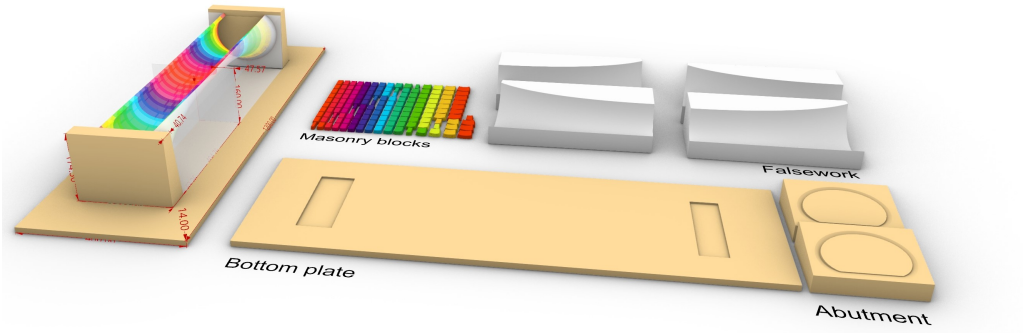

Figure C.8: *The geometric modelling of the bridge in Grasshopper3d.*

The masonry blocks were 3D printed using an SLS printer ProJet CJP 660 (Figure C.9). The material is similar to gypsum, and the printed parts can be fragile during handling. Thus, the blocks were impregnated with 3D Systems ColorBond, which is a type of resin used to increase the strength of the prints and make them less fragile.

The model was assembled (Figure C.10) as dry masonry, meaning there is no glue or mortar applied during assembly. Since the concept relies on the weight of the fill, the falsework was not removed until the fill had been applied, which in this model was finely-grained sand. The final model can be seen in Figure C.1 and Figure C.11.

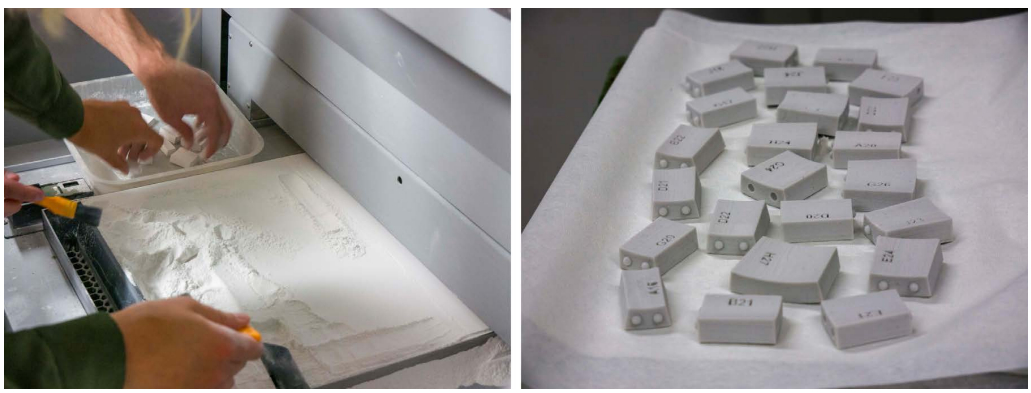

Figure C.9: *Left, 3D printed blocks being taken out of the 3D printer. Right, blocks dry after being impregnated with resin improving their strength and making them less fragile.*

C.6 Evaluation and future work

Even though the fabrication and assembly were a success, proving the fundamental aspects of the concept, future work would be to perform structural analysis and load tests on hydrostatic masonry bridges to see how well they perform. The analysis methods could

Figure C.10: *Left, the assembly in progress on the false work. Middle, the bridge before adding fill. Right, adding the necessary load from fill such that the false work could be removed.*

Figure C.11: *Close-up of a physical model of a single-span hydrostatic masonry bridge built during a workshop in 2022.*

include the *discrete element method* (Sarhosis et al., 2016) and established methods for masonry arch bridges (Heyman, 1982). The results of such studies could improve the understanding of masonry shells interacting with fill and further improve the design of

these types of bridges to be implemented in a real project.

Acknowledgement

The design and geometric modelling of the bridge model were performed by Emil Adiels, together with Fredrik Boman, Erik Wigh and Chris Williams.